Imperial College
London

POLYMER FIELD-EFFECT TRANSISTORS

RUTH RAWCLIFFE

A thesis submitted in fulfilment of the requirements for the degree of Doctor of Philosophy of the University of London and the Diploma of Imperial College London.

May 2006

Declaration of originality

"Except where specific reference is made to the work of others, this work is original and has not been already submitted either wholly or in part to satisfy degree requirements at this or any other university."

Ruth Rawcliffe

In loving memory of

John D. Oldham, Flora J. Philpot,

And Thomas P. Dorairaj

Acknowledgements

Doing a PhD is certainly a unique experience and I would like to take this opportunity to thank all those who contributed, directly or indirectly, to this. To begin with, I'd like to thank my supervisor Alasdair Campbell for all of his help and encouragement during these past four challenging years – as well as ensuring I always had a topped up Guinness! I am indebted to the tremendous kindness and support shown by Maxim Shkunov: who not only let me use the facilities at Merck, but also employed me when my funding ran out! I am also appreciative of the support given by Donal Bradley, the head of the group at Imperial.

It was a pleasure working with Theo Kreouzis – who taught me everything I know about TOF, Jo Wilson, Xuhua Wang, Jingsong Huang and George Heliotis. Thanks also to Dmitri Poplavskyy for the useful discussions about charge transport and SAMs, and to Saghar Khodabakhsh for help with KP measurements. Thank you also to Steve Cussell, and to Carolyn Dale and Loli Sanchez for their administrative support. On a personal level, I'd like to thank all those who contributed to my life at Imperial, especially those who contributed to the entertaining office atmosphere: 'The Basque Bull', Mariano for always seeing the artist within, Miguel for trying to keep me focussed, and Martina.

'Externally' I'd also like to thank Kristel Fobelets in Electronic Engineering for use of her analyser, probe station and wire bonding facilities. I am also grateful to David Smith in the Quantum and Functional Matter group at Southampton University for the loan of his spectrometer, and Roland Smith in the Optics group at Imperial for the use of his photomultiplier tube. Special thanks also go to the Polymer Electronics Group at Merck, especially Richard Simms - my personal chauffeur! Kristijonas Geneviecus, and of course I must not forget Iain McCulloch, for always

agreeing to employ me! I must also mention Dessislava Sainova and Armin Wedel for their hospitality during my stay at the Fraunhofer Institute in Gölm, and Ulrich Todt of the Fraunhofer Institute in Dresden, for the substrates provided. Thanks also to the Director and all the 'bods' at Sherkin Island Marine Station – especially Danny (my favourite plankton team member, though it was a close call) and AM.

I'd also like to my friends for all their support and understanding over the years. Ευχαριστω τον Αρη για την αγαπη και την βοηθεια του κατα τη διαρκεια αυτης της δυσκολης περιοδου της ζωης μου. Θεν θα ξεχασω ολα οσα εκανες για μενα. I am especially grateful to Sarah and Gareth for their generous hospitality during my writing-up stints in London (Hurrah for WW and Cher), Dan for our experimental cooking sessions and all the singing and dancing, Ann-Marie for our countless adventures, Leanne for understanding me, Erin for our unending hikes, Greg for always having an infallible faith in my abilities, and Barn for simply being Barn. To quote the latter: I love you guys!

Thank you also to my Godmother Janet, Grandma Lily, my Aunties and Uncles, and my cousins; though scattered over three continents I have managed to see nearly all of you during the course of this thesis! Finally, I dedicate this thesis to my parents, Eric and Santha, for the love, encouragement and the incredible support and belief they have shown me all the way through my life and education.

Abstract

There are many unanswered questions concerning the operation of polymer field-effect transistors, and this thesis aims to further our understanding of these devices. To begin with, it is shown that water vapour is more detrimental to device performance than oxygen, indicating that stable, operational transistors are achievable if fabrication and encapsulation procedures are carried out in a low humidity environment. A high ionisation potential equates to increased stability, making oxidation of the polymer chains less favourable. This in itself leads to problems with efficient injection of charge carriers, especially when device dimensions are reduced. A lateral field dependence of the mobility is observed at high electric fields (i.e. shorter channel lengths) as the pinch-off region expands into the channel when the gradual channel approximation breaks down. Light emission is observed at these high drain biases as electron injection can occur from the drain electrode. The contact resistance can be reduced by minimising the injection barrier, for example using ITO as an adhesion layer for gold or by using thiol self-assembled monolayers to raise the workfunction of the gold electrode. Silanes reduce the energetic disorder by improving molecular order at interface, also acting to passivate the silica interface by minimising the concentration of electron-trapping hydroxyl groups. Combining these self-assembled monolayers gives optimum transistor performance, as injection into the polymer and charge transport are enhanced. Finally, the difference between the bulk mobility, measured by the TOF photocurrent technique, versus the field-effect mobility is explored. The two-dimensional charge transport in transistors occurs in the first few polymer chains adjacent to the interface, making it more sensitive to disorder and interfacial traps. Temperature measurements confirm that the disparity between the bulk and interface mobility is due to increased energetic disorder and a longer interchain hopping distance at the interface.

Contents

Introduction and overview of thesis **1**

1. Charge transport in polymer field-effect transistors **5**

1.1. An introduction to organic semiconductors **6**

1.1.1. What is a polymer? 6

1.1.2. Electronic structure and bonding of carbon 7

1.1.3. What is conjugation? 9

1.1.4. How are the energy levels in conjugated materials defined? 10

1.1.5. Charge transport in conjugated polymers 16

1.2. Polymer field-effect transistors **17**

1.2.1. Operational principles of polymer field-effect transistors 17

1.2.2. Device characterisation of polymer field-effect transistors 21

1.2.3. Determining the mobility of polymer field-effect transistors 25

1.2.4. Gate voltage dependency of the mobility 26

1.2.5. Multiple trapping and release model (MTR) 27

1.2.6. Variable range hopping (VRH) 29

1.2.7. Polarons 31

1.3. Summary **31**

2. Experimental Techniques **35**

2.1. Device fabrication **36**

2.1.1. Fabrication of top-gate and bottom-gate transistors 36

2.1.2. Materials used in thesis 38
2.1.3. Substrate preparation 42
2.1.4. Solution preparation and spin-coating 43
2.1.5. Patterning of contacts 44
2.2. Device characterisation 46
2.2.1. Electrical measurements 46
2.2.2. Kelvin probe measurements 47
2.2.3. Contact angle measurements 50
2.2.4. Annealing and differential scanning calorimetry 51
2.2.5. Thickness profiling 51

***3. Ambient stability of thiophene-based polymer field-effect transistors* 54**

3.1. The effect of regioregularity on the transistor characteristics 57
3.2. Ambient stability of P3HT transistors 60
3.3. The effect of humidity on P3HT transistors 62
3.3.1. Experimental techniques 64
3.3.2. Stability of 90% RR P3HT transistors in low environmental humidity 65
3.3.3. Stability of 90% RR P3HT transistors in high environmental humidity 68
3.3.4. Stability of 97.5% RR P3HT transistors 71
3.3.5. The effect of regioregularity on the stability of P3HT transistors 74
3.4. How does the humidity affect transistor characteristics? 76
3.4.1. Electrochemical stability and redox processes 77
3.4.2. Hysterisis and trapping effects caused by water 85
3.4.3. Morphology and diffusion related instability 90
3.4.4. Summary of the mechanism for ambient doping of P3HT 91
3.5. Increasing the air stability of P3HT via the introduction of dopants 92
3.5.1. Experimental techniques 93

3.5.2. Increasing the stability of P3HT transistors using 0.05% DDQ 94

3.6. Ambient stability of syn-pBTTT and ant-pBTTT transistors 97

3.7. Encapsulation and device performance 102

3.8. Conclusions and further work 103

***4. Short- channel effects in polymer field-effect transistors* 109**

4.1. Short-channel effects in the linear regime 111

4.1.1. Contact resistance of syn-pBTTT transistors 111

4.1.2. Lowering R_C via an ITO adhesion layer 115

4.2. Short-channel effects in the saturated regime 122

4.21. Lateral field dependence 122

4.2.1. Finite output conductance 126

4.2.3. Electron injection at high electric fields 129

4.3. Light-emission in PFETs 129

4.3.1. What are excitons? 130

4.3.2. Absorption and emission spectra of conjugated polymers 132

4.3.3. Electroluminescence 134

4.3.4. Light-emission in OFETs 135

4.3.5. Experimental techniques 138

4.3.6. Light emission from syn-pBTTT transistors 139

4.3.7. Mechanism of light emission 141

4.4. Conclusions and further work 145

5. Controlling the characteristics of PFETs using SAMs *149*

5.1. Injection into organic materials **150**

5.1.1. The metal/organic interface 152

5.1.2. Charge injection 156

5.2. Modification of hole injection using thiols **157**

5.2.1. Why use thiols? 157

5.2.2. Formation of thiol monolayers 159

5.2.3. Workfunction measurements of thiol modified gold 162

5.2.4. I-V characteristics 166

5.2.5. Wettability and contact angle measurements 171

5.2.6. The effect of thiols on the contact resistance 173

5.2.7. How do thiols affect the mobility? 177

5.2.8. Summary of transistor performance with thiol modified electrodes 177

5.3. Improving interfacial molecular order using silanes **178**

5.3.1. Formation of silane monolayers 178

5.3.2. I-V characteristics 180

5.3.3. The effect of silanes on ambipolar transport in transistors 183

5.3.4. Wettability and contact angle measurements 185

5.3.5. Contact Resistance 186

5.3.6. Temperature studies 188

5.3.7. Summary of silane treatments 195

5.4. Combination of surface treatments **196**

5.4.1. Combination of surface treatments for syn-pBTTT 196

5.4.2. Combination of surface treatments for ant-pBTTT 198

5.5. Conclusions and further work **200**

6. Bulk and interface mobility comparison **205**

6.1. Differences in the bulk and interface mobility **206**

6.2. Experimental techniques **209**

6.2.1. The time of flight photocurrent technique 209

6.2.2. Device fabrication 212

6.2.3. Time of flight measurements 213

6.2.4. Diode (SCLC) measurements 215

6.3. Room temperature mobility measurements **217**

6.3.1. Bulk mobility measurements of amorphous materials 218

6.3.2. Field-effect transistor measurements of amorphous materials 221

6.3.3. Bulk and field-effect mobility measurements of F8T2 223

6.3.4. Comparisons of the bulk and field-effect mobility 228

6.4. Temperature dependence of the mobility **231**

6.4.1. The Bässler and Holstein (Arrhenius) Models 232

6.4.2. Temperature dependence of the mobility for PFB 233

6.5. Conclusions and further work **239**

7. Conclusions and further work **243**

Appendix I **249**

Organic electronics is a rapidly developing field that offers to fill a niche in the electronics market, which is at present saturated with silicon and its inorganic counterparts. Organic materials are envisioned for use in low-cost, large area applications as their ease of fabrication and mechanical flexibility could enable the realisation of reel-to-reel processing. They also have the added advantage of being tailored to suit requirements, as molecular design can easily modify their electronic and optical properties.

This thesis is primarily concerned with polymer field-effect transistors. Since the demonstration of the first organic transistor in 1986, much of the focus in this field has been concerned with improving the mobility. The field-effect mobility of amorphous silicon (α-Si) devices lies in the range of 0.1-1cm^2/Vs, values which have been approached and exceeded by organic field-effect transistors (OFETs). Currently, the record stands at 5cm^2/Vs for a vacuum-deposited small molecule pentacene device and 0.6cm^2/Vs for a transistor fabricated using a solution-processible conjugated polymer, ant-pBTTT, which is used in this work.[1,2] Industrial interest in these materials is consequently picking up, and OFETs have already been successfully demonstrated in applications such as electronic paper,[3] sensors,[4] and radio frequency identification cards (RFIDs).[5]

Fig.1 illustrates several products which were developed using this technology. The KODAK EASYSHARE LS633 Zoom Digital Camera is the first commercially available camera with an active organic light emitting diode (OLED) display.[6] These self-luminescent displays (i.e. no backlight) offer high contrast pictures when viewed from almost any angle. Also shown is an example of the first large-screen (40inch) full-colour OLED display which was developed by Seiko Epson Corporation used inkjet printing technology.[7] The largest flexible organic active matrix display (10inch) was recently demonstrated by Plastic Logic.[8]



Figure.1. (i) The KODAK EASYSHARE LS633 Zoom Digital Camera is the first commercial camera using an OLED display (ii) The first large-screen full-colour OLED display was printed by the Seiko Epson Corporation (iii) The largest flexible printed organic active matrix display using E Ink Imaging Film™ by Plastic Logic. Images taken from[6,7,8]

E Ink Imaging Film™ was designed for use in paper-like electronic displays by E Ink Corporation and consists of a layer of electrophoretic microcapsules on a transparent electrode. A printed OFET backplane is used to drive the electronic ink frontplane, by moving the black and white charged pigments towards/away from the transparent electrode.[9] All in all, the thickness of the flexible, laminated display is just 0.4mm, opening up widespread possibilities for display technologies.

This thesis is concerned with the fundamental issues associated with the device performance of polymer field-effect transistors. Chapter 1 and 2 present a brief introduction into their operation and fabrication, before tackling the problem of ambient instability in Chapter 3. This is one of the main drawbacks of organic

materials as their low ionisation potential renders them susceptible to oxidation by reactive ambient species, like molecular oxygen and water vapour. Polymers with higher ionisation potentials are in general more stable. However, this can lead to problems as gold ($\Phi_{Au} \sim 5.1eV$) is typically used as an injecting contact in PFETs. Chapter 4 discusses the problems associated with the contact resistance of a polymer with $I_P \sim 5.3eV$, as well as looking at the short channel effects that can arise when the channel length of a transistor is reduced. A spin-off of this was the observation of electroluminescence (EL) near the drain electrode at high drain biases!

Chapter 5 provides a solution to the problem of contact resistance by using a class of self-assembled monolayers (SAMs) called thiols to modify the workfunction of the injecting contact. The molecular order at the interface is also improved by using trichlorosilane SAMs, which results in dramatic improvements of the mobility. Finally, a comparison is made between the field-effect mobility and the bulk mobility of polyfluorene material systems in Chapter 6. Temperature measurements confirm that the disparity between the bulk and field-effect mobility is due to increased energetic disorder and a longer interchain hopping distance at the interface. A summary of this and the other Chapters is given in Chapter 7, in which the main conclusions and related further work is presented.

References

1. P. F. Baude, D. A. Ender, M. A. Haase, T. W. Kelley, D. V. Muyres, S. D. Theiss, *Appl. Phys. Lett.* **82** 3964 (2003)

2. I. McCulloch et al., *To be published in Nature Materials* (2006)

3. G. H. Gelink, *Nat. Mater.* **3** 106 (2004)

4. Z.-T. Zhu, *Apply. Phys. Lett.* **81** 24 (2002)

5. D. Voss, *Nature* **407** 442 (2000)

6. www.kodak.com

7. www.epsom.com

8. www.plasticlogic.com

9. B. Comiskey, J. D. Albert, H. Yoshizawa, J. Jacobson, *Nature* **394** 253 (1998)

Chapter 1

Charge transport in polymer field-effect transistors

This chapter discusses how the conjugated system in polymers enables charge transport by considering electronic structure and transport mechanisms. The operation and characterisation of polymer field-effect transistors is then introduced before reviewing the models currently used to describe them.

Nowadays, many traditional materials such as wood, ceramic, metal and glass have been replaced with synthetic polymers. They are incredibly versatile and can be tailored to possess an impressive range of material properties. An example of this diversity is the polymer polyvinylchloride (PVC), which can be used to manufacture window frames, credit cards and cling film! If asked whether plastics can conduct electricity, most people would answer "No", which is hardly surprising as PVC is used as the insulating sheathing of electrical wires. Naturally, the question arises of how a traditionally insulating material can function as a semiconductor.

The purpose of this Chapter is to resolve this issue and provide a general background to the charge transport properties and operation of polymer field-effect transistors (PFETs), which can then be built upon in subsequent Chapters. Features of the charge structure and electronic properties of conjugated polymers will be introduced in the first part of this Chapter. The principles behind polymer field-effect transistors will then be explained, concluding with a discussion of the mechanisms for charge transport and related models. As this thesis is primarily concerned with conjugated polymer transistors, the focus will be as such.

1.1. An introduction to organic semiconductors

1.1.1. What is a polymer?

Let us first consider what a polymer is. The word polymer derives from the Greek πολυ μεροι, literally meaning many parts, and chemically speaking consists of a macromolecule made up of repeat units (monomers). If the polymer comprises of identical units it is classified as a homopolymer, and if it contains more than one monomer is a copolymer. These can be further classified as block, alternating or statistical copolymers, depending on the arrangement of repeat units, as illustrated in

Fig.1.1. It is clear that there is an unlimited range of possible combinations, each possessing different properties, allowing a polymer to be designed to meet specific requirements.

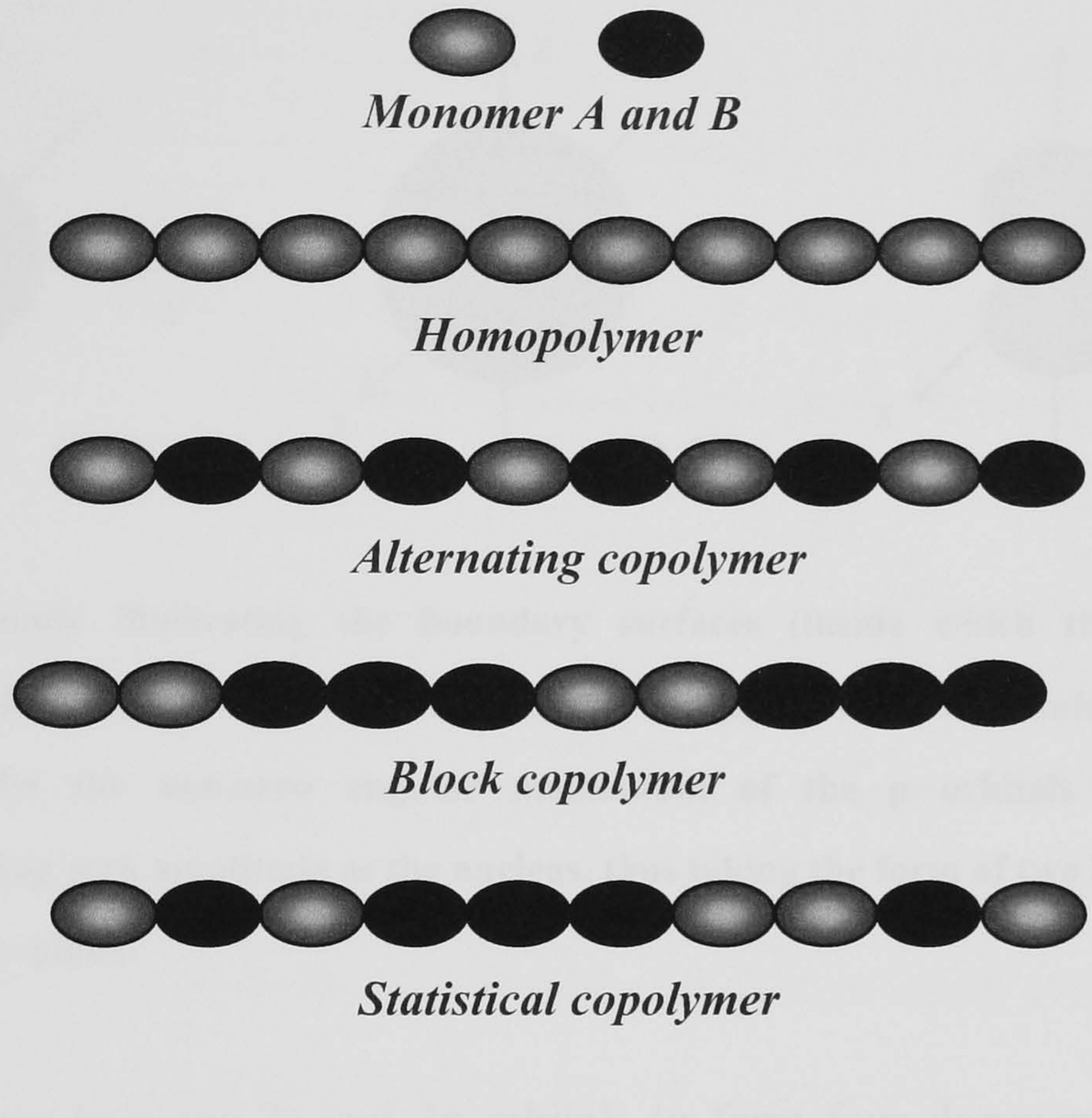


Figure.1.1. Examples of polymers formed with different combinations of monomer units are represented above by either grey (A) or black (B) ovals. The repeating units making up a homopolymer are identical. A copolymer contains more than one monomer species. This classification can further be segregated as alternating copolymers (alternating sequence of monomer units A and B), block copolymers (repeating sequence of blocks, each block comprising of several identical monomer units, of monomers A and B), and statistical copolymers (a random arrangement of monomers A and B)

1.1.2. Electronic structure and bonding of carbon

The term 'organic' is used in chemistry to describe carbon based systems and applies to the small molecules and polymers considered here. Carbon has the ground state electronic structure $1s^2 2s^2 2p_x^1 2p_y^1$ and according to valence band theory should only form two bonds. However, carbon is tetravalent as an electron can be promoted

from a $2s^*$ to a 2p orbital, enabling four bonds to be formed (excited state electronic configuration is $1s^2 2s^1 2p_x^1 2p_y^1 2p_z^1$ - there are four unpaired electrons in separate orbitals).

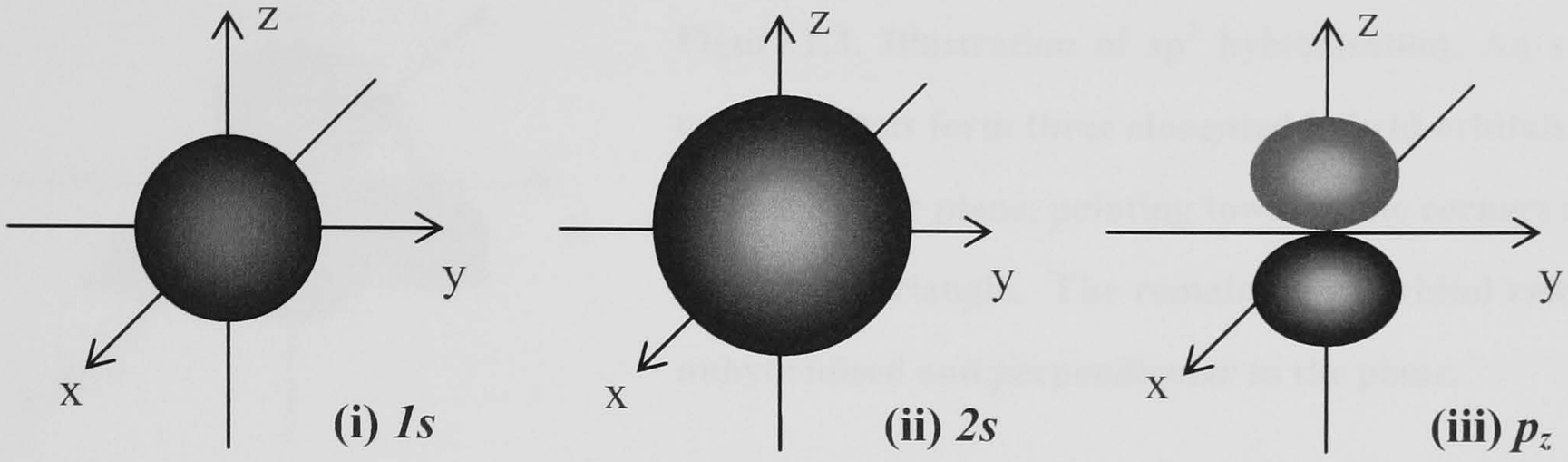


Figure.1.2. Schematic illustrating the boundary surfaces (inside which there is a 90% probability of finding the electron) of (i) 1s (ii) 2s and (iii) p_z orbitals. S orbitals are spherically symmetrical whilst the non-zero angular momentum of the p orbitals results in the wavefunction having zero amplitude at the nucleus, thus taking the form of two lobes above and below the nodal xy-plane.

Mixing can occur between 2s and 2p orbitals to form four degenerate sp^3 hybrid orbitals that lie in a tetrahedral fashion around the central carbon atom (109.47° between bond axes), as is the case for methane. This hybridisation can be thought of as the four atomic orbitals behaving as waves centred around a nucleus that interfere constructively and destructively, giving rise to a hybrid orbital. Constructive interference between the s orbital and positive lobes of the p orbitals results in enhanced electron density near the nucleus, so the bond strength is greater than that of an unhybridised orbital (repaying some of the energy required to promote the 2s electron in the first place).[1] In the case of partial sp^2 hybridisation an s and two p orbitals are superimposed forming three new hybrid orbitals in the same plane at 120°, leaving a p orbital perpendicular to the hybridisation plane unaltered. This

---

*The energy of a shell is given by the quantum number n =1,2,3… For the n = 2 level 2s and 2p orbitals exist with s and p denoting different subshells (with angular momentum l = 0 and 1 respectively)

type of hybridisation is illustrated in Fig.1.3 and is the bonding normally found in semiconducting carbon-based polymers.

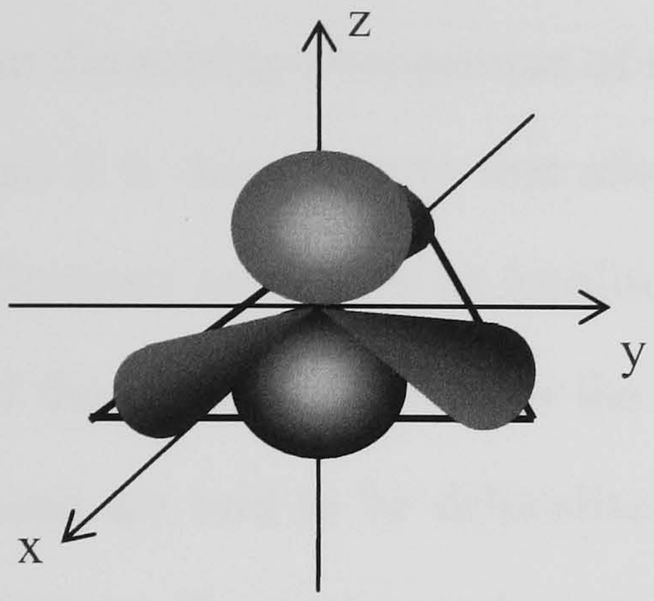


Figure.1.3. Illustration of sp^2 hybridisation. An s and two p orbitals form three elongated hybrid orbitals that lie in the same plane, pointing towards the corners of an equilateral triangle. The remaining p_z orbital remains unhybridised and perpendicular to the plane.

Three axial σ-bonds (single bond) can be formed via the overlap of the sp^2 orbitals of neighbouring carbon atoms (or with the 1s orbitals of adjacent hydrogen atoms). C-C and C-H σ-bonds thus form the framework of the system and if planar, the remaining unhybridised p orbital on each adjacent C atom could overlap sideways, forming a weaker π-bond (double bond).

1.1.3. What is conjugation?

The structure of benzene (C_6H_6) proved to be a problem for chemists when explaining why monosubstituted derivatives, such as chlorobenzene, displayed no isomers. This suggested that the six carbon atoms must occupy equivalent positions. In 1865 the German scientist Friedrich Kekulé supposedly had a dream in which a snakelike atomic chain caught hold of its own tail, forming a circular structure. He suggested that benzene possessed a cyclic structure of alternating single and double bonds.[2] Today it is explained as π-electrons forming a delocalised electron cloud above and below a planar σ-bonded framework. Indeed if a comparison of bond lengths in cyclohexane is considered it is found that a single bond has a length of

0.15nm, a double of 0.13nm, with the actual length in benzene being equidistant at 0.14nm![3]

An alternating arrangement of single and double bonds is called a conjugated system and it is this property that allows organic materials to function as semiconductors. Electrons are said to be localised if they are located in the region between the nuclei of the bonded atoms, as is the case for the electrons in a σ-bond. Electrons in a π-bond are said to be delocalised as they are not specifically confined to the region between the nuclei, and so form a cloud of electron density above and below the plane of the σ-bond. Their π-electron clouds can spread out over nearby single bonds, creating a delocalised system over the entire molecule.

The conjugation length of a polymer is defined as the length of an oligomeric (an oligomer is a 'small molecule' constructed of only a few monomers – again from the Greek λιγα μεροι meaning small parts) segment with the same value of E_G as the disordered polymer chain. This can simply be thought of as the average number of repeat units between conjugation breaking defects. The conjugation length is estimated to be 3-5nm for most polymers, though it should be noted that this definition assumes that each conjugated segment is completely decoupled from its neighbour. In reality there is bound to be some degree of overlap and leakage of the π-electron system between segments.[4]

1.1.4. How are the energy levels in conjugated materials defined?

Every solid contains electrons. The important question to consider, if concerned with conductivity, is how they respond to an applied electric field. The electrons in an isolated atom have a distinct set of energy levels. If two identical atoms an infinite distance apart are brought closer together, the interaction between them splits

the previously degenerate energy level into two levels, one higher and one lower than that of then isolated atom. The electrons in a crystal are periodically arranged in a closely spaced ordered lattice and interact to form two continuous energy bands, separated by a 'forbidden energy' band gap E_G. The upper band is called the conduction band, and the lower is entitled the valence band. The material behaves as an insulator, semiconductor or metal depending on how its valence electrons fill these bands, the size of E_G, and the presence of any dopants.

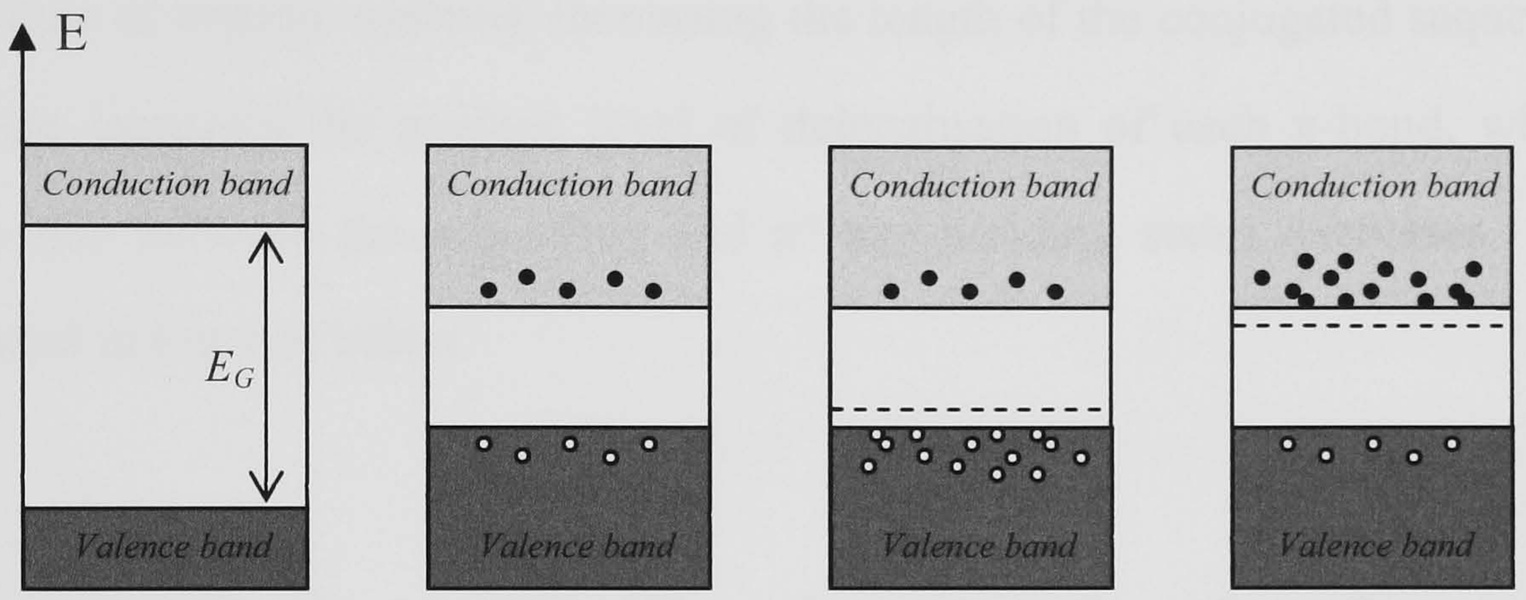


Figure.1.4. Energy bands of (i) an insulator (ii) an intrinsic semiconductor at room temperature (iii) a p-type semiconductor with the dashed line showing the acceptor energy levels and (iv) a n-type semiconductor. In this case the dashed line represents the donor energy levels. The energy gap E_G of a semiconductor is smaller than that of an insulator, enabling electrons to be thermally excited into the conduction band at room temperature. 'Free to move' holes and electrons are illustrated by white and filled circles, respectively.

Good conduction occurs in a metal as the bands are only partially filled so there are vacant energy states adjacent to occupied ones. Alternatively, band overlapping can occur. If the valence electrons completely fill or empty these bands, electrons can not move on the application of an electric field and the material behaves as an insulator. As the model of an insulator suggests (See Fig.1.4 (i)), the lower energy state is completely filled and the higher empty, so an electron must be promoted to

the higher energy band for a current to flow. This happens in the case of semiconductors as the energy gap is smaller so electrons can be thermally excited into the conduction band at room temperature. At absolute zero the energy bands of an intrinsic semiconductor should be as for an insulator. The addition of donor (or acceptor) impurities to an intrinsic semiconductor creates additional energy levels at the bottom of the conduction (or top of valence) band that increases the conductivity by changing the carrier density.[5, 6]

In the case of organic systems, increasing the length of the conjugated sequence in a molecule increases the average level of delocalisation of each π-bond, whilst the energy gap between the π-bonding and π*-anti-bonding states decreases. This is illustrated in Fig.1.5, below.

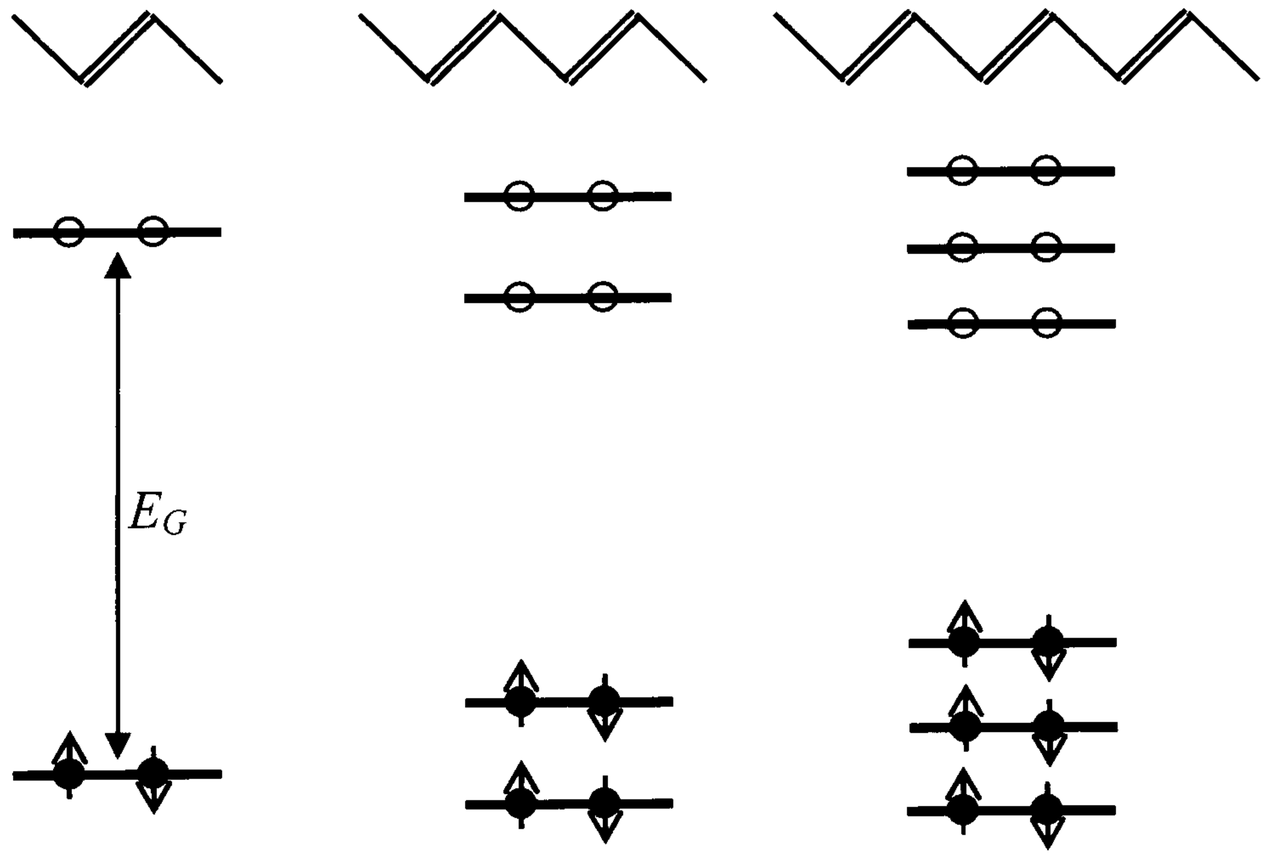


Figure.1.5. Schematic illustrating how the energy levels change as the length of a conjugated molecule is increased. As the conjugated length and level of delocalisation of the system is increased, the energy gap between the highest occupied molecular orbital (HOMO) and lowest occupied molecular orbital (LUMO) decreases. Adapted from[7]

However, the gap remains finite in the long chain limit as preserving some bond alternation achieves a lower total energy than delocalising the whole π-bonding electron system. This is known as the Peierls instability.

Constructive or destructive interference between orbitals results in π-bonding or π* anti-bonding orbitals. Anti-bonding orbitals are denoted with an asterisk. An anti-bonding orbital acts against the cohesion holding the two atoms together if occupied – as the nuclei would be attracted to an electron density region outside the internuclear bonding area. Consequently, the energy of the molecule is increased, relative to the separate atoms. The highest filled state can be referred to as the highest occupied molecular orbital (HOMO) and the lowest empty state as the lowest unoccupied molecular orbital (LUMO). These are the frontier orbitals, and are analogous to the concept of the conduction and valence bands in inorganic semiconductors.

Fig.1.6 illustrates the differences in energetic structure of a conjugated molecule in isolation, and in an ordered crystalline film. The energy required to remove an electron from the HOMO to infinity is the ionisation potential I_P and the energy required to add an electron to the LUMO from infinity is termed the electron affinity A. The shift in the energy levels between the gas and crystalline phase is mainly due to polarisation interactions between the molecules. This is easy to explain if you consider what happens if a positive (removal of an electron) or negative (addition of an electron) charge is added to a molecule. If the conjugated molecule is in a solid, the additional charge can polarise the surrounding π-electron systems of neighbouring molecules, reducing its energy. Although this is the dominant process, charge coupling between these induced dipoles can also contribute to the electronic polarisation energy.

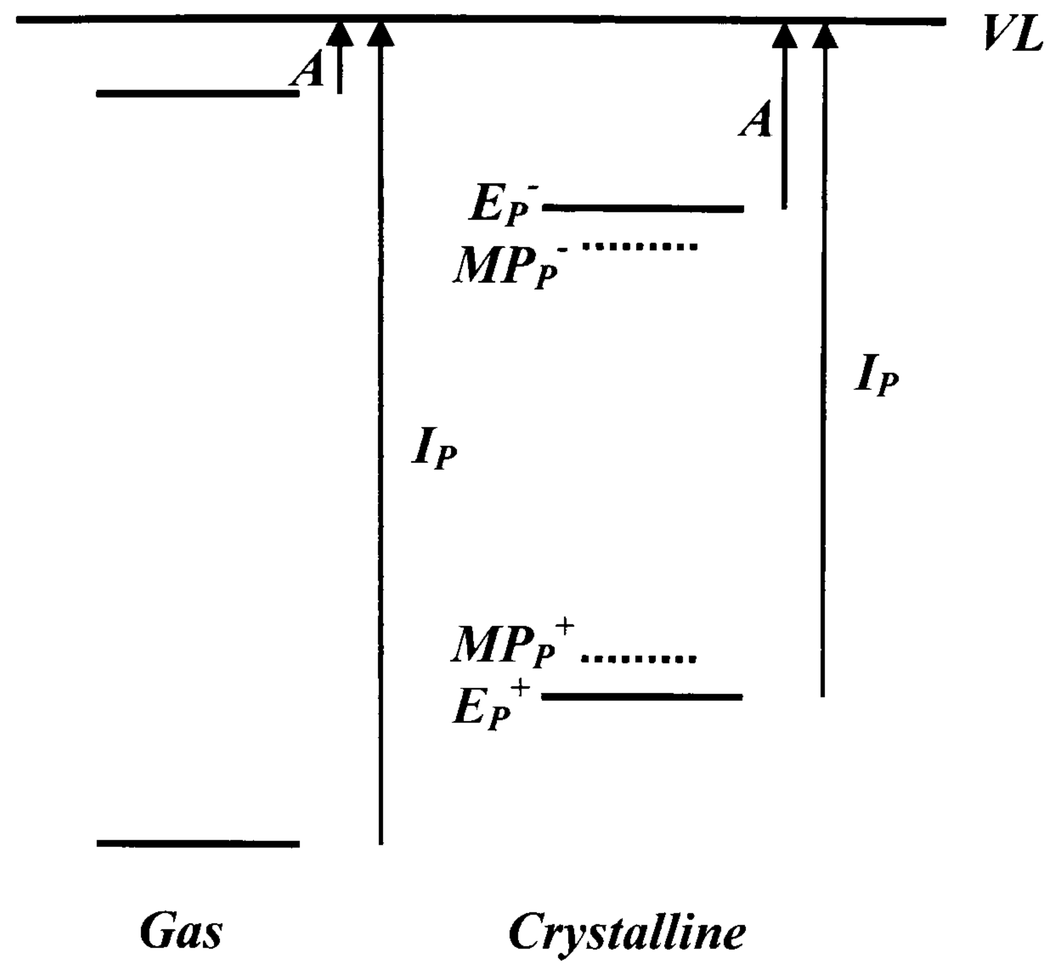


Figure.1.6. This schematic illustrates the difference in energy levels of a single conjugated molecule in isolation (gas) and in a crystalline solid state (crystalline). I_P represents the ionisation potential, in other words the energy required to remove an electron from the HOMO to infinity (i.e. above the vacuum level VL), and A represents the energy required to accept an electron from infinity to the LUMO - the electron affinity. In the crystalline system, additional states are formed in the energy gap by the addition or removal of an electron, with E_P and MP_P referring to the electronic and molecular polaron levels, respectively. Adapted from[7]

Unlike covalently bonded bulk crystalline semiconductors such as silicon and germanium, the addition or removal of an electron to a conjugated system causes a reorganisation of the bonding. The resulting structurally relaxed charged state is called an electron polaron (if an electron is added) or hole polaron (if an electron is removed)*. This bond reorganisation results in extra states being formed in the energy gap – the molecular polaronic levels (MP). The relaxation time for electronic polarisation interactions (10^{-16} to 10^{-15}s) is quicker than polaron coupling to the lattice (10^{-15} to 10^{-14}s), so injected charge initially sits in the electronic polaron levels

* These structurally relaxed charged states are termed molecular polarons. The polarisation interactions can be referred to as electronic polarons.

before undergoing interactions with lattice and relaxing into the molecular polaron levels.[7]

A polymer chain can take up a range of different conformations by rotating or by twisting and distorting its backbone bonds. In addition, it will contain chemical defects (saturated units or chain branches), which would also contribute towards a breaking up of the conjugation in the chain. The backbone electron system consequently becomes less delocalised along the chain and the size of the carrier energy gaps increases - resulting in a distribution of energy states. The case is further complicated as each molecule (or conjugated section of chain) is randomly orientated and is surrounded by a range of molecules with different orientations and positions. Thus the polarisation interactions will also be spread out over a range of energies. The resulting level of energetic disorder can be approximated by a Gaussian distribution about the HOMO and LUMO levels as follows:

$$g(\varepsilon) = \frac{N_0}{\sqrt{2\pi\sigma}} \exp\left(-\frac{\varepsilon^2}{2\sigma^2}\right) \qquad \{1.1\}$$

where N_0 is the total density of states, ε is the energy of the states, and σ is the standard deviation of the density of states (DOS).

In a conjugated polymer a range of conjugation lengths is present. This conformational disorder has the effect of increasing the energetic disorder, with a typical distribution of σ for small molecules and polymers being 0.1eV. Further evidence to justify the use of a Gaussian function is that absorption bands of disordered organic materials normally have a Gaussian shape with a typical variance of $\leq$ 0.1eV so it seems reasonable that the transport DOS has a similar distribution and energetic parameters.[8, 9]

1.1.5. Charge transport in conjugated polymers

Consider the representation of an amorphous polymer film in Fig.1.7, consisting of a range of conjugated segments. In each section, the charged excitations can move relatively easily along individual chains in the direction of the electric field since their wavefunctions are delocalised over similar repeating units. In order to transfer onto another chain, the excitation has to hop between chains, so charge carriers traversing a thin film will be a combination of carriers moving between localised sites along the chains (intrachain) as well as hopping between chains (interchain). The latter is the rate-limiting step when concerned with charge transport and gives an upper mobility limit of 10^{-4} to 10^{-3} cm^2/Vs in amorphous films.[10] It follows that charge transport is sensitive to the morphology and local structural order within the film, with structural and energetic disorder playing an important role in determining the mobility.

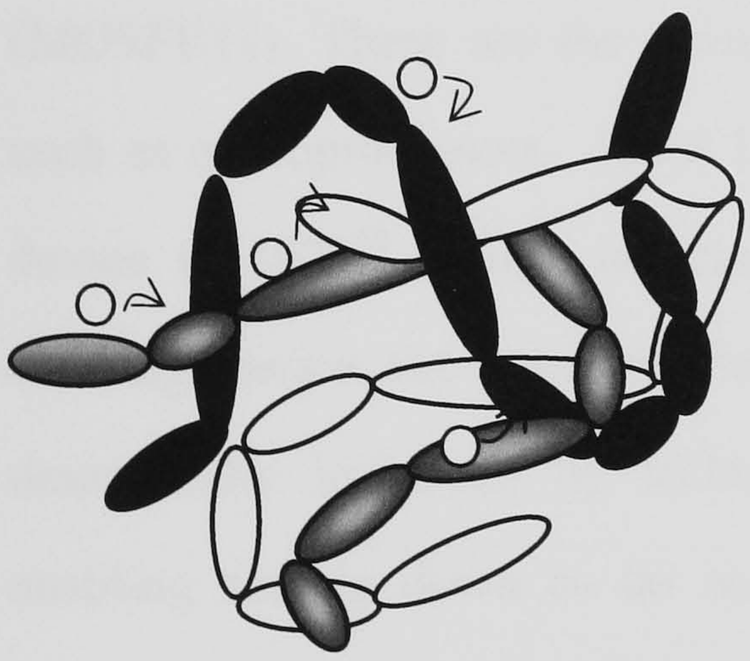


Figure.1.7. Diagram illustrating intrachain (along chains) and interchain (between polymer chains) hopping. Holes are represented by the empty circles and conjugated segments of the chains are represented by ovals. Thus, the hole at the far left of the picture is hopping along the grey chain, whilst the hole adjacent to it is hopping between different chains. The latter is the rate determining step.

In the next section, we will consider the operational principles of polymer field-effect transistors. A brief synopsis of organic field-effect transistors was presented in the introduction. Much of the work has been concerned with improving the mobility and performance of transistors but, to an extent, the more fundamental

device physics has been neglected. The basic concepts behind transistor operation will be explained, before discussing characterisation techniques, and describing several models that can be used to quantify the charge transport properties of devices. The background gained will be built upon in the following Chapters, where specific aspects of transistor behaviour will be investigated.

1.2. Polymer field-effect transistors

These days it is virtually impossible not to encounter transistors as part of daily life as they are hidden in all manner of everyday items, from washing machines to toasters. The first integrated circuit[11] realised in 1958 contained just two transistors. Considering that the Intel Pentium 4 microprocessor currently contains over 55million transistors, it is clear that silicon technology has been a rapidly advancing field over the last thirty years.

Most transistors in use today are metal-oxide-semiconductor field-effect transistors (MOSFETs). These are the primary components of large scale integrated circuits such as microprocessors. Julius Lilienfield proposed the basic principle behind this device in 1925[12] though inadequate material-processing techniques resulted in a working device not being fabricated until 1960. Since then devices have been dramatically improved by technological and material processing advancements enabling scaling down as far as subnanometer channel lengths, the point where operational and processing limits are predicted to reach in a decade or so.[13]

1.2.1. Operational principles of polymer field-effect transistors

A FET utilises the field-effect principle to amplify weak signals. It is a three terminal device in which the current flow between two of the terminals, the source

(usually grounded) and the drain, can be controlled by modulating the bias on the third, the gate. Charge carriers travel between the source and drain contacts along a semiconducting path called the channel. The channel has a length in the direction of the current flow, L, and a width perpendicular to the current and parallel to the surface, W.

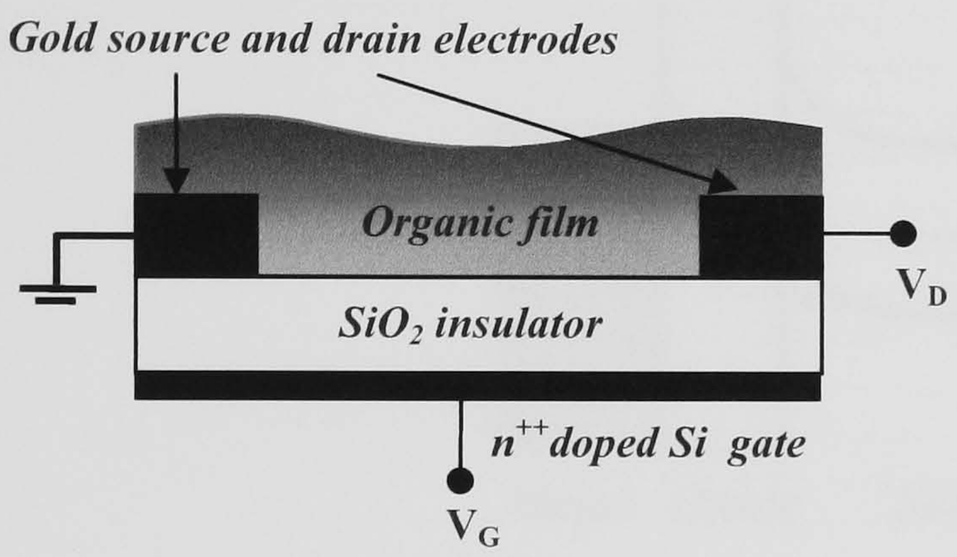


Figure.1.8. Schematic for an OFET using n^{++}- doped silicon as the gate electrode with gold source and drain electrodes. A thermally grown layer of silicon dioxide (~200nm thick) acts as the dielectric, and the organic layer is spin-coated, drop-cast or vacuum deposited on top.

There is essentially no current between the gate and the channel as the oxide layer functions as a dielectric. The gate and channel can consequently be thought of as two plates of a capacitor. Thus, a positive charge on the gate would induce an equal amount of negative charge in the channel and vice versa. The application of a small bias to the drain would induce a current to flow in the channel, the magnitude of which would be dependent on the number of carriers present. It follows that a small change in gate voltage can cause a large variation in the current, which is how a transistor amplifies signals.

Organic field-effect transistors predominantly function as accumulation-mode enhancement transistors. If a negative bias is applied to the gate, the voltage would be dropped over the insulator and semiconductor near the insulator/semiconductor interface. The system is no longer in electronic equilibrium so the Fermi levels of the metal and semiconductor realign via a redistribution of charge at the interface, giving rise to band bending. The situation looks similar to that of a p-type inorganic

MOSFET in accumulation and is illustrated in Fig.1.9. The main difference is that there are in effect no free charges in an undoped organic semiconductor at zero gate bias (neglecting any unintentional dopants), bar a thin region of a few nm near the contacts of charge that has been thermally excited from the metal.[4]

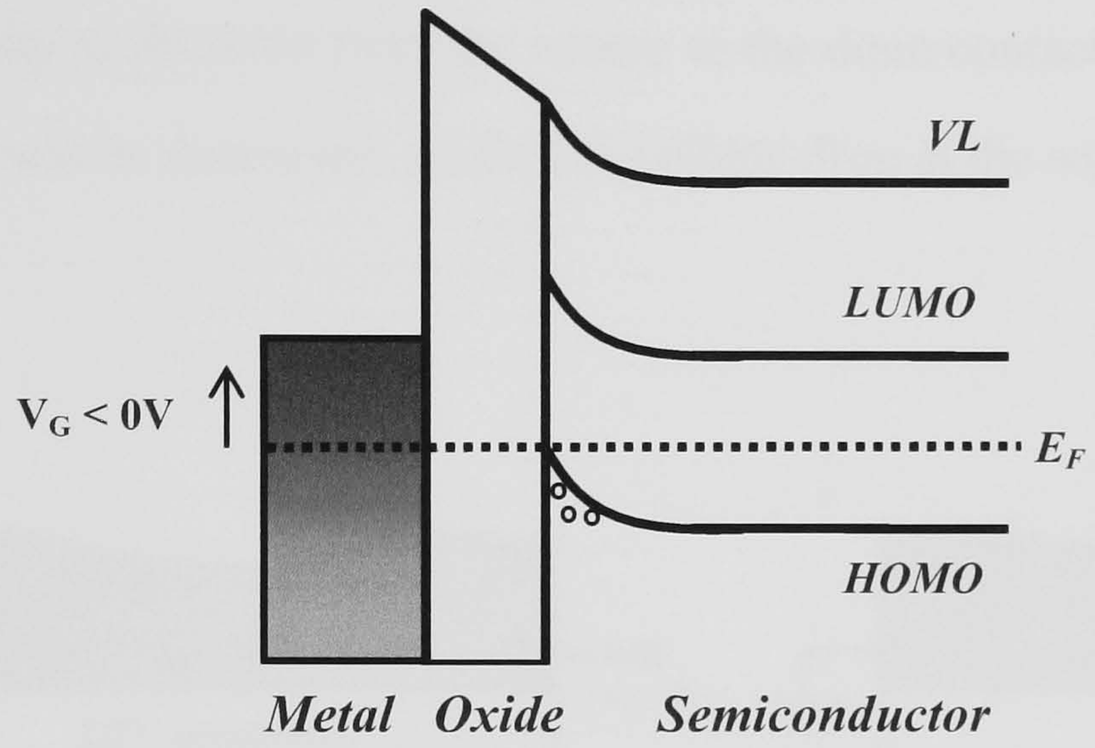


Figure.1.9. This diagram describes the band bending in an undoped p-type OFET with an applied negative gate bias, operating in the accumulation regime. On the application of a negative gate voltage the E_F of the metal is raised by eV_G and holes are accumulated at the interface as the semiconductor bands bend upwards to accommodate.

It follows that the charges needed to form the accumulation layer must be injected into the polymer by the source and drain electrodes. Organic materials generally transport holes more efficiently than electrons and behave as p-type semiconductors with ionisation potentials ranging from 4.5 to 5.9eV.[14] An Ohmic contact between the electrodes and the polymer is required for efficient injection so gold is commonly used as it provides a good contact to most materials since is relatively non-reactive and possesses a workfunction of 5.1eV.[15]

A negative gate bias would cause holes to be injected from the source electrode into the polymer layer. An equal and opposite charge is stored at the gate/insulator and polymer/insulator interface and the charge per unit area will be uniformly

accumulated throughout the transistor channel. As in the case of an inorganic MOSFET, a current flows in the channel on the application of a bias between the source and the drain. At very low drain bias the accumulation layer will still have an approximately constant charge density[16] and the drain current will increase linearly with drain voltage. An increasingly negative drain bias would cause the accumulated charge density to decrease from the source to the drain contact as the voltage drop at the drain would be decreased, whilst the voltage drop at the source electrode remains the same.

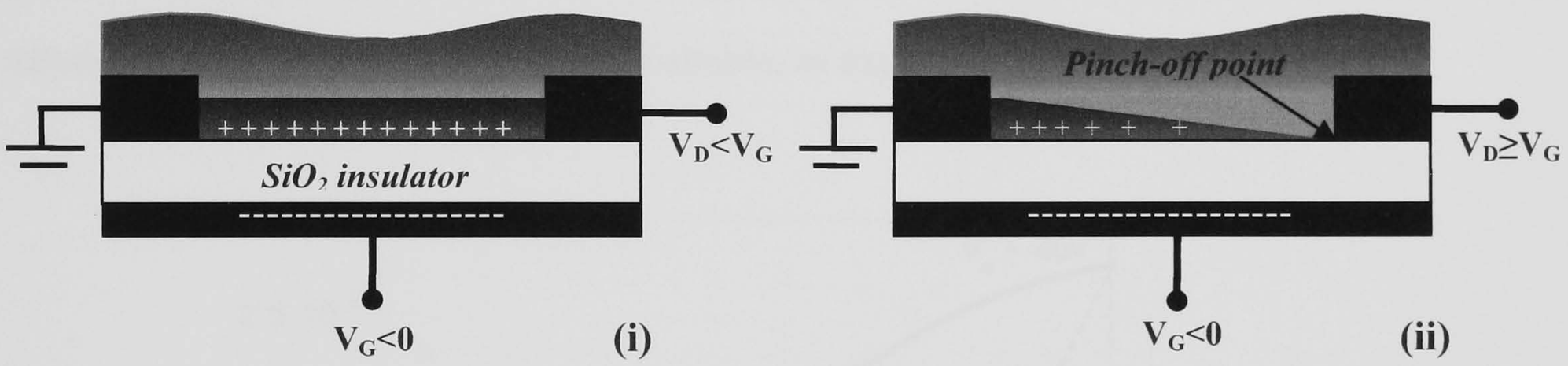


Figure.1.10. Schematic of channel formation in the (i) linear and (ii) saturation regime. As a negative bias is applied to the gate electrode, positive charge is accumulated at the insulator/polymer interface. This forms the channel in the transistor. At low drain biases, the charge density in the channel is approximately constant, but at higher drain voltages the channel is pinched-off at the drain as $V_D \geq V_G$.

Further increasing the drain causes the current to increase sub-linearly until the channel gets 'pinched off' before the drain electrode ($V_D \geq V_G$). The accumulated charge density and voltage drop across the insulator are zero at the 'pinch off point'. Beyond the pinch-off point the drain current is essentially the same, as the current flowing between the drain and source is constant since the number of carriers arriving from the source per unit time remains the same. This is termed saturation, and the linear and saturation regimes can be clearly identified from an output plot.[13]

1.2.2. Device characterisation of polymer field-effect transistors

As with inorganic devices, there are several standard techniques used to characterise OFETs. Transfer and output measurements provide the minimum data to extract material and device properties such as the field-effect mobility, turn-on voltage, on/off ratio and contact resistance. Output characteristics are measured by sweeping the drain bias from 0 to -60V at constant gate voltages, ranging from 0 to -60V in 10V steps, and recording the drain current. A typical output plot is shown in Fig.1.11 for a (poly (2,5-bis(3alkylthiophen-2-yl)thieno[2,3-b thiophene) (syn-pBTTT) transistor with 10μm channel length and 1cm channel width. The linear and saturation regimes are clearly distinguishable, as expected from MOSFET theory.

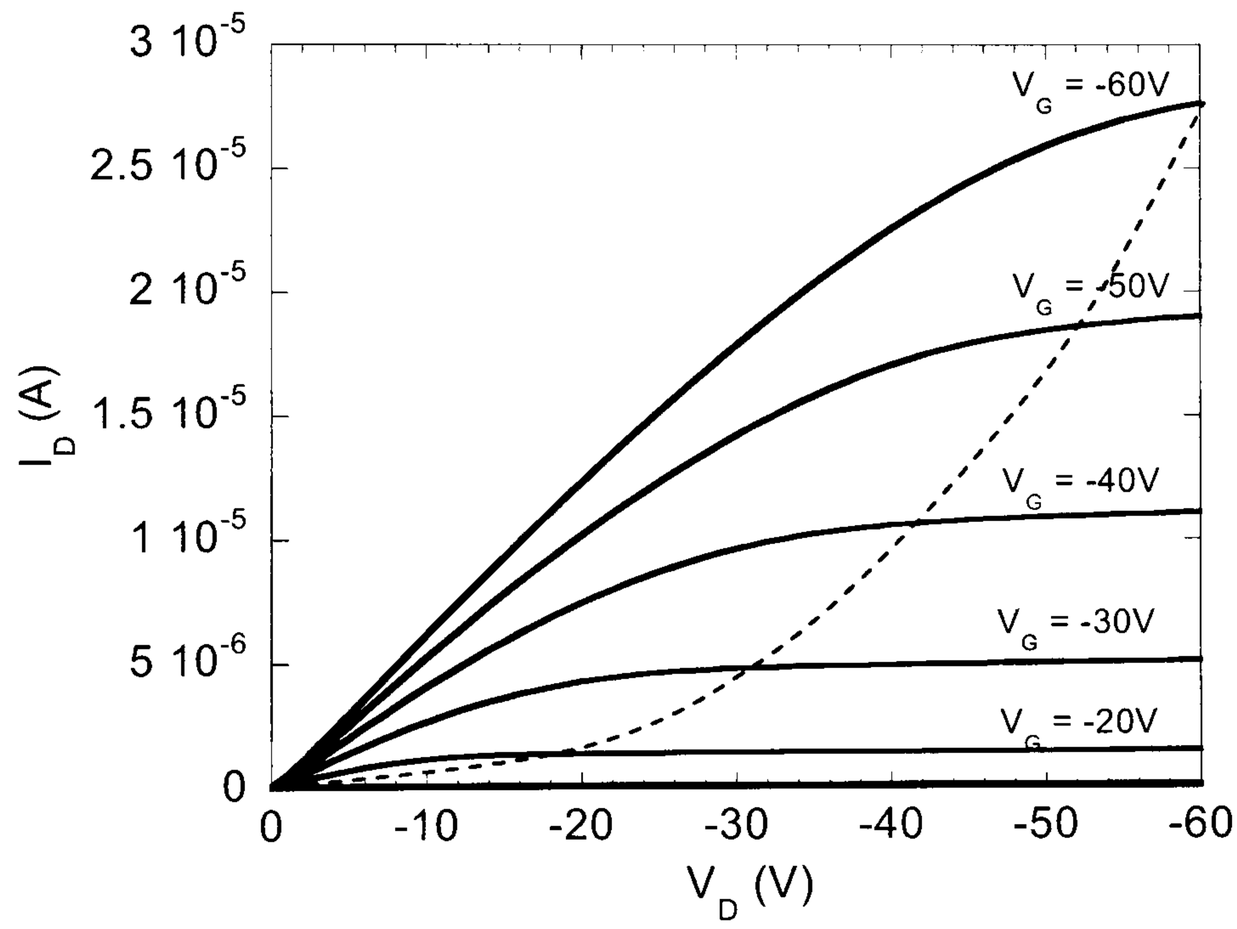


Figure.1.11. Output characteristics for a syn-pBTTT transistor with channel dimensions L=10μm and W=1cm, at increasing gate biases. The locus of I_{DSAT} and V_{DSAT} is represented by the dashed line and the linear and saturation regimes can be clearly distinguished to the left and right of this, respectively.

Fig.1.12 shows typical examples of linear and saturated transfer characteristics for a syn-pBTTT transistor of channel length 10μm. The plot on the left (i) includes the

gate current (dashed line), which is useful as it gives an indication of the level of leakage currents at the gate. The gate current is negligible (~nA) in comparison to the source and drain currents and good symmetry is observed between the currents measured at the source (dotted line) and drain (solid line) electrodes, indicating good transistor behaviour. The second plot (ii) shows only the drain current in a semi-logarithmic format. In semi-logarithmic format, it is evident where the transistor turns on (V_0) as the current rapidly increases.

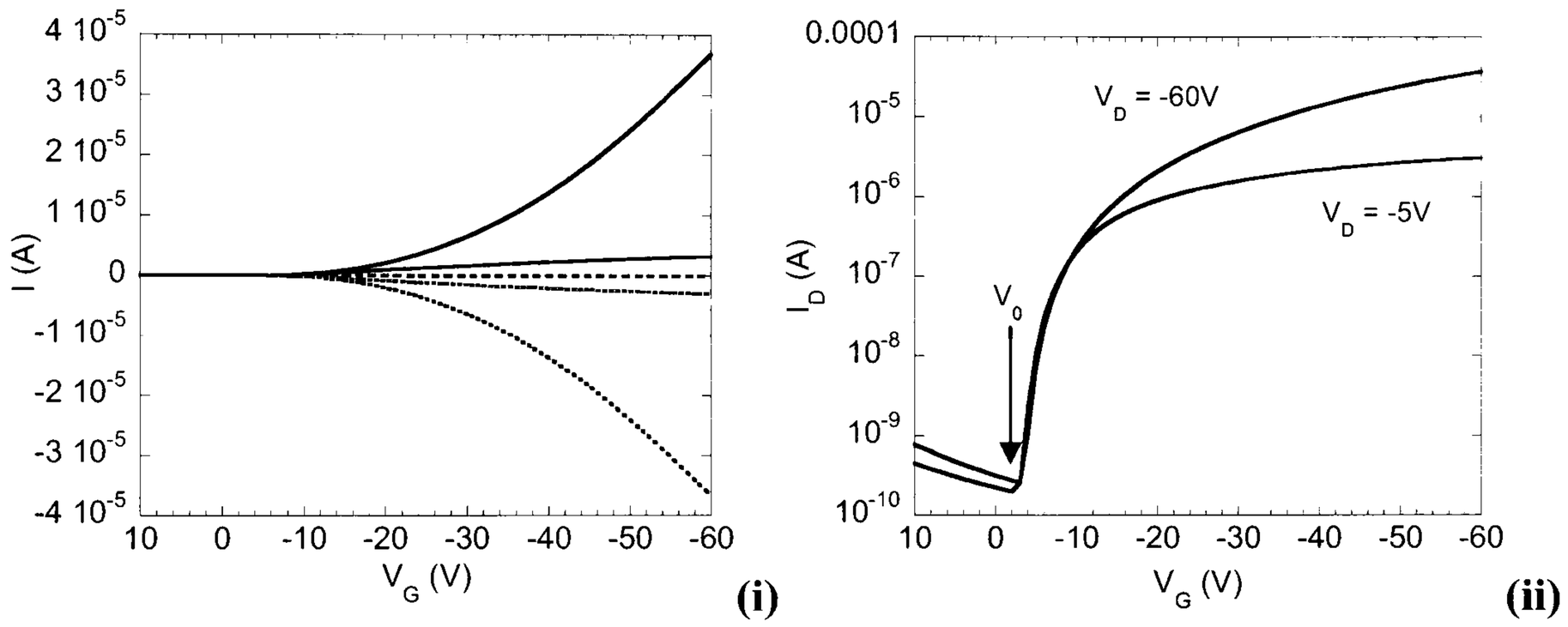


Figure.1.12. Transfer characteristics for a syn-pBTTT transistor with channel dimensions L=10μm and W=1cm showing (i) the simultaneously measured source (dotted line), drain (solid line) and gate currents (dashed line) in the linear (V_D = -5V) and saturated (V_D = -60V) regimes and (ii) the linear and saturated transfer characteristics in a semilogarithmic format, enabling the turn-on V_0 of the transistor to be easily identified (See arrow).

The difference between the traditional threshold voltage V_T and the switch-on voltage V_0 is illustrated in the Fig.1.13. V_0 is estimated from the point at which the current starts to rise sharply, the turn-on of the transistor. Standard MOSFET theory derives V_T from transfer characteristics by plotting the square root of saturated drain current against the gate voltage, and is defined as the gate voltage at the onset of strong inversion.[13] The curve is fitted linearly and V_T obtained from the x-axis intercept. However, strong inversion is not seen to occur in organic transistors, so V_T

should be thought of as merely a fit parameter.[17] As an alternative, the switch-on voltage V_0 is used in this work. Though, it should also be mentioned that for practical applications, V_T might still be a reasonable approximation, as the physical current detection limits between an on and off state is of the order of μA.

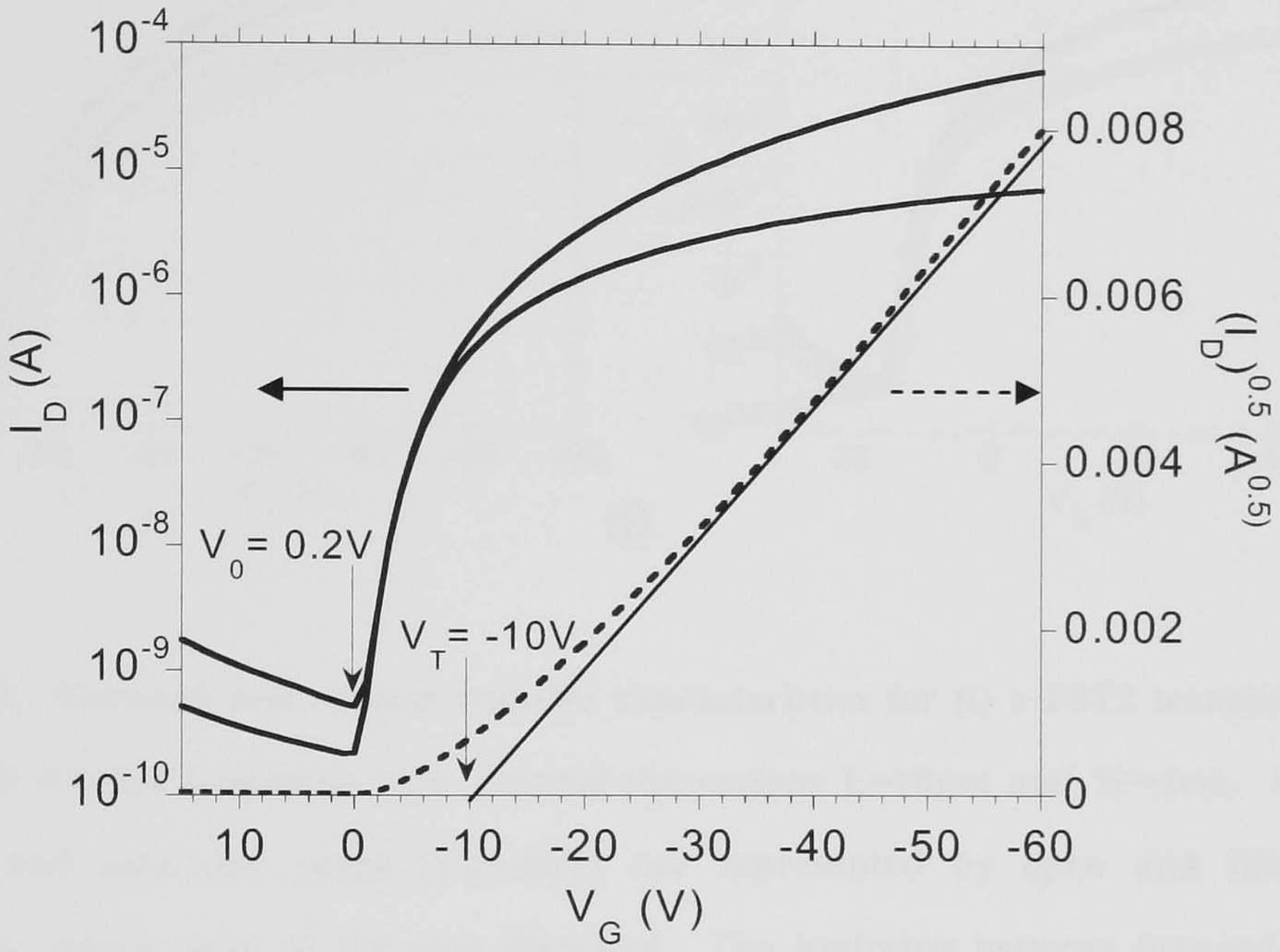


Figure.1.13. The difference between the switch-on (V_0) and threshold (V_T) voltages is clearly illustrated. V_0 is read directly from the semilogarithmic plot of the transfer characteristics (solid line), whilst V_T is extrapolated from the square route of the saturated drain current (dashed line).

Theoretically, holes should be accumulated in the channel as soon as the gate bias becomes negative. A mismatch between the workfunction of the gate Φ_G and Fermi level E_F of the bulk semiconductor has the same effect as applying a voltage to the gate, causing the bands of the semiconductor to bend at the interface until the levels are equilibrated. If the gate workfunction is lower than the Fermi level of the polymer, charge will be depleted at the interface, and if higher would cause charge to be accumulated. In the latter case, the transistor is switched on at zero gate bias and a positive bias has to be applied in order to deplete the charges present. However,

the difference $\Phi_G - E_F$ can only be of the order of 1eV and as V_0 can be as large as ±30V it cannot be the only explanation.

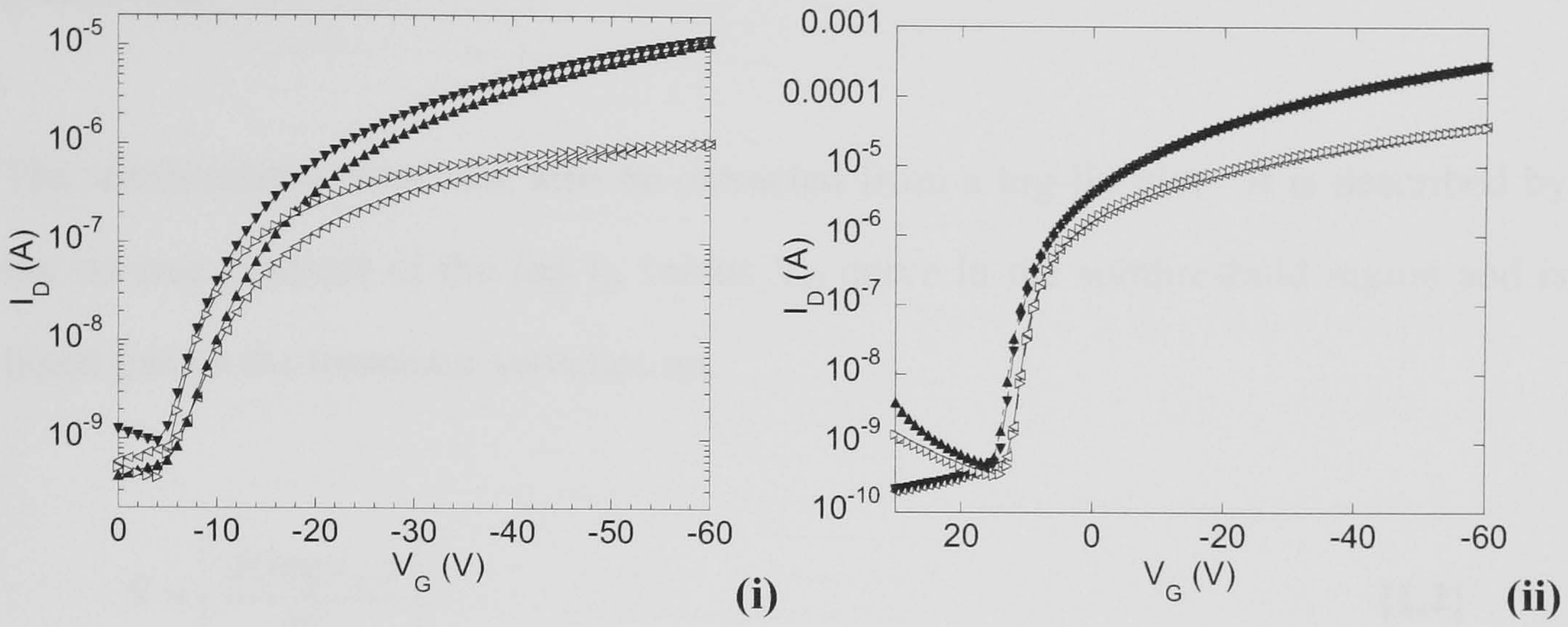


Figure.1.14. Forward and reverse transfer characteristics for (i) a F8T2 transistor and (ii) a P3HT OTS treated transistor with channel dimensions L=10μm and W=1cm. Linear scans (V_D=-5V) and saturated scans (V_D=-60V) are represented by open and filled triangles, respectively, which point in the scan direction. The hysterisis between forward and reverse scans can be clearly identified in (i).

If a negative V_0 is considered, it seems likely that in the presence of trap states accumulated charge is trapped and unable to contribute to the transistor current. A negative gate voltage raises the Fermi level, filling the trap states and enabling charge to be accumulated into transport states. This effect is common in polyfluorene transistors, which can exhibit severe bias stress that is attributed to trapping. On the other hand, polythiophene is particularly susceptible to unintentional doping and often exhibits a positive switch-on voltage in excess of +20V, suggesting significant hole accumulation is present at zero applied bias. Fig.1.14 illustrates both of these effects.

The off-current in a transistor will also be increased if the bulk conductivity is high. This is often due to the presence of impurities. The on/off ratio is useful parameter in

characterising OFETs and is defined as the ratio of current at high gate voltage (the on-current I_{ON}) to the off-current I_{OFF}, and is a means of evaluating the switching performance of the device. For most applications the switching level required is greater than 10^5.

The subthreshold slope can also be extracted from a log-lin plot. It is described by the inverse gradient of the log I_D versus V_G curve in the subthreshold region and is taken just as the transistor switches on.

$$S = \left[\frac{d(\log I_D)}{dV_G} \right]^{-1} \qquad \{1.2\}$$

This is evidence for how sharp the turn on of the transistor is and as small a value as possible is required. In practise S is affected by interface states and traps, which fill and empty as the gate bias is changed, slowing down the accumulation of carriers in the channel and the turn-on of the transistor.

1.2.3. Determining the mobility of polymer field-effect transistors

The mobility of a material can be defined as the magnitude of the drift velocity per unit electric field. There are several experimental techniques that can be used to estimate the mobility of charge in organic materials, such as the time of flight photocurrent technique (TOF), in which the transit time of optically generated carriers across thin films is measured, and derivation from diode and transistor characteristics. Let us concentrate on the definition of 'mobility' in an organic FET. OFETs are usually analysed using the standard inorganic TFT models:

$$I_D = \frac{Z\mu C_i}{L}\left[V_G - V_T\right]V_D \qquad (V_D < (V_G - V_T)) \qquad \{1.3\}$$

$$I_{DSAT} = \frac{Z\mu C_i}{2L}\left[V_G - V_T\right]^2 \qquad (V_D > (V_G - V_T)) \qquad \{1.4\}$$

with the above equations describing the drain current in the linear and saturation regions respectively. μ is the mobility, C_i the insulator capacitance per unit area, V_G the gate voltage, V_T the threshold voltage, and V_D the drain voltage.[13] If the mobility is only weakly dependent on the gate voltage, the derivative of the approximation can be equated to the slope of the transfer characteristics - if taken at a voltage in the linear regime. This is the linear mobility. Similarly, the saturated field-effect mobility can be obtained from the gradient of the square root of the saturated drain current versus the gate voltage. However, it should be borne in mind that these models are derived for inorganic materials and do not take into account the charge transport properties of organic materials, or allow for the experimentally observed charge density and electric field dependence of the carrier mobility.

1.2.4. Gate voltage dependency of the mobility

If the mobility is calculated using the above equations a deviation from a linear fit is often noticeable. This suggests that the mobility is gate voltage dependent and taking the derivative of I_{DSAT} with respect to V_G in {1.4} does indeed find that the mobility increases with gate bias. Though this effect is reduced if contact effects are considered, scanning potentiometry and transmission line analysis (TLM) both confirm the variance.[18,19] There have been several attempts to explain the gate voltage dependence using the multiple trapping and release (MTR) and variable range hopping models (VRH), specifically considering the charge density of the system.

1.2.5. Multiple trapping and release models (MTR)

Consider first the MTR model, which is commonly used in amorphous silicon transistors.[20] A density of localised levels exists near the delocalised transport bands in amorphous silicon that act as traps for charge carriers. These trapped charge carriers must thermally jump (be released) into the delocalised band in order to contribute to the current. The model assumes that most of the charge carriers are trapped in these localised states, with the energy of a trap level E_T defined by the distance from the delocalised transport level. As the trapping and release mechanisms are thermally activated processes, the ensuing 'temperature dependent' mobility exhibits an Arrhenius-like relation to the mobility in the delocalised band.

This model has been extended to organic systems, still assuming that most of the charge carriers are trapped in localised states, with the energy of a trap level defined by the distance to the transport level.[21] It is important to bear in mind that this transport energy is a statistical quantity – describing the energy at which a carrier in a tail state will probably escape to. Below this energy, carriers are trapped in the tail states of the Gaussian DOS and must thermally jump (be released) into a transport state in order to contribute to the current. Thus, it is analogous to the mobility edge in inorganic semiconductors.

The amount of temporarily released charge carriers in a transport level depends on the energy level of the localised trapped states, the temperature and the gate voltage (as V_G determines the interfacial charge density). At low gate biases the majority of the gate induced charge is only in the lower localised levels and the mobility is consequently low (operating in accumulation mode). The Fermi level approaches the transport states on increasing the gate bias, filling more traps and leading to an increase of mobile carriers in transporting states, thus increasing the effective mobility. In the linear regime the accumulation layer has an approximately constant

charge density so the linear regime equation should be valid even if the mobility is dependent on the charge density. However, in the saturation regime the charge density is not constant along the channel and varies from maximum at the source to 0 at pinch-off point. It follows that {1.3} and {1.4} are only valid for a constant mobility, which is independent of charge density – in other words not dependent on the gate bias.

This is often not the case and a gate bias dependence of the mobility can be determined from the transconductance g_m in each regime:

$$g_m^{N} = \left.\frac{\partial I_D}{\partial V_G}\right|_{V_D=const} = \frac{W C_i}{L} \mu_N V_D \qquad \{1.5\}$$

$$g_m^{SAT} = \left.\frac{\partial I_D}{\partial V_G}\right|_{V_D=const} = \frac{W C_i}{L} \mu_{SAT} (V_G - V_0) \qquad \{1.6\}$$

However, Horowitz interpreted the mobility variation of OFETs in the framework of the MTR model and though he found the mobility to be both gate bias and temperature dependent, the magnitude of the trap free mobility obtained was too low to correspond to transport in trap free transport states. If we consider that the boundary between localised and delocalised transport is between 0.1cm^2/Vs to 1cm^2/Vs, and that extended state transport is not expected to occur in amorphous organic films in which the charge carriers are strongly localised, there is controversy as to whether the MTR model can apply.

The general consensus is that delocalised transport could occur for highly ordered molecular films, but is not expected to arise in amorphous polymer films.[22] Regioregular P3HT was used in similar studies by Sirringhaus et al., and as

aforementioned can exhibit mobilities of $0.1 cm^2/Vs$.[23] This is of a similar order to the mobilities realised in polycrystalline OFETs suggesting the existence of extended transport states arising from short-range order. These small microcrystalline domains would be broken by disordered chain conformations and structural or chemical defects resulting in localised trap states below the transport states. As no assumptions are made about the nature of these localised states or the transport mechanism – MTR could be applicable to polaron transport in polycrystalline, conjugated polymers and {1.5} and {1.6} will consequently be used for the high mobility microcrystalline thiophene based polymers in this thesis.[24]

1.2.6. Variable range hopping (VRH)

In this case, the transport is governed by hopping (thermally activated tunnelling of carriers between localised states) rather than activation to a transport level. Most hopping models originate from a Miller-Abrahams jump rate model that was initially proposed to study low temperature hopping between single-phonon mediated shallow impurity states in inorganic materials.[25] It assumes that electron-lattice coupling is weak, and when applied to polymers considers the conjugated segments as analogous to nearly isolated impurity states. The hopping rate ν_{ij} between an occupied site i and a neighbouring unoccupied site j, separated in energy by E_{ij} and by distance R_{ij} is described by:

$$\nu_{ij} = \nu_0 \exp\left(-2\gamma a\left(R_{ij}/a\right)\right)\begin{cases}\exp\left(-E_{ij}/k_B T\right) & E_{ij} > 0 \\ 1 & E_{ij} < 0\end{cases} \qquad \{1.7\}$$

where ν_0 is an appropriate prefactor (related to the hopping attempt frequency), γ describes off-diagonal order effects (and is a measure of the inverse wavefunction decay constant of an energy state), and a is the average lattice constant. Mott

extended this model to include hops over greater distances so that a carrier might hop over a small distance with high activation energy or hop over a long distance with low activation energy.[26] This is the basis of the VRH model and finds the mobility to vary with temperature as:

$$\mu \propto \exp\left[-\left(\frac{T_0}{T}\right)^{1/n+1}\right] \qquad \{1.8\}$$

T_0 is inversely proportional to the density of states at the Fermi level and n is the dimensionality of the system. However, VRH assumes an isotropic wavefunction and does not take into account charge carrier species, though conjugated polymers are often anisotropic and electron interactions between charges are important.[7]

As it has been experimentally shown that the mobility of OFETs is thermally activated and gate bias dependent, a successful model should encompass all of these factors. Vissenberg and Matters used percolation theory to derive the mobility of an OFET based on VRH in an exponential density of localised states. Experimental data for a small molecule (pentacene) and polymer (polythienylene vinylene (PTV)) FETs fitted well and the mobility was observed to be thermally activated with activation energy, E_A. Hopping between localised states is dependent on the energetic distribution and distance between sites. In contrast to Mott's expression for VRH in a constant DOS an Arrhenius-like temperature dependence was found, as the hops are more like the activated jumps we find in MTR due to the exponential DOS. However, a major difference from MTR is that Vissenberg and Matters take into account tunnelling events, and interestingly found the main difference in the mobility between pentacene and PTV to be α, signifying a better electronic wavefunction overlap for the more ordered small molecule film.[27]

Already, the difficulties of finding a definitive model to describe transport in disordered systems are evident. Another point to note is that the temperature ranges of organic materials are limited making it impossible to distinguish precisely between different models. In fact charge transport is unlikely to be a consequence of any single mechanism for all conjugated systems, though as we have seen there are several models that successfully describe specific behavioural aspects. A common factor to the models mentioned so far is that the polaronic nature of charge carriers has been neglected.

1.2.7. Polarons

In conjugated systems, the formation of a polaron results in deformation of the conjugated chain by the addition of charge and the creation of molecular polaronic levels within the energy gap. Brown found a gate dependent mobility and activation energy using the linear transconductance and explained this using polaron hopping.[28] The variation of the activation energy is attributed to disorder and in this case the activation energy is equated to the polaron binding energy.[29] Deep localised states can exist within the energy gap as a result of spatial disorder. As charge is introduced these states will be occupied first so at increasingly negative biases (and charge) the Fermi level would move towards 'typical' polaronic levels and be pinned there. The density of states within the gap is relatively low so charge transport can be approximated as thermally activated from the localised polaronic states at the Fermi level to a larger density of localised transport states.

1.3. Summary

This chapter introduced the concept of conjugated polymers and their use in field effect transistors. The first section explained how their semiconducting properties

arise, with delocalised π-electron systems enabling charge transport via the movement of electron or hole polarons. The theory and characterisation of polymer field-effect transistors is then reviewed. Moving on to the final part of the Chapter, the difficulties of modelling charge transport in such devices is discussed. Disordered systems give rise to localisation of charge, with transport occurring via hopping between charge transport sites. The MTR model used for amorphous silicon has been used successfully to describe the temperature and gate voltage dependence of the mobility in small molecule and polycrystalline FETs, though whether this is truly applicable to organic systems remains uncertain. Transport in disordered amorphous semiconductors is best described by VRH, and a number of models have evolved to take into account problematic aspects of such systems. However, the experimental window available for measuring temperature dependence is limited and the similarity between theories leaves it impossible to determine which is ultimately correct. What seems certain is that a model describing all aspects of charge transport in conjugated polymers still eludes us, and for the present, models should be chosen with respect to the system to be studied.

References

1. P. W. Atkins, *Physical Chemistry*, 5th Edition, Oxford University Press (1994)

2. Josef Loschmidt, an Austrian schoolteacher, published a booklet in 1861 introducing the idea of ring structures for organic compounds that Kekulé dismissed as confusing.

3. M. Vokins, *Nuffield Advanced Science Chemistry Students Book*, 3rd Edition, Longman Group Ltd. (1994)

4. I. H. Campbell and D. L. Smith, *Physics of Organic Electronic Devices*, in Solid State Physics **55,** Academic Press (2001)

5. C. Kittel, *Introduction to Solid State Physics*, 7th Edition, John Wiley & Sons (1996)

6. J. R. Hook and H. E. Hall, *Solid State Physics*, 2nd Edition, John Wiley & Sons (1999)

7. T. H. Richardson, *Functional Organic and Polymeric Materials: Molecular Functionality – Macroscopic Reality*, John Wiley & Sons (2000)

8. H. Bässler, *Phys. Stat. Sol. (b)* **175** 15 (1993)

9. A. Dieckmann, H. Bässler, P. M. Borsenberger, *J Chem. Phys.* **99** 8136 (1993)

10. W. Warta and N. Karl, *Phys. Rev. B* **32** 1172-1182 (1985)

11. With a revelation that all parts of a circuit could be constructed from silicon, Jack Kilby built a flip-flop (bistable multivibrator-memory device) at Texas Instruments in 1958. Robert Noyce of Fairchild Semiconductor was thinking along similar lines and was awarded a patent for a more complex "unitary circuit" in 1961.

12. US patent 1745,175. Oskar Heil was awarded a British patent (439,457) in 1935 for a structure similar to a MOSFET.

13. S. M. Sze, *Physics of Semiconductor Devices*, 2nd Edition, John Wiley & Sons (1981)

14. A. R. Brown, C. P. Jarrett, D. M. de Leeuw, M. Matters, *Synth. Met.* **88** 37-55 (1997)

15. H. Ishii, K. Sugiyama, E. Ito, K. Seki, *Adv. Mater.* **11** 605 (1999)

16. This is not strictly correct as the charge density in the accumulation layer is not uniform as it depends on the distance from the interface, as described by C. Tanase, E. J. Meijer, P. W. M. Blom, D. M. de Leeuw, *Organic Electronics* **4** 33-37 (2003)

17. E. J. Meijer, C. Tanase, P. W. M. Blom, E. van. Veenendaal, B.–H. Huisman, D. M. de Leeuw, T. M. Klapwijk, *Appl. Phys. Lett.* **80** 20 (2002)

18. L. Bürgi, H. Sirringhaus, R.H. Friend, *Appl. Phys. Lett.* **80** 16 (2002)

19. G. Horowitz, *J. Mater. Res.* **19** 7 (2004)

20. P. G. Le Comber, *Phys. Rev. Lett.* **25** 509 (1970)

21. G. Horowitz, P. Lang, M. Mottaghi, H. Aubin, *Adv. Funct. Mater.* **14** 11 (2004)

22. G. Horowitz, *Adv. Mater.* **10** 5 (1998)

23. H. Sirringhaus, N. Tessler, R. H. Friend, *Science* **280** 1741-1744 (1998)

24. H. Sirringhaus, N. Tessler, D. S. Thomas, P. J. Brown, R. H. Friend, in *Advances in Solid State Physics* **39** 101-110, B. Kramer. Ed. (Vieweg, Braunschweig, Germany) (1999)

25. A. Miller and E. Abrahams, *Phys. Rev.* **120** 745 (1960)

26. N. F. Mott and E. A. Davies, *Electronic Processes in non-crystalline materials,* 2nd Edition, Oxford University Press (1979)

27. M. C. J. M. Vissenberg and M. Matters, *Phys. Rev. B* **57** 20 (1998)

28. A. R. Brown, C. P. Jarrett, D. M. de Leeuw, M. Matters, *Syn. Met.* **88** 37 (1997)

29. According to Holstein's theory the activation energy should correspond to half of the polaron energy, as described in **22.**

Chapter 2

Experimental techniques

This Chapter introduces the general experimental techniques used in this thesis. A brief account of the polymers used is presented in the first section, before describing the step by step procedures necessary to fabricate polymer field-effect transistors. Device characterisation and other useful techniques such as Kelvin probe and differential scanning calorimetry are also touched on.

This Chapter focuses on the experimental techniques involved in the fabrication and characterisation of polymer field-effect transistors (PFETs). The first section describes the fabrication of PFETs and the materials used. The experimental techniques used to analyse the material and device properties are discussed in the second section, concentrating on those relevant to transistors. Other specific experimental techniques used in this thesis, such as time of flight, will be dealt with within the relevant Chapters.

2.1. Device fabrication

2.1.1. Fabrication of top-gate and bottom-gate transistors

Transistors were fabricated on both glass and silicon substrates in 'top' and 'bottom' gate configurations. Corning barium borosilicate glass (7059) slides were used as they have a low alkali content (<0.3%), minimising any diffusion of sodium ions into the polymer layer.[1] Fig.2.1 is a schematic for a top-gate FET structure.

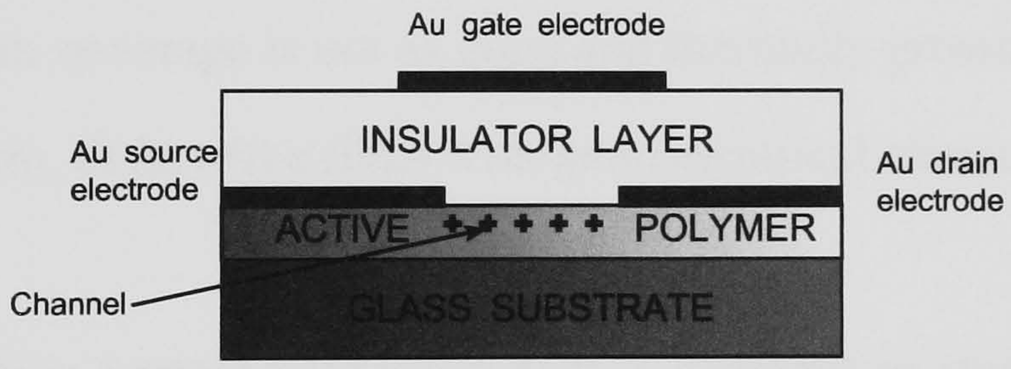


Figure.2.1. Diagram of a top-gate structure organic FET. A glass or flexible plastic substrate can be used to support the semiconducting polymer layer. Source and drain electrodes are then patterned via shadow mask evaporation or printing techniques. An insulator immiscible in the active polymer is then coated before deposition of the final gate electrode.

A top-gate geometry consists of the active polymer layer directly spin-coated onto the substrate, later evaporating the source-drain contacts. The charge which forms

the accumulation layer of a transistor has to be injected from the source or drain electrodes. Gold is generally used as in most cases it provides a good ohmic contact to the semiconducting polymer. The polymeric gate insulator is then spin-coated and finally the gate electrode deposited on top, hence the terminology 'top' gate. The bottom gate construction is simply the reverse. There is more success with the top gate FETs on glass, most likely due to less disruption to the surface of the polymer layers when spin-coating over the electrodes.

However, the bottom gate structure is favoured for silicon substrates, as if the silicon is suitably doped it can act as the gate electrode with a silicon oxide or silicon nitride layer grown on top to function as the gate insulator. The oxide can be grown by thermal oxidation or chemical vapour deposition (CVD). Thermal oxidation involves reacting the silicon substrate with gaseous oxygen (dry oxide) or water vapour (wet oxide) in a furnace at about 1000-1200°C. CVD can be used to grow silicon nitride layers as well and can be done on any type of substrate by combining gaseous silane and ammonia at 700-900°C (SiO_2 is grown by replacing the ammonia with oxygen). Though lower temperatures are required and film growth is faster with CVD, the film coverage is not as good and thermally grown oxide layers should be used for uniform, defect-free films with good electrical characteristics.

In the case of silicon bottom gate transistors, a coplanar or staggered geometry can be used, as illustrated in Fig.2.2. The staggered design is less susceptible to high contact resistance as the effective area of the contact is larger as, unlike coplanar devices, the vertical component of the electric field is applied over the entire contact (assuming there is an overlap of gate and source and drain electrodes) aiding injection.

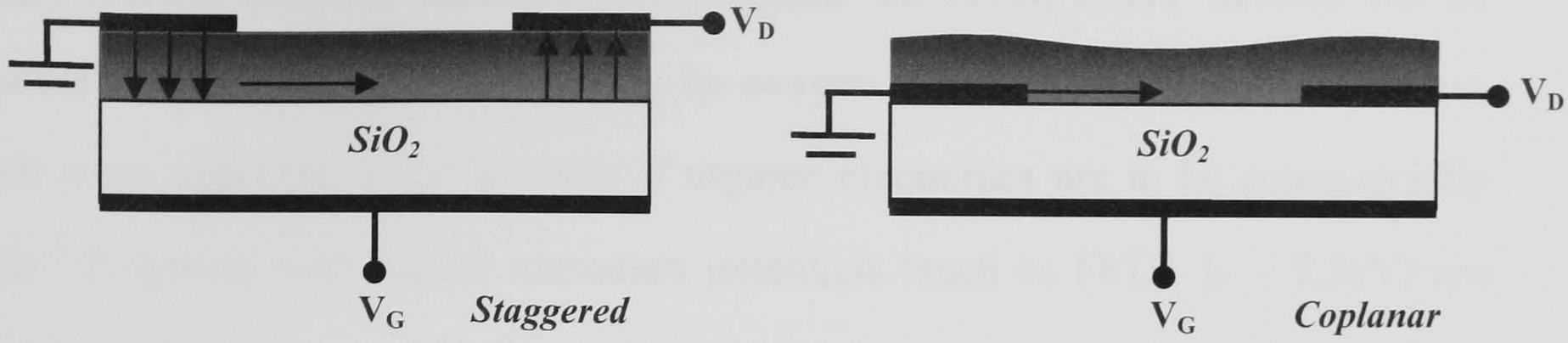


Figure.2.2. Schematic of a staggered and coplanar transistor geometry illustrating the larger effective contact area for the staggered configuration. Adapted from[2]

There is also likely to be less disruption of the polymer film at the interface for staggered devices, as with top gate structures. However, the energetic levels of metal on organic and organic on metal interfaces are not always symmetrical. Evaporating metal contacts can lead to metal atoms diffusing into the polymer layer or chemical interactions at the polymer/metal interface, since the vaporised metal atoms are highly reactive. This can lead to the formation of new energy levels, which has been demonstrated to reduce the hole injection barrier in a Mg/Alq_3 system.[3] An advantage of using the coplanar structure is that it enables more precise channel patterning as photolithographic techniques can be used. Devices prepared on bottom-gate pre-patterned gold source and drain silicon substrates, provided by the Fraunhofer Institute in Dresden, were extensively used this work as they allowed for reliable comparisons to be made.

2.1.2. Materials used in this thesis

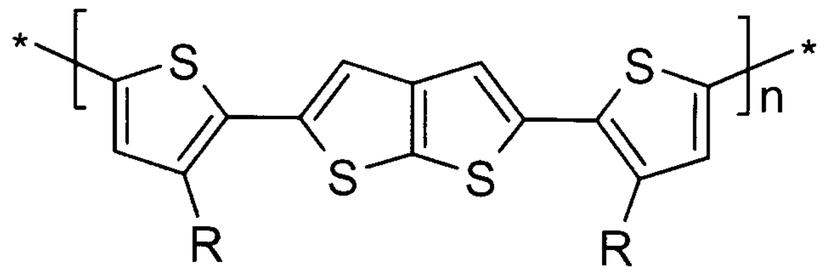
In this work, transistors were fabricated from polyfluorene and polythiophene based materials. Polythiophenes and their use as the active layer of OFETs have been widely studied, especially since regioregular head to tail poly(3-hexyl-thiophene) (P3HT) transistors were found to exhibit mobilities as high as $0.1cm^2/Vs$.[4] These high charge carrier mobilities are thought to derive from the crystalline nature of the films and x-ray diffraction studies confirm that well ordered lamellae with co-

facially stacked polymer backbones are formed. However, P3HT devices can be sensitive to unintentional p-type doping by oxygen if fabricated and operated in air, which is an important issue to solve if organic electronics are to be commercially viable.[5] Polymers with higher ionisation potentials (such as F8T2, I_P ~ 5.5eV) are less susceptible to oxygen doping and relatively air stable. Chapter 1 explained how decreasing the conjugation length of a polymer can increase the ionisation potential (the energy required to remove an electron from the HOMO to infinity). Practically, this could be achieved by increasing the rotational freedom of the backbone, thus reducing π overlap between adjacent thiophene rings, or by introducing a less conjugated unit into the backbone which would inhibit delocalisation.

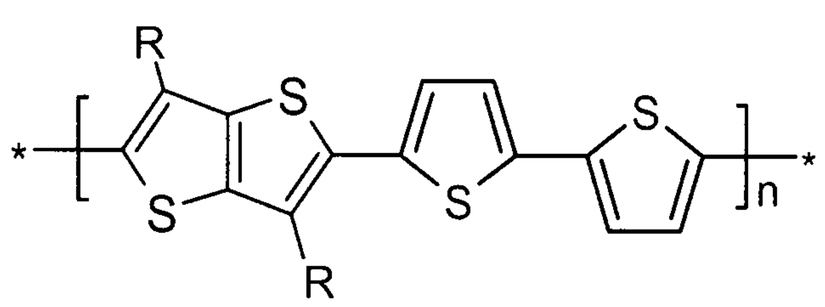
The next three chapters are mainly concerned with transistors fabricated from a novel polythiophene based polymer synthesised by Merck Chemicals Ltd., (poly (2, 5-bis(3alkylthiophen-2-yl)thieno[2, 3-b thiophene) (syn-pBTTT). In this case, the incorporation of an aromatic heterocycle thieno [2, 3-b] thiophene unit into the backbone breaks up the conjugation path whilst resulting in a planar conformation that encourages close π-π interactions. Preliminary wide angle x-ray scattering measurements on spin-coated films of syn-pBTTT reveal ordered lamellae with an intermolecular spacing of 17Å and π-π stacking distance of 3.7Å and an ionisation potential of 5.3eV. X-ray diffraction measurements were carried out by Martin Nielson and Jens Andreasen of Risoe National Laboratory, Denmark and ultraviolet photoelectron spectroscopy AC-2 measurements by Masayoshi Suzuki of Merck, Japan.

The conjugation is broken to a lesser extent in poly (2,5-bis(3-alkylthiophen-2-yl) thieno [3,2-b] thiophene) (ant-pBTTT), also synthesised by Merck Chemicals Ltd. In this case the ionisation potential is decreased to 5.1eV. Similar transport should

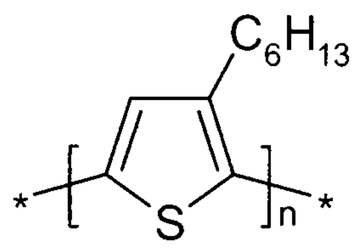
occur as in P3HT for both of these polymers, but enhanced air stability can be expected. [6,7] The chemical structure of these polymers are shown below:



(i)



(ii)

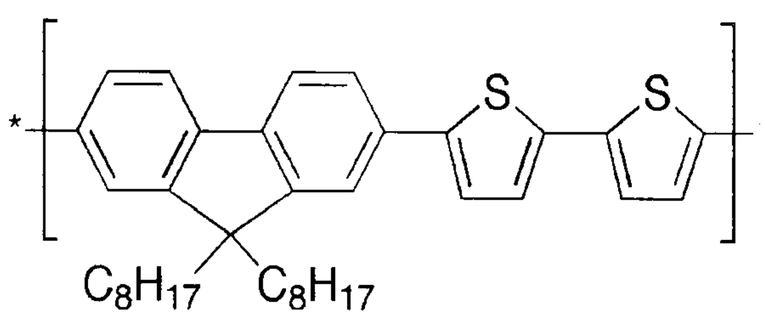


(iii)

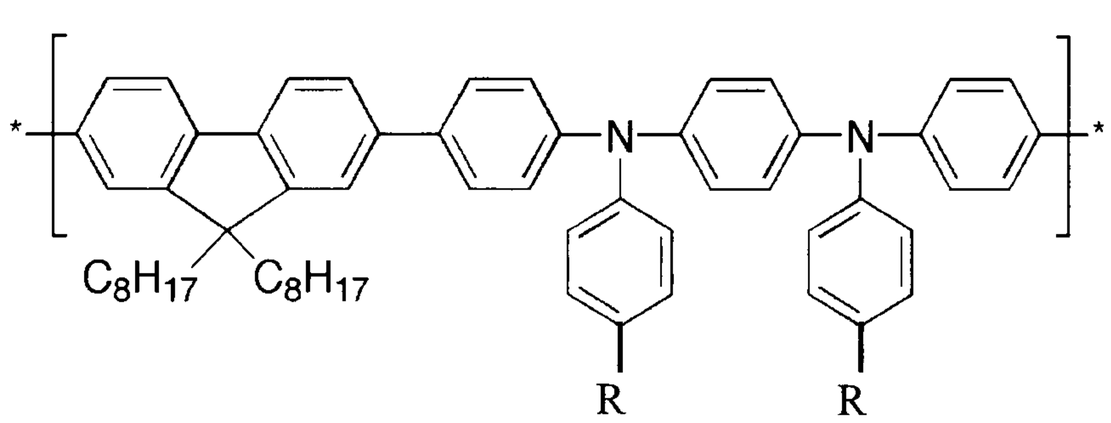
Figure.2.3. Chemical structure of (i) syn-pBTTT ~ poly(2,5-bis(3alkylthiophen-2-yl) thieno[2,3-b thiophene (ii) ant-pBTTT ~ poly(2,5-bis(3alkylthiophen-2-yl) thieno[3,2-b thiophene) [R=$C_{12}H_{25}$] (iii) P3HT ~ poly (3-hexyl) thiophene

Three hole transporting polyfluorene based polymers were also investigated. These materials are copolymers characterised by an alternating arrangement of a 9, 9-dioctylfluorene unit and another aromatic group, allowing their emissive properties to be controlled by varying the alkyl side chains or aryl group. Poly (9, 9-dioctylfluorene-co-bithiophene) (F8T2) is a green-emitting material widely used for PFETs. Mobilities of $10^{-2}cm^2/Vs$ have been realised using alignment, as it exhibits liquid crystalline properties with a nematic glass transition phase at 265°C.[8] Poly (9,9-dioctylfluorene-co-bis-N,N'-(4-butylphenyl)-bis-N,N'-phenyl-1,4-phenylene diamine (PFB) and poly (9,9-dioctylfluorene-co-bis-N,N'-(4-methoxyphenyl)-bis-N,N'-phenyl-1,4-phenylenediamine (PFMO) are both blue-emitting amorphous

materials. Their glass transition temperature can only be estimated from slight changes in heat capacity to be in the range 90 to 140°C as differential scanning calorimetry (DSC) data are ambiguous.[9] Though they exhibit lower mobilities in PFETs, they are known to provide good ohmic contacts to gold and are non-dispersive, which will be further discussed in Chapter 6. Their chemical structures are displayed below:



(i)



(ii)

Figure.2.4. Chemical structure of polyfluorene copolymers (i) F8T2 ~ poly (9,9-dioctylfluorene-co-bithiophene) (ii) PFB ~ poly (9,9-dioctylfluorene-co-bis-N,N'- (4-butylphenyl)-bis-N,N'-phenyl-1,4-phenylenediamine [R=C_4H_9] and if R is substituted by R=OCH_3 PFMO ~ poly (9,9-dioctylfluorene-co-bis-N,N'-(4-methoxyphenyl)-bis-N,N'-phenyl-1,4-phenylenediamine

These materials were provided by the Dow Chemical Company and device preparation and characterisation involving their use was carried out at Imperial College London. Similarly, experiments involving Merck materials were carried out at Merck Chemicals Ltd. in Chilworth.

2.1.3. Substrate Preparation

Cleanliness is of the utmost importance when fabricating OFETs. The transistor characteristics are affected by the ordering of the polymer film at the interface, since the conducting channel only extends up to 5nm into the bulk film.[10,11] It follows that any dust particles or impurities would disrupt the film quality, inhibiting charge transport or even causing shorts in the device. The following cleaning procedure was used for all samples. In the case of pre-patterned substrates two 15-minute acetone washes in an ultrasonic bath (60°C) were initially needed to remove the layer of photoresist.

1. Rinse substrates in ultrasonic bath for 10 minutes in water
2. Dry with nitrogen gun
3. Rinse substrates in ultrasonic bath for 10 minutes in acetone
4. Dry with nitrogen gun
5. Rinse substrates in ultrasonic bath for 10 minutes in isopropanol (IPA)
6. Dry with nitrogen gun
7. Finally ozone treat for 10 minutes to remove any organic residue

HPLC grade solvents (Aldrich) were used for cleaning purposes.

To improve the adhesion of the organic (non-polar) layer, silylating agents such as 1, 1, 1, 3, 3, 3-hexa-methyldisilazane (HMDS) and octyltrichlorosilane (OTS) were used. This makes the surface hydrophobic (less polar) by replacing hydroxide (-OH) groups with methyl ($-CH_3$) groups, and will be expanded upon in the Chapter 5.

2.1.4. Solution Preparation and Spin-Coating

Solutions were prepared under nitrogen in an MBraun MB200B glove box using the subsequent concentrations:

Active layer: 3-7mg polymer/ml of solvent

AnalaR grade (>99.5% purity) dichlorobenzene (DCB) or chloroform was used for syn-pBTTT, ant-pBTTT, and P3HT, and p-xylene for the F8T2, PFB and PFMO. To aid dissolution the solutions were heated on a hotplate, ensuring that the plate temperature was well below the boiling point of the solvent, and were then filtered with a 0.45μm filter. Glass syringes, pipettes and vials, and PTFE filters and lids were used to minimise contamination and individual glassware was used wherever possible to prevent cross-contamination.

A model SCS 6712D spin-coater was used and the spin speed, acceleration and time chosen depended on the thickness required and type of solvent used, as evaporation times vary. Generally it was 3000rpm at 1s acceleration for 45s, which gives 40-60nm thick films. If hydrophobic surface treatments were used, the film was left to stand for a couple of minutes before spinning, as this allowed the edges to dry and form a barrier to encourage the film to stick to the modified surface when spun. In the case of the polymeric insulators, slower spin speeds were used as thicker layers of up to 1μm are required, and the samples consequently baked to remove excess solvent. 1500rpm was the minimum speed used, as below this films were warped and uneven.

2.1.5. Patterning of Contacts

Gold is used to provide a hole-injecting electrode for the p-type polymers as it has a relatively low work function. The material of the gate electrode is not important so gold or aluminium was used. The contacts are usually 40 to 50nm thick for bottom gate coplanar devices, so as not to disrupt the surface of the polymer films. For staggered or top gate geometries the contacts are 80 to 100nm thick. Evaporation is initially carried out slowly (0.1Å/s) to prevent damage and diffusion of metallic atoms into the polymer layer. After 50 or so monolayers, the rate can be increased to 0.5-1Å/s, so as to reduce the time the sample is exposed to the heat. Thin wires were attached to the mask so the polymer film was not directly in contact with it, so as to prevent any surface damage. It is also important when evaporating the contacts to spin-coat or evaporate the appropriate layer as soon as possible to prevent the formation of any surface states.

The main problem experienced was shorting between the source and drain electrodes due to the shadow effect. This can be minimised by:

(i) increasing the distance between the source and the sample, so that the particles arrive at less of an angle.

(ii) making the source as much of a point source as possible, for the same reason as the above. This was achieved by using a 5mm alumina crucible, rather than the standard molybdenum filament or boat.

(iii) ensuring the samples sit flush with the mask.

Microscopic observations showed that the minimum shadow effect for the apparatus set up was 45μm. This seriously limits the feature resolution (channel definition) of the transistors.

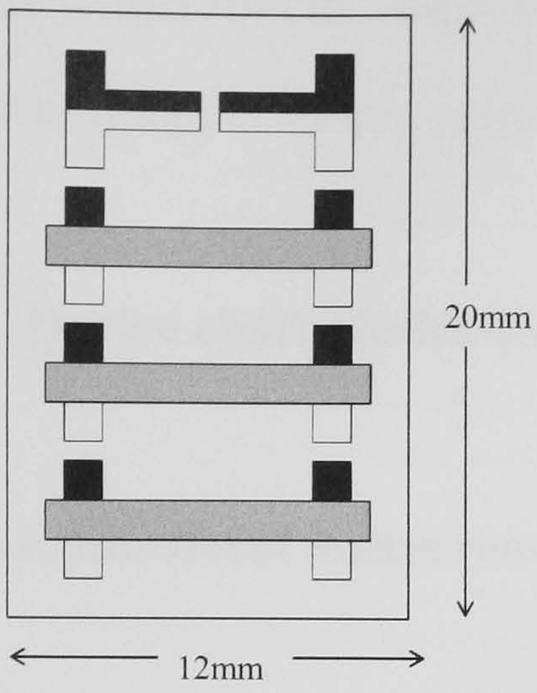


Figure.2.5. Shadow mask design. 8 transistors of channel length 30 or 90μm are evaporated in each block using n^{++}-doped silicon/silicon dioxide or Corning 7059 glass as the substrate. Each pair of source or drain electrodes are represented in black and white. The gate electrode (shaded strip) is evaporated over the channel area (if required) and is not illustrated for the first two transistors to enable visualisation of the source/drain electrode design.

The channel lengths of the shadow mask were 30 and 90μm, and the mask design is depicted above in Fig.2.5. The evaporators at Imperial College were problematic, but use of the custom built thermal Kurt J. Lesker evaporator at Merck enabled definition of 30μm length channels, as it was specially designed with a distance between source and sample of 45cm. However, unless otherwise stated, bottom-gate interdigitated pre-patterned source and drain silicon substrates of configuration pictured in Fig.2.6 were used in the results presented, as it allowed for reliable comparative studies to be undertaken.

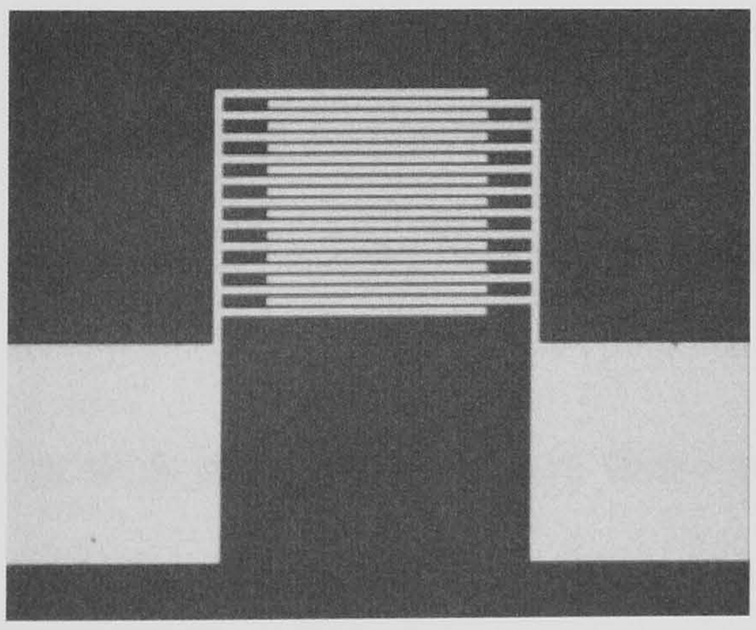


Figure.2.6. Optical micrograph of gold (5nm Cr adhesion layer) interdigitated source-drain patterned transistor structures on n^{++}-Si substrate (gate electrode) with a 230nm thick thermally grown oxide with dimensions L=5μm and W=1cm. The polymer is simply spin-coated/drop cast on top.

These were provided by the Fraunhofer Institute in Dresden, and contained 16 transistors per substrate; 4 each of 2.5, 5, 10 and 20μm channel lengths with a channel width of 1cm. As is standard practise, a 5nm chromium adhesion layer was used to promote adhesion of the gold contacts. The silicon dioxide layer was 230nm

thick with 17nFcm^{-1} capacitance, thermally grown on an n^{++}-doped silicon substrate. The polymer is simply spin-coated or drop cast on top.

2.2. Device characterisation

2.2.1. Electrical measurements

As oxygen and water are known to degrade PFET performance, the majority of measurements and device preparation were carried out under nitrogen in a M200 MBraun glove box. The oxygen and water levels were kept at a ppm level, which allowed intrinsic device properties to be measured. Electrical measurements were made using a Hewlett Packard 4155A or 4145B semiconductor parameter analyser. This enabled the source, drain and gate currents to be measured simultaneously, which is essential for checking the present of leakage currents. To minimise parasitic currents, individual transistors were isolated on the common substrate by carefully scratching boundaries using a wooden toothpick. The silicon dioxide was scratched off a corner of the substrate using a diamond scribe, forming a connection to the gate electrode. Contact was made to the source, drain and gate electrodes using a set of 3-D translational Karl Suss microprobes or by applying conductive silver paste and attaching thin wires to the contacts.

As with inorganic devices, there are several standard techniques used to characterise OFETs. Transfer and output measurements provide the minimum data to extract material and device properties such as the field-effect mobility, turn-on voltage and on/off ratio. Transfer scans involve holding the drain bias at a constant value, usually in the linear or saturation regime, whilst sweeping the gate bias and monitoring the drain-source current. The measurement parameters are chosen over a

range that the transistor is plainly in an on or off state and exhibiting clear linear or saturation behaviour. Typical values are represented in the table below.

		V_{DS} (V)	**V_{GS} Start (V)**	**V_{GS} Stop (V)**	**V_{GS} Step (V)**
Linear Regime	Forward Scan	-5	+10	-60	-1
	Reverse Scan	-5	-60	+10	1
Saturated Regime	Forward Scan	-60	+10	-60	-1
	Reverse Scan	-60	-60	+10	1

Figure.2.7. Typical applied biases used in transfer scans.

Each measurement is performed twice, first 'switching on' from a state in which the device is off towards one in which it is on (forward scan), with the second measurement sweeping the voltage in reverse (reverse scan). This allows any hysteresis due to bias stress effects or trapping to be observed. Output characteristics are measured by sweeping the drain bias from 0 to -60V at constant gate voltages, ranging from 0 to -60V in 10V steps, whilst recording the drain current.

2.2.2. Kelvin probe measurements

A useful technique to characterise surfaces is that of the Kelvin probe. This was particularly useful for characterising thiol formation on gold (See Chapter 5) as it enables changes in the workfunction of a surface to be measured. This method relies on the principle that the Fermi levels of two metals with different workfunction will align if contacted. Consider two metals with workfunction Φ_1 and Φ_2 in isolation with the familiar analogy of a parallel plate capacitor.

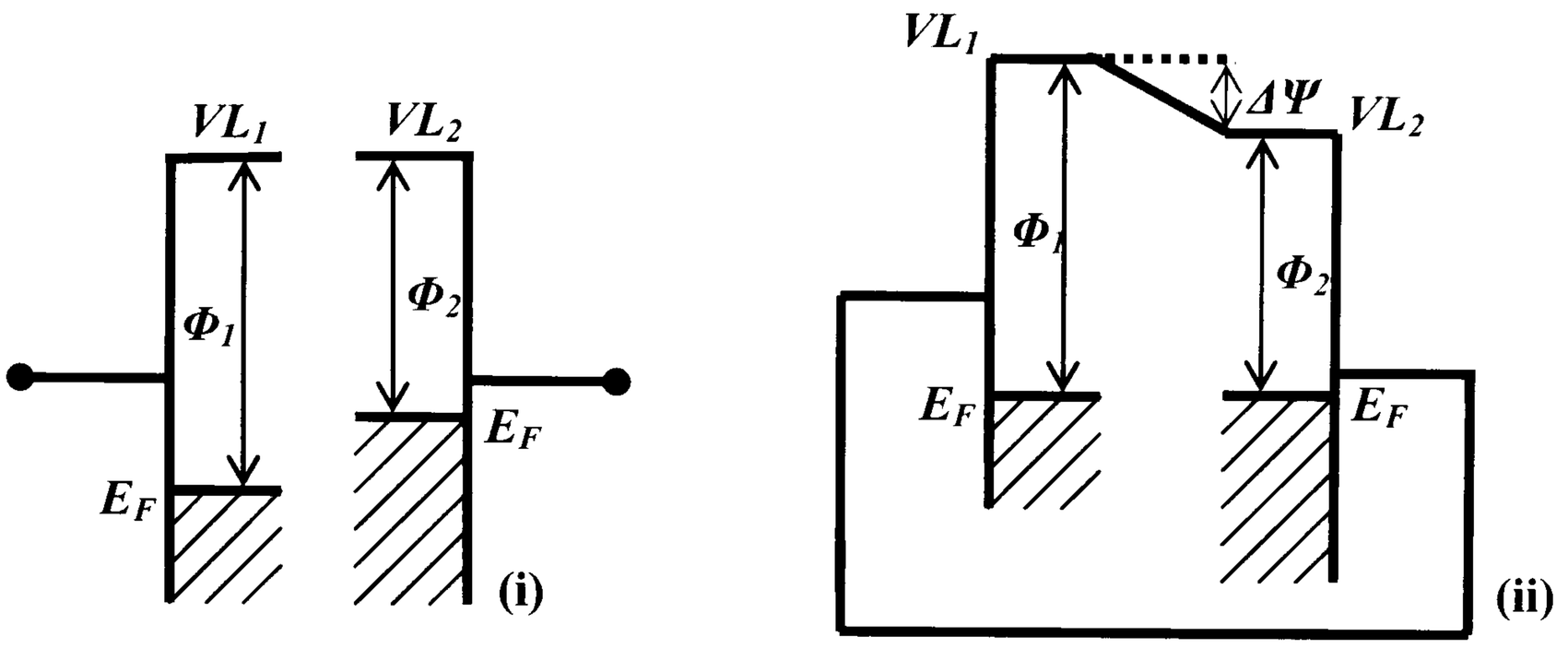


Figure.2.8. Schematic band diagram of a parallel plate capacitor formed from two different metals with workfunctions Φ_1 and Φ_2 in (i) isolation and (ii) short-circuited so that the Fermi levels align and the contact potential difference $\Delta\Psi$ is equivalent to their difference. Adapted from[12].

Both metals share the same vacuum level (VL), but when an electrical connection is made the system is no longer in equilibrium and the Fermi levels align until this is re-established. Thus the potential difference between the 'plates', in other words the contact potential difference, is equivalent to the difference in workfunction as can clearly be seen from the diagram. Kelvin suggested that the contact potential difference could be measured by applying an external voltage to compensate for it so that there is no charge flow between the plates when short circuited - the capacitor is in effect discharged.

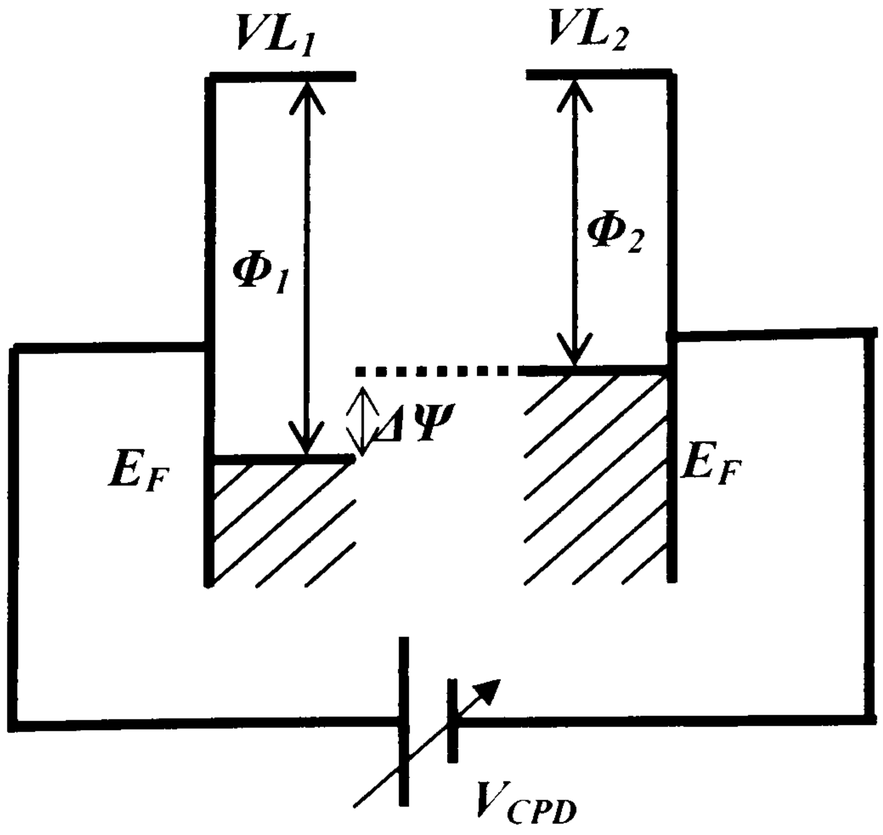


Figure.2.9. Schematic band diagram of the same parallel plate capacitor with a DC voltage (equal to the built-in potential) applied across the plates (V_{CPD}). This is equivalent to the contact potential difference ($\Delta\Psi$). Adapted from[12].

Modern Kelvin probes use a periodically vibrating plate, which is brought in close proximity to the sample surface. The time varying capacitance induces an AC current within the circuit which would be annulled if the capacitor was discharged.

The probe and supplementary electronics used in these measurements were purchased from Besocke Delta Phi GmbH in Jülich, Germany. The probe consisted of a 2.5mm diameter gold mesh circle attached to an electrically driven piezoelement. The probe was vibrated at a frequency of 170Hz and 0.5mm amplitude about 1mm above the surface to be measured. This distance could be varied with micrometer precision, as the sample is mounted on a 3-D translational stage. A lock-in amplifier with a high gain current voltage preamplifier was used to detect the AC current at a resonance frequency. The signal could be compensated for by applying a DC bias voltage that corresponds to the V_{CPD}.

It should be clarified that the Kelvin probe method is a relative rather than absolute method. Changes of workfunction can be measured with good precision if the workfunction of the probe is stable, but to translate data to more absolute values the actual workfunction of the probe has to be precisely known. Workfunctions for atomically flat or very clean metallic surfaces in ultra-high vacuum (UHV) systems are well characterised, but the workfunction of the same metal in a gas ambient may be modified due to possible chemical reactions and adsorption of gaseous molecules at the surface.[3] All Kelvin probe measurements were performed inside a nitrogen-filled dry glove box in order to remove any possible effects from oxygen or water. Still, the effects of nitrogen adsorption onto the surface may be important and it has previously been reported that the workfunction of gold can be significantly reduced from its UHV value of 5.1-5.2eV when it is placed in air or nitrogen.[13]

Gold is relatively inert material and it can be assumed that its workfunction remains stable in a constant environment. The workfunction of freshly cleaved highly orientated pyrolitic graphite (HOPG) is known to be reasonably independent of ambient atmosphere and equal to 4.5eV, and was consequently used as a reference sample to base absolute workfunctions on. In fact, based on the expected workfunction of HOPG, the probe workfunction was estimated to be 4.5-4.6 eV, significantly lower than the tabulated value for gold of 5.1-5.2 eV. This calibration work was undertaken by Dmytro Poplavskyy.[12] The typical accuracy of a single reading of the V_{CPD} was 10 mV. Measurements could not be taken directly from the transistor substrates as the areas of gold were too small, but off cuts with larger gold areas were cleaned and prepared alongside the transistor substrates for use. Values were recorded for three different positions on the sample and the average taken.

2.2.3. Contact angle measurements

The contact angle is a quantative measure of the wetting of a solid by a liquid. It is defined geometrically as the angle formed by a liquid at the three phase boundary where a liquid, gas and solid intersect. Low values of contact angle indicate that the liquid spreads well, while high values indicate less complete wetting. So, an ideal hydrophyllic liquid on an ideal hydrophyllic surface would exhibit a contact angle of 0°, and accordingly an angle of 180° would be expected for an ideal hydrophobic substrate. This is always observed to be less in practise. As a general rule, if the angle is less than 90° the liquid is said to wet the solid and if greater it is said to be non-wetting.

Contact angle measurements were performed using a Kruss Drop Shape Analysis System, DSA 10. 40µl of HPLC grade water was dropped onto the substrate using a µl pipette and the contact angle extracted from the resulting droplet shape by the relevant software. It was not possible to measure a contact angle for water on an

ozone cleaned surface, indicating complete wetting. This was clearly not the case after surface treatments and typical values for HMDS prepared substrates were between 90° and 95°, with OTS and ODTS surfaces exhibiting angles of 105° and 110°, respectively. Measurements were carried out on at least three different areas and an average taken. Errors were found to be well within ±2°, and this range could be reduced to ±0.5° for the trichlorosilanes with optimised surface preparation.

2.2.4. Annealing and differential scanning calorimetry

Differential scanning calorimetry (DSC) can be used to study thermal transitions in conjugated polymers. A few milligrams of the solid material are sealed into an aluminium pan, and placed along with a reference pan in the adiabatic enclosure of the TA Instruments DSCQ1000 differential scanning calorimeter. The pans are heated and cooled in a cycle with a fixed temperature rate, and the change in enthalpy is measured as a function of temperature by monitoring the heat flow of the sample pan relative to the reference. The crystalline or nematic transitions of the material can be identified by the points at which the heat is absorbed, appearing as endothermic features as they require latent heat. Exothermic features, such as the recrystallisation temperature, are apparent on cooling. Annealing the sample on a hotplate or Linkam at the required temperature before 'quenching' or cooling slowly enable different structural phases of the material to be investigated.

2.2.5. Thickness profiling

A Dektak^3 surface profiler was used to perform thickness measurements on the polymer films. A straight line was scratched into the polymer film using a scalpel and the surface scanned in the range so that the scratch was midway from the start and end of the scan. A cross-section of the profile was displayed from which the depth of the scratch (thickness of polymer) could be computed. An indication of the

surface roughness could also be observed. The thickness was measured at three points on the samples and an average value taken.

References

1. D. B. A. Rep, A. F. Morpurgo, W. G. Sloof, T. M. Klapwijk, *JAppl. Phys.* **93** 4 (2003)

2. R. A. Street A. Salleo, *Appl. Phys. Ltt* . **81** 15 (2002)

3. H. Ishii, K. Sugiyama, E. Ito, and K. Seki, *Adv. Mer.* **11** 8 (1999)

4. H. Sirringhaus, N. Tessler, R. H. Friend, *Sience* **280** 1741-1744 (1998)

5. M. S. A. Abdou, F. P. Orfino, Z. W. Xie, M. J. Deen, S. Holdcroft, *Adv. Mer.* **6** 11 (1994)

6. M. Heeney, C. Bailey, K. Genevicius, M. Shkunov, D. Sparrowe, S. Tierney, I. McCulloch, *JAm. Chem. Sc.* **127** 1078-1079 (2005)

7. I. McCulloch et al., To be published in *Nture M terials* (2006)

8. H. Sirringhaus, R. J. Wilson, R. H. Friend, M. Inbasekaran, W. Wu, E. P. Woo, M. Grell, and D. D. C. Bradley, Appl. Phys. Lett. **77** 3 (2000)

9. M. Redecker, D. D. C. Bradley, M. Inbasekaran, W. W. Wu and E. P. Woo, *Adv. M.* **11**, 241-246 (1999)

10. G. Horowitz, *JMer. R es.* **19** 7 (2004)

11. C. Tanase, E. J. Meijer, P. W. Blom, D. M. de Leeuw, *Organic Electronics* **4** 33-37 (2003)

12. D. Poplavskyy, *PhThe sis* (2003)

13. W. N. Hansen and K. B. Johnson, *Srf. Si.* **316** 373-382 (1994)

Chapter 3

Ambient stability of thiophene-based polymer field-effect transistors

This Chapter discusses the problem of ambient stability in polythiophene derived field-effect transistors. These materials are susceptible to forming charge transfer complexes via redox reactions with molecular ambient species. This is dependent on the ionisation potential of the polymer and as a guideline, materials with an $I_P > 5eV$ will be less vulnerable to oxidation. The dependence of operational stability on environmental humidity was also systematically studied. Operation in dry air results in very stable device characteristics. A high concentration of ambient water degrades device characteristics more severely than oxygen alone. This can be attributed to a separate mechanism, by which the polar water molecules diffuse into the film increasing the off-currents and switch-on voltage, but decreasing the on-currents. Higher regioregular films (i.e. more crystalline) are more susceptible to this degradation due to an increased concentration of grain boundaries. Encapsulation using hydrophobic fluorinated insulators was found to significantly prolong device lifetimes and is necessary for the fabrication of high-performance stable polymer field-effect transistors.

Chapter 3 Ambient stability of thiophene-based polymer field-effect transistors

There are several problems to overcome before organic electronics can become commercially viable. Unlikely to compete with inorganic semiconductors in conventional devices requiring high mobilities and switching speeds, the most promising aspect of polymer electronics is their ease of processing and the eventual realisation of all-organic printable integrated circuits. Such reel-to-reel processing or printing techniques would provide an economical means of mass producing low-cost electronics for 'low' performance applications, such as RF-ID tags and flexible displays, filling a niche in the silicon dominated semiconductor market. However, a major difficulty to overcome is that these materials are susceptible to degradation in ambient conditions. Processing could be carried out in inert environments, employing encapsulation techniques to prolong device lifetimes, but an understanding of the mechanisms behind air instability is nonetheless vital to finding the optimum solution.

The ionisation potential of most conjugated polymers lies in the range of the oxidation potential of oxygen (~5.1eV), implying that charge transfer can take place.[1] This redox charge transfer reaction acts as a p-type doping mechanism and results in higher transistor off-currents, which reduces the current modulation and consequently the performance of the transistor. F8T2 is commonly used as a material in PFETs and is known to be relatively air stable as it has a relatively high ionisation potential (I_P) of 5.52eV.[2] However, this high I_P can lead to hole injection problems from the gold or PEDOT: PSS electrodes ($\Phi_{Au/PEDOT:\ PSS}$ ~ 5.1/5.2eV),[3] inhibiting device performance. Field-effect mobilities of up to $10^{-2}cm^2/Vs$ (2-3 orders of magnitude higher than the unaligned material) have been obtained using alignment techniques, but temperatures in excess of 265°C are required to reach the nematic phase.[4] P3HT is a more promising solution-processible material, exhibiting high field-effect mobilities of up to $0.1cm^2/Vs$, as a result of its microcrystalline structure.[5] The ionisation potential of P3HT is lower than F8T2 at ~ 5.0eV, making

it easier to form an Ohmic contact, but more susceptible to doping in ambient conditions.[6]

A high performance, air stable and solution-processible material is still elusive. As greater delocalisation along the conjugated polymer backbone reduces the ionisation potential, it follows that breaking the conjugation of the backbone should lead to a higher I_P. This was the reasoning behind the development of syn-pBTTT, a polythiophene derivative in which conjugation is broken along the backbone by using cross-conjugated bi-thiophene units (Fig.2.3 (i)). This results in extension of the π-conjugation over only four thiophene units.[7] Fusing the thiophene units in a fully conjugated configuration (ant-pBTTT) results in a lower ionisation potential than syn-pBTTT, though the high mobility associated with regioregular P3HT is still mantained.[8] A comparison of the ambient stability of the aforementioned materials should provide an indication of the effect of the ionisation potential, as all these materials are polymers based on thiophene aromatic rings.

Crystalline packing is known to inhibit the diffusion of ambient species into an organic film.[9] If the regioregularity (RR) of P3HT is considered, a higher RR sample should have increased crystallinity if compared to a similarly fabricated batch of synthesis route and molecular weight. This also has the effect of decreasing the I_P, as increased crystallinity should lead to improved molecular order and increased conjugation lengths. The effect of humidity on the system will also be discussed, as preliminary results indicated that the presence of water has a greater effect on device performance than oxygen, if measured in the dark. Systematic studies of varying humidity will therefore also be presented before suggesting possible degradation mechanisms for the behaviour observed.

3.1. The effect of regioregularity on the transistor characteristics

Regioregular poly (3-hexylthiophene) (RR P3HT) films self-organise to adopt nanocrystalline but highly ordered anisotropic lamellae structures in which the polymer chains lie in the substrate plane, with the thiophene rings orientated perpendicularly. These lamellae can pack closely together, though these charge transporting planes are separated by the long insulating alkyl chains (ranging between 1.2 - 3.0nm), which are attached at right angles to the backbone to aid solubility. As the accumulation width of the transistor channel is up to 5nm, charge transport is dominated by a single lamella plane at the interface, and this two-dimensional molecular order enhances the efficiency of in-plane transport leading to higher mobilities.[10]

The device characteristics of a microcrystalline polymer such as P3HT vary significantly with batches of different molecular weight and regioregularity. As with all polymer synthesis, a range of chain lengths would be produced and the average molecular weight estimates the size of a typical polymer chain. If the molecular weight is increased, the mobility should be improved as the average chain length could be longer and fewer grain boundaries would exist. However, this is not always the case as the conjugation length is typically ~ 8 repeat units so is not necessarily dependent on the molecular weight. Zen et al. attribute this mobility increase to a more planar backbone configuration.[11]

This work is initially concerned with the effect of regioregularity on transistor characteristics. Regioregularity (RR) is defined as the percentage of head-to-tail coupled thiophene units. Other types of coupling (head-to head or tail-to-tail) induce steric hindrance along the backbone and reduce the planarity of the molecule. Thus RR can give an indication of the degree of crystallinity and molecular order in the

film. A higher RR material would signify better molecular order, which acts to enhance charge transport and consequently the mobility. To avoid any other discrepancies in the reasoning, both P3HT batches were synthesised by the same route and had similar molecular weights of approximately 50,000gmol^{-1}.

A reduction in the ionisation potential would also be expected due to increased crystallinity, as this leads, on average, to better packing and longer conjugation lengths. This could also further improve device performance as may act to improve the two-dimensional delocalisation of charges in the transport plane and reduce the barrier to hole injection at the electrode/polymer interface. Ultraviolet photoelectron spectroscopy (UPS) comparative measurements of the ionisation potential for 97.5% RR P3HT estimated it to be 4.8eV, and 5.08eV for a 90% RR batch, thus illustrating that the I_P can range by over 0.3eV with a RR difference of just 10%. UPS measurements were carried out by Masayoshi Suzuki of Merck, Japan.

Fig.3.1 and 3.2 show a comparison of the transfer characteristics for both polymers measured under nitrogen, in a graphical and tabular format, respectively.

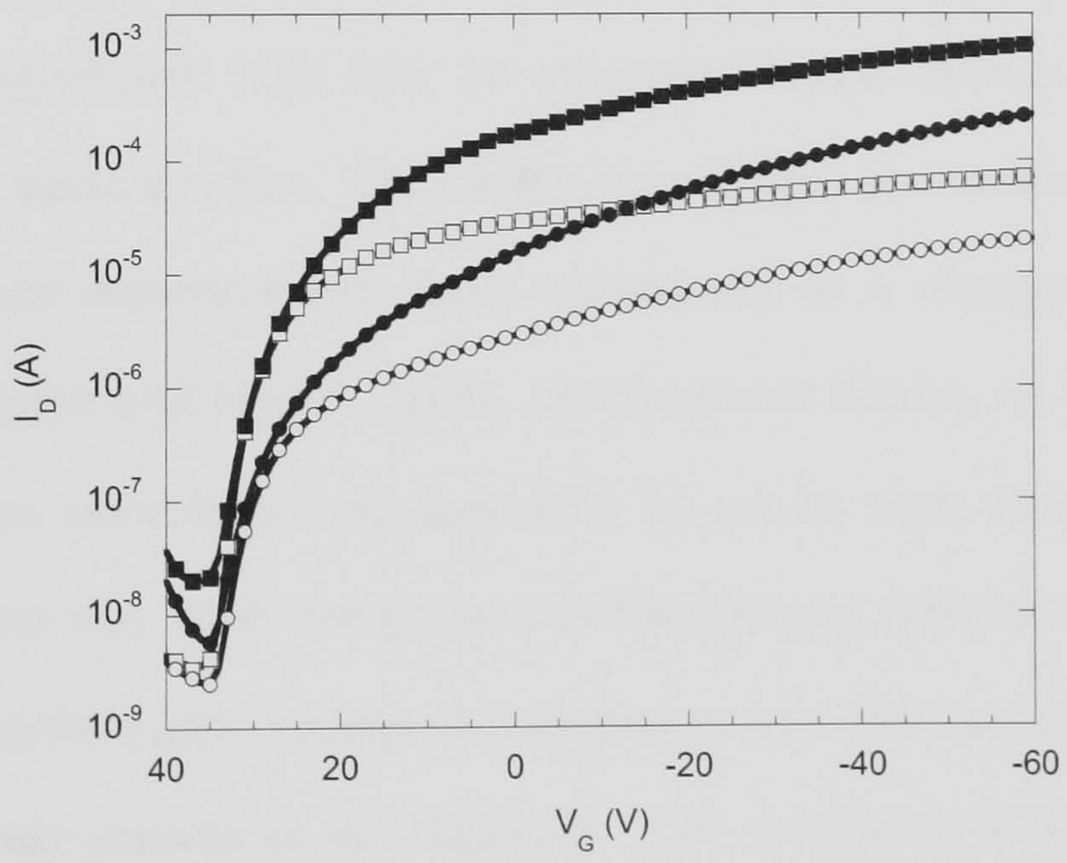


Figure.3.1. Linear (open shapes) and saturated (filled shapes) transfer scans for 90% RR (circles) and 97.5% RR (squares) P3HT transistors. The channel length is 10μm and the channel width is 1cm.

Regioregularity (RR)	Measurement Regime	Mobility (cm^2/Vs)	V_0 (V)	I_{ON} (mA)	I_{OFF} (nA)
90% RR	**Linear**	0.0016	+35.0	0.020	2.42
	Saturated	0.0132	+35.0	0.071	3.25
97.5% RR	**Linear**	0.0039	+35.0	0.235	5.06
	Saturated	0.0251	+35.2	1.056	19.1

Figure.3.2.Table comparing the transistor properties of 90% and 97.5% RR P3HT.

The silica interface of all the transistors was treated with octyltrichlorosilane (OTS) to passivate hydroxyl groups and improve the molecular order of the polythiophene. Further discussion of this can be found in Chapter 5. Results were consistent over all measured transistors, noting that all devices used for direct comparison were prepared side by side, the only variable being the batch of polymer used.

The ionisation potential of the 97.5% RR polymer is closer to that of gold, but both polymers should provide a good Ohmic contact to the gold source and drain electrodes. In agreement with this, no injection-limited characteristics are evident from the output characteristics. The switch-on voltages are similar at +35V. Though all fabrication and measurements were carried out in a nitrogen atmosphere with typically O_2 < 2ppm and H_2O < 2ppm, unintentional doping or impurities left over from synthesis are present in both materials, as can be seen from the large positive V_0. This indicates that holes are present in the channel without the application of a gate bias, as a positive gate voltage is required to turn the transistor off (i.e. deplete the charges already present in the channel). The similarity of V_0 for both polymer batches suggests that any bulk traps, interface states, impurities and/or dopants present are of a similar magnitude. The off-currents are higher for the 97.5% batch,

doubled for the linear regime and increased by 6 times for the saturated transfer characteristics. This indicates that there is an increased level of impurities in the 97.5% RR batch, though these are of a nA-scale and not enough to solely account for the dramatic increase in the on-currents.

The 97.5% RR sample shows mobilities approximately double that of the 90% RR batch. The on-currents are 12 and 15 times higher in the linear and saturated regimes, respectively. Higher regioregularity certainly seems to improve the charge transport and consequently the mobility of P3HT transistors - but what effect will this have on the ambient stability of the transistor?

3.2. Ambient stability of P3HT transistors

This section discusses the ambient stability of polythiophene transistors. The components of ambient atmosphere consist mainly of nitrogen, oxygen and water vapour. On exposure to ambient, these gaseous species could diffuse into the polymer matrix and oxidise the material via charge transfer reactions. More inert gases such as nitrogen and argon are known not to degrade device performance, so measurements of 'pristine' polymer systems are usually carried out in such atmospheres or under vacuum. Most of the measurements in this thesis were carried out in a nitrogen filled glove box where the levels of water and oxygen were kept below 2ppm as it is important to know how the device acts in a stable environment. Such transistors were found to have a shelf life of over two years with negligible degradation to device performance. In this Chapter, device testing was also carried out in a controlled ambient environment, though (unless otherwise stated) all samples were initially prepared and tested under nitrogen before exposure to ambient conditions, as a control.

Oxygen and water are the more reactive species present in the atmosphere and both molecules are known to cause degradation. The majority of work done to date has been concerned with the effect of oxygen. It is widely accepted that molecular oxygen forms a reversible charge transfer complex with P3HT.[9] A charge transfer complex (CTC) is formed via the association of a molecule with low ionisation potential with one of high electron affinity. The degree of charge transfer and magnitude of the equilibrium constant for complex formation is supposed to be a function of ionisation potential and morphology. Abdou et al. suggested that this charge transfer complex was responsible for generating excess charge carriers in polythiophene on exposure to air. The exact nature of the interaction between the species was not specified, though it was firmly established that charge withdrawal occurred from the delocalised π-electron system of P3HT. [9] It is also known that these polymers are especially susceptible to degradation in the presence of oxygen and light. The dominant reaction is purported to be photosensitisation of singlet oxygen, which could be generated via dissociation of an excited CTC by irradiation.

Abdou et al. investigated P3HT transistor characteristics under varying oxygen pressures. The presence of oxygen caused a loss of saturation character in the output characteristics.[9] This effect was completely reversed on the removal of oxygen. Meijer et al. carried out a systematic study in which a shielded (to minimise effects from parasitic currents) transistor structure was measured at different oxygen pressures as compared to vacuum.[12] An extra contribution to the current was clearly evident as a 'second shoulder' in the transfer characteristics at higher oxygen levels and was attributed to transport in the bulk becoming more dominant than transport in the channel, as the concentration of oxygen-induced dopants in the bulk film increased. However, measurements were carried out in the dark, suggesting that photoinduced oxygen doping is not the entire story. They also observed a separate effect of a shift in the V_0 which was attributed to interfacial charging at the

semiconductor/insulator interface, though the origin and nature of the charges was not specified.

3.3. The effect of humidity on P3HT transistors

Thin films of polythiophene are semicrystalline, as compared to amorphous films in which molecular packing is looser. A more crystalline film hinders diffusion of molecular species into the bulk, though there is evidence to suggest that water can diffuse at grain boundaries to reach the polymer/dielectric interface. Thus, polymers possessing low ionisation potentials and with an amorphous nature (to allow easier diffusion) are likely to be most susceptible to CTC formation with molecular oxygen or water. The ionisation potential of the 97.5% RR P3HT is reduced with respect to the 90% RR batch and is estimated to be 4.8eV rather than 5.08eV. This should result in a higher susceptibility to doping with ambient species for the higher regioregularity batch.

The molecular weight of both polythiophene batches is approximately the same at 50,000gmol^{-1}, the main difference being the degree of regioregularity. The stability in air could be dependent on the crystallinity of the polymer film as well as the ionisation potential. The morphology of the 97.5% RR polymer should have better packing than the 90% RR batch, indicating that the latter should be more susceptible to oxygen doping if diffusion morphology is the main issue. Improved stability with the more regioregular batch could then be attributed to closely-packed molecular ordering and worsened stability could indicate increased susceptibility to reactive species as the 97.5% RR polymer is easier to oxidise. However, increased crystallinity may result in a greater proportion of grain boundaries within the film, enabling easier diffusion of ambient molecular species these points. X-ray

diffraction studies are needed to verify this as this could determine the size of the crystallites.

Routine measurements occasionally demonstrated an unexplainable variation in stability for samples fabricated from the same polymer batch. This was eventually attributed to changing levels of moisture in the air, varying with respect to the weather conditions outside!

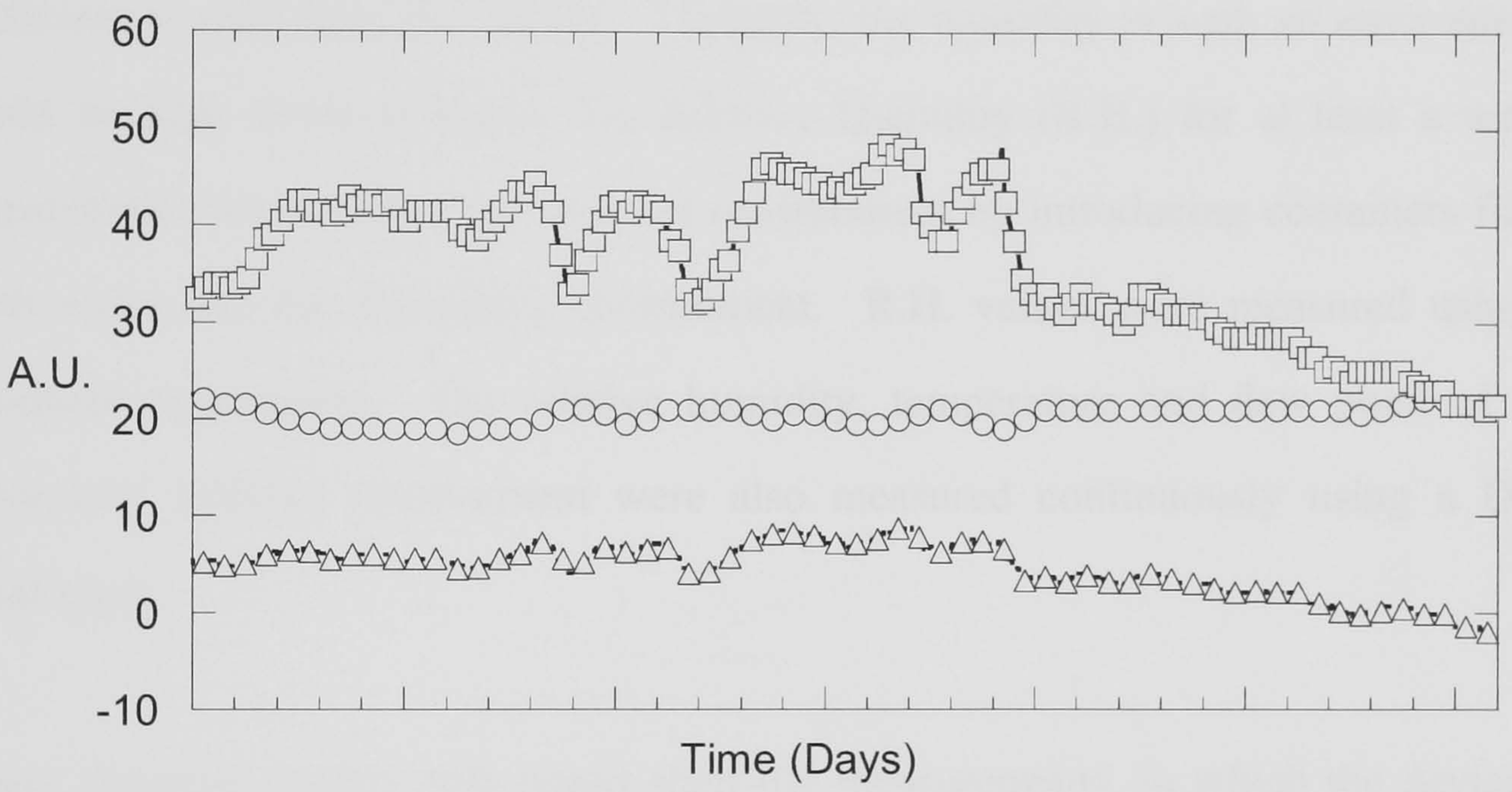


Figure.3.3. This graph shows the changes in the laboratory environment over a period of ten days in January. The y-axis represents the relative humidity (%) by open squares, the temperature (°C) by open circles and the dew point of water (°C) by the open triangles.

Fig.3.3 shows the differences in the temperature, relative humidity and dew point in the laboratory over a period of just ten days in January. The temperature remains fairly constant at 20°C, but humidity values vary by as much as 30% over this short period. Stability measurements were thus carried out in controlled dry and wet atmospheres, all in the presence of oxygen, in order to isolate the effect water has on the system.

3.3.1. Experimental techniques

Measurements in air were carried out in the dark in an enclosed metal box. Initially a climate chamber was used, and though this allowed the temperature and humidity to be controlled, the vibrations from the cooling pump caused the probes to move when continuous measurements were taken. Using a dehydrated 3nm alumina zeolite molecular sieve in a sealed box enabled continuous measurements to be carried out in dry air. If hydrated, heating in an oven at 100°C for an hour was sufficient to dehydrate the zeolite. Typically, the humidity in such an environment could be kept stable at below 5% Relative Humidity (R.H.) for at least a week. Experiments were carried out in a wet environment by introducing containers filled with water into the measuring environment. R.H. values were measured using a handheld hygrometer. The relative humidity, temperature and dew point of the laboratory ambient environment were also measured continuously using a USB datalogger.

Many literature studies only report shelf-life measurements, in which the device is stored in ambient for a specified period of time before measuring. This provides no indication of the operational stability, which is of interest in this work. The HP 4145B semiconductor parameter analyser was set to scan the sample continuously at set time intervals. V_G was typically scanned +40V and -60V at V_D=-5V or -60V. At least 20 minutes was left between scans to ensure that the device had recovered, as the bias stress of continuous operation can also affect the characteristics. After 6 hours the scan was changed to measure hourly, and then to measure twice daily if the transistor was still operational after 3 days. Each set of samples was subjected to the same electrical stress. Similar continuous measurements under nitrogen showed no noticeable change, so the variation in device characteristics can definitely be attributed to other ambient species.

3.3.2. Stability of 90% RR P3HT transistors in low environmental humidity

Let us first consider the 90% RR sample. Fig.3.4 demonstrates how the transfer characteristics evolve over 7 hours in 5% relative humidity.

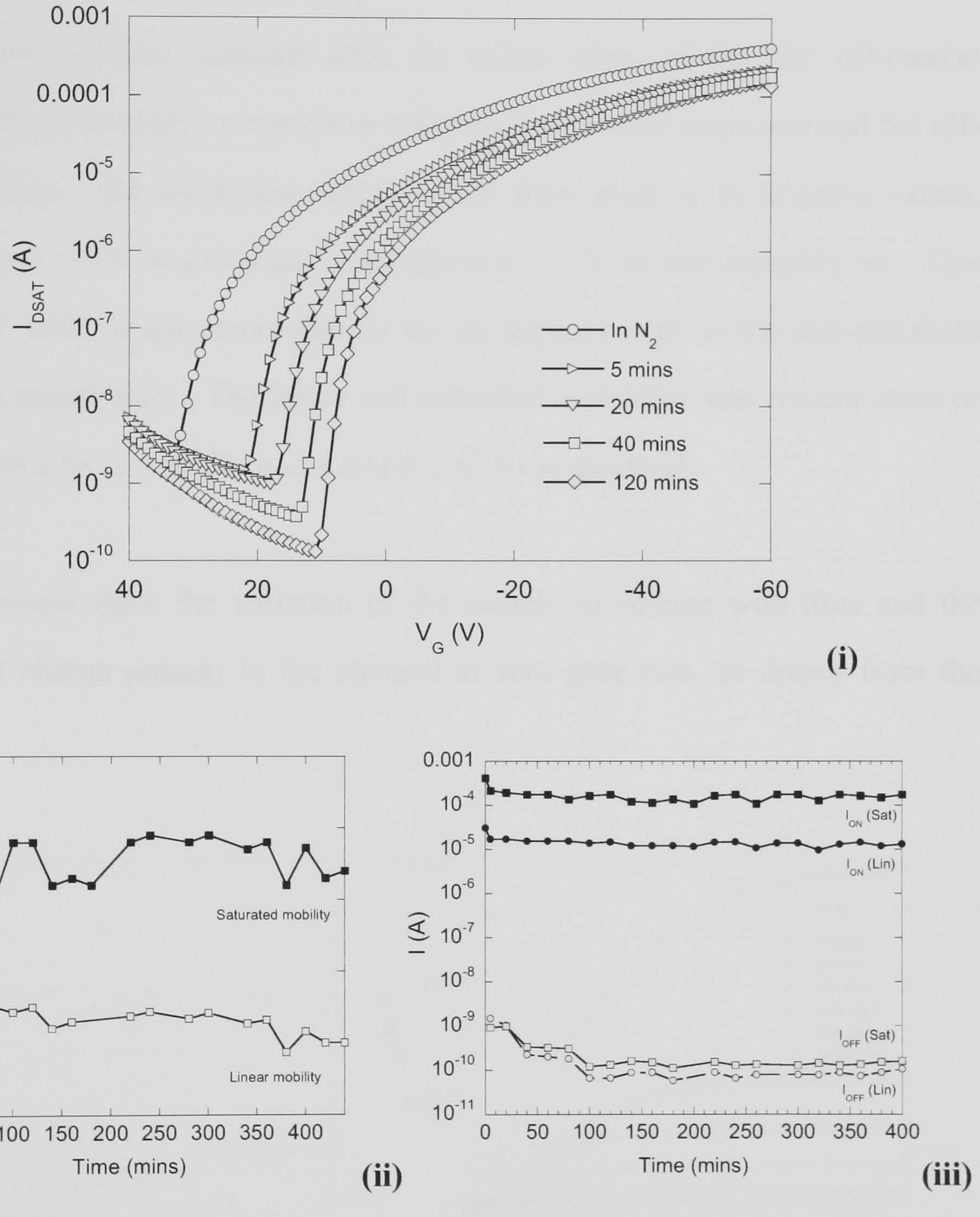
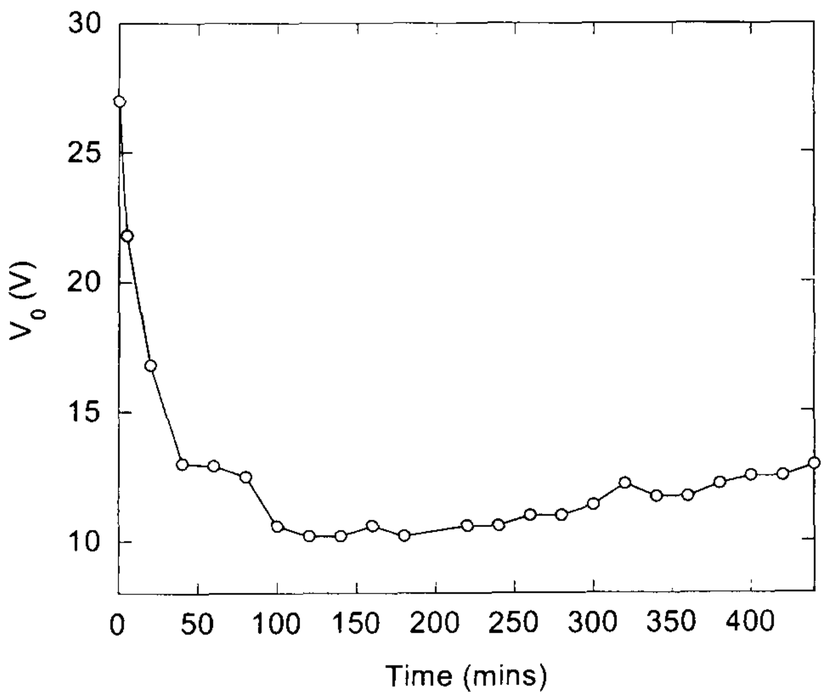


Figure.3.4. (i) Saturated transfer characteristics for the 90% RR P3HT OTS treated transistor measured in low humidity (<5%) air for 2 hours after exposure. The channel length is 10μm and the channel width is 1cm. The evolution of the linear and saturated mobility and associated on and off-currents with time is illustrated in (ii) and (iii), respectively, over a period of 7 hours.

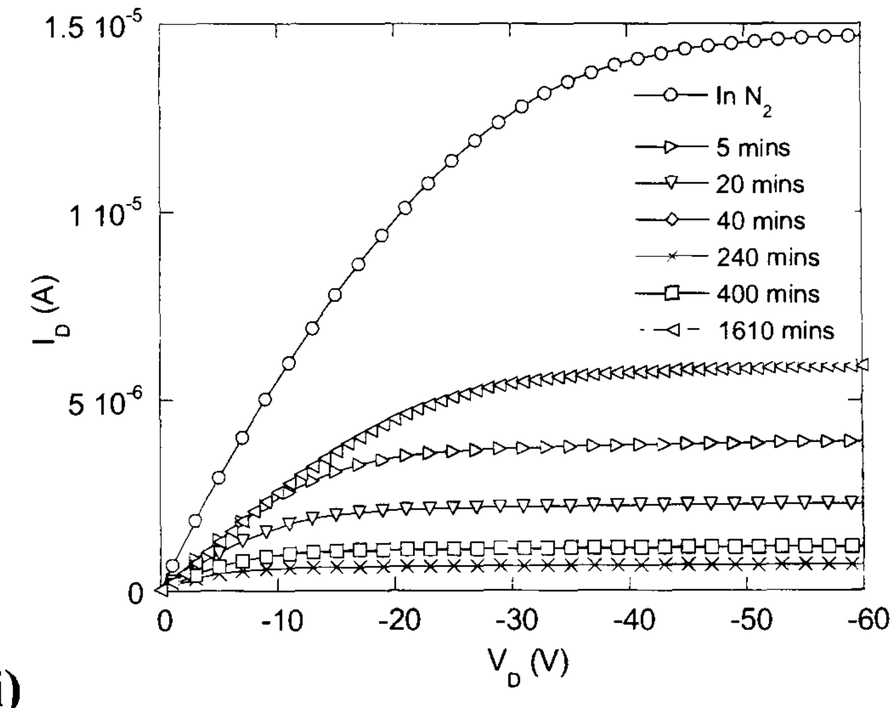
Similar characteristics and trends were obtained for environments with humidity as high as 20% R.H. The results show an unexpected trend. The negative shift of the switch-on voltage and decrease in the off-currents show the opposite trend to that expected and previously reported in the literature.

The on-current remains constant after an initial drop, whilst the off-current decreases. This is contrary to reports in which the on-current decreases and the off-current increases. The switch-on voltage shifts from positive to negative values, decreasing from +35V in a nitrogen atmosphere to +12V in low humidity air. This negative 23V shift is also accompanied by an improvement in the sub-threshold slope and the on/off ratio. The linear and saturated mobilities also remain more or less constant at $2.5\times10^{-3}cm^2/Vs$ and $4.8\times10^{-3}cm^2/Vs$ respectively.

The graphs below show the variation of the switch on-voltage with time and the magnitude of charge present in the channel at zero gate bias, as drawn from the output plots.



(i)



(ii)

Figure.3.5. (i) The variation of the switch-on voltage with respect to time and (ii) output characteristics at zero applied gate bias, giving an indication of the charge present in the channel for the 90% RR P3HT OTS treated transistor measured every 20 minutes in low humidity (<5%) air. After decreasing for 3 hours, V_0 and I_D (V_G=0V) slowly increase. The channel length is 10μm and the channel width is 1cm.

Accumulation in the channel at zero gate voltage can be due to workfunction mismatch, trapped interfacial charges, and or dopants. In this initial timescale, the transistor seems to dedope rapidly, corroborated by an exponential negative shift of V_0 and decrease in current at zero gate bias. This indicates that charges are being trapped, or could suggest that the polymer is being reduced – if we assume that it is initially doped (V_0 = +35V under N_2) it would be capable of accepting electrons and could act as an oxidant. This all depends on the energetics of the chemical reactions, which will be further discussed in the next section.

However, after 3 hours, V_0 starts to move back towards positive voltages. Fig.3.6 shows this second stage of behaviour, which is more generally observed in these polymer systems.

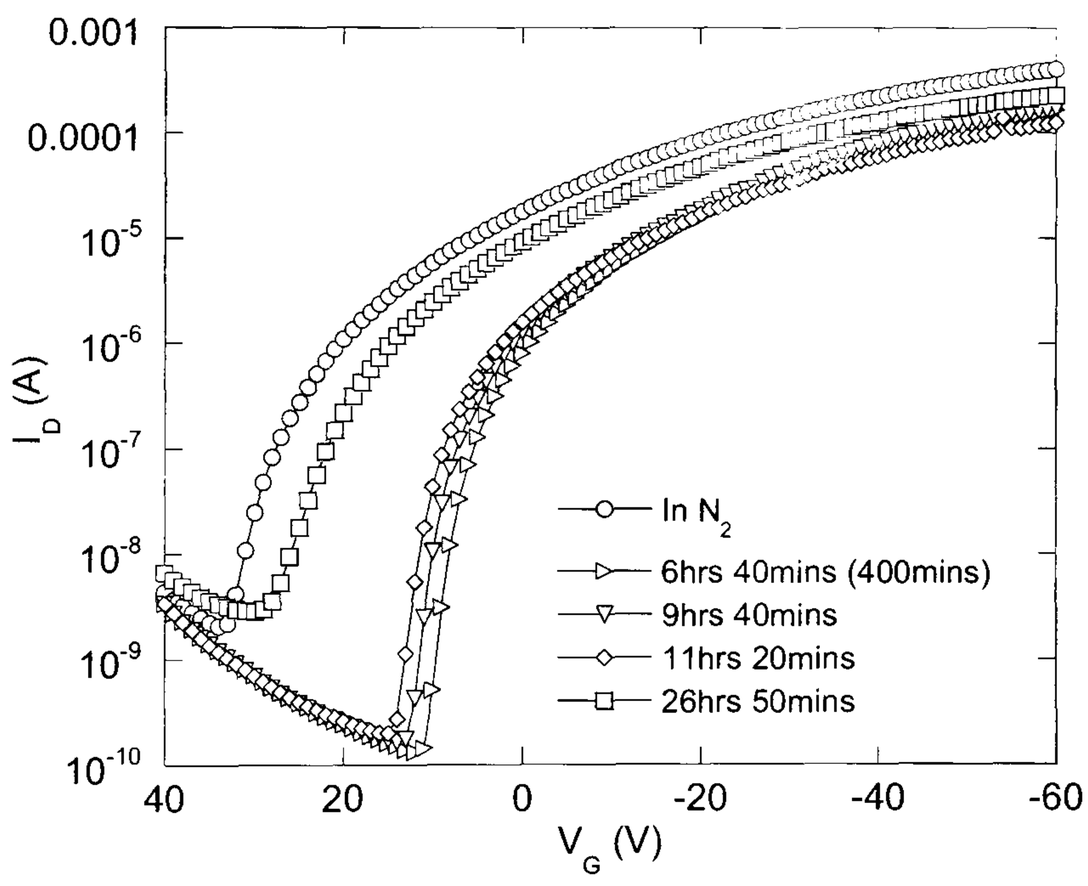


Figure.3.6. Saturated transfer characteristics for the 90% RR P3HT OTS treated transistor measured in low humidity (<5%) air. This is an extension to Fig.3.4 (i) as data measured over a longer timescale is shown. The off-currents, V_0, and the subthreshold slope gradually increase over the 20 hours. The channel length is 10μm and the channel width is 1cm.

This is more consistent with what one would expect on exposure to air. The turn-on voltage shifts gradually to more positive values at an approximate rate of +0.65V per hour. The off currents also increase. Both these effects are easily explainable by the

(neutral) polymer being oxidised, resulting in an increased dopant concentration and higher bulk conductivity in the film. Let us first look at the effect of an identical sample exposed to a moisture rich environment before discussing possible mechanisms for this behaviour.

3.3.3. Stability of 90% RR P3HT transistors in low environmental humidity

The transistors used in the high and low humidity experiments were made side by side and showed no differences when initially measured under nitrogen. The transfer scans with respect to time for 50% R.H. conditions are shown in Fig.3.7. These show a marked difference to the transistor measured in <5% R.H. – essentially dry air.

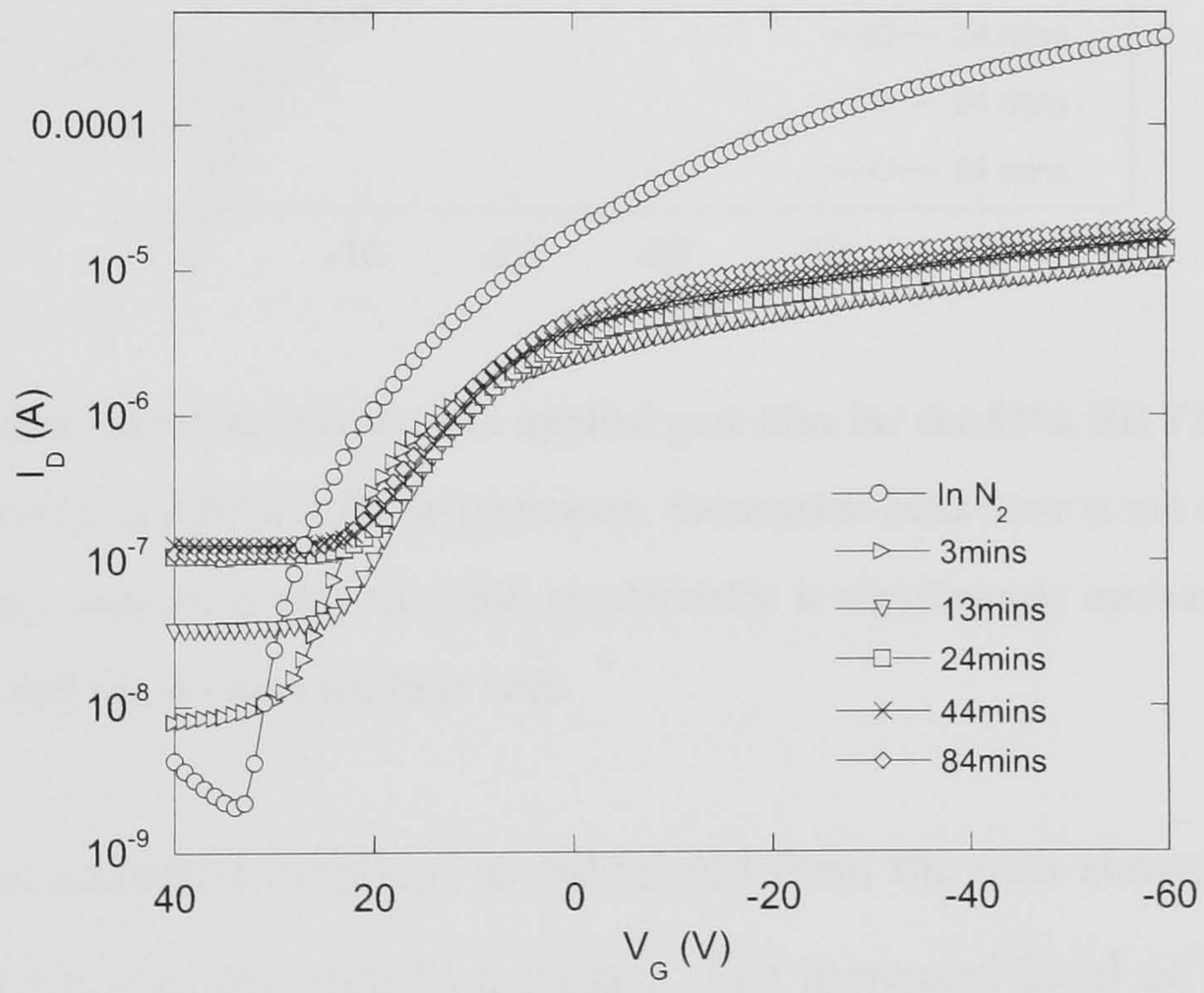


Figure.3.7. Saturated transfer characteristics for the 90% RR P3HT OTS treated transistor measured in a 50% R.H environment. The off-currents, on-currents and the subthreshold slope increase rapidly and the on/off ratio is reduced to 10^2 after just 44 minutes. The channel length is 10μm and the channel width is 1cm.

In this case the switch-on voltage does not shift to the extent it did in the dry air case, and after an initial negative shift of -3V after 13 minutes in wet air, it remained constant. The off-currents increase rapidly with time and after just 44 minutes the on/off ratio has decreased from 10^5 to 10^2. On comparison to the previous case in dry air, water seems to act as the main dopant in the bulk, as the drain current at zero gate bias reaches μA levels almost immediately (Refer to Fig.3.8). These levels are only reached after a day in the drier air.

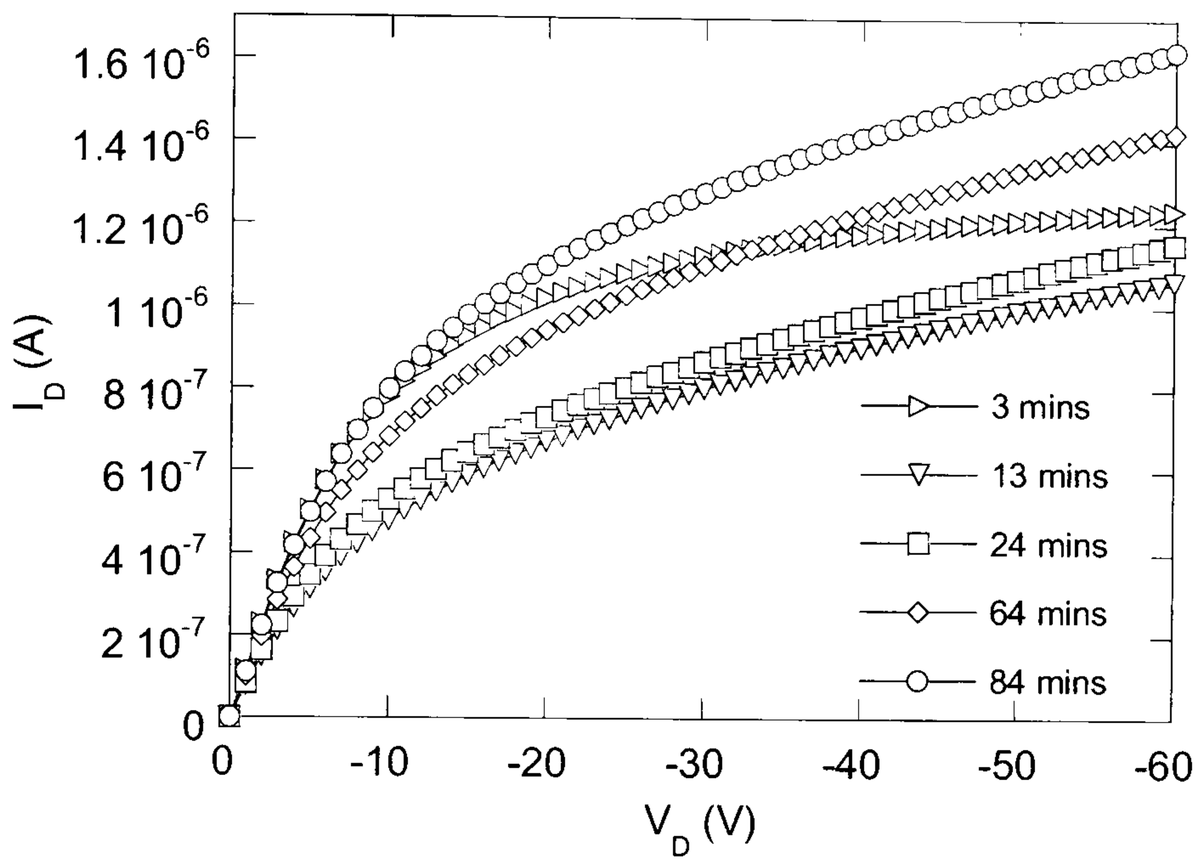


Figure.3.8. Output characteristics at zero applied gate bias for the 90% RR P3HT OTS treated transistor measured in a 50% R.H. environment. Saturation behaviour is not observed after 13 minutes exposure indicating that the bulk conductivity is significantly increased. The channel length is 10μm and the channel width is 1cm.

The linear and saturated mobility, as calculated from the data shown in Fig.3.7 are shown in Fig.3.9, and are seen to increase. The increased level of dopants acts to increase the on-currents, and as V_0 remains constant, the mobility appears to increase, though is 16 and 8 times worse than that measured under nitrogen for the saturation and linear regimes, respectively.

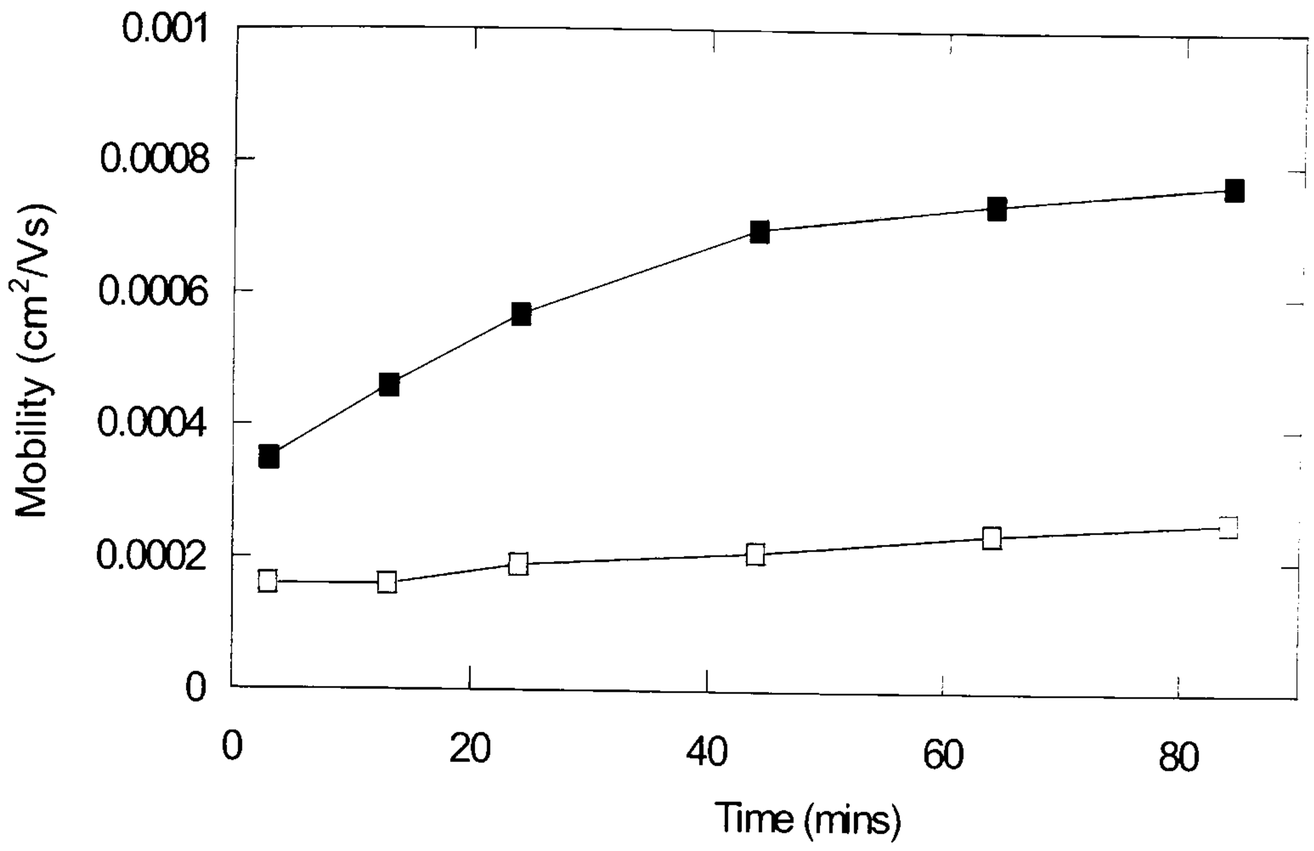


Figure.3.9. Variation of the linear (open squares) and saturated (open circles) mobility of the 90% RR P3HT OTS treated transistor measured in a 50% R.H. environment. The mobility increases, corresponding to an increase in the on-current of the device. The channel length is 10μm and the channel width is 1cm.

Unfortunately it was not possible to carry out the experiments in completely dry air at the time these measurements were carried out, but comparison of behaviour in a high and low humidity environment is sufficient to demonstrate the main differences in device operation. Water is more detrimental to device performance than oxygen alone, and the increase in off-currents happens on a much more rapid time scale if humidity is high. As low levels of water are still present in the 5% R.H. results, this is suggestive of a time dependent process. It takes ~150 minutes of exposure to 5% R.H. air for the transfer characteristics to exhibit a positive voltage shift and increase in off-current. If the R.H. is increased to 18%, the same effects are seen after just 60 minutes (These results are not presented). In 50% R.H. an increase in the off-current is seen immediately, though a negative then positive shift in V_0 is not observed. Whether this is because the initial dedoping process does not occur, or because it is masked by the rapid increase of dopants in the bulk, or because it occurs in a timescale that is too quick to be observed, is unclear.

A final confirmation that this is indeed a time dependent process was provided by the recent installation of a dry air glove box at Merck Chemicals Ltd. in Southampton. This enabled the fabrication and characterisation of devices in dry air with <0.1% R.H. Similar experiments with ant-pBTTT polymer (See section 3.5.) have shown any switch-on voltage shifts to be even more retarded, gradually shifting to more negative values over a matter of months rather than 4 days, as is observed in a laboratory environment.

3.3.4. Stability of 97.5% RR P3HT

What should we expect if the polythiophene has a greater degree of regioregularity? We know that the device characteristics are improved if measured under nitrogen, but does the lower ionisation potential make the 97.5% RR P3HT more unstable in ambient conditions? Fig.3.10 illustrates the change in the saturated transfer characteristics with respect to time in an environment with <5% R.H. for the 97.5% RR P3HT transistor.

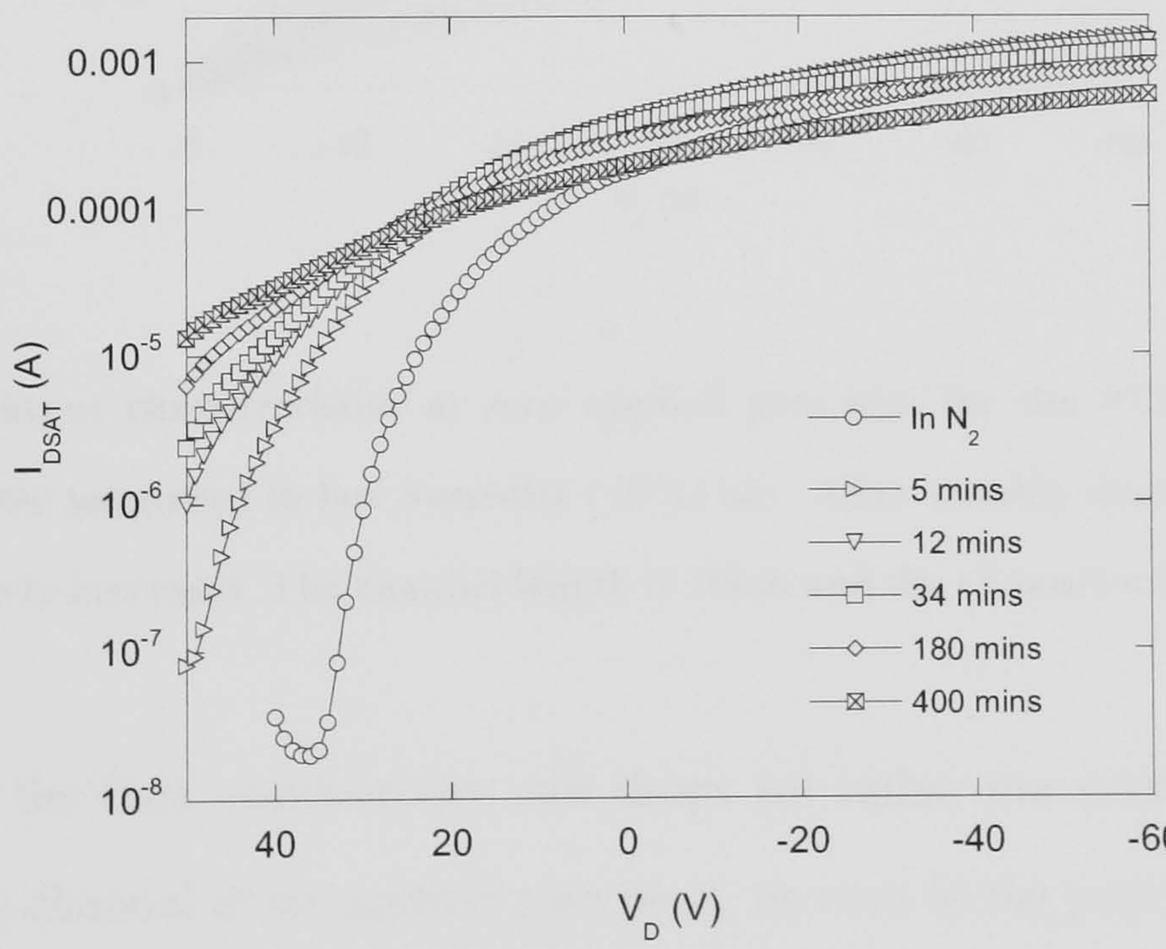


Figure.3.10. Saturated transfer characteristics for the 97.5% RR P3HT OTS treated transistor measured in low humidity (<5%) air. The channel length is 10μm and the channel width is 1cm.

The most noticeable difference is the significant positive shift of the switch-on voltage from the original value, as measured under nitrogen. After just five minutes exposure to low humidity air, V_0 is +50V. It was then not possible to extract V_0 from the transfer scans. Increasing the scan range to more positive values could have enabled the switch-on voltage to be extracted, but the magnitude of the biasing regime could also affect the stability. The polymer is more likely to degrade at higher biases, so similar scan ranges were chosen to allow for comparable results. The initial negative shift observed for the 90% RR P3HT does not appear to happen with this sample.

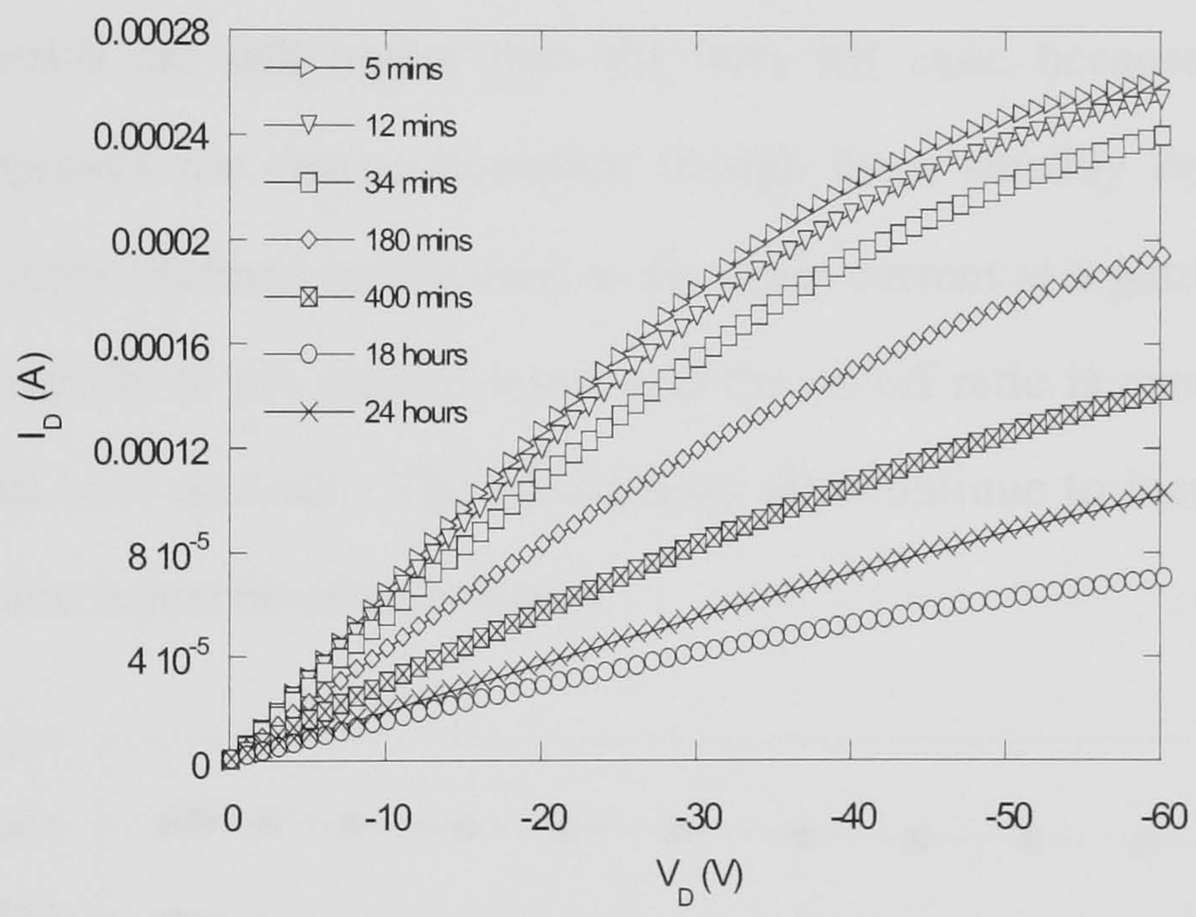


Figure.3.11. Output characteristics at zero applied gate bias for the 97.5% RR P3HT OTS treated transistor measured in low humidity (<5%) air. After steadily decreasing for 18 hours, I_D (V_G=0V) slowly increases. The channel length is 10μm and the channel width is 1cm.

Surprisingly, the bulk conductivity still drops (or rather our estimation of charges present in the channel at no applied gate bias), as seen in the previous case for 90% RR P3HT. This is consistent with the observed decrease in the on-current, though the off-current increases significantly. This decrease of the drain current at V_G=0V continues for up to 18 hours when it reaches 70μA at an applied drain voltage of -

60V. It then starts to increase again and after 24 hours exposure to 5% R.H. air has reached a current level of 0.1mA. This dedoping/redoping effect happens over a longer timescale for the more regioregular polythiophene transistor, as the current due to accumulated charge at zero gate bias started to increase again after just 150 minutes in the 90% RR P3HT. The currents were much higher than for the 90% RR P3HT transistors, even if compared to the sample measured in a wet environment. These higher current levels (i.e. a higher charge carrier density) in the film could mask any shifting of V_0, which in the lower regioregularity case corresponds to the decrease and increase of these non-gate bias induced currents.

The on-currents are still higher than the 90% RR case, because better molecular packing improves the charge transport, though these steadily decrease with time. The off-currents (defined in this case as the drain current at a gate voltage of +50V) deteriorate rapidly to μA current levels and the on/off ratio is consequently reduced to 10^3 in just over an hour. The off-currents also continue to increase with time so the on/off ratio is just 80 after 24 hours.

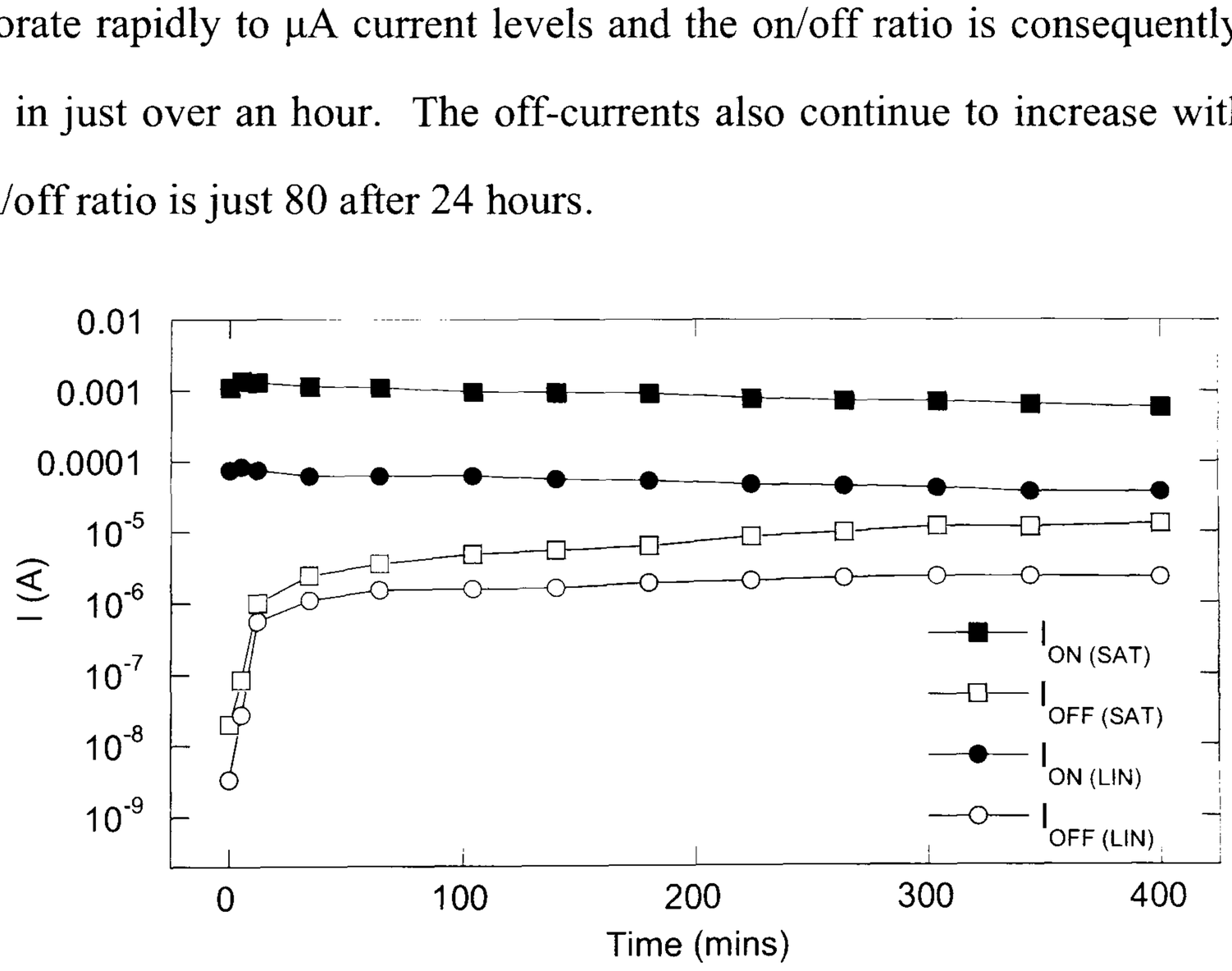


Figure.3.12. On and off-currents measured for the 97.5% RR P3HT OTS treated transistor measured in low humidity (<5%) air. The on-currents decrease steadily, whilst the off-currents increase rapidly at first. The on-off ratio is reduced to 10^3 in an hour. The channel length is 10μm and the channel width is 1cm.

This is clearly evident from plotting the on and off-currents with respect to time in Fig.3.12. The on/off ratio was 10^5 in the 90% RR case after 6 hours in dry air and $8.1 \cdot 10^4$ after a day of exposure to the same humidity environment. The 97.5% RR P3HT certainly exhibits more unstable behaviour in dry air, than the less regioregular batch.

The deterioration of characteristics in 50% R.H. appeared to be instantaneous, with an on/off ratio of less than 20 and a switch-on voltage well above +50V measured for the first scan after exposure.

3.3.5. The effect of regioregularity on the stability of P3HT transistors

The two polythiophene batches exhibited different behaviour on exposure to wet and dry air. In dry air the less regioregular P3HT transistor exhibited a gradual negative then positive shift in V_0, which was reflected in the declining then rising level of charges present at zero applied gate bias. The off-current also followed this pattern and decreased to 10^{-10}A before gradually increasing for the remainder of the measurements. The time scale for this changeover was 150 minutes. The on-currents and saturated and linear mobilities decreased slightly and were 5 and 3 times lower than those measured previously under nitrogen. When the humidity was increased to 50% R.H., the on and off-currents increased rapidly and the switch-on voltage remained constant after an initial -3V shift. This resulted in an increasing mobility. There was also a clear loss of saturation in output characteristics indicative of increased bulk conductivity.

The characteristics of the 97.5% RR P3HT transistor in wet air were immeasurable as the switch-on voltage was immediately shifted to > +60V with an on/off ratio of less than 20. Device performance was improved in dry air, though V_0 was shifted

positively to > +50V. Much higher currents were present than for the 90% RR sample, though the on/off ratio diminished with time as the on-currents decreased and off-currents increased rapidly. The number of accumulated charges present at zero gate bias followed the previously observed gradual decrease, before increasing after 18 hours. This did not seem to correspond to any change in V_0 or the off-current, though this effect could have been screened by the increased density of dopants present.

The same behaviour was also seen on comparing a different batch of more crystalline P3HT of higher regioregularity with a similarly synthesised batch of lower regioregularity (These results are not presented). No negative shift in the switch-on voltage or off-current was observed for the high RR device, and the transfer characteristics displayed a rapid positive shift of V_0 and increasing off-currents. The bulk conductivity decreased for both samples. The lower regioregularity batch exhibited a negative then positive V_0 shift and an initial decrease of the off-currents. This is further evidence that the differences in performance are due to the regioregularity – higher regioregular batches being more unstable in ambient conditions. This is likely to be due to the lower ionisation potential making it easier to oxidise the polymer, though the increased crystallinity should hinder diffusion of molecular species into the bulk.

However, all results indicate that water exerts a more detrimental effect on device characteristics, as measurements in lower humidity displayed more stable characteristics and degradation was shown to be a time dependent process related to the concentration of water.

3.4. How does the humidity affect transistor characteristics?

Recently, a number of environmental stability studies with varying relative humidity (R.H.) have been undertaken for OFETs.[13-17] There are several interactions that can affect the ambient stability of conjugated polymers and we have already suggested that ambient stability will be increased in materials with high ionisation potential (more electrochemical stability) and a less amorphous nature (hindering diffusion through the bulk). The majority of work on the effect of humidity on transistor performance has been carried out on the small molecule pentacene.

Qiu et al. looked at the stability of pentacene transistors and found that device stability worsened with higher humidity levels as water was adsorbed at the crystalline grain boundaries.[14] FTIR studies showed the appearance of a hydroxyl radical absorption peak in the spectra after 100 hours exposure to ambient, and AFM studies clearly confirmed the appearance of water at the grain boundaries. They postulated that the water molecules can diffuse in between these grain boundaries, increasing the concentration of traps and reducing the mobile charges in the channel when the transistor is operating. The presence of polar molecules is also known to decrease the charge transport by increasing the amount of energetic disorder present through charge-dipole interactions.[15]

Li et al. also studied the effect of humidity on pentacene transistors by increasing the relative humidity of a nitrogen environment.[16] They attribute the reduction in the mobility and on-current to polar water molecules at the grain boundaries interacting with charge carriers. The diffusion of water molecules into grain boundaries changes the intermolecular interactions by increasing the energy barrier for charge intergrain transport or by the ions screening the electric field and lowering the concentration of accumulated charge carriers in the channel. They also noted that

the threshold voltage shifted to more positive values and the off-current increased with increasing R.H. A higher density of grain boundaries was found to directly contribute to higher moisture sensitivity, and as the deposition of pentacene onto gold results in smaller grain sizes than that deposited on silicon dioxide, bottom contacts proved to be the most susceptible to high humidity degradation.

A brief introduction to the electrochemistry will be given in the next section, before describing the effect redox processes could have on the observed ambient degradation characteristics. In this case, the ionisation potential is the determining stability factor as this gives an indication of whether the oxidation/reduction process is likely to proceed if thermodynamically favourable. The effect of trapping and interface states, and how the morphology can affect the diffusion rate of molecular species into the film will also be discussed. Finally, a possible mechanism by which P3HT transistors degrade on exposure to ambient conditions will be put forward.

3.4.1. Electrochemical stability and redox processes

First, let us consider the electrochemical stability of the system. Electrochemistry can be defined as the study of charge-transfer phenomena. Oxidation involves the loss of electrons and conversely, reduction involves the gain of electrons. It follows that a combination of these reactions is termed a redox reaction. In other words, a reaction that occurs via the loss of electrons from one species and the gain of electrons by another. The oxidising agent (or oxidant) accepts electrons readily and the reducing agent (or reductant) is an electron rich species which can supply electrons. Whether a reaction actually happens is governed by the thermodynamics of the system. For a reaction to be spontaneous (have a natural tendency to occur) the overall Gibbs free energy ΔG of the reaction (ΔG depends on the enthalpy and entropy of the reaction) should be negative.[18]

If we split a redox reaction into the reduction and oxidation parts, we are left with two half reactions – one in which the species gains electrons (reduction) and one in which a species loses electrons (oxidation). Convention dictates that these half reaction 'couples' are written in the format of reduction processes. The free energy of the overall reaction is consequently the difference of the free energies of the two half reactions. As these reactions must always occur in pairs (hence the term redox couple) and we are only concerned with their relative values, we can take one half reaction to have $\Delta G = 0$. This reference electrode is usually taken to be the reduction of hydrogen ions to hydrogen gas or a standard calomel electrode (Hg/Hg_2Cl_2). The potential that corresponds to ΔG of a half reaction is called the standard reduction potential E ($\Delta G = -nFE$ where n is the number of moles of electrons and F is Faraday's constant – the charge per mole of electrons) and is a measure of the relative oxidising/reducing power of different species. This can then be used to predict which species will be reduced or oxidised.

For example, consider the case of a redox reaction combining the half reactions 1 and 2 in which Red stands for the reduced species and Ox for the oxidised species with standard electrode potentials E_1 and E_2 respectively. Movement of electrons are not shown:

$$Red_1 + Ox_2 \Leftrightarrow Ox_1 + Red_2 \qquad \{3.1\}$$

E must be greater than 0 (note the negative sign with respect to ΔG) so $E = E_2 - E_1$ must be positive ($E_2 > E_1$) for species 1 to be reduced. Thus, oxidised species with high positive standard potentials are strong oxidising agents and reduced species with large negative potentials are strong reducing agents.

De Leeuw et al. described the ambient stability of n-type doped conducting polymers using this reasoning.[19] The standard electrode potentials of conducting polymers are not readily available, so the values were approximated from the middle potentials of the anodic and cathodic waves in cyclic voltammograms. Cyclic voltammetry measures the current through an electrode as the potential is increased then decreased, linearly.[18]

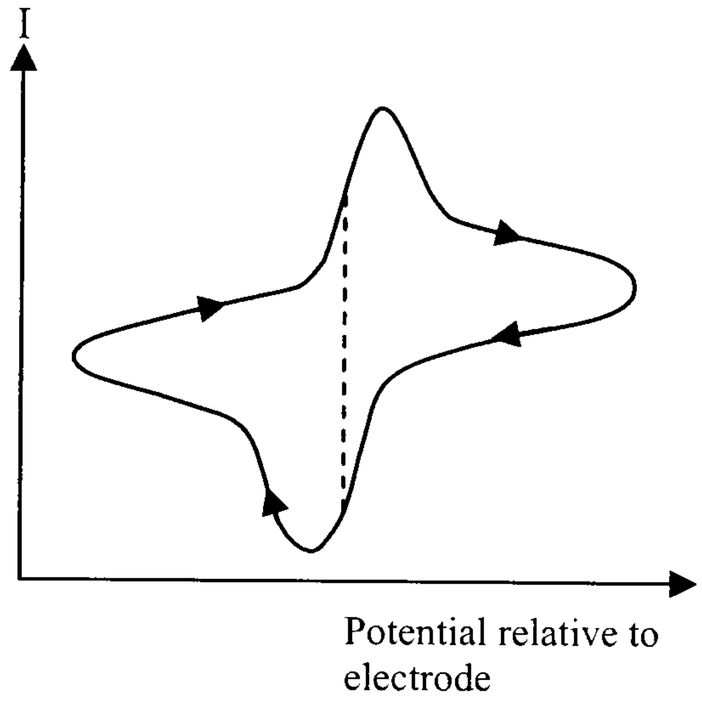


Figure.3.13. Cyclic voltammetry scan showing the evolution of current with respect to the potential applied. The direction of the scan is denoted by the arrows and the dotted line represents the electrode potential E. Adapted from[18]

Consider a solution containing the redox couple X^0/X^{-1}. If a highly negative potential is initially applied, X^0 near the electrode will be reduced to X^{-1}, and the current will be small as the concentration of X^0 (oxidised species) will be low. If the potential is scanned to more positive values, oxidation of X^{-1} will begin as the potential approaches E and the current will increase. As the potential exceeds E, X^0 is now the dominant species at the electrode, and the current falls again at these high positive potentials. On reversing the potential sweep direction a current begins to flow as the potential is reached, this time for reduction of X^0, with the current peaking as the concentration of X^{-1} dominates. These peaks lie either side of the electrode potential, which is shown by the dotted line in the Fig.3.13.

The diagram in Fig.3.14 includes the most likely redox reactions for water and oxygen, and illustrates the stability of neutral and doped p-type polymers with

respect to this. So far, we have neglected any overpotential. In many cases a reaction requires a free energy of activation to proceed which can be supplied by an excess voltage. These values have not yet been reported, but could be up to 1V. Thus, it should be borne in mind that the stability thresholds could be shifted by this amount.

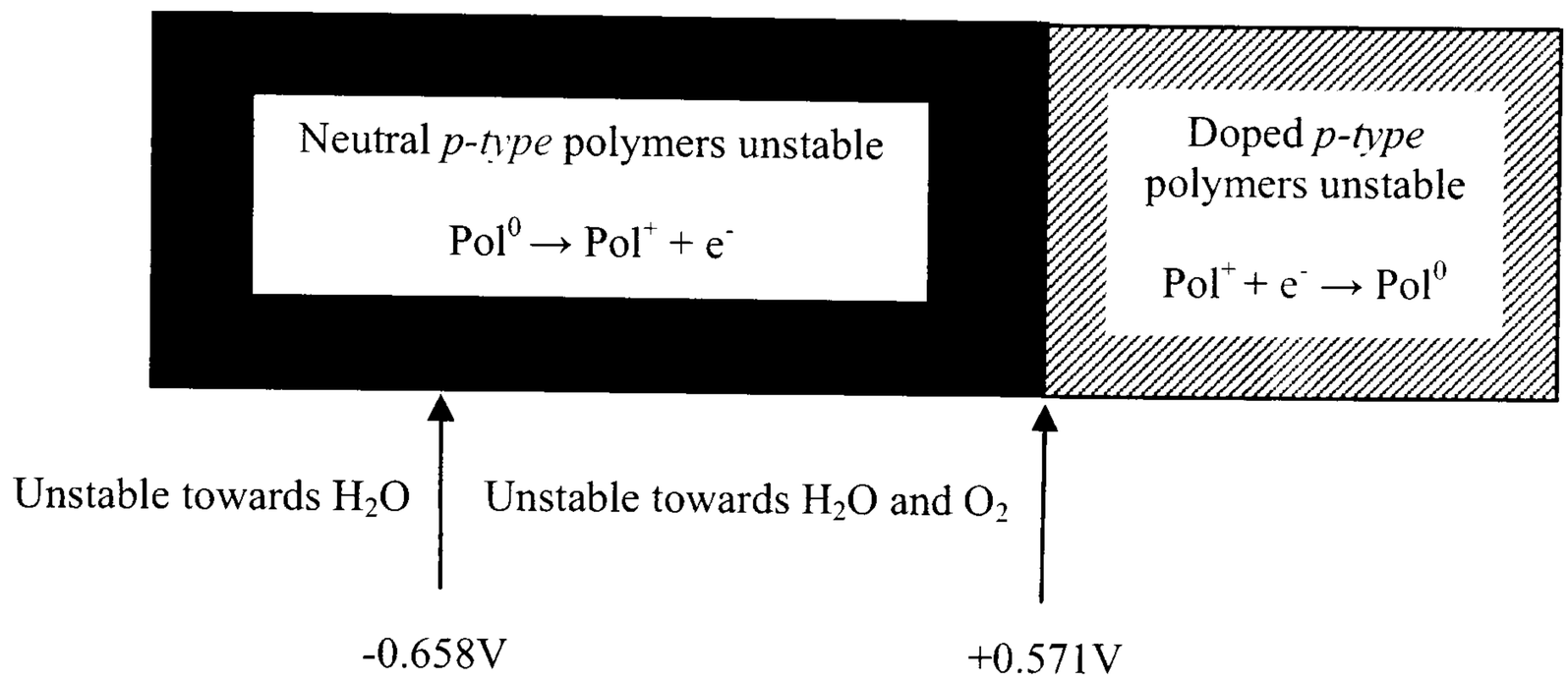


Figure.3.15. Schematic illustrating the stability of p-type polymers with respect to water and oxygen. If the electrochemical potential of a neutral p-type polymer is less than -0.658V it can be oxidised by water and if less than +0.571V can be oxidised by water and oxygen, as illustrated by the filled region. The instability of doped p-type polymers is depicted by the shaded block. Adapted from[19].

Let us consider an example reaction. A p-type polymer is capable of accepting electrons and is an oxidant whilst an n-type polymer is capable of donating electrons and is thus a reductant. The solid state ionisation potential of a p-type polymer is equal to the electrochemical potential at which the polymer can be oxidized plus 4.4V.[19] Thus, as the I_P of the 97.5% RR P3HT is 4.8eV, the electrochemical potential is approximately +0.4V. The less regioregular batch has a higher I_P of 5.08eV, implying an electrochemical potential of +0.68V. According to the diagram, the potential at which a neutral p-type polymer can be oxidised is >-0.658V to be stable towards water and >+0.571V to be stable towards oxygen and water. Alternatively, for p-type doped polymers, the oxidation potential should be lower

that +1.412V to be stable towards oxidation of oxygen to ozone, lower than +1.118V to be stable towards H_2O_2 and lower than +0.571 to be stable against oxygen and water. Thus, if we consider the 90% RR P3HT to be undoped it should be stable with respect to both oxygen and water, whilst the 97.5% RR P3HT would be oxidised by these species.

This reasoning agrees with what we expected in terms of instability, but can it explain the switch-on voltage shift? If the polymer is oxidised, as in the case of the 97.5% RR P3HT, it loses electrons such that $Pol^0 \rightarrow Pol^+ + e^-$. Combining this half reaction with that for the reduction of oxygen to water:

$$O_2 + 4H^+ + 4e^- \rightarrow 2H_2O \quad E = +0.571V \qquad \textbf{\{3.2\}}$$

$$4Pol^0 \rightarrow 4Pol^+ + 4e^- \quad E = +0.4V\ (+0.68V) \qquad \textbf{\{3.3\}}$$

$$4Pol^0 + O_2 + 4H^+ + 4e^- \leftrightarrow 4Pol^+ + 4e^- + H_2O \qquad \textbf{\{3.4\}}$$

$\rightarrow$ Energetically favourable for 97.5% RR P3HT

$\leftarrow$ Energetically favourable for 90% RR P3HT

Thus, the 97.5% RR polymer will be oxidised with respect to the reaction shown, but the free energy of the 90% RR polythiophene would be positive and unlikely to proceed. The above reactions can proceed in both directions - depending on the equilibrium reached. By similar logic you could expect the reaction:

$$4Pol^+ + 4e^- + H_2O \rightarrow 4Pol^0 + O_2 + 4H^+ + 4e^- \qquad \textbf{\{3.5\}}$$

to be favourable for the lower regioregular polymer. The switch-on voltages of both polymers are large, even as measured under nitrogen, indicating that there must be

some impurities/dopants present even without exposure to ambient. These are likely to be due to any catalyst residue or unintentional doping from processing. If we say that the polymer is initially doped, this in essence means that is has an excess of holes and can accept electrons to be come neutral. 'Doped' 90% RR P3HT would in this case be unstable with respect to water and oxygen, but 'doped' 97.5% RR P3HT would be stable!

Returning to our results, experimentally we observed that:

(i) V_0 shifted negatively then positively (time dependent on the amount of water present) for the 90% RR polymer. No negative shift was observed for the more regioregular polymer, as V_0 was immediately shifted to high positive voltages.

(ii) In a low humidity environment, a decrease then increase in the drain current at zero applied gate bias was evident for both polymers. The changeover was prolonged for the more regioregular polymer, though V_0 was >+50V so the off-currents were not observed.

(iii) The off-currents increase rapidly in wet environments, for both polymers.

Is electrochemical theory enough to explain this behaviour? Let us consider the shift of switch-on voltage first. Water is a weak acid and can dissociate into H^+ and OH^- ions. The 97.5% RR P3HT is susceptible to oxidation by molecular oxygen and H^-. Positively charged polymer ions have the effect of increasing the bulk current, so that even when the channel is depleted (on application of positive gate bias) the carriers in the bulk can contribute to the current. Thus, the switch-on voltage is shifted to more positive values. A higher bulk conductivity also corresponds to the higher off-currents observed.

The 90% RR polymer is supposedly stable to oxidation. However, if the polymer is unintentionally doped so that the polymer cations can be reduced, the polymer will return to its neutral state and V_0 should shift negatively. This negative shift is dependent on the concentration of water in the system. At increased relative humidity, V_0 and the off-current reach their most negative and lowest value sooner. This suggests that the 'doped' polymer is being reduced to its neutral state, before the process of oxidation ($Pol^0 \rightarrow Pol^+ + e^-$) starts to dominate. The dedoping reaction should occur quicker if a higher concentration of water is present, which is as observed.

The situation is clearly not simple, and it is hard to provide a complete explanation with regards to electrochemistry without further experiments. Electrochemistry can be thought of as a minimum requirement for air stability, as it doesn't take into account alternate chemical reactions between molecular ambient species and the polymer. Both polythiophene batches are 'borderline' with regards to stability in oxygen and water, so establishing equilibrium due to concentration of products and reactants and reaction kinetics may result in this shifting behaviour. This discussion has also neglected to mention any overpotential, which in practise can be as much as 1V and acts to shift the potential of the reactions by this amount.[18,19] It should also be remembered that there is a distribution of polymer chain lengths with different conformations and different ionisation potentials!

Hoshino et al. also looked at the effect of water on P3HT FETs.[17] Their study focussed more on shelf-life rather than operational stability. Ambient stability differences can be due to operational stress. The characteristics of an unmeasured transistor are always better that those of a measured device on the same substrate, even though both devices have been exposed to air for the same time. However, degradation occurs more rapidly if the new device is then subjected to continuous

measurements. Optical measurements of polymer film are often carried out under ambient conditions, and no apparent degradation is observed for short timescales. Operational stress either provides a different mechanism though which the material degrades, accelerates the degradation process, or electrical measurements enable observation of electronic effects that can not be observed optically. In any case, the difference between operational stress and stability is beyond the scope of this thesis and further experiments should be carried out to examine these phenomena.

However, Hoshino et al. also found that device operation was significantly influenced by water, even in an environment without oxygen (wet nitrogen). Enlarged off-state conduction and deterioration in saturation behaviour of output characteristics seemed to be due to the presence of water rather than oxygen. They attributed this to the adsorption of polar water molecules on the surface increasing the charge carrier density, similar to that described for pentacene transistors. These observations agree with our findings, though no information was provided about the variation of the switch-on voltage as their transistor characteristics focussed on output rather than transfer scans. Measurements carried out in pure oxygen resulted in a higher conductivity ($1.49 \cdot 10^{-3}$S/cm versus $0.78 \cdot 10^{-3}$S/cm in N_2 and $0.58 \cdot 10^{-3}$S/cm in vacuum) but lower mobility ($0.94 \cdot 10^{-4}$cm^2/Vs versus $1.23 \cdot 10^{-4}$cm^2/Vs in N_2 and $1.25 \cdot 10^{-4}$cm^2/Vs in vacuum) than transistors measured in nitrogen or in vacuum. This inverse correlation was explained by the scattering probability of charge carriers being increased by the formation of the charge transfer complex between the polythiophene and oxygen, as described by Abdou et al.[9]

Our measurements could not be carried out in completely dry air and the relatively humidity was typically <5%, so a low concentration of water was present. In our case, the conductivity appeared to decrease before increasing, after 3 hours for 90% RR and 18 hours for 97.5% RR polythiophene. Considering the mechanics of CTC

formation, the lower ionisation potential of the more regioregular batch should result in a larger degree of charge transfer. However, the number of scattering sites is dependent on the concentration of oxygen. The more regioregular film is more crystalline so acts to inhibit oxygen diffusion into the bulk. Molecular oxygen would diffuse quicker into the 90% RR film, so the threshold of scattering sites at the interface needed to increase the conductivity is reached sooner. Molecular oxygen is physically bigger than a water molecule, so takes longer to penetrate into the film, which could also explain why its effects take longer than water.

On the other hand, as the 97.5% RR P3HT is easier to oxidise, there would be a greater concentration of OH^- ions in the film. This would make any doped polymer chains more susceptible to reduction via nucleophillic substitution reactions with the OH^- ions.[20] These hydroxyl ions could also affect the energetic disorder, field distribution and act as traps (as could non-dissociated polar water molecules). Threshold voltage instabilities and deterioration of device performance in wet conditions have also been attributed to trapping and ionic diffusion in the polymer film. Zilker et al. found strong positive threshold shifts in the presence of water.[21] It remains unclear whether water provides the mobile ions or if a network is formed inside the insulator (in our case thermally grown silicon dioxide is used so this can be neglected), or whether the water generates high mobility paths for already present impurities (we know that these exist for P3HT due to large V_0 anyway). These effects will be discussed in the following two sections before summarising the most likely mechanisms for the effects observed.

3.4.2. Hysterisis and trapping effects caused by water

Electronic defect states at the semiconductor interface and in the dielectric can cause instabilities in the threshold voltage and V_0. Matters et al. reported negative

threshold voltage shifts due to charge trapping with applied gate bias stress measurements.[22] This was more pronounced in the presence of water than in vacuum or dry air and was attributed to trapping of charges in less mobile states. Accumulated charges fill these states under application of a negative gate bias and are released when the applied bias is stopped. This effect is accelerated by applying a positive gate voltage. Better performance was observed if the interface was initially treated with a hydrophobic agent such as HMDS, as this reduces the number of hydroxyl states at the silica interface.

Street et al. suggested that charge trapping occurs due to formation of low mobility bipolarons by the reaction of two polarons, though some groups have been unable to detect the spectroscopic signature of this.[23,24] These bipolarons are immobile and deplete the channel of mobile holes, shifting the threshold voltage accordingly. The voltage shift can also be recovered by illumination of the sample with light above the band gap of the polymer, which generates electron-hole pairs in the organic semiconductor near the trapped charge. The photogenerated electron then has a chance of recombining with the trapped hole leaving behind a mobile hole. This indicates that these trap states must be in semiconductor or at the interface. It has also been reported that positive gate voltage stress leads to a positive threshold voltage shift, which is explained by the injection and trapping of electrons.

Fig.3.15 illustrates the dramatic difference in hysterisis for the 90% RR P3HT transistors exposed to dry air for 18 hours and just 44 minutes in wet air. The hysterisis in the low humidity environment is negligible. The same effect was also observed for the more regioregular polymer, though a small degree of hysterisis was also evident in the <5% R.H. case. But what is actually happening?

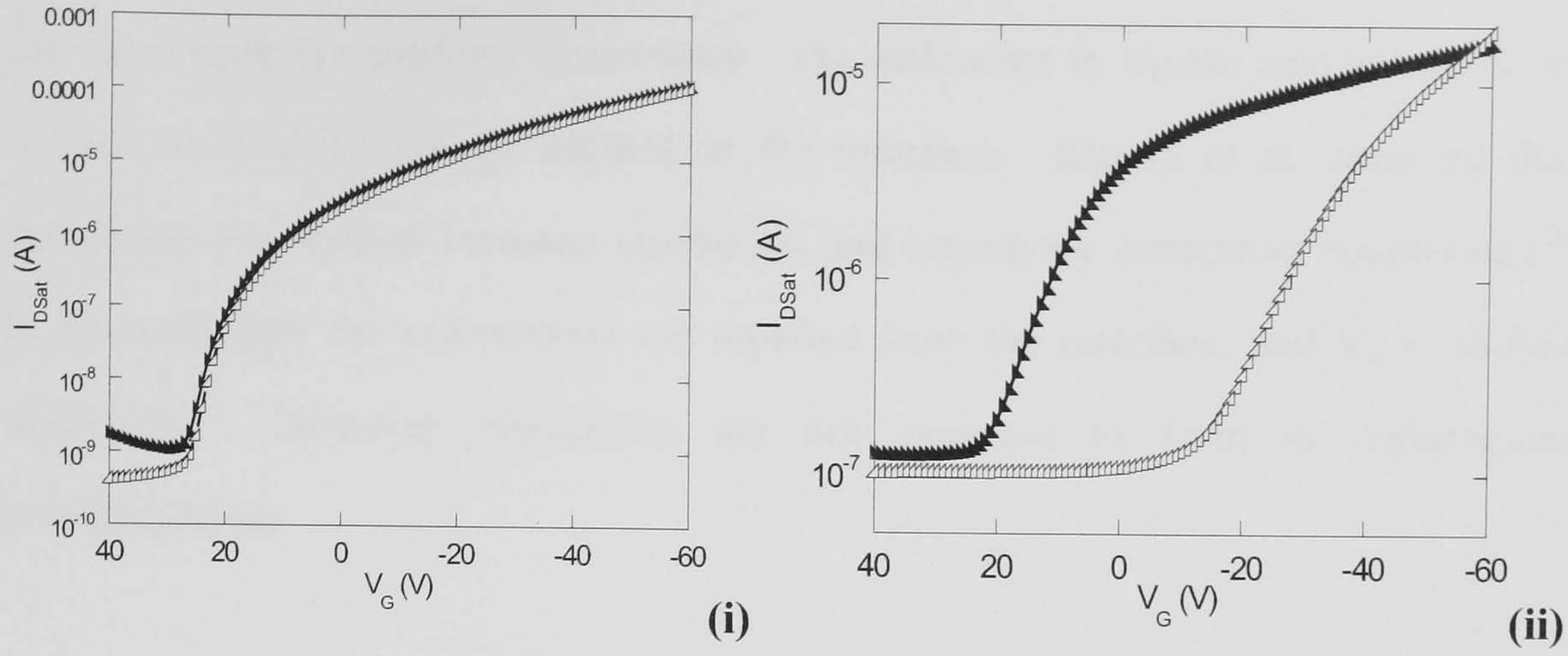


Figure.3.15. Forward (filled triangles) and reverse (open triangles) saturated transfer scans for the 90% RR P3HT OTS treated devices after (i) 18 hours in less than 5% R.H. and (ii) just 44 minutes in 50% R.H. environments. The scan was swept from positive to negative and then reversed.

The currents are higher on the forward sweep than the reverse sweep, though the current at the beginning of the reverse sweep is slightly higher that at the end of the forward sweep as the gate bias was switched off momentarily between measurements. In the forward scan an increasing negative bias is applied and positive charges are accumulated by the applied bias. There is a significant hole current at +20V, suggesting that charges are already present in the bulk of the film without the application of a gate bias – as a positive gate voltage has to be applied in order to deplete the channel. The more negative V_G is, the more holes are accumulated and the higher the drain current will be. On the reverse scan, the bias is scanned to more positive values. This acts to deplete positive charges. There are fewer mobile holes available in the reverse scan, as lower 'positive' voltages are required to deplete the channel.

Rep at al. looked at the hysterisis caused by mobile ions.[25] In our case, the hole current was decreased when the voltage was scanned positively. Let us assume that water introduces mobile negative ions in the film. In accumulation, these negative

ions would gather around the source electrode. When the bias is removed the ions can relax back to a uniform distribution. The difference in V_0 can also be explained if there is positive charge trapped at the interface. Kirova et al. assumed that complexes are formed between bipolarons and negatively associated counterions.[26] In accumulation the counterions are repelled from the interface, and V_0 is shifted negatively. However, bipolarons are not expected to form in regioregular polythiophenes.

Water clearly increases the level of hysterisis in both polymers. In 20% R.H. hysterisis effects are more pronounced than in the dry air case – but still much less than in 50% R.H. With a greater concentration of water there is a greater concentration of mobile OH^- ions. If the transistor is operated in accumulation a negative voltage is applied to the drain electrode, forcing the anions to cluster around the source electrode. This would raise the contact resistance and would lower the charge carrier density of the reverse scan.

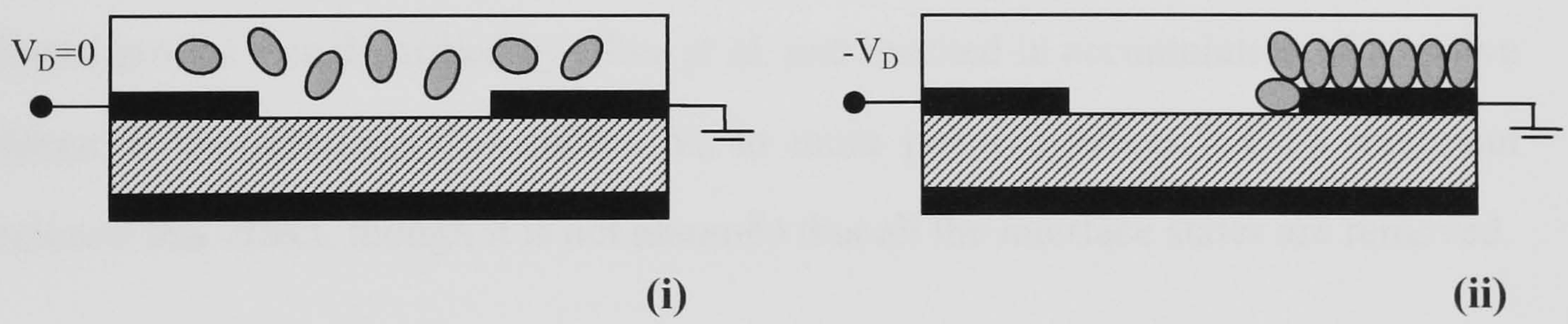
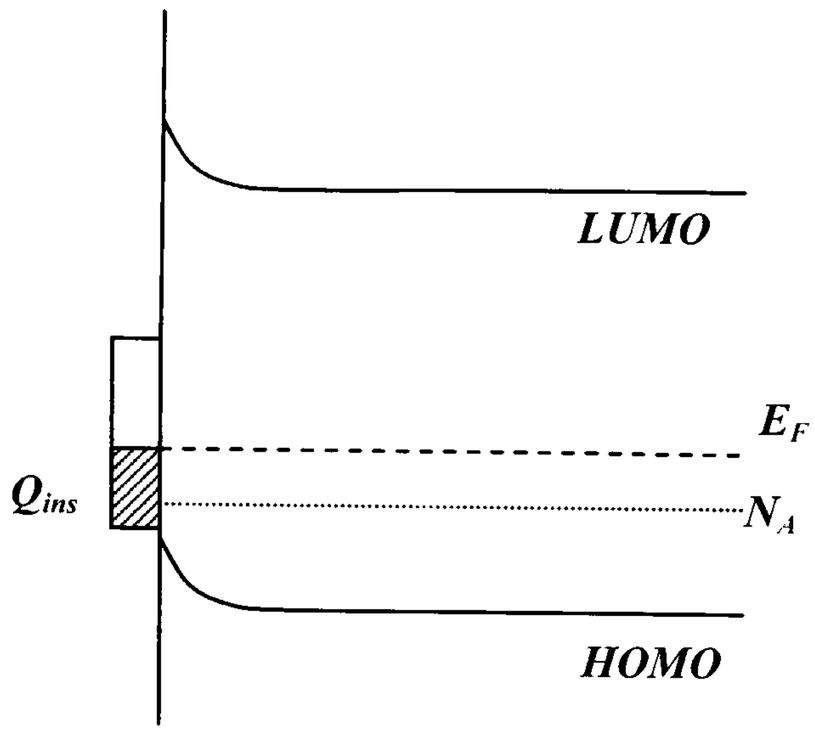


Figure.3.16. illustrates the movement of negatively charged mobile ions (ovals) on application of a negative bias to the drain. The application of a negative gate bias accumulates positive charge carriers in the channel, but these firstly need to be injected from the source electrode. This is not depicted. In (i) there is no applied drain bias and the negative ions are randomly distributed throughout the film. In (ii) a bias is applied, and the ions are repelled from the drain electrode and cluster around the source contact. This inhibits injection and the OH^- ions can also act to trap positive charges.

We have also observed that transistors with smaller channel lengths, for example 2.5μm, deteriorate more rapidly than those with longer channel lengths. This suggests that water or its associated ions are adsorbed or attracted near to the vicinity of the contacts, increasing the contact resistance, hysterisis and off-currents whilst reducing the on-currents.

Water (or OH^-) could also act to trap positive mobile charge carriers. Let us assume that water can trap charge carriers and that these trap states exist at the interface and grain boundaries. The shift in V_0 could be due to emptying or charging of these interface states. A negative switch-on voltage shift indicates that hole traps are being filled (the interface becomes more positive so a less positive gate bias is required to turn off the transistor) and a positive shift that hole traps are being emptied (or alternatively that electron traps are being filled). We know that treating the interface with a hydrophobic layer such as octyltrichlorosilane (OTS) reduces hysterisis effects, even in the presence of water vapour. Such passivating treatments are known to reduce the concentration of polar hydroxyl groups that can act as trapping interface states. A mechanism for these hydroxyl groups trapping electrons to form silanol groups was described by Chua et al, and resulted in accumulation of negative charge at the interface that shifted V_0 to more positive values.[27] OTS treatment lessened this effect, though it is not assumed that all the interface states are removed.

Literature studies of the effect of humidity on pentacene, suggest that water molecules or mobile ions are preferentially attracted to grain boundaries where they can act as hole traps.[14-16] At higher concentrations of water, there would be a greater proportion of traps and the hole currents would be decreased. As water can act as a p-type dopant, greater concentrations increase the acceptor density driving the Fermi level down towards the HOMO of the polymer. This changes the Fermi level at the interface and empties the interface and trap states, shifting V_0.



The HOMO level (I_P) of the 97.5% RR polythiophene is 4.8eV so the acceptor level would lie closer. Thus, ionisation is easier, the material dopes faster and shifts are more dramatic with increasing H_2O concentration.

Figure.3.17. Diagram showing the energy levels of the semiconductor at the interface. Interface states are depicted by the block, with the filled states (shaded section) having charge Q_{ins}. Water is a p-type dopant and its incorporation into the film would increase the acceptor density level N_A so that it, and the Fermi level, shift closer to the HOMO. Charge is subsequently released from the interface states.

A consequence of this is that the interface states have to be distributed in energy and must be intersected by E_F. Polythiophene is a polycrystalline material and it is plausible that traps exist at grain boundaries and the interface with a distribution of energies (considering the different conjugation lengths and polarisation interactions). Also, if traps were related to grain boundaries, the 97.5% RR polymer is more crystalline, thus more traps would be expected and the charge in these states should be higher thus shifting the switch-on voltage to higher values.

3.4.3. Morphology and diffusion related instability

Let us consider the effect increased crystallinity has on stability from a diffusion standpoint. Small molecules are known to have good air stability as their crystalline nature inhibits the diffusion of oxygen and water, though problems with diffusion at grain boundaries have been noted. The batch of polythiophene with higher regioregularity possesses a greater degree of crystallinity and the molecular packing

in the film should be improved. This alone should hinder the diffusion of species through the film as compared to the 90% RR polymer. A more regioregular film should contain more crystalline regions, so one could assume that it also contains more grain boundaries. The exact difference in the concentration of grain boundaries in the two films is not known, and x-ray diffraction studies are needed to clarify this. However, the degradation of the 97.5% RR polythiophene was far more rapid, with respect to a positive switch-on voltage shift and decrease of on/off ratio, indicating that the increased crystalline regions have a greater concentration of grain boundaries (which enable easy diffusion of ambient molecular species) or that electrochemical interactions and trap effects play a more dominant role.

3.4.4. Summary of mechanism for ambient doping of P3HT

It has also been suggested that water molecules can exert an electronic effect on device operation through adsorption on the surface layer. The large dipole moment of water (1.94D) could generate holes near the surface of the polymer if the molecular vertex made contact with the polymer.[15] Poor saturation of output characteristics in wet conditions suggests that the dominant conduction path is not affected by the depletion regime originating from the drain electrode which usually results in saturation behaviour. Hoshino et al. described the operation of a P3HT transistor in dry and wet nitrogen using the same mechanism.[17] As mentioned previously, nitrogen is relatively inert and not expected to undergo any reaction with the polymer. They observed a loss of saturation in the output characteristics in wet nitrogen, as well as increased conductivity.

This clearly indicates that at least two mechanisms must be occurring. On one hand, the bulk conductivity of the polymer is increased due to water diffusing into the bulk of the film. This results in loss of saturation behaviour (as seen when comparing

output characteristics of high and low humidity measurements) and decreasing on/off ratios. On the other hand, the ionisation potential of the polymer has a clear effect on the stability of the system with regards to ambient conditions and humidity. Measurements were carried out in identical environments with the same humidity levels, and systematic differences were found between higher and lower I_P materials. The closer the ionisation potential is to that of the reduction potential of oxygen, the less stable the polymer is in ambient, which can also be represented by a shifting switch-on voltage. This is dependent on whether the polymer is initially oxidised (doped) as if it is then reduced V_0 will shift negatively, whilst if it is oxidised V_0 can shift positively.

This is still conjecture, but so far we have been able to conclude that water is most detrimental to device performance. This is promising as dry environments are easier to maintain than completely inert atmospheres. For example, Philips insert a desiccant into their encapsulated polymer light emitting diodes (PLEDs). Increased stability is observed at R.H. of 20% rather than 50%, which can occur naturally in lab so it is not unfeasible to carry out any initial fabrication steps (before encapsulation) in this environment.

3.5. Increasing the air stability of P3HT via the introduction of dopants

Semiconducting polymers generally have a low level of conductivity if no dopants are present. As we have just seen, p-type dopants can be introduced unintentionally by redox charge transfer reactions with oxygen and water. The main effect of this is to increase the off-current and shift the switch-on voltage to more positive values. A high on/off ratio is an important parameter for good transistor behaviour and this is greatly reduced on exposure to ambient conditions. The conductivity can be increased by increasing the doping level as more carriers can transport charge in the

film. There are controlled ways of doping polymers. Protonic doping using strong acids results in a loss of solubility and processibility and decreases the effective conjugation length as sp^2 carbon atoms are protonated (electron removed) to form sp^3. This reduces the conductivity though raises the ionisation potential of the polymer, affecting the stability.[28]

Unlike protonic doping, oxidative doping involves oxidation of the polymer backbone in association with a negative counterion. As we have just discussed, a requirement of this is that the reduction potential of the oxidant is more positive than the oxidation potential of the polymer. The difference between the reduction and oxidation potentials of these chemicals says whether a reversible charge complex forms (as in the case of oxygen) or whether complete electron transfer occurs. Thus, one way to increase the air stability of P3HT is to dope it in order to change the density of states distribution of the HOMO and LUMO levels in order to make it more oxidatively stable.

3.5.1. Experimental techniques

A 2-3% wt. solution of P3HT in dichlorobenzene (DCB) was made up with 0.05% (2, 3-Dichloro-5, 6-dicyano-1, 4-benzoquinone) (DDQ). This dopant is an electron acceptor and its chemical structure is illustrated in Fig.3.18. A control sample containing no dopant was made up at the same time, so that comparisons could be made. All preparation steps and initial measurements were carried out under nitrogen. The sample was then removed to air and measured continuously, as described in Section 3.2.

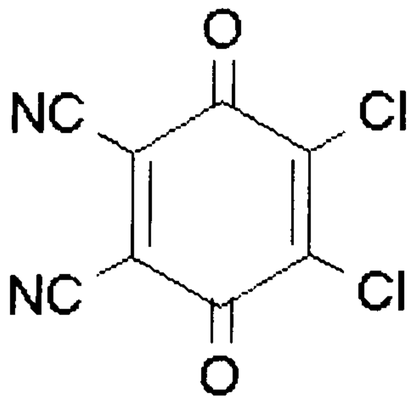


Figure.3.18. Chemical structure of DDQ.

3.5.2. Increasing the stability of P3HT transistors using 0.05% DDQ

Fig.3.19 compares two transistors of 92% RR P3HT taken into air. There is a marked difference in the stability of the doped sample with regards to the undoped sample. As one would expect, on and off currents are higher for the doped transistor by an order of magnitude. The switch-on voltage is more than doubled, being +87V under nitrogen. The increased switch-on voltage can be explained by the fact that mobile charges have been introduced in the channel.

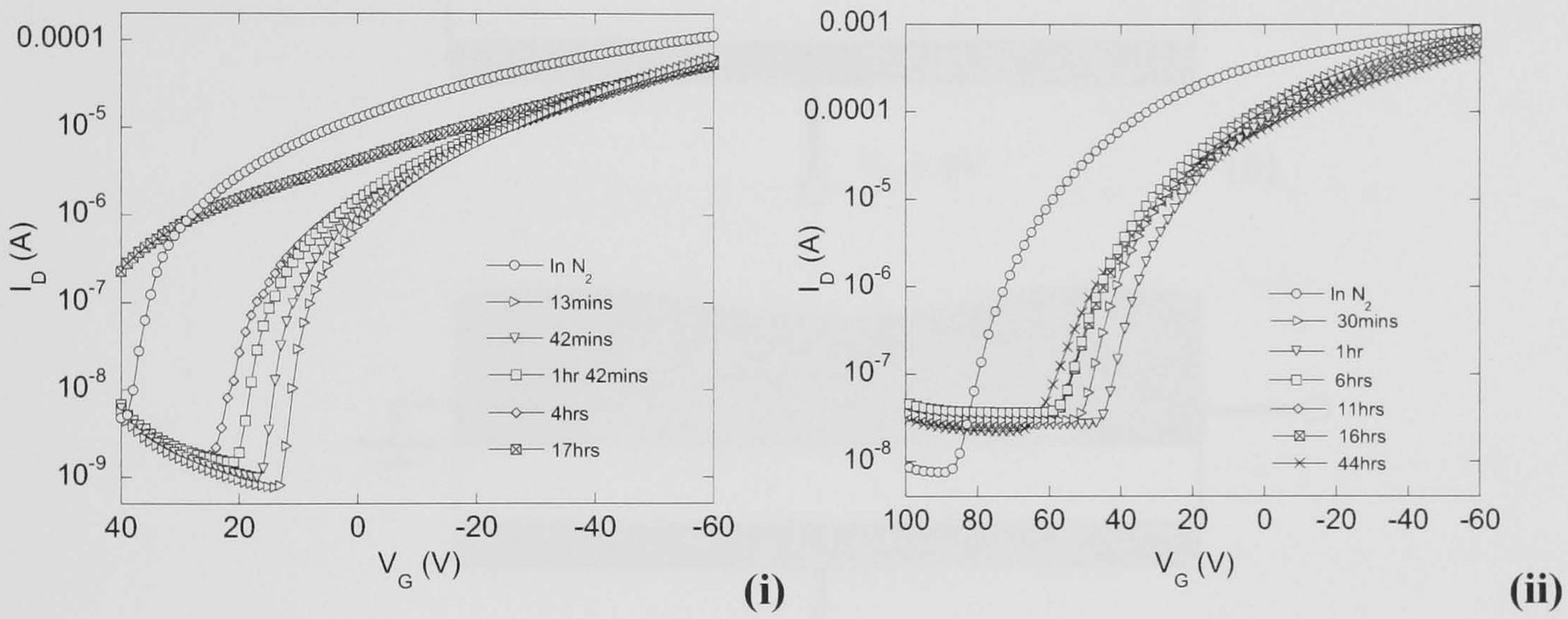


Figure.3.19. Saturated transfer scans run continuously over time for (i) non-doped and (ii) 0.05% DDQ doped P3HT transistors in ambient. These data were provided by Richard Simms.

In accumulation the charge density is dependent on the applied gate bias. However, there is an additional flow of current through the bulk material as the oxidised polymer cations (DDQ oxidises the polymer by accepting electrons) are associated with negative counterions. If the transistor is operated in depletion (positive applied gate bias), holes are depleted from the interface. Bulk conduction can still occur, as in this case, mobile ions are also present in the bulk. Thus a higher positive V_G is required to deplete all the positive charges in the film, as illustrated in Fig.3.20.

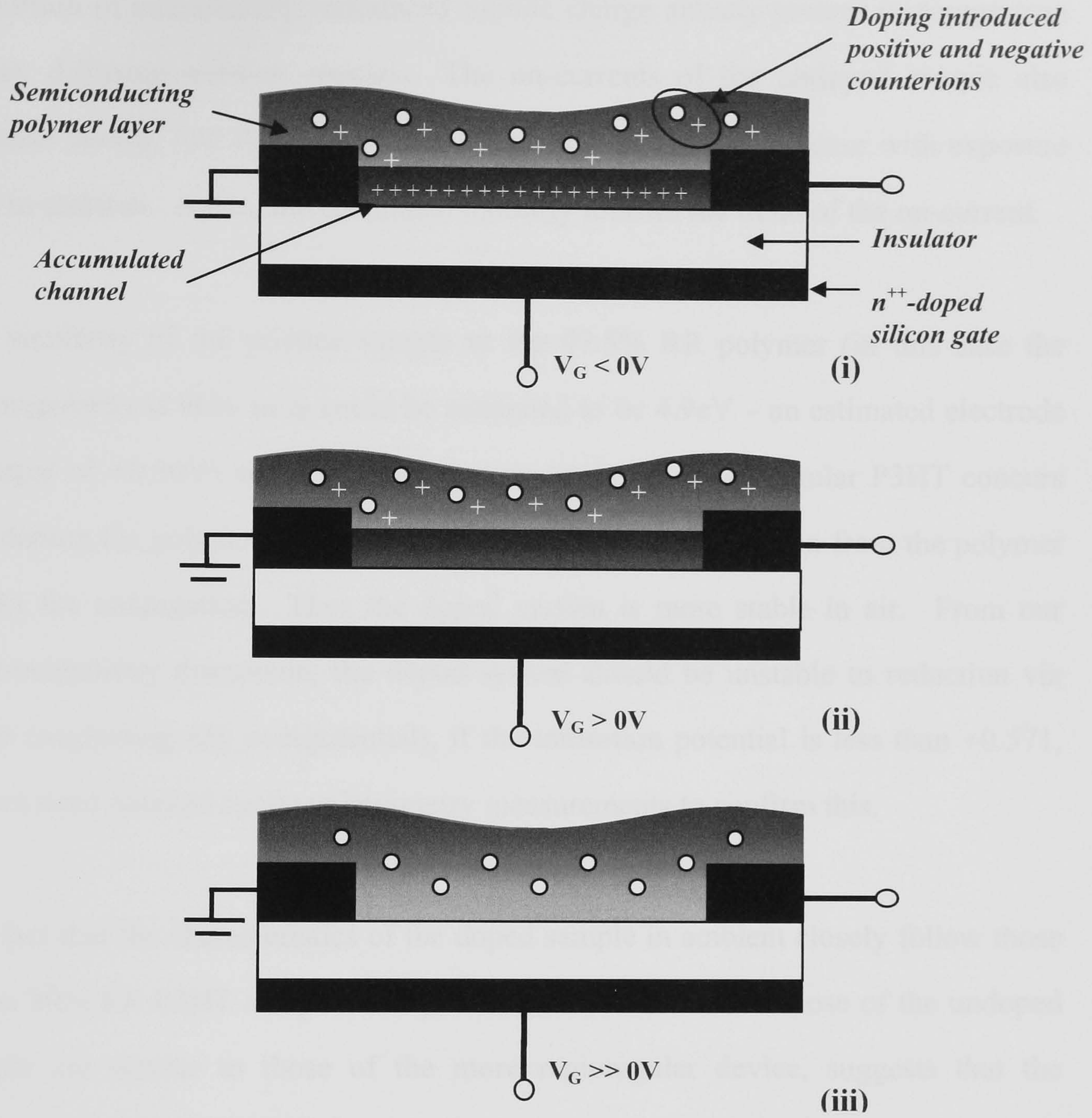


Figure.3.20. If V_G is negative a conducting channel of positive charge accumulates at the interface. If the semiconductor is doped, there will be an extra flow of current through the bulk due to these extra mobile charges, as depicted in (i). As the gate voltage is shifted to positive values a depletion region forms in the channel, but conduction can still occur in the bulk (ii). The transistor will not switch off until the entire semiconductor is depleted (iii) shifting the switch-on voltage to more positive values. Figure adapted from[19].

Though the measurement scan ranges are different, we can see that the stability of the doped sample is improved with respect to the non-doped sample. A negative then positive V_0 shift is seen for the doped sample – shifting positively after an hour of air exposure. The on-currents decrease slightly though the off-currents remain relatively stable for the doped sample. This could be due to there being a larger

proportion of intentionally introduced mobile charge already present in comparison to any diffusing ambient species. The on-currents of the undoped sample also decrease slowly, and the off-currents and switch-on voltage increase with exposure time to ambient. Again, the calculated mobility follows the trend of the on-current.

The similarity of the pristine sample to the 97.5% RR polymer (in this case the regioregularity is 96% so I_P could be estimated to be 4.9eV – an estimated electrode potential of +0.50V) and the doped sample to the less regioregular P3HT concurs that doping the polymer raises the I_P as the removal of an electron from the polymer breaks the conjugation. Thus the doped system is more stable in air. From our electrochemistry discussion, the doped system should be unstable to reduction via water (neglecting any overpotential), if the ionisation potential is less than +0.571, but we need detailed cyclic voltammetry measurements to confirm this.

The fact that the characteristics of the doped sample in ambient closely follow those of the 90% RR P3HT sample on exposure to dry air, and that those of the undoped sample are similar to those of the more regioregular device, suggests that the difference between the doped and undoped sample is centred around the ionisation potential. We do not know the exact proportion of oxidised polymer in the doped system but we can assume a range of conjugation lengths is available and that depending on the oxidation state and I_P of each chain, oxidation or reduction can occur. Both water and oxygen are necessary requirements for these reactions. Faced with the similarity of the doped p-type polymer with the 90% RR device, we can conclude that an initial negative voltage shift due to dedoping via reduction or nucleophillic substitution of the polymer cations is reasonable.

Even if the ambient measuring environment is the same, clear differences in the behaviour of different regioregular polymer transistors are evident. Though

deterioration of device characteristics is clearly time dependent with regards to the concentration of water molecules present, this dependence does rely on electrochemical stability. This is reflected in the ionisation potential, which can be tailored to resist oxidation by:

(i) Reducing the regioregularity, though this worsens device characteristics as charge transport is worsened.

(ii) The addition of dopants, though high V_0 and off-currents result due to increased mobile charges. This also increases the on-currents and mobility.

(iii) Manipulation of the chemical structure so the conjugation along the backbone is reduced.

The latter point will now be discussed.

3.6. Ambient stability of syn-pBTTT and ant-pBTTT transistors

Solution-processible polymers containing thiophene backbones are widely used in transistor applications. Regioregular polythiophene transistors have demonstrated mobilities of $0.1 cm^2/Vs$, as the polymer chains self-organise to form well-ordered lamellae with co-facially stacked backbones. This enables efficient charge transport along the π-π conjugated backbone, leading to relatively high mobilities.[10] The ionisation potential of polythiophene ranges between 4.8-5.1eV, making it prone to p-type doping via oxygen. This instability in air leads to increased off currents and instabilities in the switch-on and threshold voltages, in some cases shifting by as much as ±20V.

Ong et al. at Xerox have also recently reported an air stable solution-processible polythiophene derivative poly (3, 3''-dialkyl-quaterthiophene) (PQT), tailored to retain structural order whilst containing unsubstituted thienylene moieties that act to lessen the conjugation, in turn increasing the oxidative stability of the system.[29,30] Heeney et al. at Merck Chemical Ltd. developed a thiophene based co-polymer with increased stability in ambient conditions. This was achieved by breaking the conjugation along the backbone by the insertion of fused thieno [2, 3-b] thiophene units. The cross conjugated central double bond inhibits π-π delocalisation along the backbone, decreasing the conjugation length and increasing the ionisation potential to 5.3eV, suggesting a better stability to p-type oxygen doping as compared to polythiophene.[7] The polymer structure of (poly (2, 5-bis (3alkylthiophen-2-yl) thieno [2, 3-b thiophene) (syn-pBTTT) is illustrated in Fig.2.3 in the materials section of Chapter 2. The table summarises data for the three polymers.

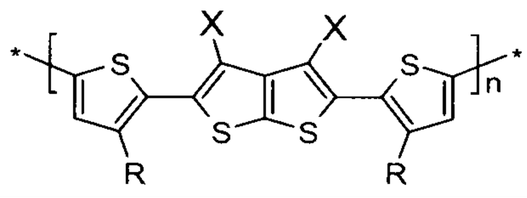
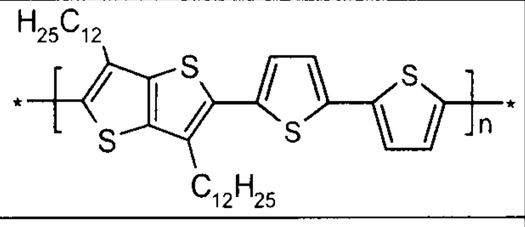
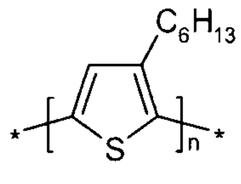
Polymer Name	Chemical Structure	I_P/E (eV/V)	Mobility (cm^2/Vs)	Operational time (Days)
Syn-pBTTT		5.3 (0.9)	0.03	84
Ant-pBTTT		5.1 (0.7)	0.14	4
P3HT		5.0 (0.6)	0.03	1

Figure.3.21. Table comparing the ionisation potential I_P (the calculated electrode potential is given in brackets), saturated mobility and stability in ambient of three thiophene based polymers.

Ant-pBTTT also consists of a fused thiophene unit breaking up the conjugation but to a lesser extent, as the sulphur atoms are anti-symmetric. The ionization potential

in this case was 5.1eV.[8] This improves the hole injection barrier with respect to syn-pBTTT so better device performance and worsened stability is observed. The best stability is achieved with syn-pBTTT, though the mobilities are lessened. However, the decrease in mobility with time of syn-pBTTT is much more retarded than ant-pBTTT, as the saturated mobility drops immediately to $10^{-2}cm^2/Vs$ on exposure to ambient conditions, whilst after 83 days the mobility of syn-pBTTT drops from $2.3 \cdot 10^{-2}cm^2/Vs$ to $1.5 \cdot 10^{-2}cm^2/Vs$. As all experiments were carried out under the same conditions and on the same substrates, differences can be attributed to the ionisation potential and consequent stability towards oxygen. The electrode potentials are shown in brackets in the table of Fig.3.21.

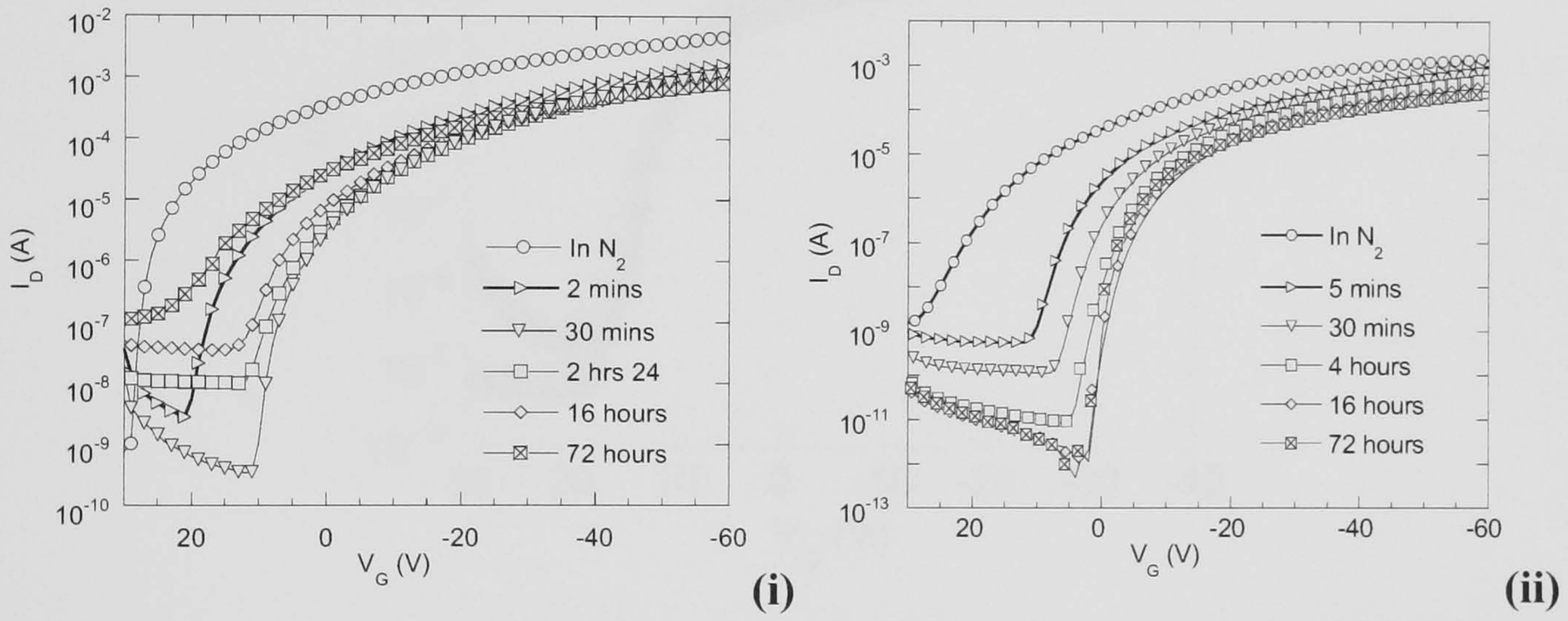


Figure.3.22. Evolution of saturated transfer characteristics of 20μm channel length ant-pBTTT transistors with time, as measured in (i) laboratory ambient and (ii) <5% R.H air.

Fig.3.22 shows differences of the saturated transfer characteristics of ant-pBTTT FETs in ambient and low humidity conditions with respect to time. A negative V_0 shift is initially observed for both devices, but this shifts back to positive values after the second scan, for the transistor measured in ambient, whilst the off-currents start to increase. If an identical device is measured in drier air (<5% R.H.), a slower negative switch-on voltage shift is observed, stabilising after 16 hours. Again, this is a dramatic difference of material behaviour in the presence of higher water concentrations, following the same trends as observed for the 90% RR polythiophene

transistor (with $I_P \sim 5.08eV$). The high initial V_0 also indicates that the material could be unintentionally doped, and the negative shift and decreasing off-currents could then correspond to the polymer being reduced by water.

Fig.3.23 shows a comparison of ant-pBTTT transistors made in and measured in dry air. In this case, all fabrication and measurement steps, including solution preparation and annealing, were carried out in a dry air glove box (purged with compressed air – R.H. >0.1%).

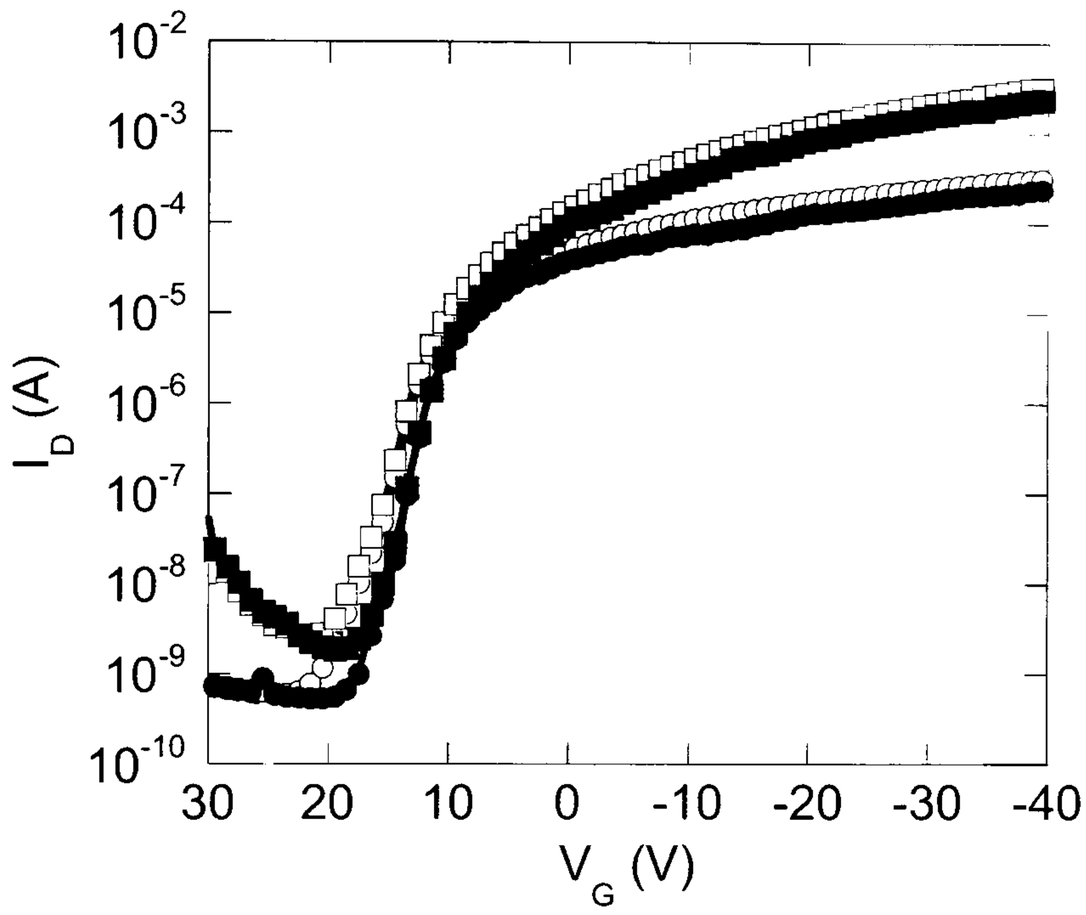


Figure.3.33. Linear (circles) and saturated (squares) transfer characteristics for ant-pBTTT made and measured in dry air immediately after fabrication (open shapes) and after a weeks exposure (filled shapes).

High mobilities of $0.15cm^2/Vs$ were achieved with stable device characteristics for at least four months. These are very promising results if we consider that large-scale processing is easier to carry out in dry air rather than an inert environment. As low water levels stave off degradation, perhaps initial fabrication steps could be carried out in such as an environment, using encapsulation techniques to prolong device stability in harsher conditions.

The ionisation potential is an important factor when it comes to designing materials for use in polymer electronics. Charge carriers have to be injected into organic systems, so an I_P similar to the injecting contact is necessary for efficient hole injection. Gold or PEDOT:PSS are the most commonly used electrodes with $\Phi \sim$ 5.1eV and Mallarias et al. have proposed that the contact is Ohmic as long as the workfunction difference is $\leq$0.3eV.[31] Unfortunately this leaves the material prone to oxidation by the ambient species, water and oxygen. A trade-off between a higher ionisation potential and consequent limitations to device performance has to be realised. All polymers showed excellent stability under nitrogen, no matter what the ionisation potential of the material was. Water degrades device performance to a greater extent than oxygen alone and degradation can be noticeably retarded by operating the transistor in a low humidity environment. If the penetration of oxygen and water into the polymer matrix could be obstructed this should have the same effect.

3.7. Encapsulation and device performance

There have recently been mixed reports concerned with the air stability of P3HT transistors. Ficker et al. submitted top gate P3HT FETs and ring oscillators to shelf life and device tests in an ambient environment (without exposure to direct sunlight).[32] Shelf life measurements compared the characteristics of an as-prepared transistor with one tested a year later. The on-currents decreased by 14%, whilst the off currents increased by 40%. However, the on/off ratio was still suitable for integrated circuit applications. Operational stress tests were also carried out by continuously running a transistor with V_{DS} of -10V and a 0 to -10V 1 kHz alternating bias applied to the gate. The response was measured over a period of 42 days and although fluctuations due to light (which increases the output current) were observed, the signal remained relatively stable.

Ring oscillators also remained operational for up to 9 days. Though the devices measured were technically unencapsulated, the active polythiophene layer was to an extent protected as the device structures were top gate. Thus, the insulator (and metallic electrodes) acts as a shielding layer hindering diffusion of oxygen and water species into the air sensitive polymer. Increased degradation in performance would be expected for bottom gate devices in which the semiconducting polymer has an open surface. Devices were also prepared in air, so any initial deterioration in characteristics (which is typically observed on comparing a device measured in air after removal from the glove box to its previous characteristics) may not be observed.

Encapsulation is a method used to isolate the active polymer layer from the environment, and though operational stability is significantly improved, another manufacturing step is added. So far all measurements have been carried out on bottom gate transistors with bottom contacts, exposing the entire polymer surface to ambient. It certainly seems that a sort of encapsulation is needed to make such devices useful in longer term applications. This has been confirmed by comparing the characteristics of top gate devices with bottom contact structures. Bottom contact structures in effect possess an open surface which is more susceptible to direct attack for ambient species. Top gate devices consist of the polymer active layer being shielded by metallic contacts as well as the insulating layer. A method of protecting bottom contact devices is to spin-coat a layer of insulator on top of the polymer layer to hinder diffusion of the water and oxygen molecules. This gives devices with approximately triple the lifetime of the open surface. The best result we found was with a hydrophobic fluorinated insulator dissolved in butanone.

The graph in Fig 3.34 compares an as prepared ant-pBTTT 20μm channel length transistor with a continuously measured unencapsulated device three days later, and

a device encapsulated with a hydrophobic fluorinated insulator. The initial characteristics of the encapsulated and unencapsulated devices were similar, so for clarity only the transfer characteristic of the encapsulated device is shown. Use of the encapsulation layer, significantly improves device performance as the off-current only increases slightly, whereas the uncapped sample has an off-current of μA after the three days. The physical barrier to the diffusion of water and oxygen is clearly effective and is necessary for stable devices.

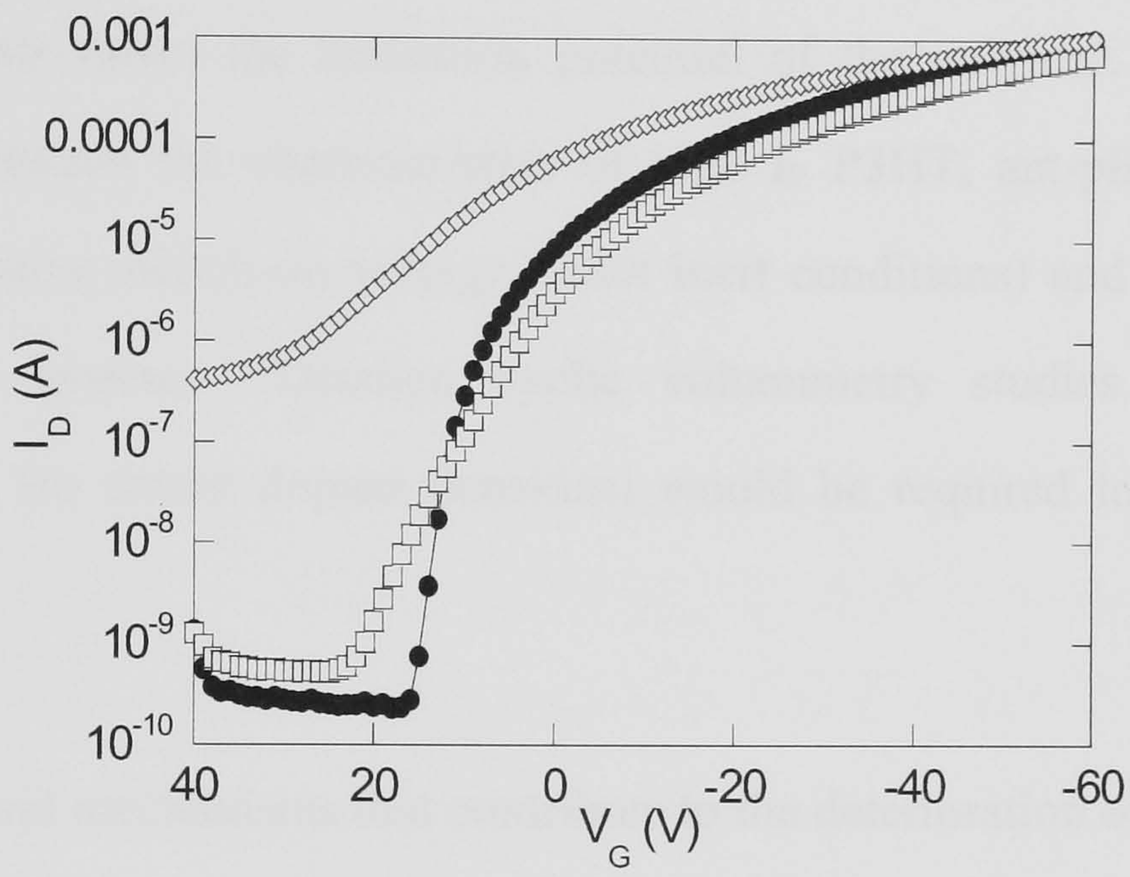


Figure.3.34. Saturated transfer characteristics for 20μm channel length ant-pBTTT transistors made and measured under ambient conditions. The filled shapes indicate the first scan, the open diamonds the transistor as measured after 3 days without encapsulation, and the open squares the transistor with a hydrophobic fluorinated encapsulation layer spin-coated on top.

3.8. Conclusions and further work

The ionisation potential is an important parameter for determining stability, as can be seen from the trend of increased stability with ionisation potential. The ambient stability of thiophene based polymers in this work support this order as syn-pBTTT > ant-pBTTT > 90% RR P3HT > 97.5% RR P3HT. A distribution of conjugation lengths and conformations leads to a range of ionisation potentials. Estimations of

the HOMO of P3HT suggests it is borderline stable to electrochemical attack, and could be oxidised or reduced. If a neutral polymer chain has an I_P less than 4.97eV it can be oxidised by oxygen and water. Alternatively, if an oxidised polymer chain has an I_P more than 4.97eV it can be reduced. This discussion neglects any overpotential necessary for the reactions to occur. The high V_0 of P3HT (even if fabricated and measured under N_2) indicates that the device could be unintentionally doped, so it seems reasonable that on exposure to ambient both reduction and oxidation processes can occur. Doping of the P3HT also results in improved stability, as this raises the ionisation potential of the polymer. There are close similarities between the characteristics of high I_P P3HT, ant-pBTTT (which also exhibits a positive switch-on voltage under inert conditions) and the doped low I_P polythiophene system. Detailed cyclic voltammetry studies and capacitance measurements (to detect dopant densities) would be required to fully understand these effects.

There are several mechanisms that contribute to the deterioration of characteristics in ambient. Photoinduced oxidation and the formation of a charge transfer complex with oxygen are two of the most recognised mechanisms. Both water and oxygen both influence device characteristics and both are necessary for electrochemical redox reactions to occur. Water affects device characteristics most severely. Exposure to high humidity levels results in increasing off-currents, switch-on voltages and hysterisis. These effects have been observed in wet, oxygen-free environments indicating that this process relies only on the presence of water. Deterioration is a time dependent process, depending on the rate of diffusion of water into the polymer film. The close packed structure of crystalline systems are most resistant, though there is evidence that water can diffuse and reside at grain boundaries trapping charge carriers. A polar molecule such as water and its associated ions (H^+ and OH^-) could also disrupt charge transport by screening the

applied electric field, and increasing the energetic disorder. This work has shown that water is the main culprit in instability to ambient conditions. Fabrication and operation of devices in dry air significantly prolongs device lifetimes as does encapsulation with a 1μm thick hydrophobic insulating layer, simply spin-coated on top of the polymer layer of a bottom contact device. The latter forms a physical barrier to diffusion of ambient species into the polymer film. From an industrial point of view, it is easier and more cost-effective to fabricate devices in a low humidity (rather than inert) environment. Significant improvements in performance are seen for a relative humidity of 20%, so fabricating the device in such an environment combined with encapsulation would result in more stable and reliable devices.

Relative humidity in laboratory conditions can vary from 50% to 20% over a period of several days so a controlled measuring environment is necessary to obtain meaningful results. Industry standard uses 85% R.H. and 85°C conditions to test device performance, but it should be noted that there are significant differences between shelf-life and operational stability. There is no standard for ascertaining the stability of these materials so it is hard to make comparisons from literature studies. This work only provides an introduction to the causes of instability in these systems and though the effects of humidity and ionisation potential were discussed, further work needs to be done to confirm the precise mechanisms involved. The addition of antioxidants has also been shown to improve ambient stability, as has blending insulators with the semiconducting polymer.[33,34] There is also a great deal of further work to be done in this field involving combining spectroscopic measurements (such as photoluminescence photo-oxidation and FTIR studies), cyclic voltammetry, and modelling of dopant densities using capacitance measurements. Clear differentiation should also be made of operational and shelf-life stability before we can fully understand the processes contributing to degradation.

References

1. A. R. Brown, C. P. Jarrett, D. M. de Leeuw, M. Matters, *Syn Met.* **88** 37-35 (1997)
2. H. Sirringhaus, T. Kawase, R. H. Friend, T. Shimoda, M. Inbasekaran, W. Wu, E. P. Woo, *Science* **290** 2123-2126 (2000)
3. G. Horowitz, *Adv. Mer.* **20** 365-377 (1998)
4. H. Sirringhaus, N. Tessler, R. H. Friend, *Science* **280** 1741-1744 (1998)
5. H. Sirringhaus, N. Tessler, D. S. Thomas, P. J. Brown, R. H. Friend, in *Advances in Solid State Phys ics* **39** 101-110, B. Kramer. Ed. (Vieweg, Braunschweig, Germany) (1999)
6. As estimated from photoelectron spectroscopy AC-2 measurements by Masayoshi Suzuki of Merck, Japan.
7. M. Heeney, C. Bailey, K. Genevicius, M. Shkunov, D. Sparrowe, S. Tierney, I. McCulloch, *JAm. Chem. Soc.* **127** 1078-1079 (2005)
8. I. McCulloch et al., To be published in *Nature M terials* (2006)
9. M. S. A. Abdou, F. P. Orfino, Z. W. Xie, M. J. Deen, S. Holdcroft, *Adv. Mer.* **6** 11 (1994)
10. H. Sirringhaus, P.J. Brown, R. H. Friend, M. M. Nielsen, K. Bechgaard, B. M. W. Langeveld-Voss, A. J. H. Spiering, R. A. J. Janssen, E. W. Meijer, P. Herwig, and D. M. de Leeuw, Nature **401** 685-688 (1999)
11. A. Zen, J. Pflaum, S. Hirschmann, W. Zhang, F. Jaiser, U. Asawapirom, J. P. Rabe, U. Scherf, D. Neher, *Adv. Finct. Mer.* **14** 8 (2004)
12. E. J. Meijer, C. Detcheverry, P. J. Baesjou, E. van Veenendaal, D. M. de Leeuw, T. M. Klapwijk, *JAppl. Phys.* **93** 8 (2003)
13. T. Jung, A. Dodabalapur, R. Wenz, S. Mohapatra, *Appl. Phys. Lett.* **87** 182109 (2005)

14. Y. Qiu, Y. Hu, G. Dong, L. Wang, J. Xie, Y. Ma, *Appl. Phys. Lett.* **83** 8 (2003)

15. Z.-T. Zhu, J. T. Mason, R. Dieckmann, G. G. Malliarias, *Appl. Phys. Lett.* **81** 24 (2002)

16. D. Li, E. J. Borkent, R. Nortrup, H. Moon, H. Katz, Z. Bao, *Appl. Phys. Lett.* **86** 042105 (2005)

17. S. Hoshino, M. Yoshida, S. Uemura, T. Kodzasa, N. Takada, T. Kamata, K. Yase, *J Appl. Lett.* **95** 9 (2004)

18. D. F. Shriber, P. W. Atkins, C. H. Langford, *Inorganic Chemistry*, 2nd Edition Oxford University Press (1998)

19. D. M. de Leeuw, M. M. J. Simenon, A. R. Brown, R. E. F. Einerhand, *Syn. Met* . **87** 53-59 (1997)

20. Personal communication with J. Owen in the Electrochemistry Group at the University of Southampton

21. S. J. Zilker, C. Detcheverry, E. Cantatore, D. M. de Leeuw, *Appl. Phys. Lett.* **79** 8 (2001)

22. M. Matters, D. M. de Leeuw, P. T. Herwig, A. R. Brown, *Syn. Met* . **102** 998-999 (1999)

23. R. A. Street, A. Salleo, M. Chabinyc, *Phys. Rev. B* **68** 085316 (2003)

24. T. Lindner, G. Paasch, S. Scheinert, *J Appl. Phys.* **98** 114505 (2003)

25. D. B. A. Rep, A. F. Morpurgo, W. G. Sloof, T. M. Klapwijk, *J Appl. Phys.* **93** 4 (2003)

26. N. Kirova, S. Brazovskii, *Syn. Met* **76** 229 (1996)

27. L.-L. Chua, J. Zaumseil, J.-F. Chang, E. C.-W. Ou, P.K.-H. Ho, H. Sirringhaus, R. H. Friend, *Nature* **434** 194-199 (2005)

28. M. Lauritzen, *M Thes is* (1998)

29. B.S. Ong, Y. Wu, P. Liu, S. Gardner, *J Am . Chem. Soc.* **126** 3378-3379 (2004)

30. B.S. Ong, Y. Wu, P. Liu, L. Jiang, K. Murti, *Syn. Met.* **142** 49 (2004)

31. J. C. Scott and G. G. Malliaras, *Chem. Phys. Lett.* **299** 115 (1999)

32. J. Ficker, A. Ullmann, W. Fix, H. Rost, W. Clemens, *J Appl. Phys.* **94** 4 (2003)

33. A. Asimakis, *PhD Thesis* (2005)

34. As seen in preliminary results undertaken whilst at Merck Chemicals Ltd.

Chapter 4

Short channel effects in polymer field-effect transistors

This Chapter looks at the so-called short channel effects observed in polymer field-effect transistors. Downscaling device dimensions should result in increased switching speeds and mobility, but contact resistance becomes a problem if the channel length is decreased to < 5μm. This is due to injection problems, either a large barrier due to workfunction mismatch and/or bad morphology near the contacts. The effects can be reduced if ITO is used as an adhesion layer for gold instead of chromium. Additionally, we find the there is lateral field dependence of the mobility, as the pinch-off region expands into the channel when $V_D > V_G$. At high drain biases electron injection can occur from the gold electrode so that light emission is observed. This electroluminescence is in agreement with photoluminescence spectra so we can conclude that it is a property of the material. Emission is sensitive to trapping effects, as even low oxygen levels or the application of a continuous gate bias inhibit the EL.

Recent advances in material and device fabrication techniques have considerably improved the performance of polymer transistors. The field-effect mobility of devices has increased from 10^{-5} to 10^{-1}cm^2/Vs over the last few years, such that it is now competitive with that of amorphous silicon ($\mu_{\alpha\text{-Si}} > 0.1\text{-}1$cm^2/Vs).[1] Previously the poor mobility of organic materials resulted in the current of a transistor being mainly limited by the channel resistance. Higher currents make contact resistance a more significant factor and consequently, injection can be severely inhibited at shorter channel lengths with non-linear characteristics commonly observed in the output characteristics of polymers having non-ohmic contacts.[2]

Downscaling of device dimensions should result in enhanced currents, a higher operational frequency and a higher mobility, as the drain current is inversely proportional to L and the maximum switching frequency is proportional to μ/L^2. Another benefit of downsizing is that more components could be fitted onto an integrated circuit chip. However, as channel lengths become shorter, adverse effects can arise. These so-called short-channel effects are also observed in silicon MOSFETs due to the depletion layer widths of the source and drain junctions being of comparable magnitude to the channel length. This leads to carrier velocity saturation at higher electric fields, resulting in reduced currents. These effects are usually compensated for by scaling down the applied voltages and device dimensions accordingly, so that the internal electric fields remain similar to those of a long-channel device.[3]

The operation of a transistor can be thought of as two regimes, the linear and saturation, differentiated by the point at which $V_D \geq V_G$. The output characteristics of a long-channel transistor should show a clear differentiation between linear and saturation regimes. If the channel length of an OFET is decreased to $L \leq 5\mu$m (for typical insulator thicknesses (i.e. 200-300nm SiO_2)), the drain current exhibits non-

ohmic, superlinear behaviour at low V_D and the drain saturation current has a non-zero slope, implying a finite output conductance in the saturation regime. There appear to be two different effects contributing to the observed short-channel effects, so this Chapter is split into two main parts. The first section looks at the linear regime and the effect of contact resistance on devices with channel lengths ranging from 2.5μm to 20μm. The second looks at reasons for loss of saturation and increased mobilities at higher lateral fields, before discussing the phenomenon of light-emission from PFETs.

4.1. Short channel effects in the linear regime

4.1.1. Contact resistance of syn-pBTTT transistors

Fig.4.1 compares the output characteristics of a 20 and 2,5μm channel length syn-pBTTT transistor of width 1cm and gate oxide thickness 230nm. Clear linear and saturation regimes are evident for the long channel transistor, whilst the short channel transistor exhibits a lack of saturation at high drain voltages.

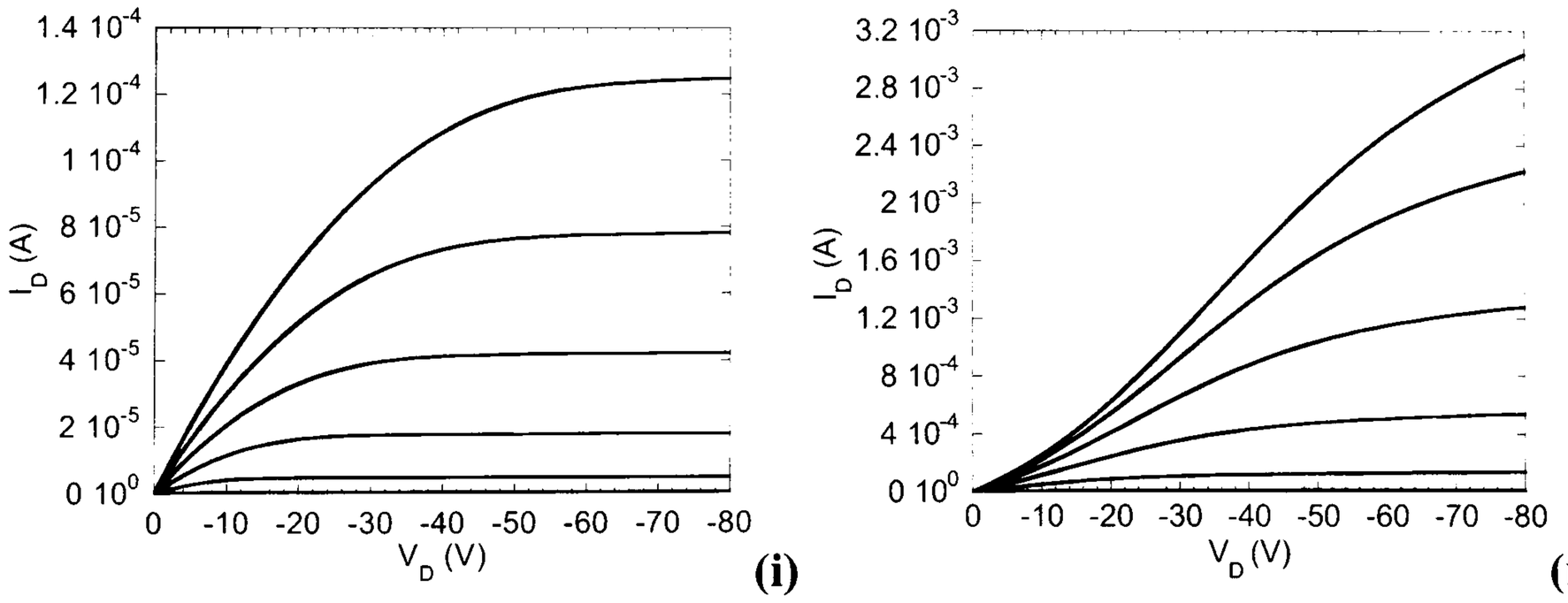


Figure.4.1. Output characteristics of a syn-pBTTT transistor with channel length (i) 20μm and (ii) 2.5μm fabricated on OTS treated gold pre-patterned Si/SiO_2 substrates. The channel width is 1cm. Both non-linearity and a lack of saturation are observed at low and high V_D, respectively, for the short channel length transistor, whilst the 20μm channel length device displays ideal behaviour.

This could be due to channel length modulation, mobility dependence on the lateral field or current induced heating effects, and will be discussed in the next section. The effect of contact resistance will firstly be considered, and is typically denoted by non-linear characteristics at low drain biases, which are clearly evident for the short channel device.

For the channel to accumulate in PFETs, charge carriers have to be injected from the source electrode. Schottky-Mott theory predicts that the contact will be ohmic if the workfunction of the injecting electrode is close to the HOMO (for holes) or LUMO (for electrons). Experimental studies and device modeling of OLEDs propose that this condition will be fulfilled if the injection barrier $\leq$0.3eV.[4] The workfunction of gold is assumed to be 5.1eV, as measured in ultra high vacuum (UHV) systems.[5] The conjugated polymer syn-pBTTT has an I_P of 5.3eV, implying that a small barrier to hole injection exists, if using gold as the injecting contact. In practice, a reasonably high contact resistance (of 10kΩ – 1MΩ order) is observed from device characteristics and quantative analysis. An explanation for this is that though gold is assumed to be relatively inert, in an ambient or a nitrogen atmosphere Φ_{Au} can drop to 4.6eV as a result of adsorbed molecules changing the surface dipole of the metal.[6] So though the hole injection barrier of 0.2eV for syn-pBTTT seems negligible, it is likely to be more than that expected from mere Schottky-Mott analysis.

Several methods have been derived to quantitatively estimate the contact resistance. The most frequently used is the transfer line method (TLM), which was developed from amorphous silicon TFT theory.[7] The resistance ($R_C = R_S+R_D$) at the contacts is assumed to be independent of the channel length and to be in series with the channel resistance, as illustrated in the circuit overleaf.

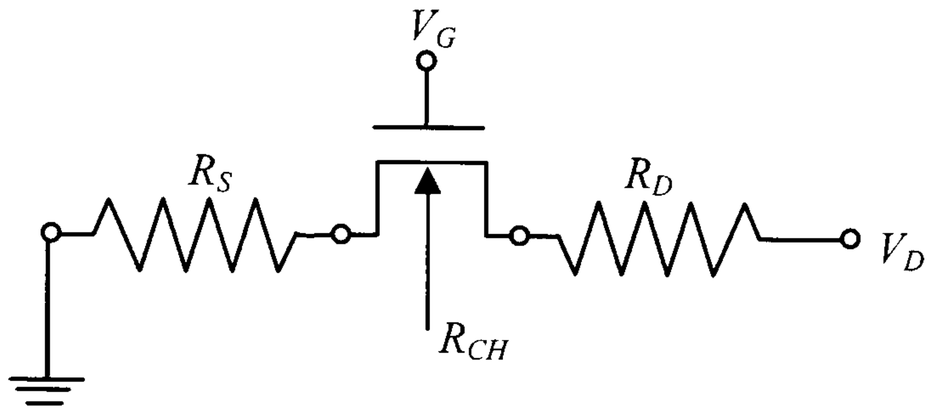


Figure.4.2. Equivalent circuit of an OFET taking into account the parasitic resistances at the source and drain electrodes, which are represented by the resistors R_S and R_D respectively. The channel is represented by a capacitor with resistance R_{CH}.

The effect of contact resistance on device performance is dependent on the magnitude of the contact resistance compared to the channel resistance. If the channel resistance is larger the contact resistance will be less pronounced. In the linear operating region of a transistor the channel resistance varies linearly with the channel length so that the total resistance, as calculated from the slope of the output characteristics in the linear regime, varies as:

$$R_{ON}(L) = \left.\frac{\partial V_D}{\partial I_D}\right| = R_{CH}(L) + R_C \qquad \{4.1\}$$

If the total device resistance is plotted as a function of channel length the contact resistance can be determined from the y-axis intercept. This is illustrated in Fig.4.3 (i). For this analysis, measurements are required for several devices. As it can't be assumed that the channel and contact resistances are identical for each device, three transistors of each channel length were typically measured on each substrate, and the average value used for analytical purposes.

The variation of the contact resistance with the gate voltage is also plotted in Fig.4.3 (ii) and R_C is observed to decrease with increasing gate bias. It ranges from 1.8MΩ

to 25kΩ for the syn-pBTTT transistor, which seems reasonable as it lies in between the values derived for P3HT (kΩ – I_P~5.0eV) and F8T2 (MΩ – I_P~5.5eV).[8]

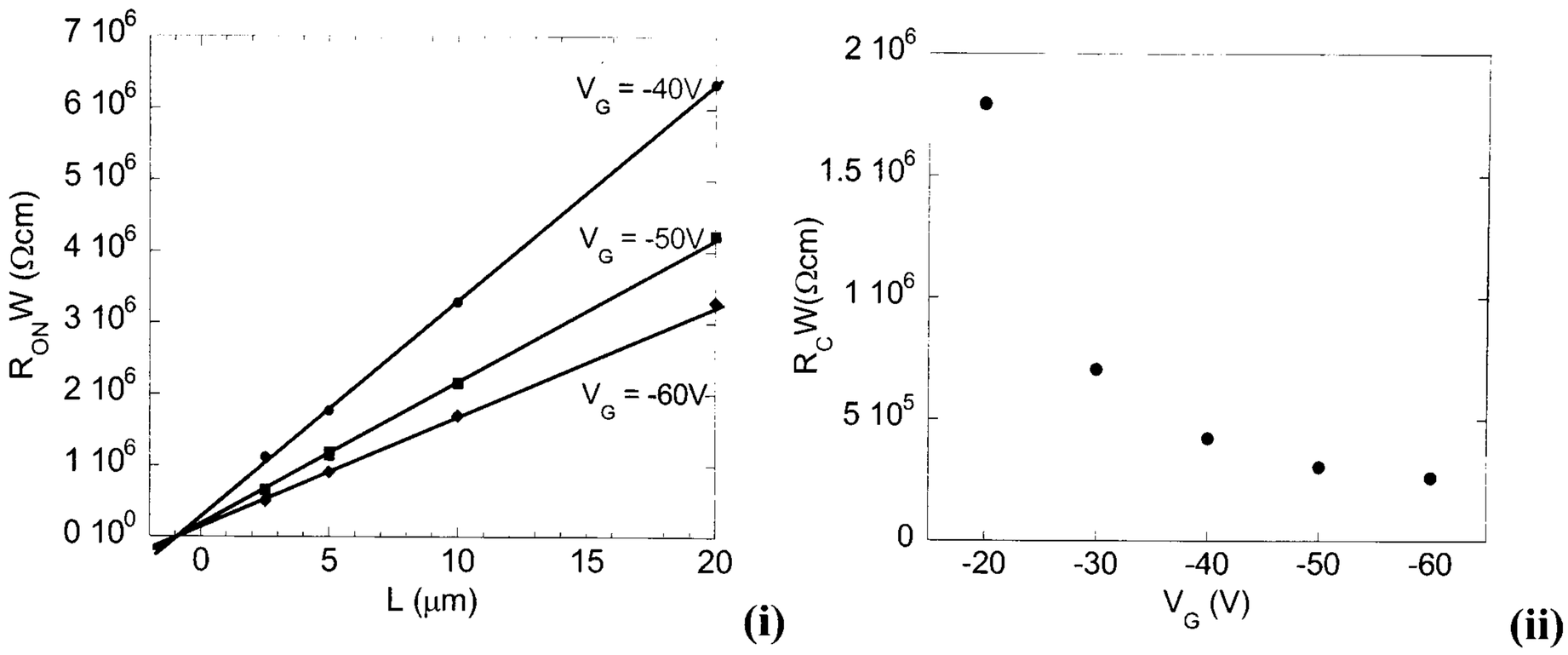


Figure.4.3. Analysis of contact resistances for OTS treated syn-pBTTT transistors with gold source-drain electrodes. (i) Width normalised channel resistance as a function of channel length for 3 different gate voltages. (ii) The contact resistance as a function of gate voltage.

From the gradient of Fig.4.3 (i) we find the channel resistance, the inverse of which is equivalent to the channel conductivity. Plotting this against the gate voltage should yield a straight line as:

$$\frac{\partial\left[\left(\frac{\Delta R_{ON}}{\Delta L}\right)^{-1}\right]}{\partial V_G} = \mu_{FE}(V_G)WC_i \qquad \{4.2\}$$

This can then provide a value for the mobility, corrected for the parasitic resistance and independent of the channel length.

A corrected mobility of 0.01cm^2/Vs and threshold voltage of -13V is extracted from the slope and intercept of the linear least squares fit. This matches the value derived from a conservative estimate of the saturated mobility (using V_0 rather than V_T) of

0.01cm^2/Vs and is 5 times larger than the mobility estimated from the linear equation of 0.002cm^2/Vs for a transistor with 2.5μm channel length. This method corrects for the contact resistance satisfactorily and shows that the R_C should be taken into account, especially if there is a significant difference between the mobility values derived from the linear and saturated regimes.

Another method of directly calculating the contact resistance was pioneered by Bürgi et al. and involved measuring the potential profile of an operating transistor.[9] This so-called scanning Kelvin probe microscopy (SKPM) is based on the Kelvin probe technique (explained in Section 2.2.2). In this case, changes in the resonant frequency are caused by an interaction with the surface. The contact potential is a sum of the local potential in the accumulation layer and the difference in the work function between the probe tip and the polymer film. Typically, a potential drop is evident at the injecting source and extracting drain electrodes, indicating a barrier to charge injection. In the case of ohmic contacts into P3HT they are of similar magnitude, but for a material like F8T2 with a higher predicted hole injection barrier, the potential barrier is larger at the source injecting electrode.[10]

4.1.2. Lowering R_C via an ITO adhesion layer

To promote adhesion of gold onto silicon dioxide, a thin adhesion layer of chromium or titanium is typically used. Unlike gold, chromium or titanium have good adhesion to silicon dioxide as they are more reactive metals, and form a thin oxide layer which prevents further oxidation as well as improving the sticking of gold. Leufgen et al. carried out a systematic study of the effect of varying the channel length and dielectric thickness on transistor performance.[11] By reducing the thickness of the gate oxide, good operational nanometre scale channel length transistors were realised, exhibiting reasonable saturation behaviour. The superlinear behaviour at small drain

voltages was ascribed to gate leakage currents, and was enhanced with thinner oxide thicknesses.

Analysis of contact resistance also showed that reducing the thickness of the titanium adhesion layer from 10nm to 1nm reduced R_C. The mobility was calculated from the saturated transfer characteristics using standard MOSFET theory, and although it decreased with decreasing channel length, this effect was lessened for thinner adhesion layers. This suggested that the Ti adhesion layer has a detrimental effect on device performance, and that as well as good packing of the first monolayers at the organic/oxide interface being essential for efficient charge transport, good physical contact at the electrodes is also of paramount importance. Sakanoue et al. fabricated transistors with 20nm thick photolithographically patterned gold electrodes with 10nm Cr or Al adhesion layers.[12] The drain current was on average 3 times smaller for the devices with Al/Au electrodes and hole injection was clearly worsened.

In this work, devices were fabricated on identically patterned substrates in which the adhesion layer was 5 or 3nm of chromium, or 5nm of indium (II) tin oxide (ITO).[13] ITO has a workfunction between 4.6 - 5.0eV, closer to that of gold than chromium, so using an ITO adhesion layer should have the same effect as reducing the thickness of a chromium adhesion layer. The devices prepared on substrates with an ITO adhesion layer showed improved characteristics for shorter channel devices. Transfer scans can exhibit severe hysterisis in shorter channel length transistors, with the switch on voltage shifting to more negative values on the reverse sweep. Longer channel devices on the same substrate do not exhibit this effect, similar to that observed in[14]. This hysterisis is reduced in devices with thinner chromium adhesion layers and is practically negligible in short channel transistors with ITO adhesion layers. Devices were all fabricated on the same silicon wafers with a 230nm

thermally grown oxide dielectric layer. The same polymer solution was used and all spin-coating and annealing procedures were carried out at the same time. All preparation was undertaken under nitrogen and the devices were measured in close succession to each other. These factors suggest that the hysterisis is related to the different adhesion layers.

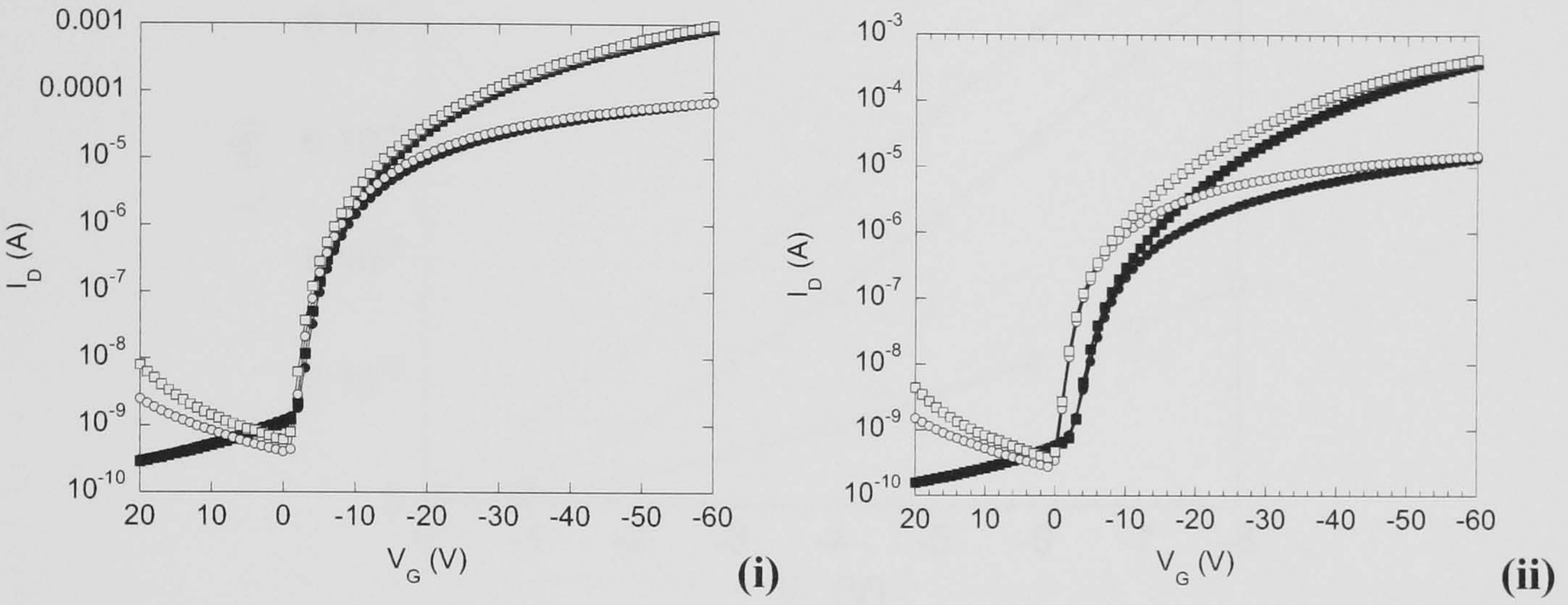


Figure.4.4. Forward (open shapes) and reverse (filled shapes) transfer characteristics in the linear (V_D = -5V) (circles) and saturated (V_D = -60V) (squares) regimes for OTS treated syn-pBTTT transistors with gold source-drain electrodes and (i) a 5nm ITO adhesion layer (ii) a 5nm Cr adhesion layer. Hysterisis between the forward and reverse transfer scans is present for the device with a 5nm Cr adhesion layer.

The devices with the 5nm Cr adhesion layer exhibit the lowest currents and most pronounced hysterisis. The ITO adhesion layer shows no hysterisis and the highest currents, and consequently mobilities, even at shorter channel lengths. 3nm Cr adhesion layer devices fall in between, exhibiting less hysterisis than 5nm Cr adhesion layer transistors but more than ITO adhesion layer devices. Increased hysterisis is suggestive of charge trapping at the contacts though the switch-on voltage does not fluctuate between devices.

Further differences are seen if the output characteristics of devices are considered. Fig.4.5 compares the output characteristics at V_G = -40V for the different adhesion layers.

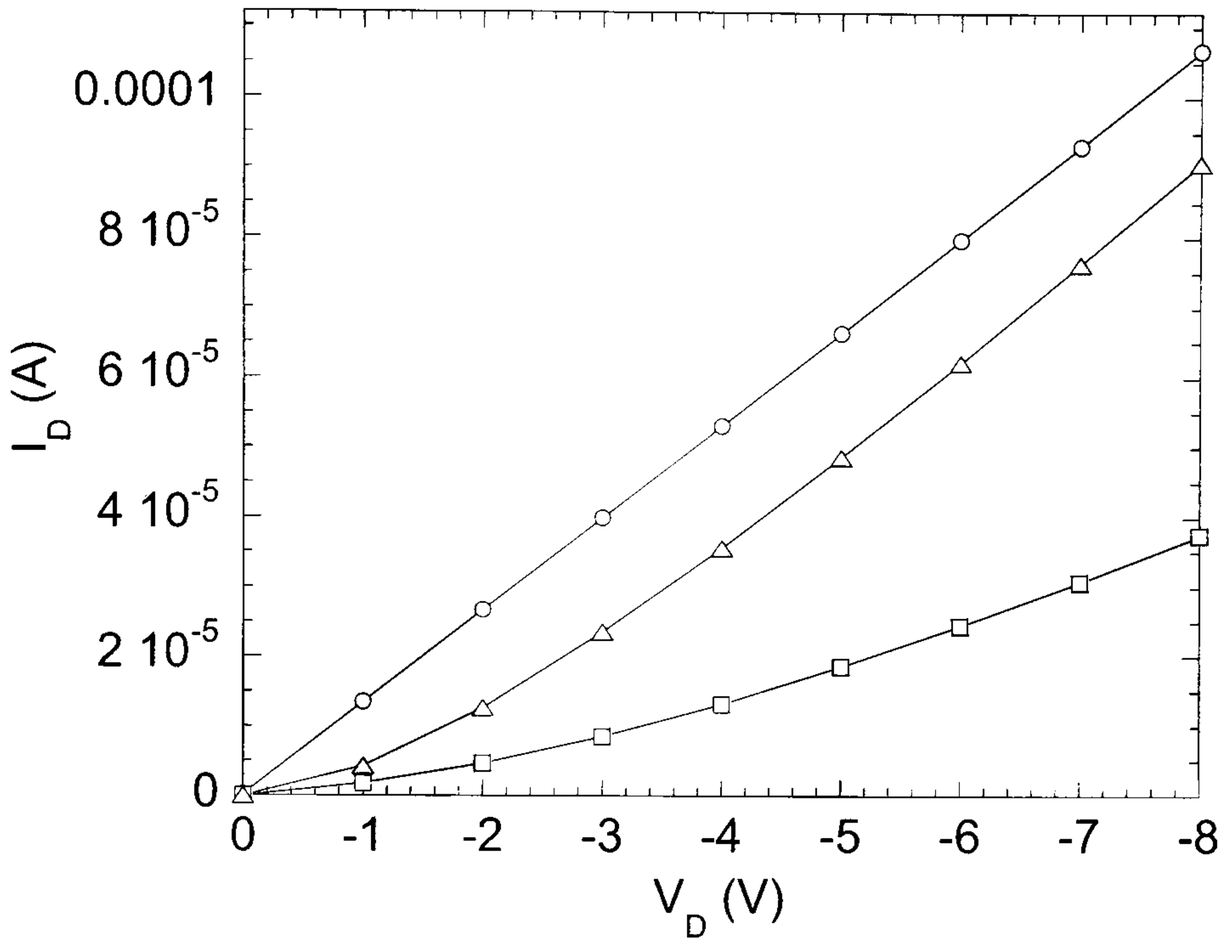


Figure.4.5. Linear output characteristics for OTS treated syn-pBTTT transistors with a 5nm ITO adhesion layer (circles), 3nm Cr adhesion layer (triangles), and a 5nm Cr adhesion layer (squares) for a gate voltage of –60V. Both the devices with Cr adhesion layers display non-linear characteristics in the linear regime, which is indicative of non-ohmic contacts.

The characteristics of the transistor with the ITO adhesion layer demonstrate higher currents and a linear relationship, indicating an Ohmic contact. The drain current progressively becomes less linear as the thickness of the chromium adhesion layer increases. This indicates that the ITO adhesion layer possesses the lowest contact resistance, and that R_C increases with increasing thickness of Cr adhesion layer. Contact resistance calculated using TLM confirmed this trend and saw a decreasing dependence with increasing gate voltage of 1.8MΩ to 250kΩ for the 5nm Cr adhesion layer, as illustrated in Fig.4.6. R_C ranged from 50kΩ to 6kΩ for the ITO

adhesion layer ~ almost an order of magnitude less. Again, the devices with the 3nm Cr adhesion lay between the two extremes, ranging from 600kΩ to 120kΩ.

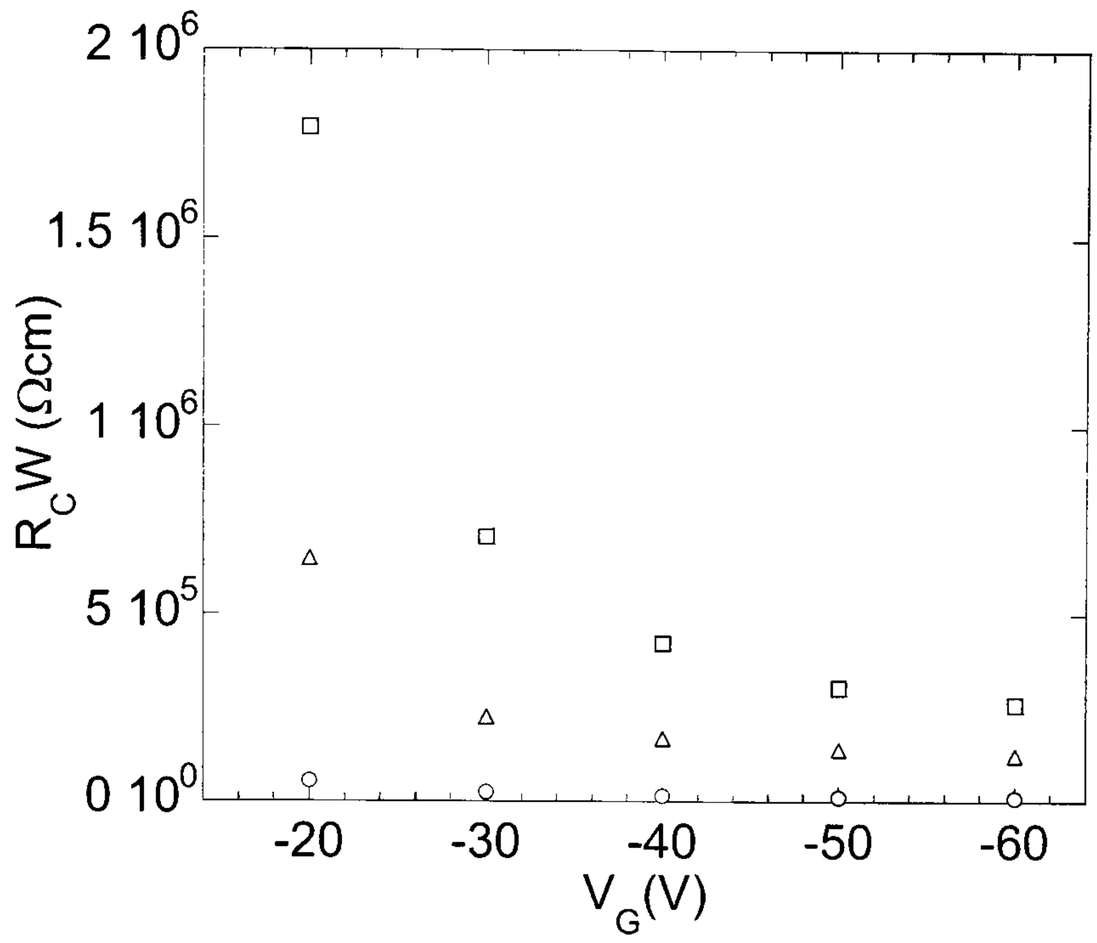


Figure.4.6. Variation of contact resistance with gate voltage for OTS treated syn-pBTTT transistors with a 5nm ITO adhesion layer (circles), 3nm Cr adhesion layer (triangles), and a 5nm Cr adhesion layer (squares).

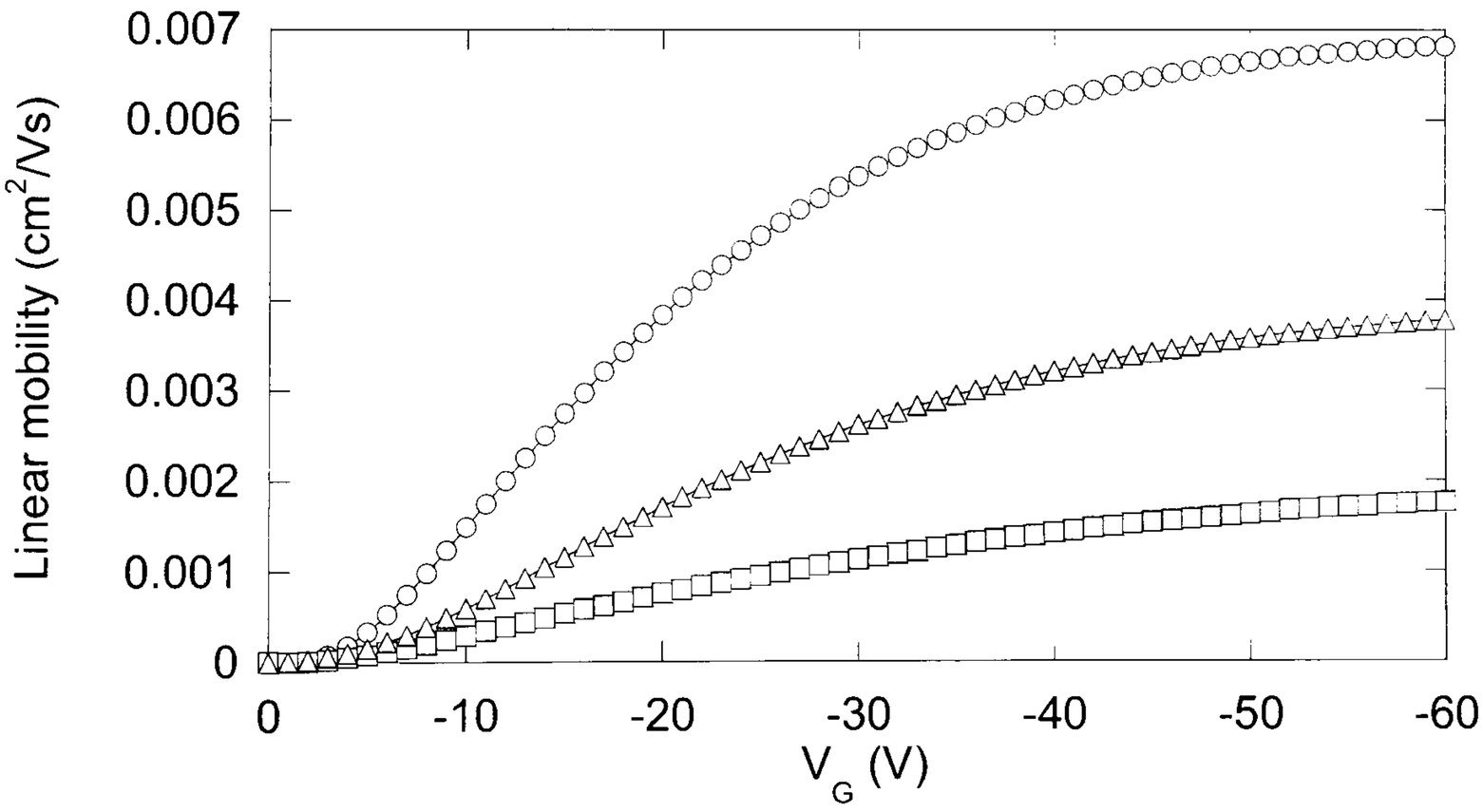


Figure.4.7. Variation of linear mobility with gate voltage for OTS treated syn-pBTTT transistors with a 5nm ITO adhesion layer (circles), 3nm Cr adhesion layer (triangles), and a 5nm Cr adhesion layer (squares) for a drain voltage of –5V and channel length of 2.5μm.

Contact resistance should only affect the mobility derived in the linear regime and the magnitude of μ_{LIN} should reflect the trend of decreasing contact resistance with ITO < 3nm Cr < 5nm Cr. The linear mobilities for the 2.5μm channel length transistors shown in Fig.4.7 adhere to this trend, being 4 times higher for the ITO adhesion layer transistor than the 5nm Cr adhesion layer device. Reducing the thickness of the Cr adhesion layer by just 2nm doubles the linear mobility. The better match of the ITO workfunction indicates that improved hole injection is responsible for the enhancement of the linear mobility.

These differences are significantly reduced for the mobility derived from the saturated characteristics, which is expected as μ_{SAT} should not be affected by R_C. However, devices with ITO adhesion layers still display higher saturated mobilities (1.5 times higher than those with a 5nm Cr adhesion layer) and the best overall performance. Another question to answer is why the hysterisis is reduced for devices with an ITO adhesion layer?

There are two possible reasons for this. Substrates with the chromium adhesion layer were fabricated with a standard lift-off technique. Reflection electron microscopy (REM) images, carried out by Ulrich Todt at the Fraunhofer Institute in Dresden, of the electrode edges show lift-off residues in the channel area.[13] These rough edges are not apparent in ITO adhesion layer structures. A different field distribution would arise as a result of these irregular features in the Cr adhesion layer case, possibly affecting the trap distribution and consequently the hysterisis. The deposition of gold onto chromium or ITO may also result in differing surface roughness, which could affect the crystallinity (and traps – related to grain boundaries) of the polymer film. AFM studies would be necessary to confirm this hypothesis.

Devices with 3nm thick Cr adhesion layers show better characteristics than 5nm thick Cr adhesion layer transistors, though the same fabrication process is used. It is accepted that the charge in the channel resides in the first monolayer at the insulator-semiconductor interface, but the distribution of charge in the accumulation layer follows a reverse square law rather than being a step function.[15, 16] A thinner adhesion layer suggests that the charge injection would be improved as the potential distribution is proportionally higher over the gold part of the electrode.

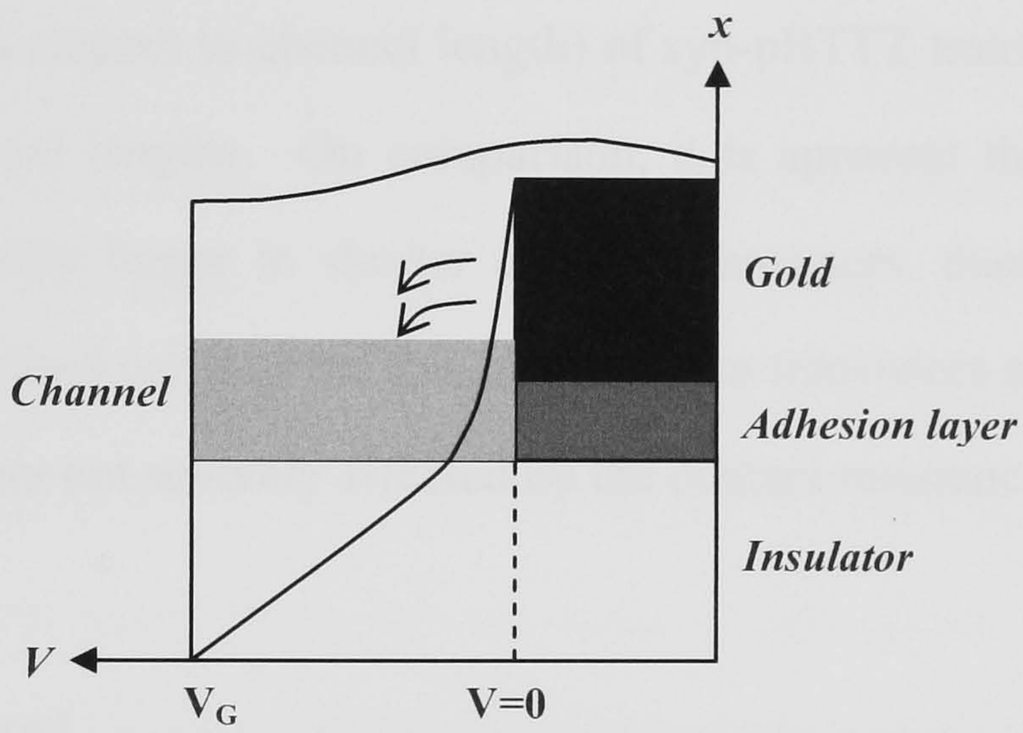


Figure.4.8. Schematic illustrating the variation of the potential distribution due to V_G in the polymer film. Gold is a better injecting contact than chromium, so the thinner the adhesion layer the more potential is dropped across the gold.

The best device performance is achieved using an ITO instead of a Cr adhesion layer, as a result of improved hole injection and better device patterning. This illustrates the importance of understanding the physics behind device operation, as the injection barrier is clearly a significant factor to consider when optimising transistor design and downscaling device dimensions. For the remainder of this Chapter, transistors with ITO adhesion layers will be used.

4.2. Short channel effects in the saturated regime

4.2.1. Lateral field dependence

It has also been seen in amorphous silicon transistors that the current and apparent mobility decrease with channel length.[7] This is attributed to a relatively larger fraction of the applied source-drain voltage being dropped over parasitic resistances, in comparison to longer channel length transistors. This is also observed in the case of P3HT and F8T2 transistors.[17,18] However, Fig.4.9 shows the normalised output characteristics (with respect to channel length) of syn-pBTTT transistors with 2.5, 5, 10 and 20μm channel lengths. On comparison, it is apparent that the normalised current is significantly larger in shorter channel transistors, than in long channel devices. The normalised currents for the 20 and 10μm transistors are comparable, as is expected if they are not severely affected by the contact resistance.

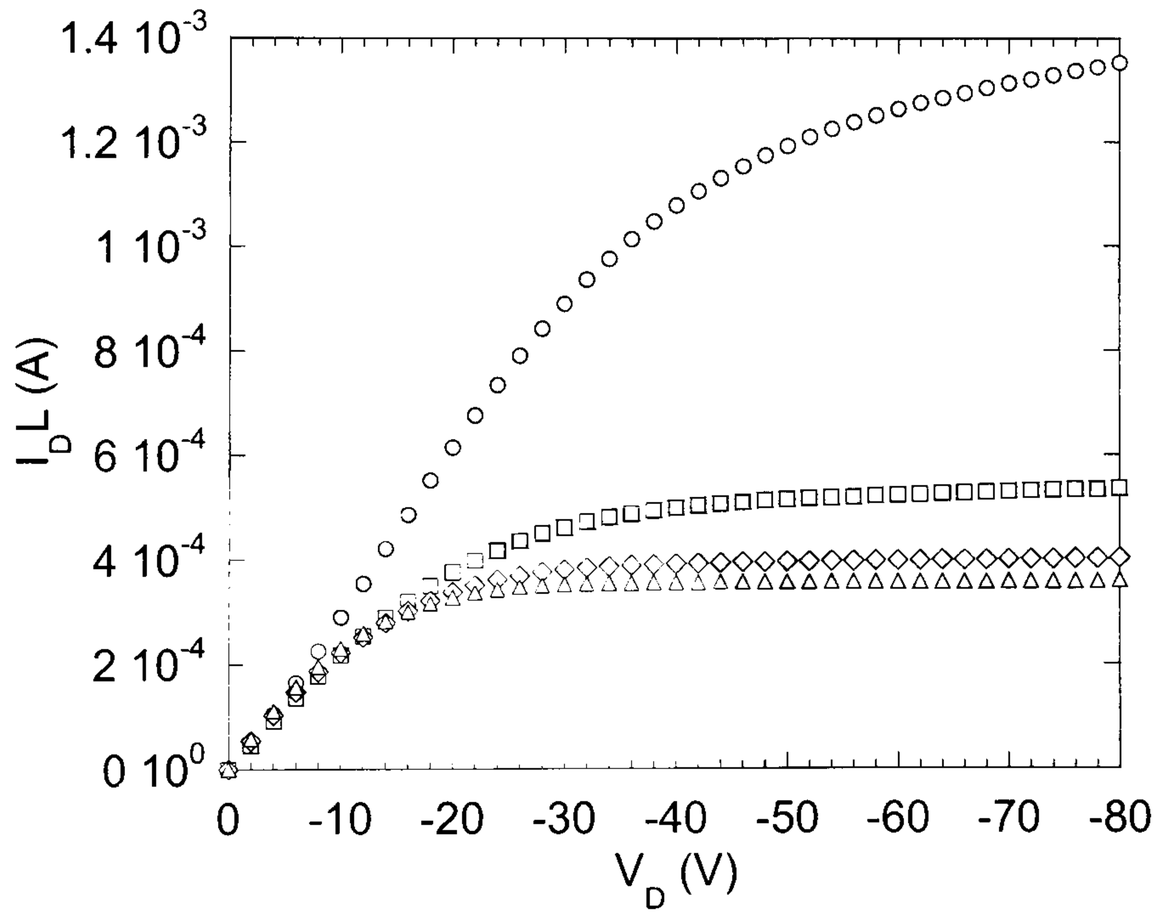


Figure.4.9. Normalised output characteristics for OTS treated syn-pBTTT transistors with a channel length of 2.5μm (circles), 5μm (squares), 10μm (diamonds), and 20μm (triangles) at a V_G of –40V.

This is contradictory to the aforementioned reports, though has also been observed in [19]. The currents are initially of similar magnitude ($V_D < -10V$), before deviating at higher drain voltages. This indicates a strong dependence on the lateral electric field.

To try and explain this lateral field dependence, the saturated derived mobilities were plotted with respect to the source-drain field V_D/L (E_x) and source-gate field V_G/d_{ox} (E_y) in Fig.4.10 and 4.11 for 20μm and 2.5μm channel length transistors, respectively. The gate voltage dependence has previously been attributed to the charge density dependence of the mobility, and increases with increasing gate bias for the long-channel transistor (L = 20μm). Increasing the lateral field E_x does not have a significant effect in this case, as E_x is a hundred times less than the field due to the gate bias E_y. At $V_G \leq -40V$, all devices should be in saturation for the lateral fields shown ($-50V \leq V_D \leq -100V$). E_x in the shorter channel transistor (L = 2.5μm) is approximately ten times higher for the same voltage range with the mobility following the same trend, also being increased ten times.

We can approximate the source-drain field strength of a 2.5μm transistor at $V_D = -5V$ as 20kV/cm and at $V_D = -60V$ as 240kV/cm. The field due to an applied gate bias of -60V is 2.6MV/cm. This is ten times more than the 220kV/cm field generated by an applied gate voltage of –5V. Compared to a transistor with a channel length of 20μm, E_x at drain voltages of –5V and –60V is just 2.5kV/cm and 30kV/cm respectively. At higher drain voltages the gradual channel approximation ($E_x << E_y$) no longer applies as the lateral and transverse fields are starting to become comparable in magnitude. In addition, these relatively high lateral fields ($E_x \geq$ 200kV/cm) are equivalent to that of a diode, in which a dependence on the transverse field is often observed. Xu et al. also noted that the dependence of the mobility on gate bias was enhanced at high lateral fields.[19]

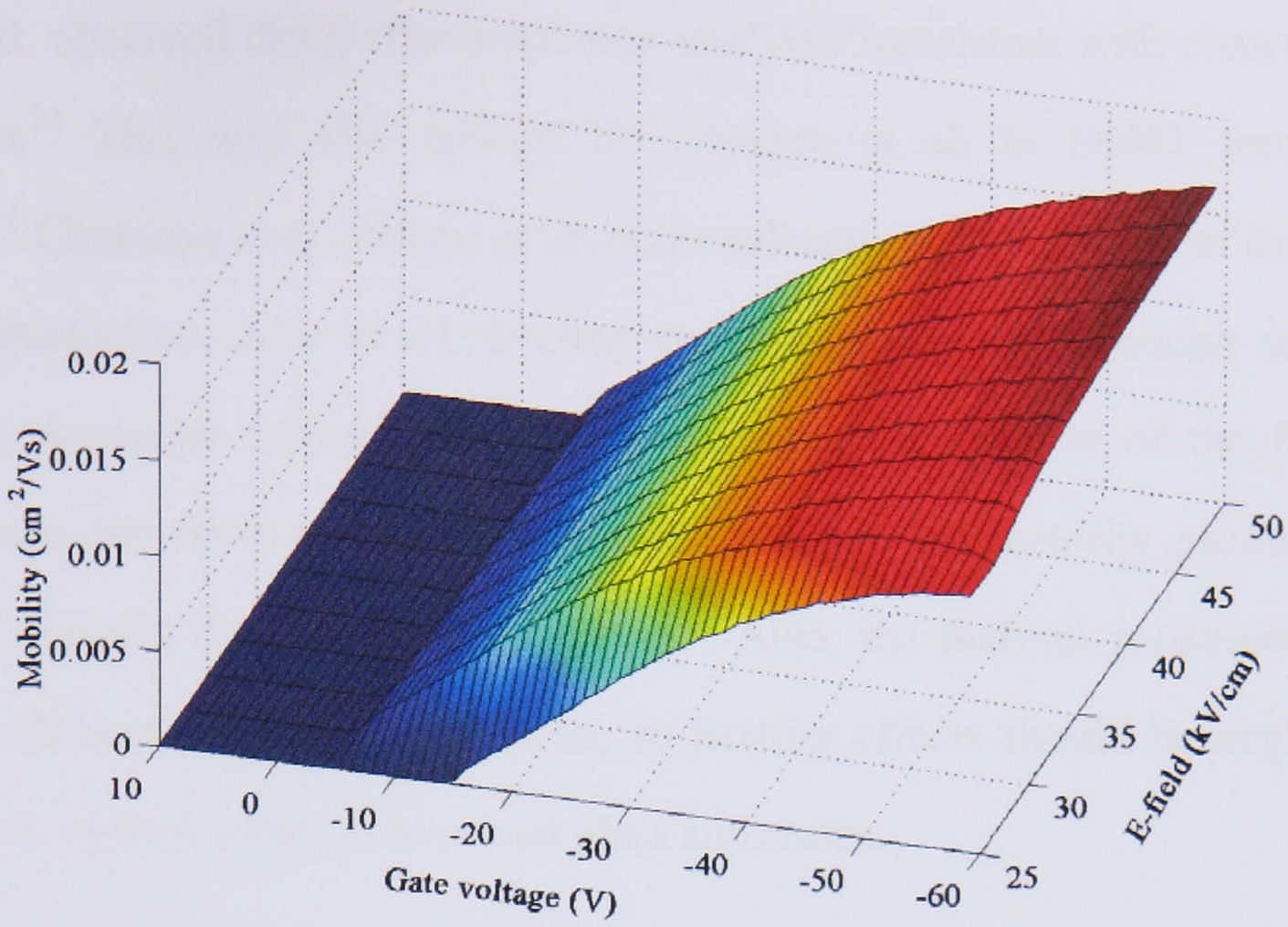


Figure.4.10. Dependence of the saturated mobility on the longitudinal and lateral E_x-fields for OTS treated syn-pBTTT transistors of channel length 20µm.

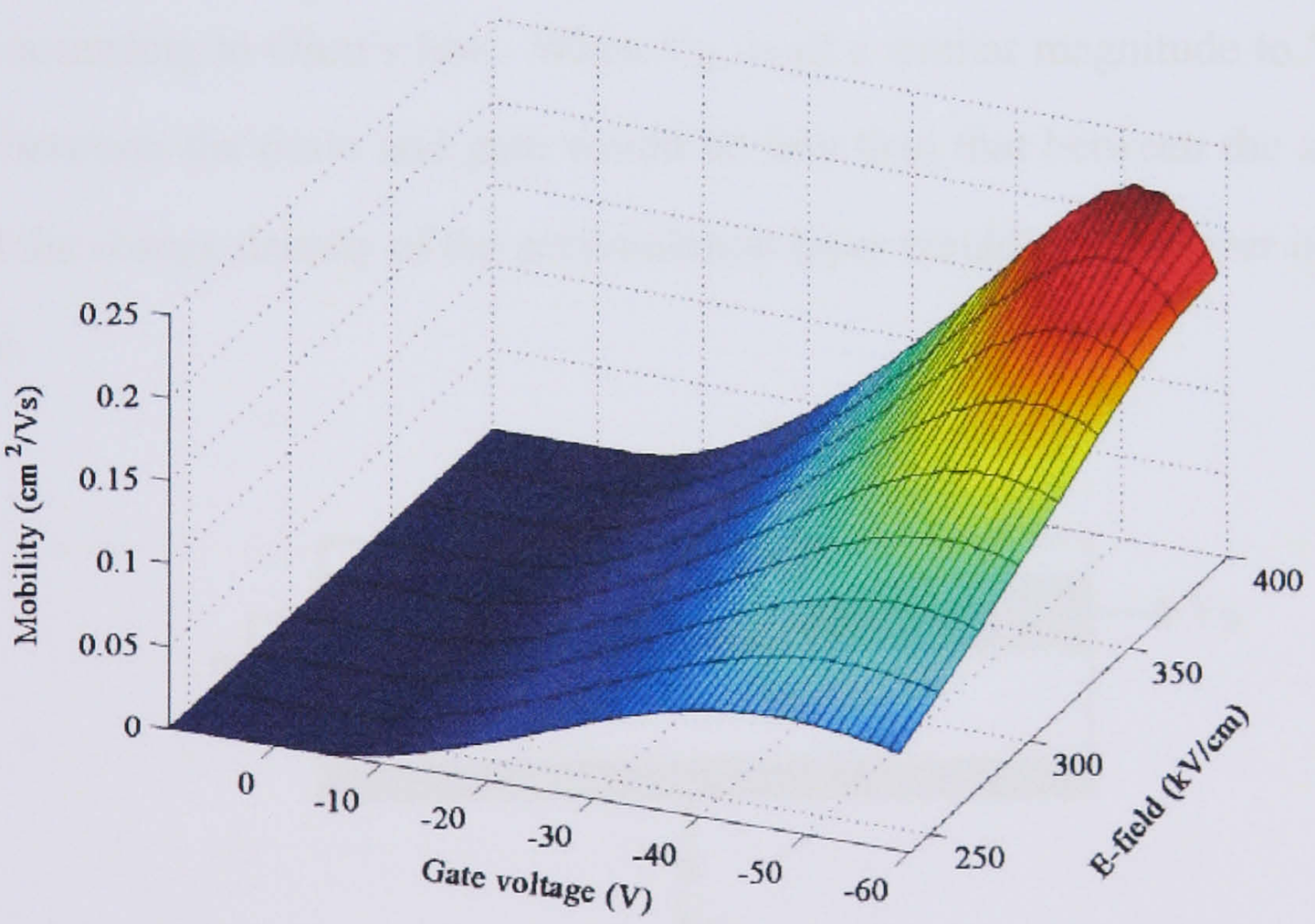


Figure.4.11. Dependence of the saturated mobility on the longitudinal and lateral E_x-fields for OTS treated syn-pBTTT transistors of channel length 2.5µm

Chou et al. observed diode-like behaviour in P3HT transistors with channel lengths of 100nm.[20] This was also noticed by Leufgen et al. in DH4T transistors of ≤100nm.[11] Chabinyc et al. looked at several explanations for the lack of saturation in PQT-12 transistors, such as self-heating and bulk-transport.[14] Though self-heating can cause increased currents due to a temperature dependence of the field-effect mobility and threshold voltage, their model did not satisfactorily account for the increased currents in the saturation region. Also, the thermal resistance is much lower for devices fabricated on silicon, so heating effects should be negligible for our devices, as their analysis involved glass substrates.

A more plausible explanation involves looking at what physically happens when the gradual channel approximation breaks down in a transistor. Let us first remind ourselves of what happens at pinch-off. At a constant V_G the number of charge carriers will be proportional to C_iV_G and at low increasing V_D the current will rise linearly according to Ohm's law. When V_D is of a similar magnitude to V_G the net voltage between the drain and gate would be less than that between the source and gate and the charge density of the accumulation layer would start to taper off towards the drain.

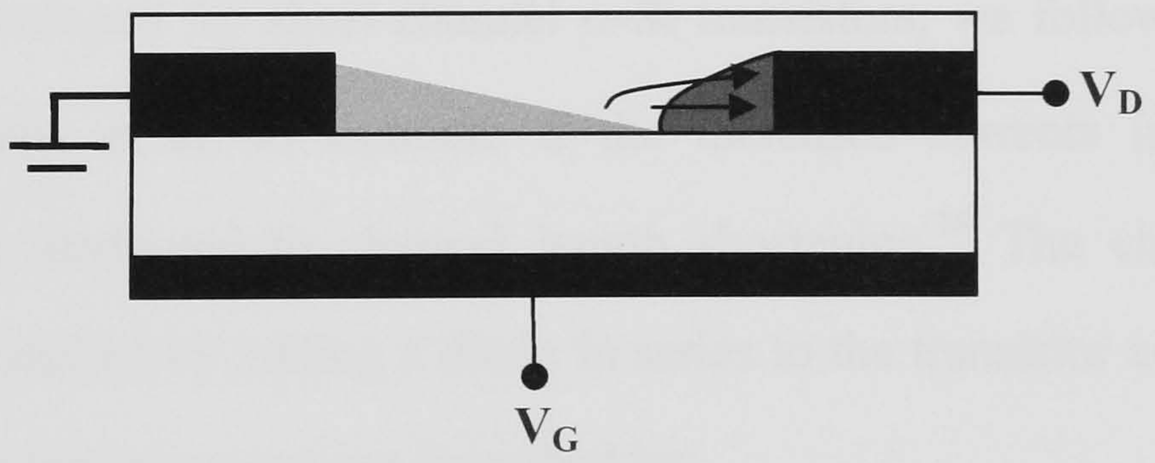


Figure.4.12. Schematic of a transistor with $V_D >> V_G$. Pinch-off has expanded into the channel (light grey area), creating a region depleted of induced carriers that favours bulk conductance. This is demonstrated by the dark grey section.

If $V_D = V_G$ the fields at the drain electrode cancel and the accumulation layer is said to be pinched-off. If $V_D > V_G$ this pinch-off region expands into the channel. The resistance in this region is high, but a large voltage drop would exist between the channel and drain electrode – which favours bulk conductance. The extent of this region into the accumulation layer would be dependent on the magnitude of the excess V_D, and can be thought of as effectively shortening the channel length. As with contact effects, this is more apparent for short-channel devices as the ratio of the channel length to the bulk region is smaller.

4.2.2. Finite output conductance

The output characteristics in Fig.4.1 shows that the drain saturation current has a non-zero slope. This indicates a finite output conductance in the saturation regime. As saturation occurs when the channel is pinched-off, further increasing V_D would lead to charge being accumulated in the pinched-off region, shortening the effective channel length by ΔL. For shorter channels this channel length modulation is significant and the saturated drain current appears to increase with increasing drain bias.

From a model developed for short channel α-Si transistors, we follow the method used by Sirringhaus et al. to estimate if the increased currents in the 2.5μm transistors can be attributed to channel length shortening.[18] The channel length shortening was modelled by adding a diode in series to the transistor and the output conductance in the saturation regime described by:

$$G_{OUT} = \frac{\partial I_D}{\partial V_D} = \frac{I_{SAT}(V_G)}{(1-\Delta L/L)^2} \cdot \frac{\partial \Delta L}{L \partial V_D} \equiv I_{SAT}(V_G) \cdot \lambda \qquad \{4.3\}$$

L is the channel length, ΔL the amount the channel length is shortened by, and λ is a measure of the channel modulation. By fitting the output characteristics in the saturated regime to:

$$I_D(V_D, V_G) = I_{SAT}(V_G) \cdot \left(1 + \lambda\left(V_D - \left(V_G - V_0\right)\right)\right) \qquad \{4.4\}$$

λ can be estimated.

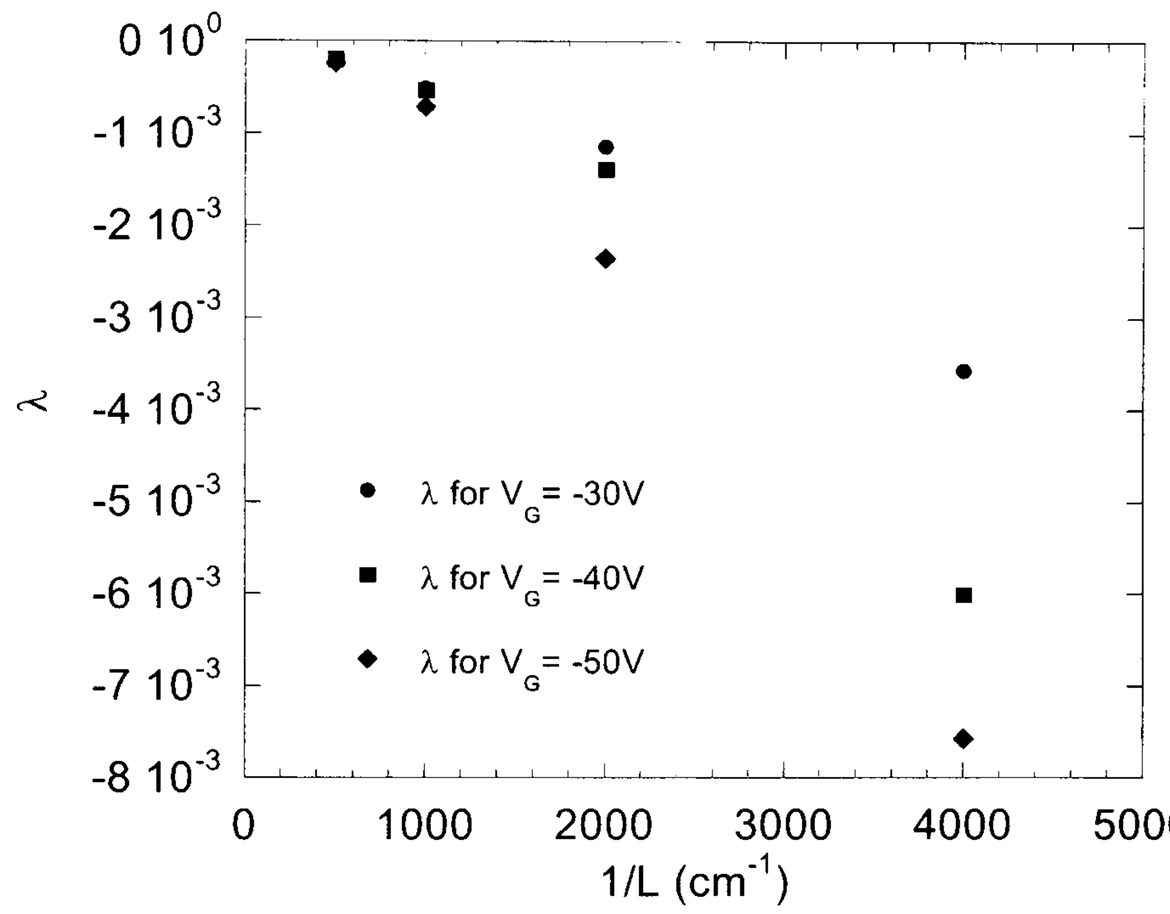


Figure.4.13. If channel length shortening is insignificant, the relation between λ and the inverse of the channel length should be linear. The above graph shows the relation for syn-pBTTT transistors. At shorter channel lengths there is a clear deviation from the linear fit.

Fig.4.13 plots the relationship between λ and L^{-1} for syn-pBTTT transistors with channel lengths 2.5, 5, 10 and 20μm. For transistors of L = 5 - 20μm, λ is proportional to L^{-1}, indicating ΔL is small and only has a weak dependence on L, as from {4.3} $\Delta L/L \approx 0$. For the 5μm device, at high applied gate bias, and the 2.5μm transistor the values deviate from the expected linear relation. This indicates that significant channel length shortening occurs at shorter channel lengths and higher gate biases.

The question arises of whether the saturation equations are valid for calculating mobility as the shorter channel devices do not exhibit true saturation behaviour. The gradual channel approximation is no longer valid, and as the mobility is calculated with respect to L, a proportionally higher value would be obtained in the presence of channel shortening.

The linear and saturated mobilities as calculated from equations {1.3} and {1.6} are shown below for OTS treated syn-pBTTT transistors of channel lengths 2.5, 5, 10 and 20μm. The trend is identical in non-OTS treated devices, except that the mobility is 10% reduced.

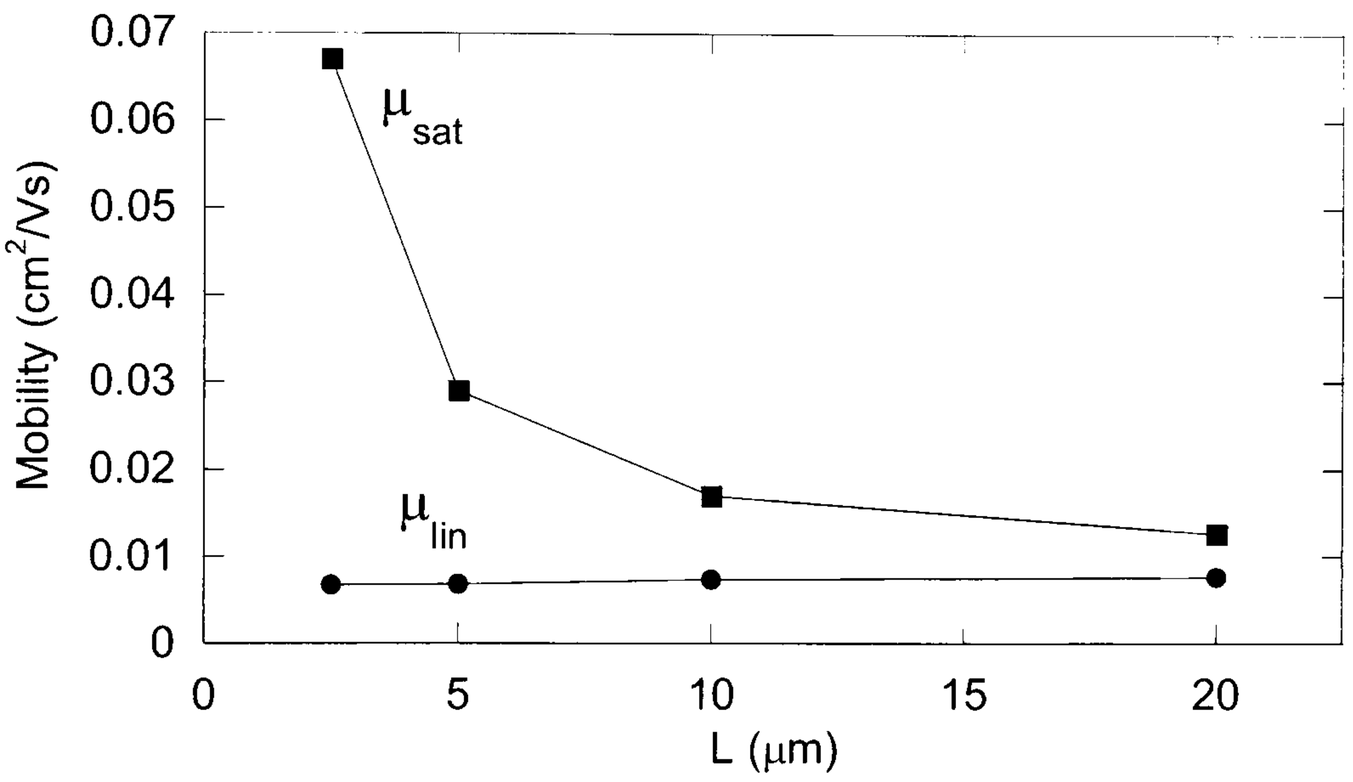


Figure.4.14. Dependence of the linear and saturated mobility on the channel length for OTS treated syn-pBTTT transistors.

The linear mobility appears to decrease with decreasing channel length, but the saturation mobility significantly increases with decreasing L. Contact resistance should affect only the linear region, and consequently the linear derived mobility. It should not have an effect on the saturation region. If we calculate the mobility using the square root of the slope of the saturated transfer characteristics for transistors of all channel lengths and estimate the channel length that gives a mobility comparable to that of the long channel transistor – in this case 0.012cm^2/Vs for 20μm, we see that it corresponds to a length of 0.5μm for the 2.5μm transistor, 2.7μm for the 5μm

transistor and 7.8μm for the 10μm transistor. This suggests that the channel length shortening is approximately 2μm, and clearly the miscalculation affects the shortest channel devices most significantly.

4.2.3. Electron injection at high electric fields

Referring back to Fig.4.11 we remember that at gate biases higher than -40V for the 2.5μm device the saturated mobility stabilises (V_D < -80V) or appears to decrease (V_D >-80V). At drain voltages ≥-80V the drain current of the output and transfer characteristics also starts to decrease. If electrons were injected at the drain at high gate voltages, this could explain the drop in the current and mobility at high fields due to charge recombination. OFETs typically operate in hole accumulation mode and electron transport is not usually observed. In OLEDs, electrons increase the total current, taken to be a sum of the electron and hole currents ($J = J_e + J_h$). In the pinch-off region of a transistor, the electron current is responsible for the drain current between the channel and drain. If the electron mobility is less than the hole mobility or the injected electron density is low, the drain current could be restricted. A larger effect is observed for short channel transistors as the magnitude of the pinch-off regime (ΔL) is large in comparison to the channel length. Further evidence to support electron injection was that whilst the 'saturated' regime of the short-channel transistors was measured, electroluminescence (EL) corresponding to the photoluminescence (PL) of the polymer was observed. This phenomenon will now be discussed in Section 4.3.

4.3. Light-emission in PFETs

Light emission was first observed at the junctions of inorganic semiconductors in the 1950s.[21] The origin of this light emission is now attributed to avalanche injection and

hot electron emission. In organic materials, charge carriers are localised on individual molecules - not a suitable case for avalanche applications. In fact, fields of 10^7-10^8 V/cm would be needed to accelerate a carrier to the kinetic energy necessary to generate holes and electrons via internal ionisation in organic semiconductor.[22] However, light emission is commonly observed in organic films due to recombination of bipolar injected charge carriers. This phenomenon is commonly exploited in organic light-emitting diodes (OLEDs). OFETs have been used to drive OLEDs as building blocks of integrated circuits, but it is only in recent years that light emission in isolated transistor structures has been observed.

Sirringhaus et al. reported integrated optoelectronic devices, which combined polymer FETs driving polymer LEDs.[23] Though these hybrid devices are promising, the realisation of low-voltage organic light-emitting transistors would represent the smallest possible integration of a light emitter and switch. Another benefit is that not only could the light intensity be set, but the location of the recombination zone could also be controlled. This section describes the basic principles behind light emission in organic materials, before discussing methods of fabricating organic light-emitting transistors (OLETs), and a suitable mechanism for the results obsereved.

4.3.1. What are excitons?

So far, the only excited species we have mentioned have been polarons. Coulombic forces, and structural relaxation around the charged states, would induce an attractive interaction between an electron and hole polaron. This species is termed an exciton, and is defined as an electrically neutral electron – hole pair bound by Coulombic interaction. For example, the absorption of a photon of suitable wavelength, could promote an electron from the HOMO to the LUMO, thus creating a bound electron –

hole pair. Alternatively, the recombination of an electron and hole polaron could also generate an exciton.

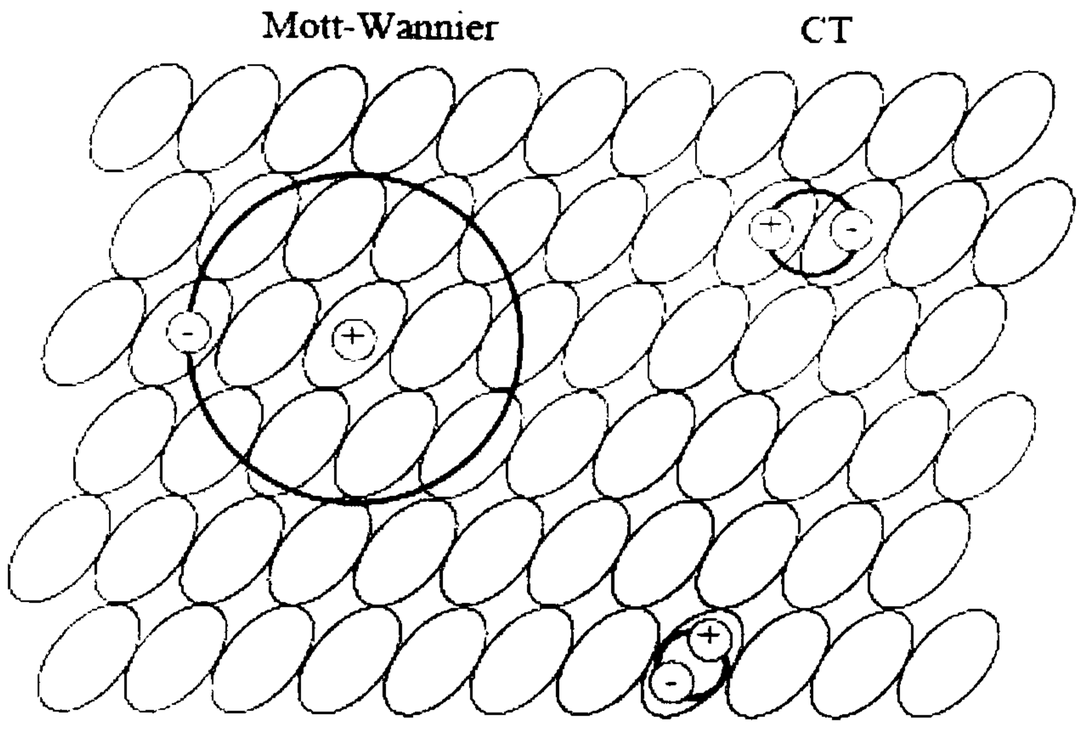


Figure.4.15. Schematic representation of Frenkel, charge transfer (CT) and Mott-Wannier excitons. Figure adopted from[24]

Excitons are classified by their size, as illustrated in Fig.4.15. The radii of Frenkel excitons are smaller than the intermolecular distance (< 5nm), so they are in effect bound on the same molecular unit. These are the type typically found in organic systems. Inorganic semiconductors favour Mott-Wannier excitons, which have radii spanning many molecular units (40 – 100nm). The intermediary case, where the excitation is spread over a few adjacent molecular units (6 - 10nm), is called a charge-transfer exciton.[25]

In addition to this, there are two further types of excitons, singlets and triplets. Quantum mechanics tells us that electrons and holes possess spin. This, coupled with the fact that the spin part of the exciton wavefunction must follow the Pauli Exclusion Principle, leads to three combinations in which the electron and hole spins combine symmetrically, and one which is anti-symmetric. Accordingly, excitons in the former case are termed triplets, and the latter singlets.

$$\left.\begin{array}{l} |\uparrow\uparrow\rangle \\ |\downarrow\downarrow\rangle \\ \frac{1}{\sqrt{2}}\left(|\uparrow\downarrow\rangle + |\downarrow\uparrow\rangle\right) \end{array}\right\} \quad S = 1 \qquad Symmetric \Rightarrow Triplet \quad states$$

$$\left.\frac{1}{\sqrt{2}}\left(|\uparrow\downarrow\rangle - |\downarrow\uparrow\rangle\right)\right\} \quad S = 0 \qquad Anti-symmetric \Rightarrow Singlet \quad state$$

As we will see shortly, light emission specifically termed fluorescence occurs via selectively allowed transitions, in which the optically excited electron returns to the ground state (HOMO). Electroluminescence (EL) is a result of the fluorescence emitted by electronically generated excitons. The fundamental difference between these mechanisms will be expanded upon in the following sections, so we can better understand the EL emitted from light-emitting transistors.

4.3.2. Absorption and emission spectra of conjugated polymers

As mentioned previously, the energy difference between the HOMO and LUMO (the band gap E_G lies between 1.3 – 3eV for most organic materials) correlates to absorption and emission in the UV/visible spectral region. These spectra can be explained by considering Fig.4.16, overleaf. Each set of curves represents the ground and first excited state of a chemical bond in a diatomic system within a potential energy (E) versus the nuclear separation (r) diagram. The molecule is in the S_0 state (with total energy S_0) when both electrons are in the π-orbital. Similarly, if the molecule is excited by promotion of an electron to the π*-orbital, the S_1 state describes the total energy of this excited state. The horizontal lines indicate the vibrational levels of the bonds, signifying the oscillation of the internuclear distances about the equilibrium bond length within the limits of the potential curve, as

illustrated. These quantised levels have ~0.1eV spacing, so it would be expected that at room temperature all electrons are at the lowest vibrational energy.

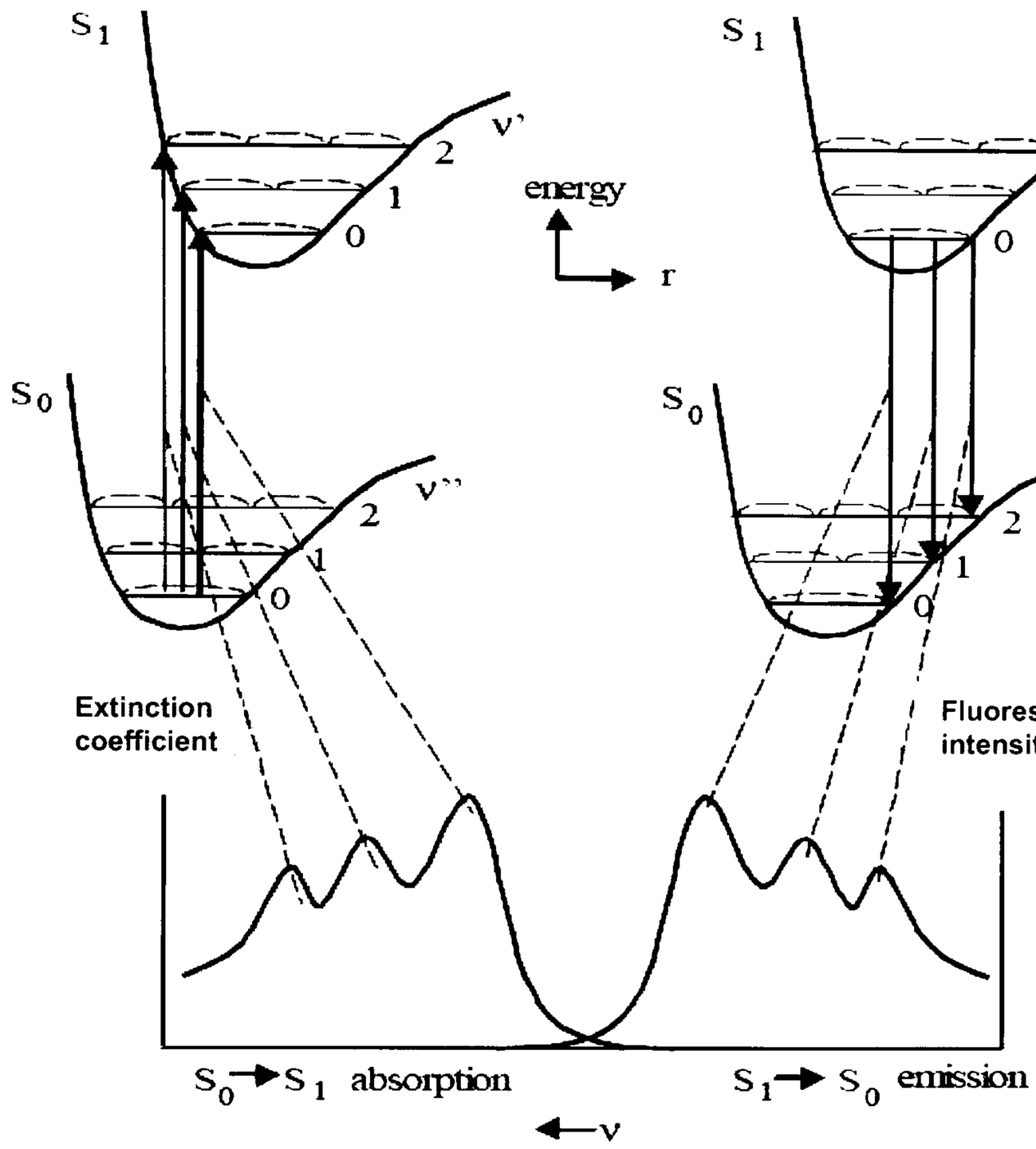


Figure.4.16. Potential energy diagram illustrating the origins of the predicted mirror symmetry of absorption and emission of a diatomic molecule. Adapted from[24]

Absorption of a photon promotes an electron from the π to the π^* state. These transitions are plotted as vertical lines, as according to the Franck-Condon principle the time it takes for an electronic transition ($\sim 10^{-15}$s) is much less than the time it takes for molecular reorganisation ($\sim 10^{-13}$s). After excitation the molecules rapidly relax ($\sim 10^{-13}$s) non-radiatively to the lowest vibrational level of the excited state. This is known as internal conversion. As this process is more rapid than electronic relaxation to S_0 all subsequent transitions are likely to occur from this state. The photon may then be re-emitted with a transition to any of the vibrational levels of the

ground state, as illustrated. In summary, the vibronic features in the absorption spectrum are indicative of the vibrational energy levels of the excited state potential, whilst the features in the emission spectrum relate to the vibrational levels of the ground state potential.[26]

The absorption and emission spectra should have mirror symmetry, which is often not observed in conjugated polymers. In general, the absorption spectra appear to be broad and featureless with little evidence of vibronic structure. So far, we have only considered an isolated molecule. In practise, the entire statistical distribution of effective conjugation lengths will be sampled – and the absorption spectrum will as a result be broadened. However, excitons are mobile and due to the energy difference of chains of different conjugation length, it is more favourable for an exciton to migrate onto a chain with longer conjugation length (lower energy). Emission therefore occurs for a smaller range of conjugation lengths and the vibronic structure can be distinguished in the emission spectrum.

4.3.3. Electroluminescence

Electroluminescence arises from the relaxation of an electrically generated exciton. A single layer organic light-emitting diode (OLED) usually consists of a sandwich structure, as illustrated in Fig.4.17, with the polymer in between a hole-injecting anode and electron-injecting cathode. Indium tin (II) oxide/PEDOT: PSS is normally used as the anode, with a low workfunction metal like calcium employed as the electron injecting electrode. On the application of a forward bias electrons and holes are injected into opposite sides of the organic layer and drift towards each other under the influence of an electric field. An exciton is consequently formed when an electron and hole approach closely and become bound together.

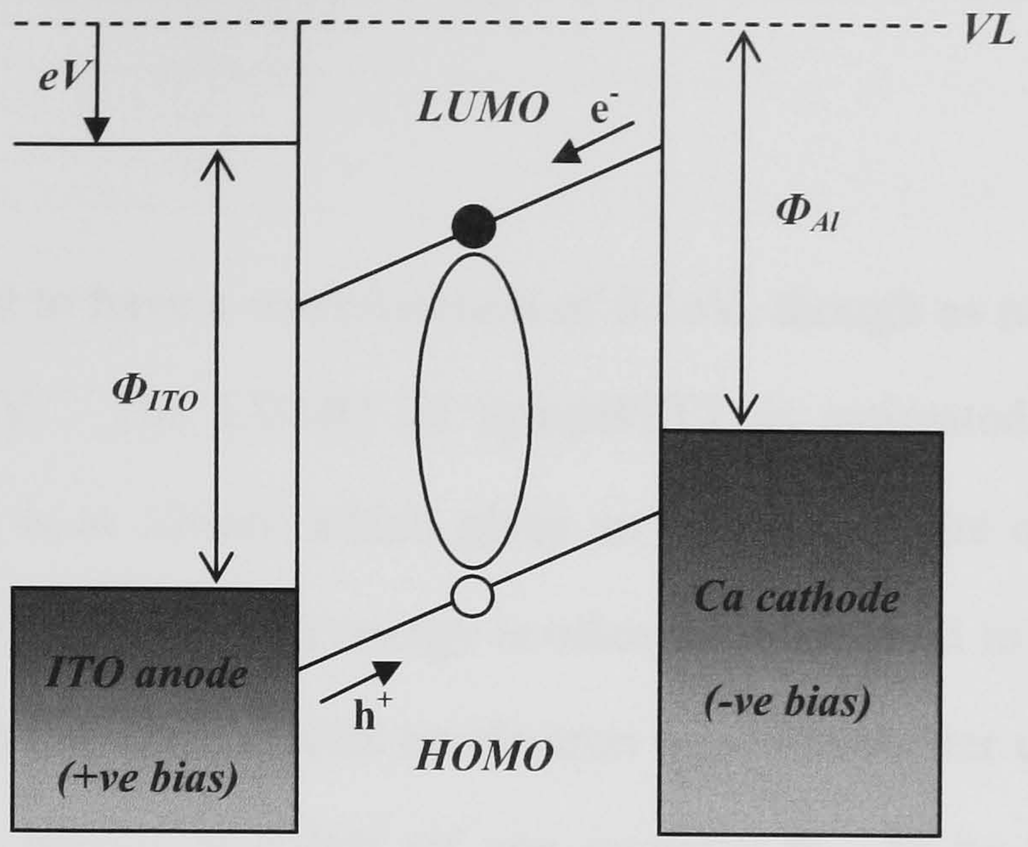


Figure.4.17. Schematic showing a simple energy level diagram of an organic light-emitting diode. The device is biased so the ITO anode injects holes, and the calcium electrode injects electrons. An electron and hole can then form an exciton (a bound electron-hole pair), which may emit light on relaxation.

From spin statistics we have seen that there are four ways to combine the spin, giving a net spin of zero for a singlet and with triplets having a spin of one. This also suggests that triplets are three times more likely to be formed than singlets, though more recent experiments indicate that the formation of singlets may be preferred in conjugated polymers. Triplets generally play no part in EL as they do not have the same spin as S_0 so the transition is radiatively forbidden.

4.3.4. Light-emission in OFETs

For light emission to occur, both electrons and holes need to be injected into the organic layer and recombine to form excitons, which could generate light. OFETs principally operate as hole accumulation devices, with horizontal planar gold source and drain electrodes positioned a couple of microns apart. This is the opposite to the vertical structure in OLEDs, in which injection is optimised for both types of carriers

using different electrodes sandwiching a polymer film several tens of nanometres thick.

Gold is expected to have a workfunction of 5.1eV, though as mentioned, this can be as low as 4.6eV. The LUMO of syn-pBTTT is estimated to be 2.6eV. The absorption edge is at 520nm which gives an estimate of the optical energy gap as 2.4eV. As the exciton binding energy is often approximated to be 0.3eV, the energy gap E_G is ~2.7eV, which suggests an electron injection barrier of 2.5eV compared to a hole injection barrier of 0.2eV (if one assumes Φ_{Au} to be 5.1eV). Even if the energy barrier was surmountable, electron transport is generally poor (with respect to holes) in organic materials. Chua et al. found that electron transport could be preserved by spin-coating a thin insulating layer of dielectric onto the silicon dioxide surface, prior to polymer deposition. This acts to passivate the interface, as electrons are electrochemically trapped by the hydroxyl groups to form immobile $Si\text{-}O^-$ ions.[27]

There has also been interesting work done on ambipolar transistors. Meijer et al. first demonstrated single layer solution-processible ambipolar transistors by blending the n-type transporter PCBM into the matrix of a p-type conjugated polymer.[28] Ambipolar operation in OFETs (supporting both n-type and p-type transport) is vital for digital circuits, similar to inorganic CMOS logic applications. Ambipolar charge transport could also give rise to exciton formation, which could be exploited in organic light-emitting transistors (OLETs).

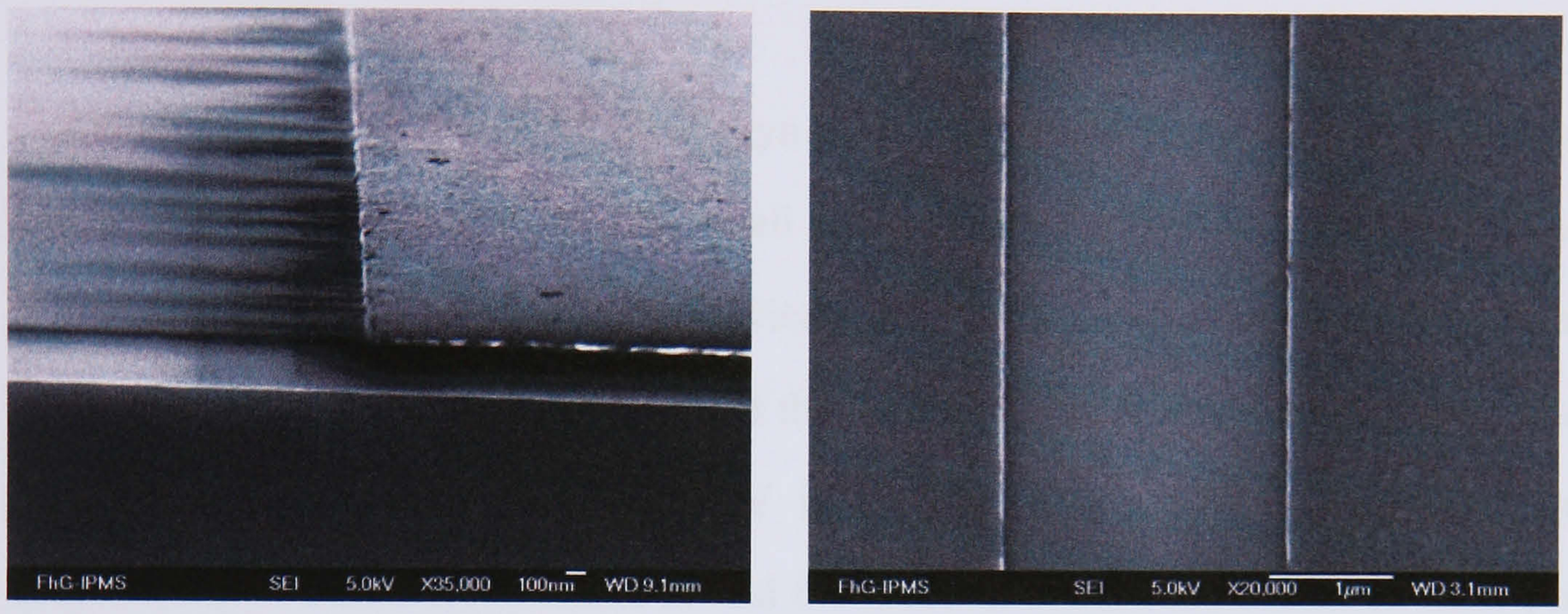
Rost et al. demonstrated ambipolar OLETs by using a co-evaporated hole and electron transporting material as the active layer and gold as the injecting electrodes.[29] Ambipolar charge transport was demonstrated and the light intensity could be controlled by both the drain and gate voltage. For n-type behaviour at positive biases, the light emission was weaker and dependent on high gate voltages.

It was independent of V_{DS}, unlike the p-type regime - in which strong light emission was observed for high drain biases, corresponding to the lack of drain current saturation in the output scans. In an extension to this methodology, ambipolar OLETs were also fabricated using bilayer hole and electron transporting materials in a heterostructure using staggered gold (bottom) and magnesium (top) electrodes.[30,31] Similar characteristics to those reported in[29] were observed, with the light output modulated by the drain and gate voltages. Strongest EL was again observed at negative biases and was correlated to the non-saturating drain current.

Light emission has also been observed in transistors with no apparent electron transport. Hepp et al. demonstrated light emission from a polycrystalline tetracene field-effect transistor with gold source and drain electrodes.[32] No n-type behaviour was detected and the light generation mechanism was explained by the under-etching of the drain electrode, which consequently acted as an OFET/OLED hybrid due to the very large electric fields possible. Similar behaviour was observed by Ahles et al. for a poly[9, 9-di(ethylhexyl)fluorine] PFET with gold electrodes.[22] Scanning electron microscopy (SEM) revealed that the electrodes were rough and under-etched by up to 2μm. The light emission was explained by physical defects at the drain electrode enhancing the electric field enabling electron injection via field emission. This was concurrent with inhomogeneous light emission at the drain and no shift of the emission zone on variation of the gate voltage. In effect, the drain electrode acts as a cathode and the accumulated holes in the channel as the anode of OLED.

Sanato et al. fabricated p-channel unipolar tetracene OLETs using gold source and drain electrodes.[33] In this case AFM studies revealed no imperfections of their electrodes. REM images of our substrates, carried out by Ulrich Todt at the Fraunhoffer Institute in Dresden, also showed no such defects, suggesting that an

alternate mechanism could be responsible. Fig.4.18 is a sample of the edge and top view of a section of channel on a 2.5μm channel length transistor. There appears to be no significant under-etching of the electrodes.



(i) **(ii)**

Figure.4.18. REM images of the electrode edges for a typical substrate from (i) a side and (ii) a top view. There is no obvious under-etching and the edge definition is reasonably sharp.

4.3.5. Experimental techniques

IVL data was taken by connecting a photomultiplier tube to the input channel of the HP 4145B Semiconductor Analyser, and running the scans simultaneously. The photomultiplier tube had a large aperture to collect maximum light and was positioned 1cm above the channel for each device. It was operated at 1.4kV. Electroluminescence spectra were recorded using an Ocean Optics 200 Spectrometer coupled to a silica fibre. The fibre was mounted onto a translational microprobe enabling precise manipulation in 3 directions. The fibre was positioned 2mm above the channel of the transistor to be measured. Ambient light was minimised by blocking off the window of the glove box with aluminium foil and switching off any light emitting equipment. Background scans were subtracted for each measurement. As the photomultiplier tube and spectrometer were on loan from Roland Smith of the Optics Group at Imperial and David Smith of the Quantum and Functional Matter

group at Southampton University, respectively, it was not possible to fully optimise the apparatus and the data recorded should be taken as such.

4.3.6. Light emission from syn-pBTTT transistors

Light emission was observed from syn-pBTTT transistors at high gate biases. Emission was observed for devices of all channel lengths, though the intensity was brightest for shorter channel length devices, indicating a dependence on the lateral field strength. An optical micrograph of the light emission from a 2.5μm length syn-pBTTT transistor at V_D and V_D=-80V is depicted in Fig.4.19. Light emission originates near to the drain electrode and the location of the recombination zone can not controlled by the drain current. This was also noted by Oyamada et al. for the EL of 2, 4-bis(4-(2'-thiophene-yl)phenyl)thiophene OFETs, with a maximum EL quantum efficiency observed for short channel transistors at high biases.[34]

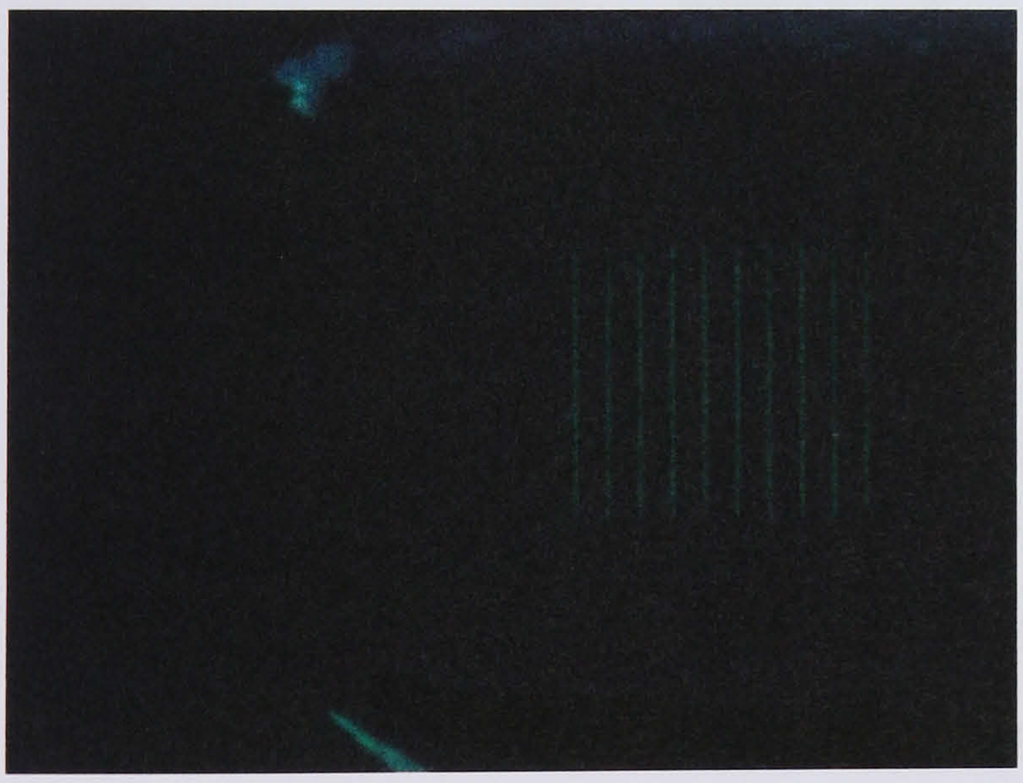


Figure.4.19. Photograph taken of operational syn-pBTTT transistor at 20x magnification and 1s exposure time. The light emission clearly originates close to the drain electrode. V_G and V_D are -80V. The channel length is 2.5μm and the width is 1cm.

The normalised absorption and photoluminescence emission spectra are plotted in Fig.4.20. The absorption spectrum does not display vibronic structure, but 0-0 and 0-1 transitions are evident from the emission spectra. The EL and PL spectra are correspondingly compared in Fig.4.21.

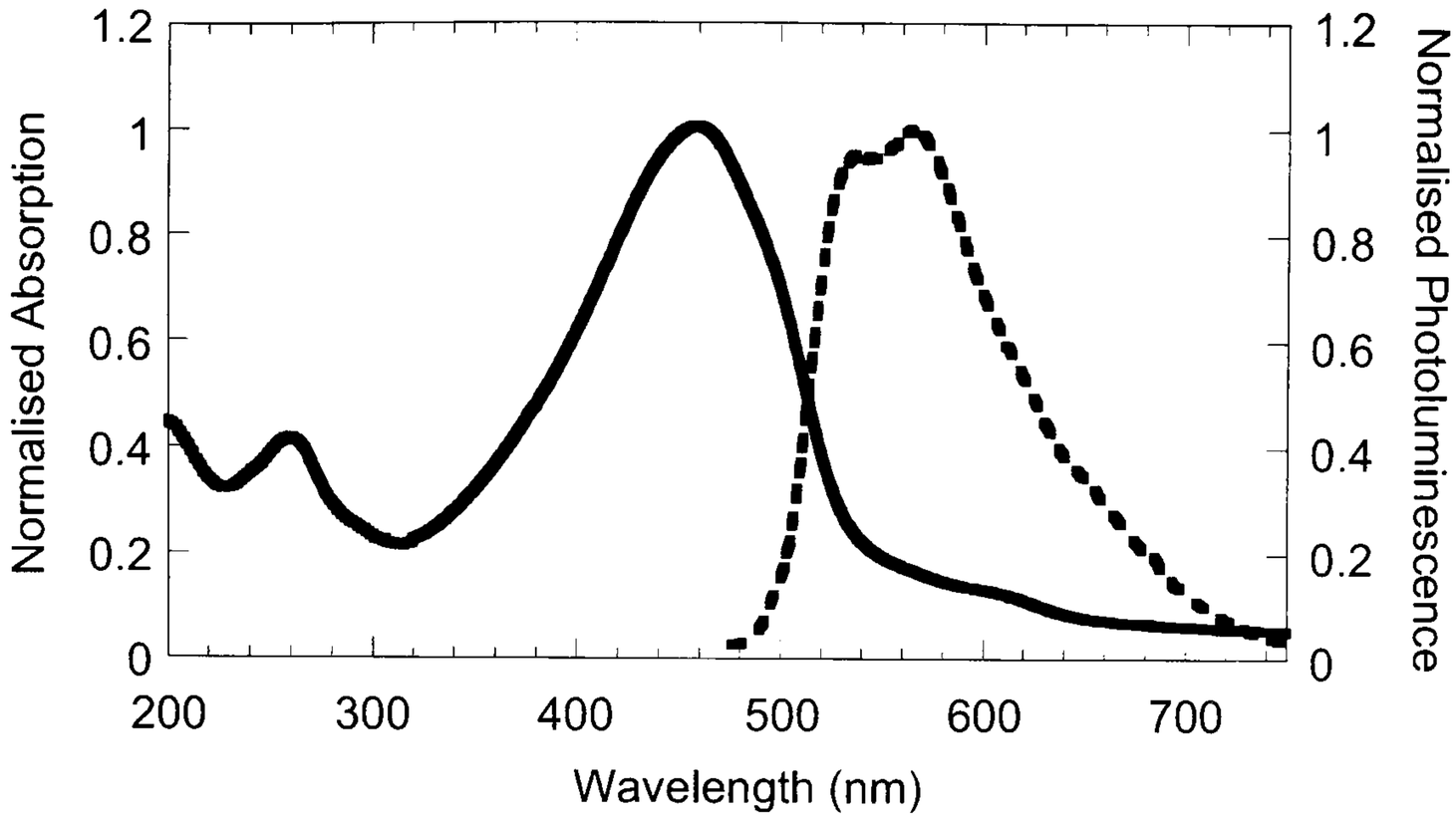


Figure.4.20. Normalised absorption (solid line) and photoluminescence (dashed line) spectra for a thin film of syn-pBTTT.

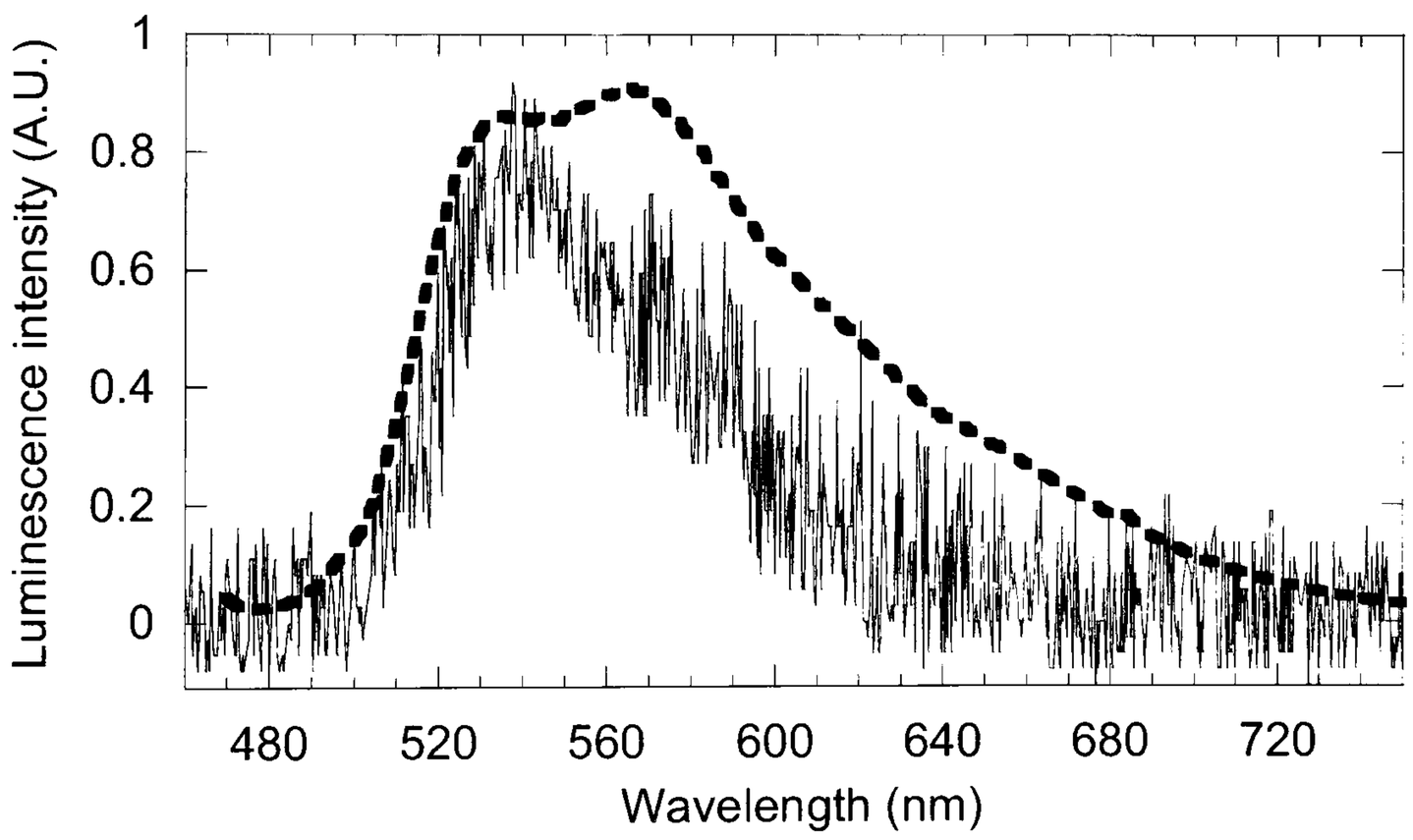


Figure.4.21. Normalised photoluminescence (dashed line) and electroluminescence spectra (solid line) for syn-pBTTT. The EL spectrum was measured from a syn-pBTTT transistor of 2.5µm channel length biased at a pulsed V_G of -80V.

The maxima are not shifted, which confirms that the emission is a property of the material, but the 0-1 transition is more pronounced in the PL spectrum. This could be an artefact, as the EL spectra were noisy but this difference was repeatedly observed. This could be a result of the polymer chains being more ordered in the

recombination zone of the FET than in the bulk of the film, though emission is expected to occur at or near the drain electrode, it would be expected that there would be disruption of order in the film around the contact, as the transistors have a bottom contact configuration. Waveguiding in the film is unlikely to reduce the emission at 560nm as waveguiding usually cuts-off shorter wavelengths closer to the absorption edge. The change in emission might also be due to a chemical interaction between the material and the gold electrode. As syn-pBTTT is a thiophene based polymer containing sulphur, which has a strong affinity to gold, this could be a likely mechanism for the change in the emission spectra.

4.3.7. Mechanism of light emission

The most puzzling question concerning the working mechanism of OLETs is how electrons are injected from gold into the polymer. As the electron injection barrier is typically 2.5eV, this process is very energetically unfavourable. However, the emission of light implies that electrons must be injected into the material. Fig.4.22 demonstrates the detected luminescence plotted in relation to a saturated transfer scan for an OTS treated syn-pBTTT transistor of channel length 2.5μm.

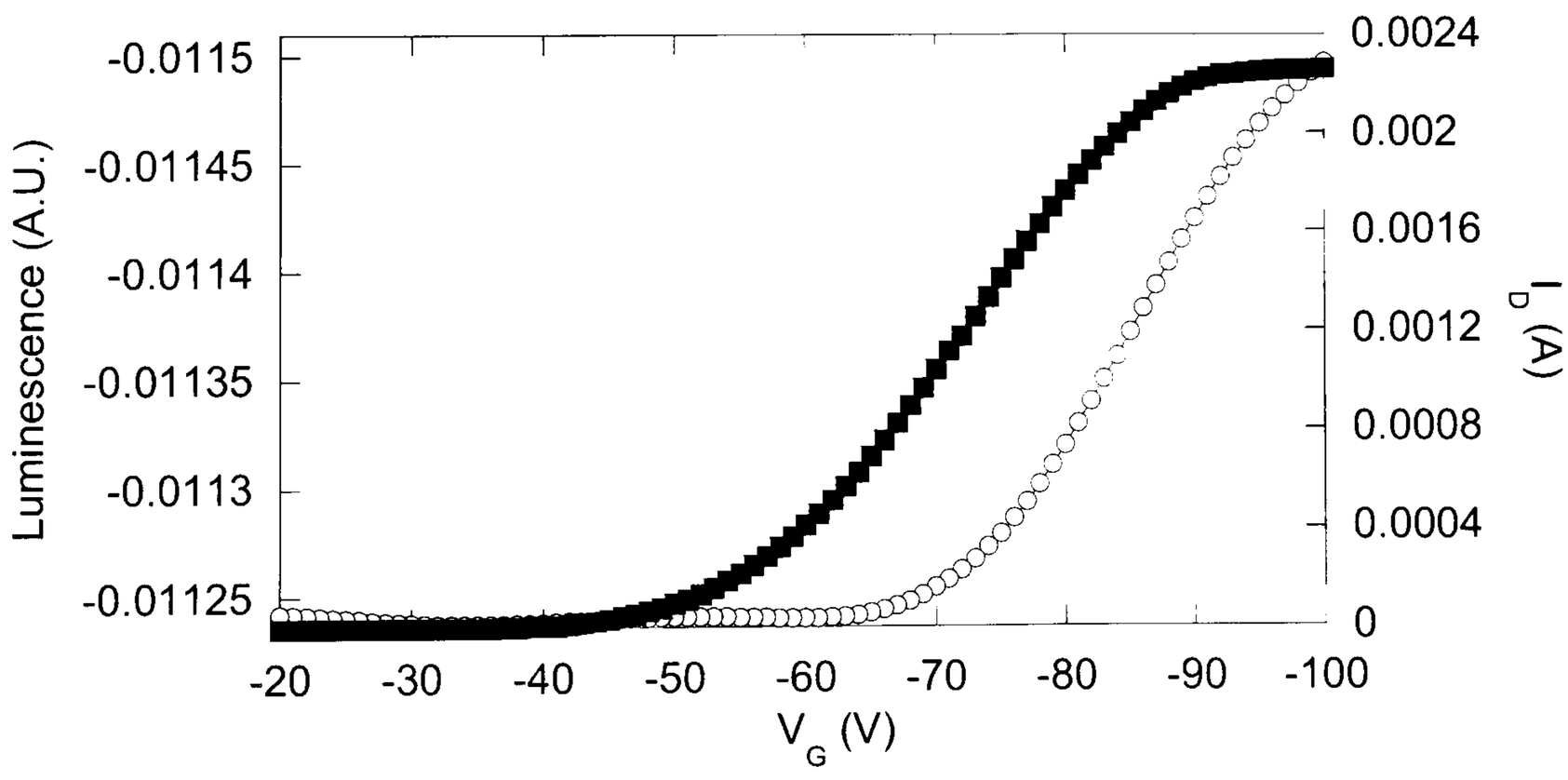


Figure.4.22. Saturated transfer characteristic (filled squares) and corresponding luminescence intensity (open circles) for a 2.5μm syn-pBTTT transistor, operated at V_D = -80V

The applied drain voltage is -80V, corresponding to a lateral electric field of 320kV/cm. This field corresponds to those present in OLED devices (~500kV/cm). No field-effect electron transport behaviour was observed in any of these devices, suggesting recombination occurs in the vicinity of the drain electrode. This lack of n-type transistor behaviour is likely to be due to trapping at the dielectric/polymer interface, as described in Chapter 5.

Electroluminescence was only observed in the saturation regime ($V_D \geq V_G$). The EL intensity increases faster than the current at higher voltages, and like I_D, the rate falls off as V_G approaches V_D. As electron–hole recombination depends on the density of holes close to the drain, as well as the injection of electrons, the number of emitted photons should be proportional to the hole current. The drain current and light emission intensity steadily increase on sweeping the gate voltage at a constant drain voltage (transfer characteristics), if the gate voltage is above a threshold value. The gate voltage determines the drain current, but should not directly influence the electron injection. The onset of the EL is at a higher voltage than the onset of the drain current, so it seems that a minimum charge density of holes is required.

For light emission to occur, electrons must be injected into the LUMO. This only seems to take place at high electric fields. As EL is only observed in saturation for high applied biases, these high lateral fields could modify the HOMO–LUMO levels of the organic material near the drain to enable electron tunnelling from the drain into the LUMO level of the organic material in the pinch-off region.[33] This confers with the optical micrograph in Fig.4.19, as light emission appears to originate close to the drain electrode. On increasing the drain-voltage the electroluminescence intensity increases faster than the drain current, as the tunnelling barrier is dependent on V_D.

Light emission was not observed if the devices were measured in air. If a transistor was measured after being taken into air, it exhibited a bright spark (appearing to correspond to the expected colour of the EL) at the voltage at which emission is seen to start, as noted from the IVL spectra measured under nitrogen. Electrical characteristics did not appear to be affected, though in some cases a dip in the drain current was observed at this point. Encapsulation using 1μm thick poly (vinylphenol) (PVP) or Cytop insulators did not prevent this, though when devices were pumped down in vacuum and re-measured under nitrogen, fainter light emission was again seen to occur. This suggests that we should also account for some sort of trapping mechanism. When tested in dry air the same effect is observed – so the atmospheric component responsible is likely to be oxygen. Probably, the diffusion of molecular oxygen into the film acts to trap electrons. The application of a continuous gate voltage also seems to contribute to trapping, as in this case no EL is observed, unlike sweeping and pulsed operating modes.

4.4. Conclusions and further work

The first part of this Chapter was concerned with contact resistance. Scaling down of device dimensions should result in enhanced currents, a higher operational frequency and a higher mobility, as the drain current is inversely proportional to L and the maximum switching frequency is proportional to μ/L^2. However, injection problems are often noticeable from the non-linearity and finite conductance of the output characteristics for shorter channel length transistors ($L \leq 5\mu m$). This was observed for syn-pBTTT transistors ($I_P \sim 5.3eV$). The contact resistance (R_C) was estimated using the transfer line method (TLM) and it was found that reducing the thickness of the chromium adhesion layer by 2nm reduced R_C at the gold electrodes. This could be because charge injection is improved as the potential distribution due to V_G is proportionally higher over the gold part of the electrode. A better

morphology near the contacts would also reduce R_C. Use of a 5nm ITO adhesion layer instead of chromium further improves device performance, as the workfunction of ITO is a closer match to that of gold. So too successfully scale down the channel length in PFETs, the thickness of the dielectric (and corresponding voltages) needs to be reduced and the barrier to hole injection minimised.

Finite conductance stems from channel length shortening at high drain biases. This, like contact resistance, is more significant in shorter channel devices and is approximated to be ~2μm for the syn-pBTTT system studied. The saturation equation can no longer be used to accurately determine the mobility as the gradual channel approximation is no longer valid ($V_D > V_G$). At these high drain voltages the pinch-off region expands from the drain into the channel, leading to enhanced transport in the bulk. Electron injection can also occur close to the drain electrode, and a decrease in currents is observed at high drain biases possibly due to recombination. In addition to this, light emission is observed close to the drain electrode when operated in the saturated regime. The EL corresponds to the PL and the luminescence intensity is dependent on the drain bias. Light emission is very sensitive to oxygen levels and trapping, as is only observed if pulsed or swept biases are applied.

An interesting trend observed concerned the polymers that exhibited electroluminescence. Polythiophene derivatives are generally not considered to be very luminescent and a luminescence efficiency of ~$2x10^{-4}$% is estimated for regioregular polythiophene.[35] Preliminary photoluminescent quantum efficiency (PLQE) measurements carried out with the help of Jo Wilson using the integrating sphere and Fluoromax estimated the quantum efficiency of syn-pBTTT to be less than 1%. Similar results were also obtained for ant-pBTTT and P3HT, which both display clearly observable EL in an OLET structure. This is interesting as more

'luminescent' materials such as PFB and PFMO did not exhibit observable light emission in a transistor structure. Perhaps the LUMO is crucial to observing this effect. All the OLET materials (including F8T2) have a LUMO over 2.6eV, whilst PFB and PFMO have a LUMO of 1.9 and 2.0eV, respectively. In this case, the injection barrier to electron injection from gold is insurmountable at the magnitude of voltages applied. On the other hand, the materials that light emission was observed from in a transistor structure all contained a thiophene group. Sulphur and gold share an affinity, which is further discussed in the following Chapter in which this property will be manipulated to induce a dipole layer at the gold surface using sulphur terminated molecules. Perhaps a chemical interaction occurs between these species that alters the interfacial energy barriers to be more favourable to the tunnelling of electrons. It would be interesting to carry out further PLQE measurements of thin films, diodes and OLET of the materials concerned to see exactly what correlation exists.

References

1. C. D. Dimitrakopoulos and P. R. L. Malenfant, *Adv. Mater.* **14** 2 (2002)

2. J. Zaumseil, K. W. Baldwin, J. A. Rogers, *J. Appl. Phys.* **93** 10 (2003)

3. S. M. Sze, Physics of Semiconductor Devices, 2nd Edition, John Wiley & Sons (1981)

4. J. C. Scott and G. G. Malliaras, *Chem. Phys. Lett.* **299** 115 (1999)

5. H. Ishii, K. Sugiyama, E. Ito, K. Seki, *Adv. Mater.* **11** 605 (1999)

6. D. Poplavskyy, *PhD Thesis* (2003)

7. S. Luan and G. Neudeck, *J. Appl. Phys.* **72** 2 (1992)

8. H. Sirringhaus, T Kawase, R. H. Friend, T Shimoda, M. Inbasekaran, W. Wu, E. P. Woo, *Science* **290** 2123 (2000)

9. L. Bürgi, H. Sirringhaus, and R. H. Friend, *Appl. Phys. Lett.* **80** 16 (2002)

10. L. Bürgi, T. J. Richards, R. H. Friend, H. Sirringhaus, *J. Appl. Phys.* **94** 9 (2003)

11. M. Leufgen, U. Bass, T. Muck, T. Borzenko, G. Schmidt, J. Geurts, V. Wagner, L. W. Molenkamp, *Syn. Met.* **146** 341-345 (2004)

12. T. Sakanoue, E. Fugiwara, R. Yamada, and H. Tada, *Appl. Phys. Lett.* **84** 16 (2004)

13. Patent No: DE 10 2005 048 774.2

14. M. L. Chabinyc, J.-P. Lu, R. A. Street, Y. Wu, P. Liu, and B. S. Ong, *J. Appl. Phys.* **96** 4 (2004)

15. G. Horowitz, *J. Mater. Res.*, **19** 7 (2004)

16. C. Tanase, E. J. Meijer, P. W. Blom, D. M. de Leeuw, *Organic Electronics* **4** 33-37 (2003)

17. E. J. Meijer, G. H. Gelinck, E. van Veenendaal, B.-H. Huisman, D. M. de Leeuw, and T. M. Klapwijk, *Appl. Phys. Lett.* **82** 25 (2003)

18. H. Sirringhaus, N. Tessler, D. S. Thomas, P. J. Brown, R. H. Friend, in *Advances in Solid State Physics* **39** 101-110, B. Kramer. Ed. (Vieweg, Braunschweig, Germany) (1999)

19. Y. Xu and P. R. Berger, *J. Appl. Phys.* **95** 3 (2004)

20. M. D. Austin and S. Y. Chou, *Appl. Phys. Lett.* **81** 23 (2002)

21. J. R. Haynes and H. R. Briggs, *Phys. Rev.* **86** 647 (1952)

22. M. Ahles, A. Hepp, R. Schmechel, and H. von Seggern, *Appl. Phys. Lett.* **84** 3 (2004)

23. H. Sirringhaus, N. Tessler, R. H. Friend, *Science* **280** 1741-1744 (1998)

24. A. Asimakis, *PhD Thesis* (2005)

25. N. C. Greenham and R. Friend, *Semiconductor Device Physics of Conjugated Polymers*, in Solid State Physics **49**, Academic Press (1995)

26. M. Pope and C. E. Svenberg, *Electronic Processes in Organic Crystals and Polymers*, 2nd Edition, Oxford Science Publications (1999)

27. L.-L. Chua, J. Zaumseil, J.-F. Chang, E. C.-W. Ou, P.K.-H. Ho, H. Sirringhaus, R. H. Friend, *Nature* **434** 194-199 (2005)

28. E. J. Meijer, D. M. de Leeuw, S. Setayesh, E. van Veenendaal, B. H. Huismann, P. W. Blom, J. C. Hummelen, U. Scherf, T. M. Klapwijk, *Nature Materials* **2** 678-682 (2003)

29. C. Rost, S. Kang, W. Riess, M. A. Loi, M. Murgia, and M. Muccini, *Appl. Phys. Lett.* **85** 9 (2004)

30. C. Rost, S. Kang, W. Riess, M. A. Loi, M. Murgia, and M. Muccini, *Syn. Met.* **146** 237-241 (2004)

31. C. Rost, D. J. Gundlach, S. Karg. W. Riess, *J. Appl. Phys.* **95** 10 (2004)

32. A. Hepp, H. Heil, W. Weise, M. Ahles, R. Schmechel, and H. von Seggern, *Phys. Rev. Lett.* **91** 15 (2003)

33. C. Santato, R Capelli, M. A. Loi, M. Murgia, F. Cicoira, V. A. L. Roy, P. Stallinga, R Zamboni, C. Rost, S. F. Karg, and M. Muccini, *Syn. Met.* **146** 329-334 (2004)

34. T. Oyamada, H. Sasabe, C. Adachi, S. Okuyama, N. Shimoji, and K. Matsushige, *Appl. Phys. Lett.* **86** 093505 (2005)

35. D. Braun, G. Gustafsson, D. McBranch, A. J. Heeger, *J. Appl. Phys.* **72** 564 (1992)

Chapter 5

Controlling transistor characteristics using self-assembled monolayers

In this Chapter self-assembled monolayers were used to tune the injection and interface properties of polymer field-effect transistors. Thiols preferentially adsorb onto gold, and if terminated with an electronegative group induce a dipole at the surface that raises the workfunction of the gold and improves hole injection into the polymer. Fluorinated aromatic thiols perform best with syn-pBTTT, increasing the mobility threefold. This corresponds to a decrease in contact resistance. Device operation can likewise be worsened by terminating the monolayer with an electron donating end group. Trichlorosilanes improved mobilities tenfold by improving molecular order in the accumulation layer, so reducing the energetic disorder and activation energy. They also act to passivate the silica interface by reducing the concentration of hydroxyl groups that can act as electron traps. N-type transport in ambipolar transistors can also be enhanced using amine terminated silanes as electrons are attracted towards the positive dipole at the interface. Finally, a combination of SAMs resulted in high mobilities of 0.041cm^2/Vs for syn-pBTTT and 0.29cm^2/Vs for ant-pBTTT transistors. Combining thiols and silanes improves the order at interface and injection into polymer, both of which are crucial for optimum device performance.

Until recently, the poor mobility of organic materials resulted in the current of a transistor being limited mainly by the channel resistance. Improvements in mobility and the need for air stable materials with high ionisation potentials have led to contact resistance being an increasingly significant problem, which was discussed in Chapter 4. In this Chapter, a solution is presented by using a class of self-assembling molecules, called thiols, to modify the workfunction of gold (Φ_{Au}). Mismatch between the Φ_{Au} and ionisation potential of the active polymer can result in an energy barrier that is inhibitive to hole injection. By grafting a layer of molecules with a permanent dipole moment onto the gold electrodes, a dipole layer can be created at the gold/polymer interface. The effective barrier to injection can be thus be modified, as it is dependent on the magnitude and direction of these induced dipoles.

This has previously been attempted for organic diode systems using poly [2-methoxy, 5-(2'-ethyl-hexyloxy)-1, 4-phenylene vinylene (MEH-PPV) with copper[1] and silver electrodes,[2] demonstrating control of injection via tuning of the Schottky energy barrier over a range of +0.5eV for holes and -1eV for electrons, respectively. This logic has also been applied to other self-assembled monolayers in organic diode systems featuring indium tin (II) oxide (ITO) as the anode. ITO is a promising candidate for OLEDs as it combines good electrical conductivity with transparency, but has a relatively low workfunction of 4.6eV.[3] Lee et al. improved the device characteristics of an OLED by using a hole transporting SAM.[4] An increase in the ITO workfunction (Φ_{ITO}) (decreasing the effective barrier to hole injection) was realised by Fujihira et al. who varied the electronegativity of the terminal groups in benzoyl chloride monolayers assembled on ITO.[5] Day et al. varied the dipole moment of phosphoric acid monolayers and found the Φ_{ITO} and device performance to increase correspondingly in an OLED structure.[6] Vilan et al. also adjusted the

barrier height of n-type GaAs diodes with gold electrodes using a series of tartaric acid derivatives with differing dipole moments.[7]

Electrode modification has not been systematically studied in transistors, though a pentacene transistor with fluorinated thiol treated gold electrodes was demonstrated by Dimitrakopoulos et al.[8] Device performance was improved, though this was attributed to increased grain boundary size and not to injection properties. A recent study involved assembling alkane thiols of different chain length onto the gold electrodes of pentacene transistors.[9] Changes in the dipole moment were not addressed, as improvements in mobility were again attributed to improved morphology.

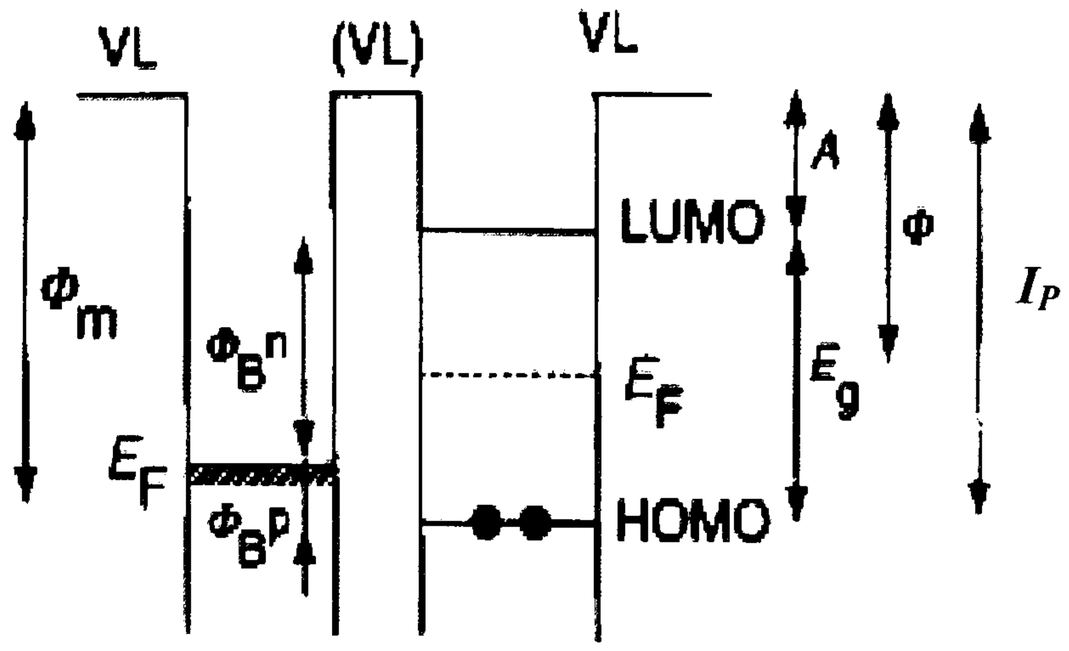
Though morphology is a more significant issue in small molecules than amorphous polymers, ordering polymers has been demonstrated to dramatically increase the mobility. If the polymer exhibits liquid crystalline behaviour, alignment methods encourage the polymer chains to orientate in a preferential direction. A simple annealing step can also facilitate the formation of microcrystalline domains within the amorphous matrix, as in regioregular P3HT and syn-pBTTT. Another commonly used method involves improving the order of the polymer at the interface using silanes. This group of molecules self-assembles due to interactions with the hydroxyl groups naturally present on silicon dioxide or glass surfaces. Charge transport can be improved as the alkyl chains present in most polymers are perpendicular to the backbone (as are only added to improve solubility), so can align in between the network of alkyl silane chains that are pointing upwards from the interface. This then enables the chains to pack closer together, improving charge transport along the conjugated system.[10]

In this work, a range of thiols was firstly chosen to investigate the effect of the dipole layer at the polymer/electrode interface. Any improvements (or worsening) in the performance were investigated by comparing device characteristics, contact resistance, and Kelvin probe measurements. The performance of silylating SAMs was also evaluated in order to optimise device performance, before finally combining both of the surface treatments.

5.1.1. The metal/organic interface

The previous chapter presented a simplistic view of injection into an organic material from a metal. Injection mechanisms are not yet fully understood, as the situation is somewhat more complicated for disordered organic materials. Simplistically, the contact is 'good' if the polymer HOMO level is close to the electrode work function (LUMO in case of n-type materials) and 'bad' if a potential barrier exists at the interface, as it would act to inhibit injection. I will start by defining and building on the basic concepts before discussing the possibilities for interfacial manipulation between an organic material and metal.

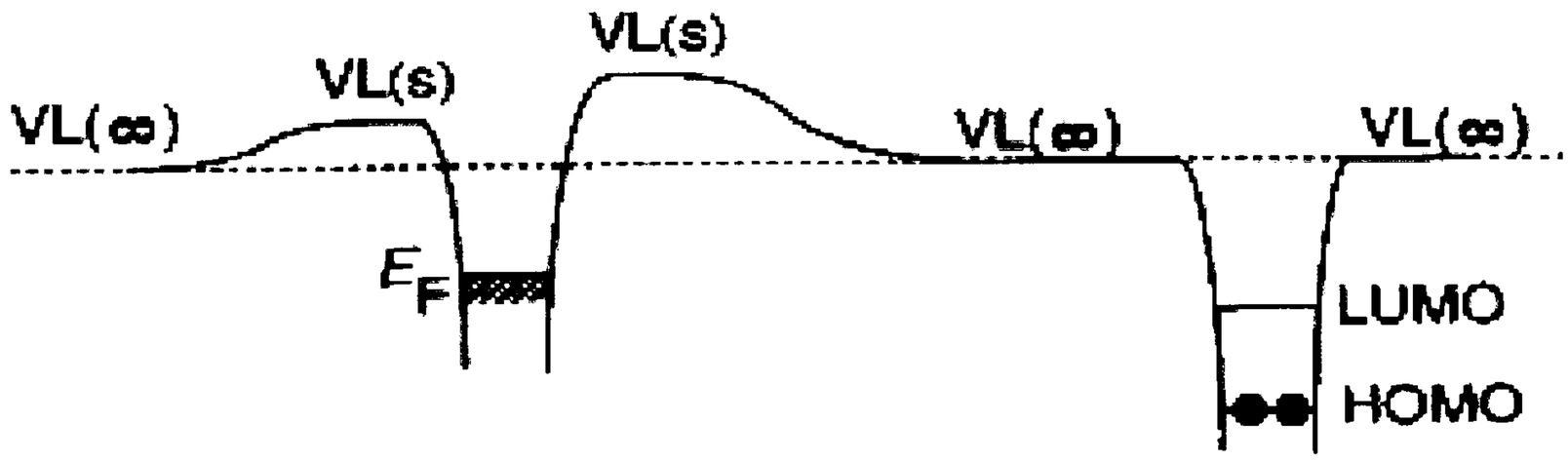
Consider the diagram below illustrating the electronic structure of a metal and organic solid at an infinite distance apart. The Fermi level, E_F, in a metal is the energy at which the probability of occupation of an electronic state by an electron is one half.[11] Thus, it generally lies midway between the 'full' valence band and 'empty' conduction band. The workfunction Φ is defined as the energy required to remove an electron from the Fermi level to a position outside the material, the vacuum level. In an organic solid the HOMO and the LUMO can be equated to the top of the filled states and bottom of the empty states, respectively. The ionisation potential I_P, electron affinity A, energy gap E_G and workfunction of the organic are assigned as shown.



Metal Semiconductor

Figure.5.1.Diagram illustrating the electronic structure of a metal and organic solid at an infinite distance apart. Φ_B^n and Φ_B^p denote the injection barriers for electrons and holes, respectively. Other abbreviations are as described in the text. Adapted from[12].

According to the Schottky-Mott rule, the hole injection barrier is the difference between the ionisation potential of the organic material and the workfunction of the metal. Similarly, the electron injection barrier is the difference between the metal work function and electron affinity of the organic film. In reality the situation is more complicated as at a metal surface there is a tailing electron density from the free surface into vacuum, thus the vacuum side of the metal will be negative in comparison to the bulk.



Metal Semiconductor

Figure.5.2. Diagram taken from[12]. Schematic representation of the common (virtual) VL of a metal and solid an infinite distance apart, illustrating the difference of vacuum level at the surface VL(s) of the metal due to the tailing electron density from the free surface into vacuum and VL(∞).

To avoid confusion a quick mention must be made to differentiate between the vacuum level at an infinite distance VL (∞) and the experimentally determined vacuum level, which is correlated to an electron at rest just outside the solid. In the latter case, the electron would still be affected by the solid's potential and this is referred to as the vacuum level at the surface VL (s). If the metal and organic solid are brought into contact the organic layer will reach the potential of the surface dipole of the metal. In addition, a further dipole layer may be formed at the interface due to various mechanisms such as charge transfer across the interface, redistribution of the electron cloud, interfacial chemical reactions and interface states or dipoles. This leads to a shift of the vacuum level by Δ as determined by the magnitude of the dipole.[12]

Scott and Mallarias modelled the currents in organic diodes and demonstrated that if the injection barrier ≤ 0.3eV, the contact is ohmic and the so-called space-charge limited current (SCLC) regime occurs.[13] As we are concerned with p-type transistors with gold electrodes, the hole-injection barrier can be approximated by subtracting the workfunction of gold from the ionisation potential of the polymer. Injection barriers could be improved by molecular design of the organic material or by modifying the workfunction of the injecting contacts. The latter technique has the advantage that the ionisation potential can remain high so the organic material is more stable in ambient conditions.

If the magnitude and direction of the dipole layer between the metal and organic layer is controlled, the energy barrier for injection can be easily manipulated. As mentioned earlier, this can be realised by grafting organic molecules possessing a permanent dipole moment onto the pre-patterned metal in order to change its workfunction. Self-assembled monolayers (SAMs) are formed by the adsorption of a specifically designed end group to the desired surface. This is a selective process

and if the molecules are designed to possess a dipole and to be orientated perpendicularly to the metallic surface, the monolayer can be engineered to possess a dipole moment that acts to reduce or increase the effective Schottky barrier to injection.

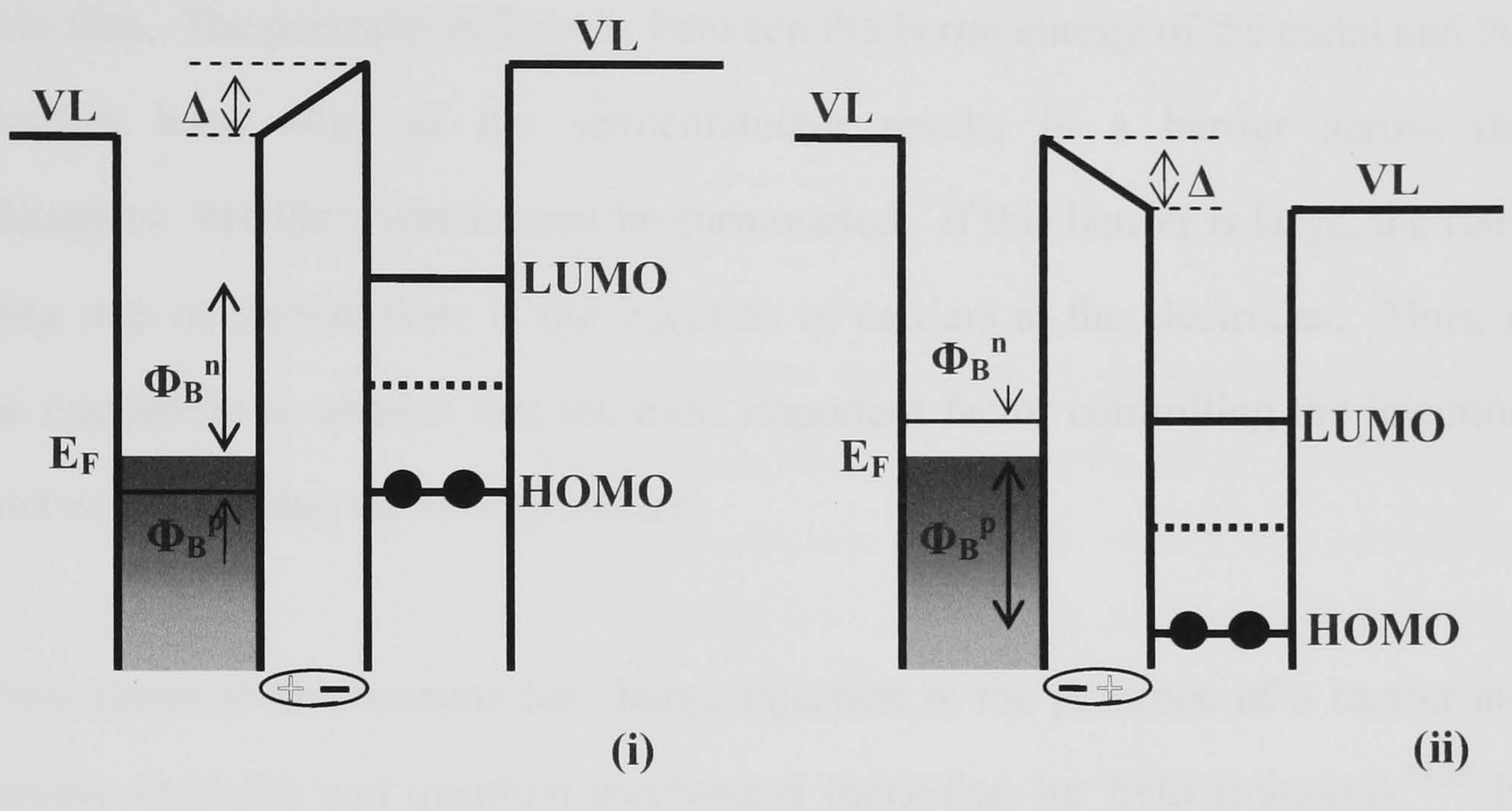


Figure.5.3. Schematic illustrating how the addition of a dipole layer pointing (i) towards the surface raises the workfunction of gold. In (ii) the opposite situation is illustrated and an increase in the hole injection barrier is observed. The direction of a dipole is defined as the direction a negative charge would move.

The diagram above illustrates how the addition of a dipole layer pointing towards the metal surface would raise the vacuum level just outside the substrate, and consequently the workfunction of the gold. Thus, the barrier to hole injection can be reduced. In the opposite situation the barrier to hole injection is increased (or the barrier to electron injection is reduced), so it would be expected that contact resistance would be increased and the transistor characteristics would be worsened.

5.1.2. Charge injection

Energy levels associated with a metal/organic interface have now been established, but for charge injection to actually occur a hole (or electron) has to be promoted from the metal into one of the HOMO (or LUMO) charge transporting states in the organic film. The potential difference between the Fermi energy of the metal and the conduction band edge of the semiconductor results in a barrier across the metal/organic interface, which must be surmounted. If this barrier is large, the rate-limiting step of current flow is the injection of carriers at the electrodes. Thus, it seems reasonable to assume that the most important factor controlling the injection process is overcoming the energy barrier.

The two classical mechanisms for charge injection in the presence of a barrier are thermionic emission and quantum mechanical tunnelling (or field emission).[14,15] In the case of conjugated polymers the injection current follows neither theory exactly, as these approaches were developed for traditional band-type materials and do not translate to disordered organic materials.

The charge carrier states of organic materials are found to be highly localised on short conjugated segments, with the energy levels of these states defined by the average energy of the HOMO or LUMO and the amount of energetic disorder in the system. The distribution of these states will also be affected by electrostatic energy due to an applied voltage, plus a potential from image charge effects (as removing a charge from the metal into the organic creates a potential energy due to attraction with the charge left behind). The injection event can consequently be described by thermally assisted hopping (tunnelling) from the metal to a localised state in the polymer, as illustrated in Fig.5.4.[16]

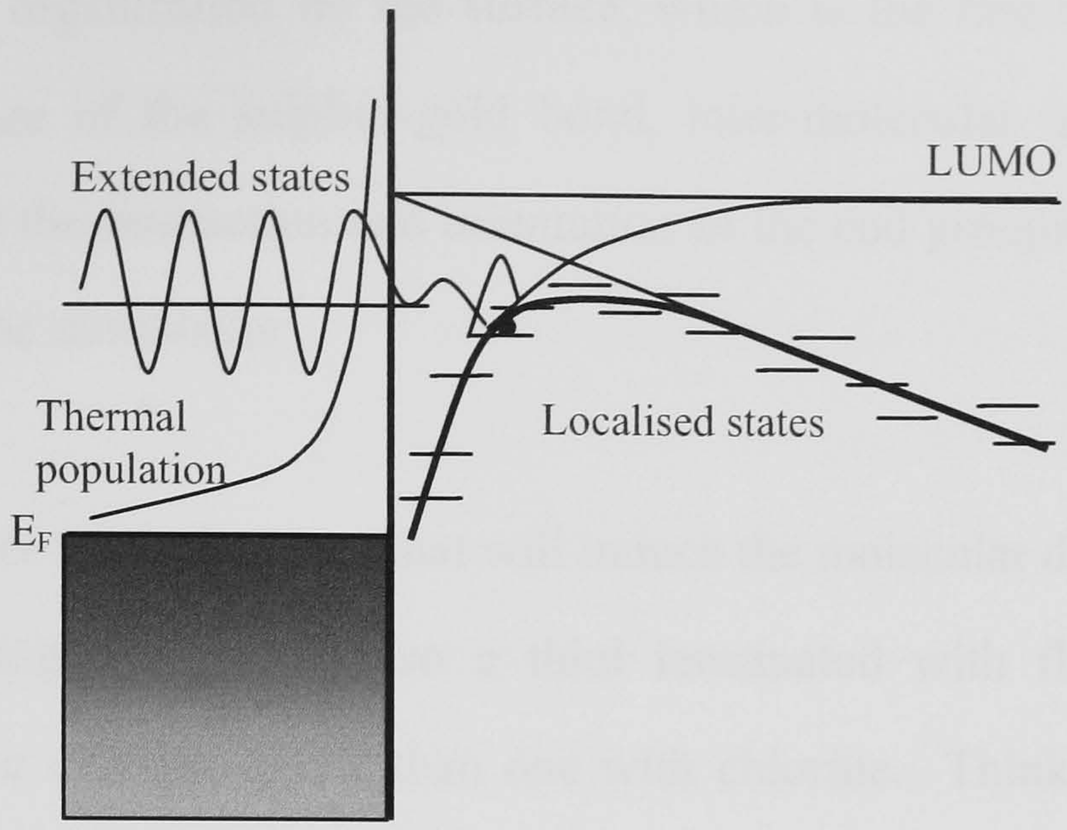


Figure.5.4. Adapted from[16]. This diagram explains the process of electron injection into an organic material. Electrons from extended states the metal (conduction band) tunnel into the localised states of the semiconductor. In this case, four parameters control the injection: the barrier height, the image potential, the potential due to the interfacial electric field, and the level of energetic disorder.

5.2. Modification of hole injection using thiols

5.2.1. Why use thiols?

The main benefits of using SAMs are their ease of preparation and the stability of the monolayers formed. Thiols, as with all SAMs, are distinguished by their molecular composition; namely a head group, which adsorbs to the surface of choice, a spacer group, and a tail group which can be chosen to induce a dipole within the molecule. Allara and Nuzzo[17] first investigated the self-assembly of thiols onto gold surfaces. The self-assembly process involves several steps, starting with bulk solution transport, surface adsorption according to:

$$R - (CH_2)_n - SH + Au \rightarrow R\text{-}(CH_2)_n - S - Au + 0.5H_2 \qquad \{5.1\}$$

followed by 2-D organisation on the surface, which is the rate-limiting step. The strength and nature of the sulphur-gold bond, inter-molecular interactions of the spacer groups and the interaction and orientation of the end groups all determine the configuration of the monolayer.

Let us first consider the end groups that will induce the molecular dipole. Fluorine is the most electronegative element so a thiol terminated with fluorine would be expected to induce a larger dipole than one with chlorine. Thinking along similar lines, an electron-donating methoxyl group should induce the opposite effect with the dipole pointing away from the surface, the opposite direction to that of fluorine or chlorine terminated molecules. The workfunction of the modified gold would raised and lowered respectively.

The range of thiols investigated is shown below:

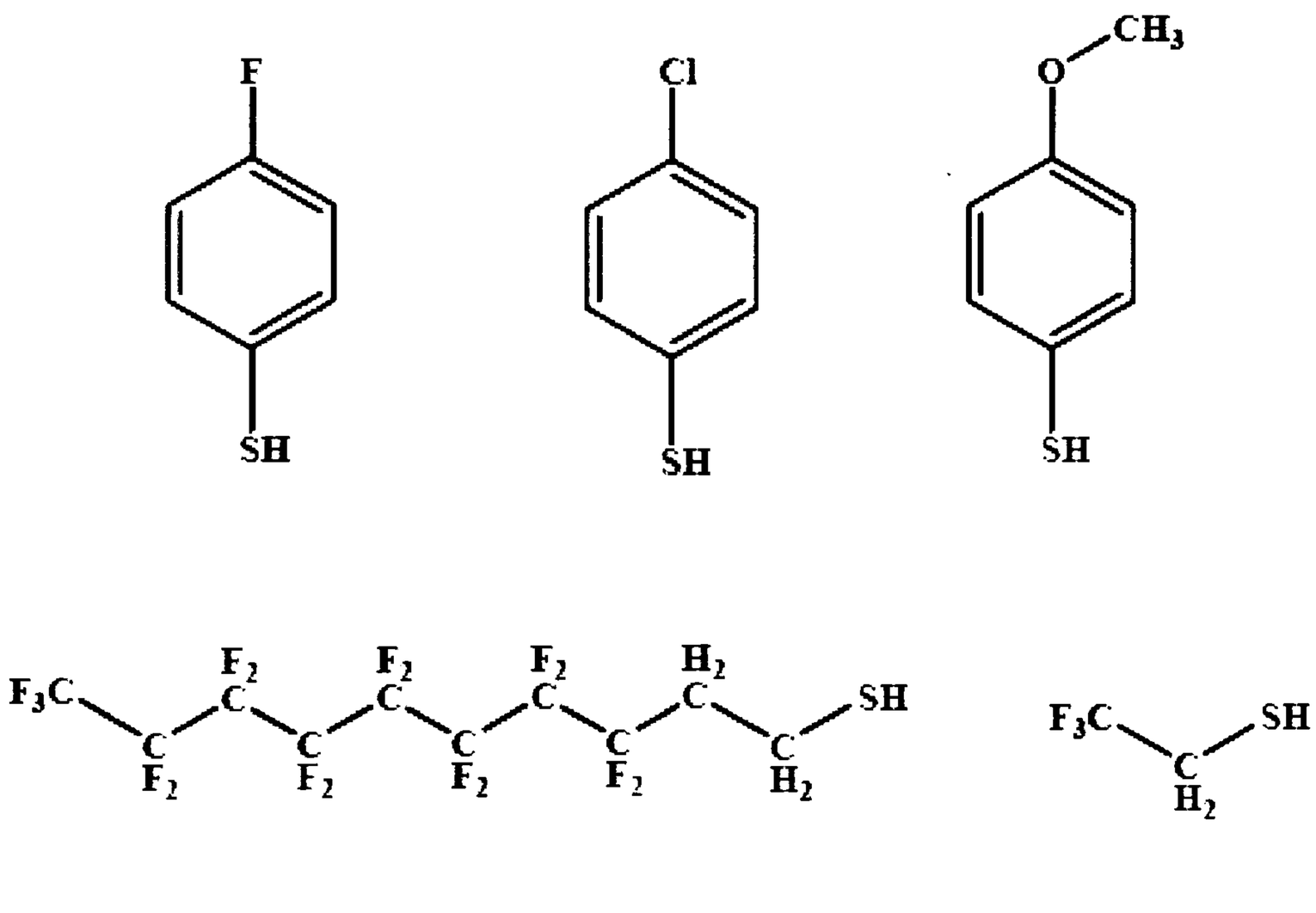


Figure.5.5. From top left going clockwise the names and chemical structures of the thiols used in this work are described: 4-fluorothiophenol (FTP), 4-chlorothiophenol (CTP), 4-methoxythiophenol (MOTP), 2, 2, 2-trifluoroethane thiol (ETSH), and 1h1h2h2h-perfluoro-1-decanethiol (LETSH)

Aromatic systems have increased inter-molecular stability as possess a more rigid backbone so have fewer degrees of conformational freedom.[18] They are also conjugated molecules so should not prove such a barrier to transport as have higher conductivities. To see the effect the dipole moment at the interface has, thiols with fluorine, chlorine and methoxyl groups substituted onto the para position of the benzene ring, were chosen. It has been shown that alkane thiols with long chains (6-7 methylene units) form more ordered, defect-free monolayers than those consisting of shorter chains. However, this could present a problem as the non-conjugated alkane segment could act as an insulating layer, inhibiting rather than increasing injection into a transistor. In order to compare any insulating effect the molecules might have, fluorinated thiols with alkyl spacer groups of differing length were also chosen.

5.2.2. Formation of thiol monolayers

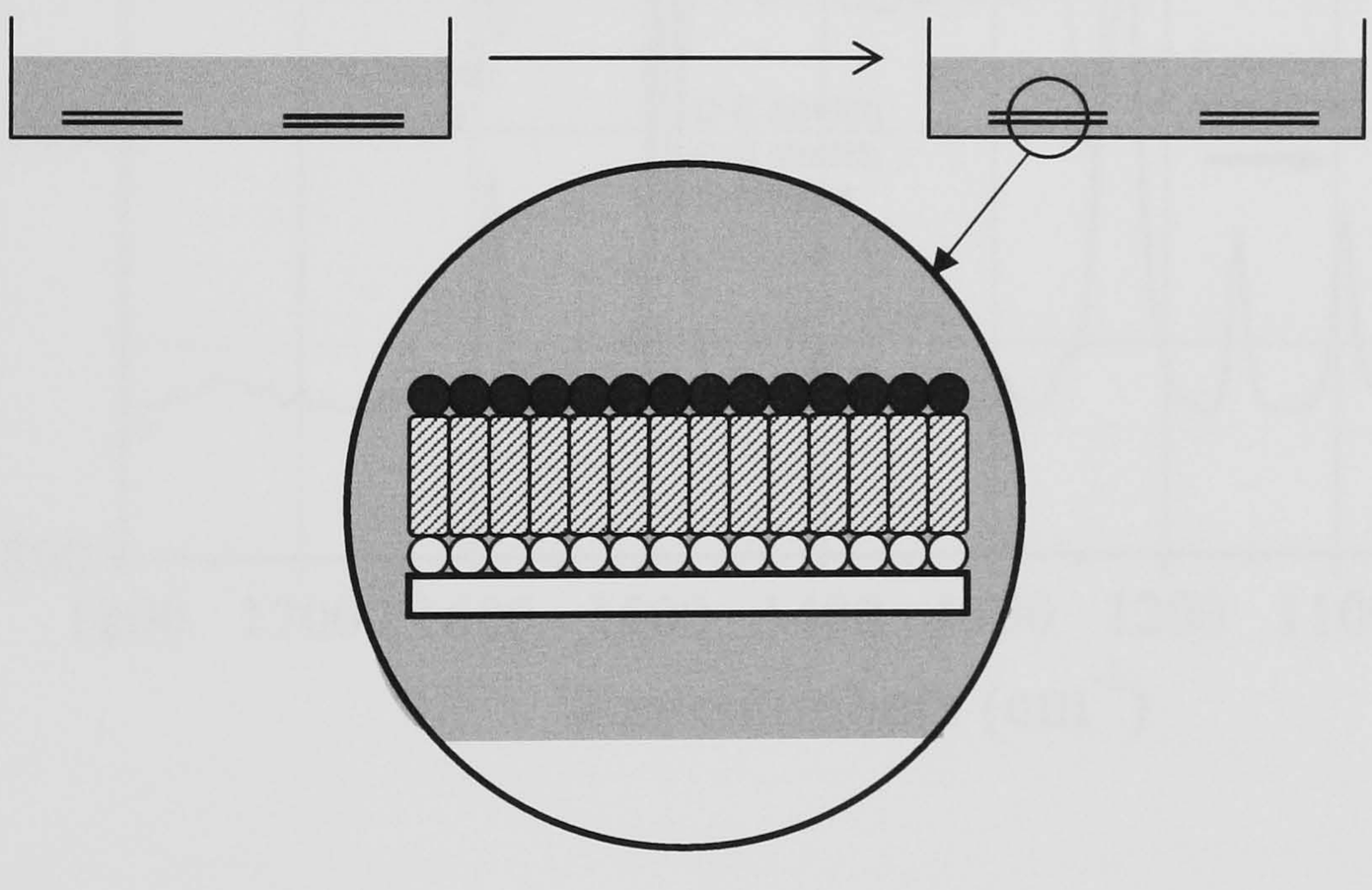


Figure.5.6. Thiols were assembled by immersing the pre-patterned transistor substrates into 1mM thiol solution in ethanol. The magnified picture denotes the sulphur head group (open circle), spacer group (shaded rectangle) and end group (filled circle) of the thiol self-assembled monolayer.

The monolayers were fabricated by immersing cleaned pre-patterned gold/SiO_2/Si substrates into 1mM solutions in ethanol. Immersion times for complete monolayer formation varied from 20 minutes to three hours and were characterised by Kelvin probe measurements. The substrates were then rinsed thoroughly in ethanol and cleaned in the ultrasonic bath for 5 minutes to remove any excess thiols. In this work, all thiol treatments were left for 12 hours to ensure full monolayer coverage.

The spectra of bulk and surface absorbed thiols on gold were measured using infrared reflection absorption spectroscopy (IR-RAS) by Saghar Khodabakhsh.[20] A typical spectrum for 4-fluoro thiophenol (FTP) is illustrated in Fig.5.7.

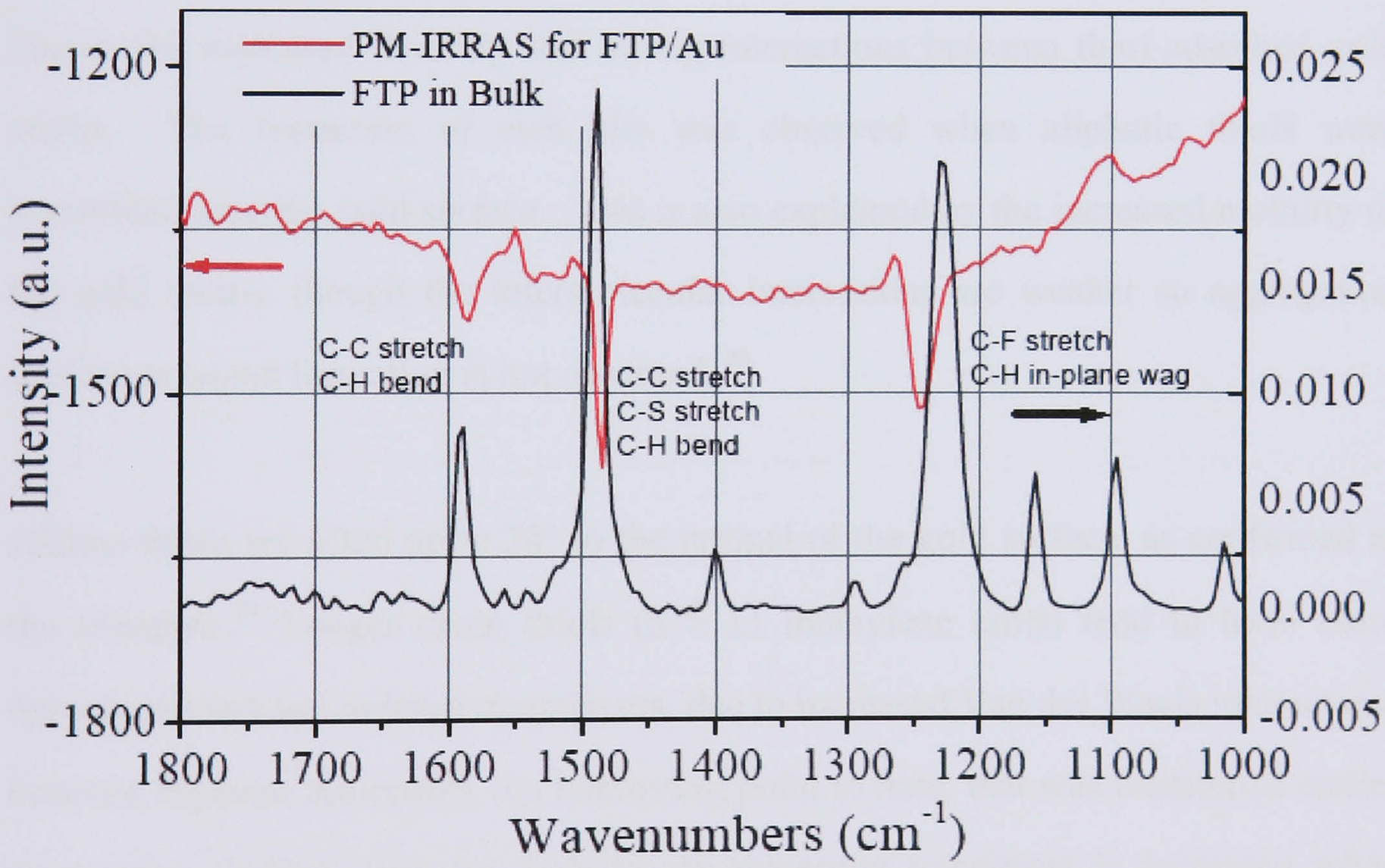


Figure.5.7. Experimental IR spectra for assembled FTP monolayer on gold and bulk FTP for 1000-1800cm^{-1} range.

For the range displayed, the spectra have three peaks in common at 1230cm^{-1}, 1485cm^{-1}, and 1585cm^{-1}, which are attributed to the C-F stretch, C-S stretch and C-C

stretch bands, respectively. According to the surface dipole selection rule, only dipoles of vibrations parallel to the plane of the molecule will be active in the IR spectrum, as dynamic dipoles aligned perpendicular to the surface are reinforced by their mirror image, whilst parallel dipoles would be cancelled out.[19] As all the dipole moments of the above vibrations are parallel to the plane of the molecule, it can be concluded that the FTP molecules are standing upright on the gold surface. Similar results were found for all the aromatic thiols.[20]

Aromatic thiols form more densely packed monolayers and are rigid with strong intermolecular interactions because of the π-electron system. This was confirmed by scanning tunneling microscopy (STM) measurements, also carried out by Saghar Khodabakhsh. Self-assembled aromatic thiols formed gold islands on the terraces due to the increased mobility and strong interactions between thiol-adsorbed gold atoms. The formation of etch pits was observed when aliphatic thiols were assembled onto the gold surface. This is also explained by the increased mobility of the gold atoms, though the intermolecular interactions are weaker so aggregation leading to island formation is not observed. [20]

Alkane thiols are tilted up to 30° to the normal of the gold surface, as confirmed in the literature.[21] Longer chain thiols (n > 11 methylene units) tend to form more densely packed and ordered monolayers, due to increased Van der Waals interactions between adjacent molecules. An interesting point to note, that was mentioned earlier concerning findings that the mobility of pentacene transistors is increased when alkanethiols with an even number of methyl groups are assembled onto the gold electrodes, is the odd-even effect. Different orientations are adopted by alkanethiols with odd or even numbers of methyl spacer groups, as illustrated in Fig.5.8.

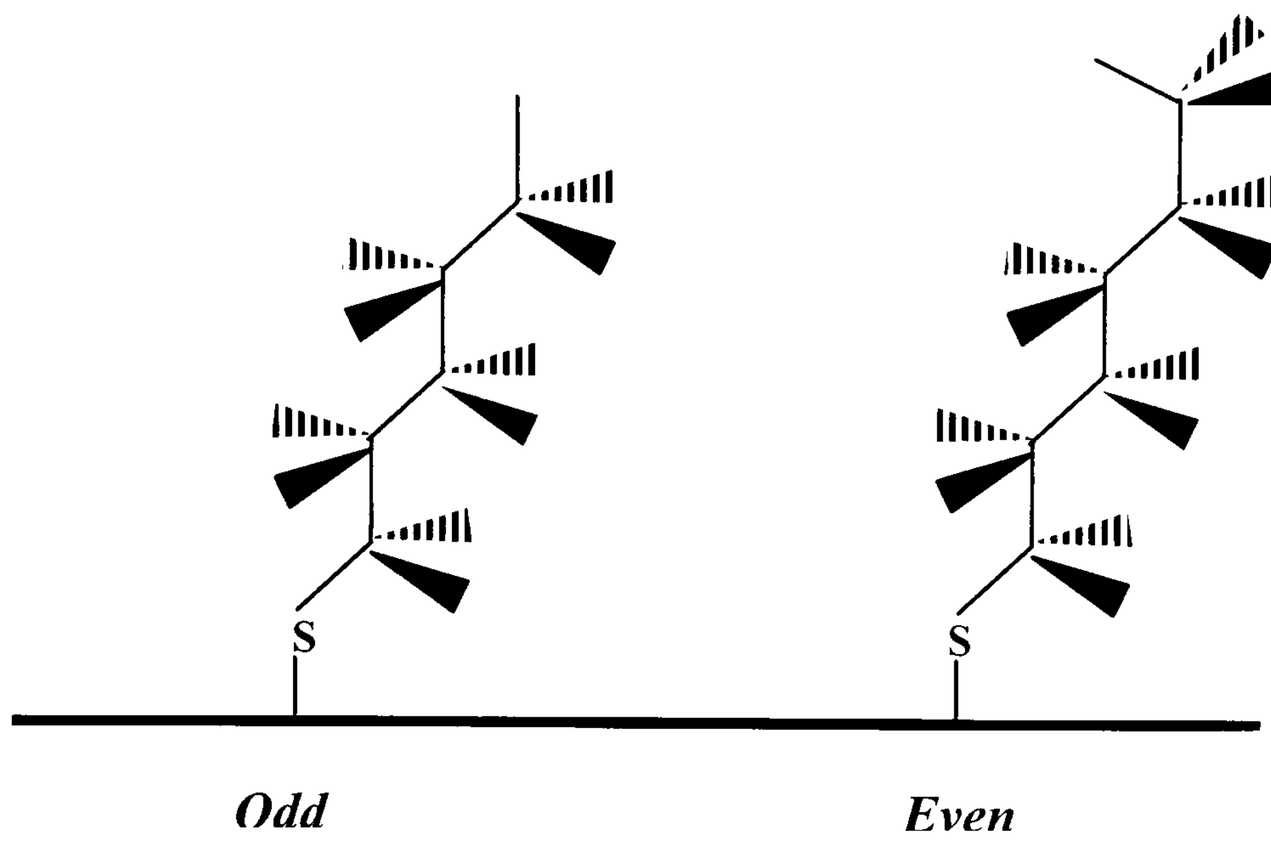


Figure.5.8. Schematic picturing the difference between alkanethiols of odd and even chain lengths. The underlying methyl units are more exposed at the surface if there are an odd number. Adapted from[22]

Monolayers of alkanethiols with an even number of methyl groups exhibit higher contact angles than monolayers with odd numbers of methyl units by ~ 10°, as the underlying methyl units of odd chains are more exposed. This leads to increased wettability and subsequently lower contact angles.[22] Though the thiols are only assembled on the gold, improved adhesion in the vicinity of the contacts could improve carrier injection. This could explain increase of mobility for even chains by providing a preferential structure for pentacene growth.

5.2.3. Workfunction measurements of thiol modified gold

The workfunction change of the gold surface with different thiol layers relative to an untreated substrate is presented in Fig.5.9, as measured by the Kelvin probe technique. The long alkylated fluorinated thiol LETSH raises the workfunction of gold the most, by +0.86eV, and the methoxyl substituted aromatic thiol MOTP actually reduces Φ_{Au} by -0.08eV. The effective hole injection barrier can clearly be modified by the interface dipole arising from the SAM.

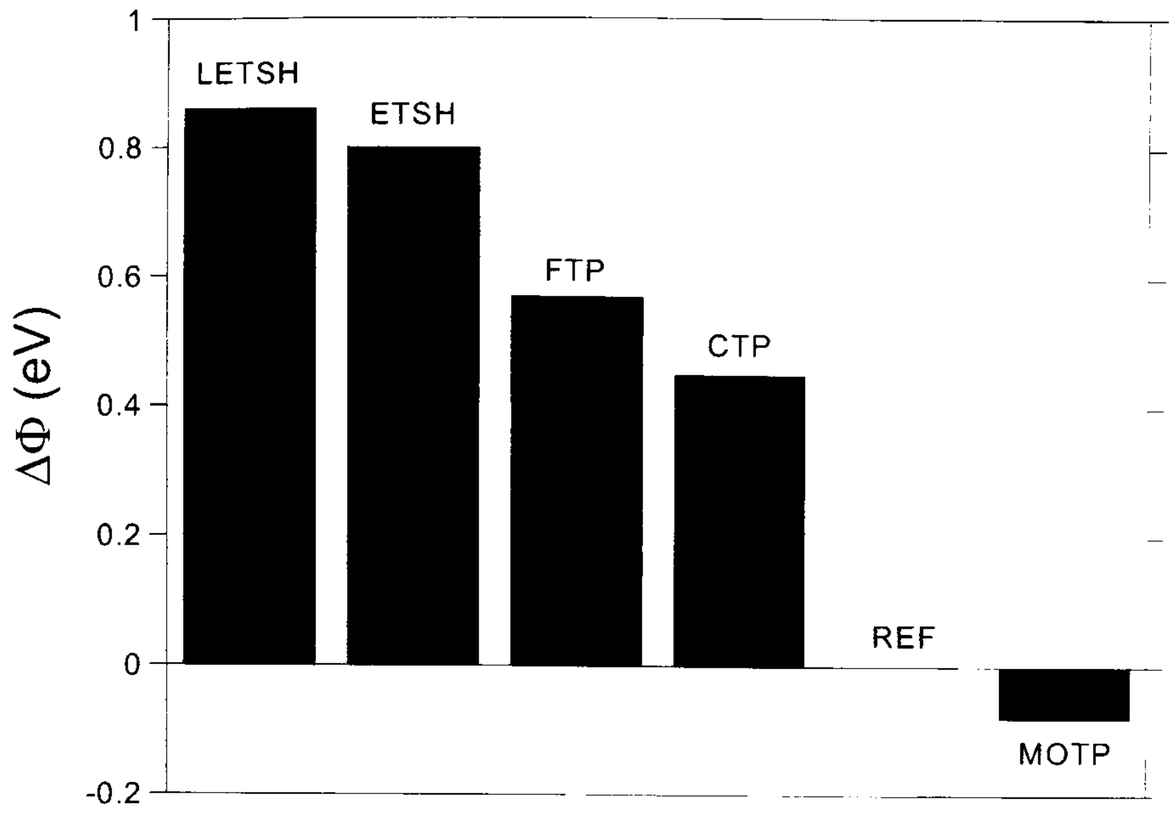


Figure.5.9. Bar chart illustrating the change in workfunction of thiol-treated gold in reference to a clean gold substrate, as measured by the Kelvin probe technique.

Space charge could be induced at the interface, and the consequent change in surface potential can be approximated by:

$$\Phi_{dipole} = \frac{N\mu\cos\theta}{\varepsilon\ \varepsilon_0} \qquad \{5.2\}$$

θ is the angle between dipole and surface normal, ε is the relative permittivity of the layer, ε_0 is the relative permittivity of free space, μ is the dipole moment, and N is the surface concentration of molecules.[7,23] The total dipole moment of the monolayer is the sum of the dipole moment of the spacer and end groups, and the polar Au-S bond. If it is assumed that the dipole moment of the Au-S bond does not change significantly for different molecular terminations, a linear relationship between the change in the workfunction (related to net dipole moment) and the dipole moment of the SAM should apply. This is also an indication that the layers have similar surface concentrations and adsorption angles.

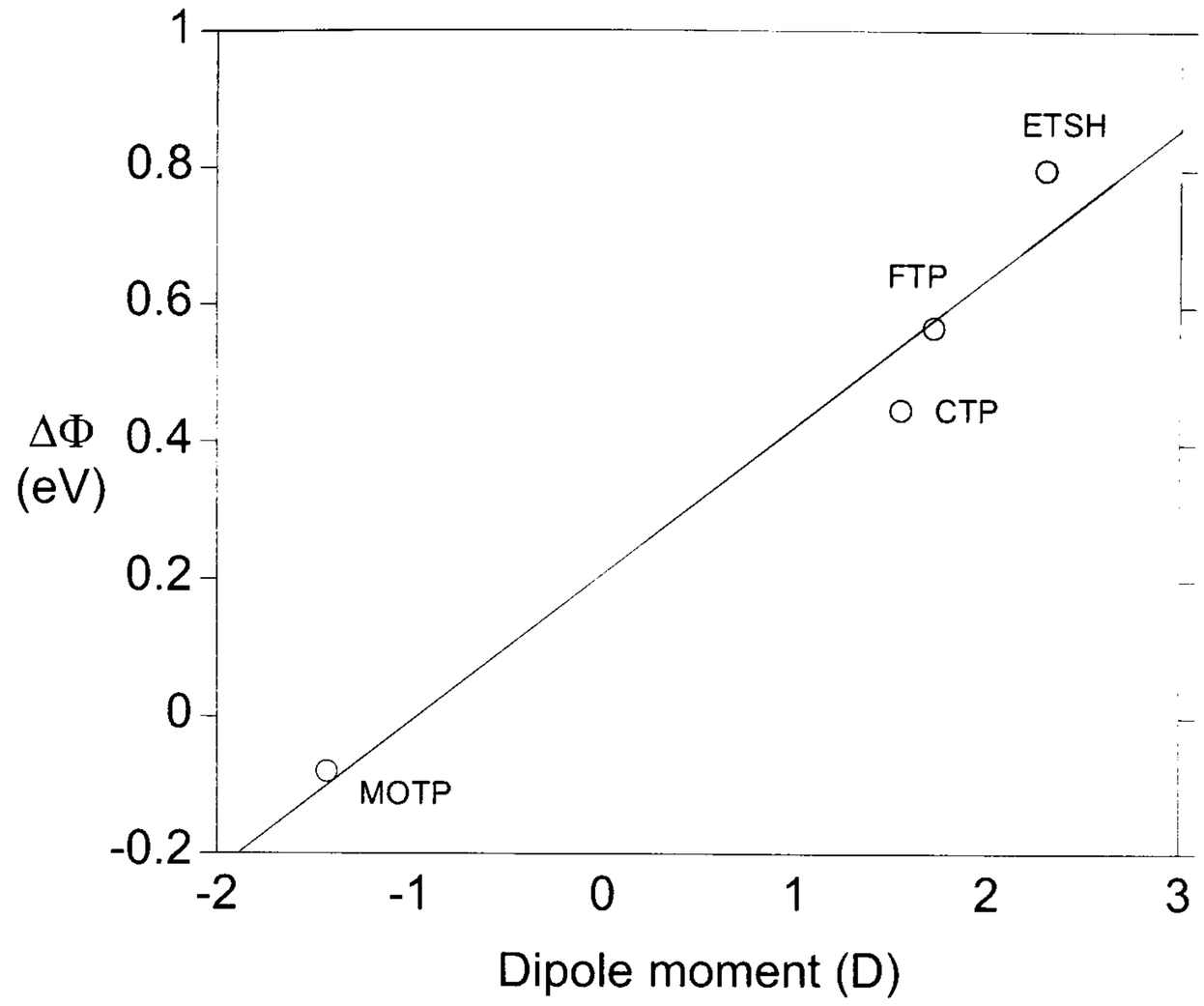


Figure.5.10. Graph showing the linear relation between the measured change in workfunction and the dipole moment of the thiols.

From the earlier discussion of dipole formation at metal/organic interfaces, it was noted that as well as the dipole expected from the adsorbed thiols, an additional dipole due to interactions with the organic layer might be formed. The energetics of the system can not be predicted by considering only the workfunction of the electrode and the ionisation potential of polymer.[12,24] More detailed studies of the composite polymer/thiol/gold interface should be carried out in future, measuring the workfunction change of the entire system and subtracting it from the ionisation potential of the polymer. However, for the purpose of this work a simple comparison of $\Delta\Phi$ of the thiols on gold electrodes will suffice as this Chapter presents a qualitative discussion of properties and how they affect the working of field-effect transistors.

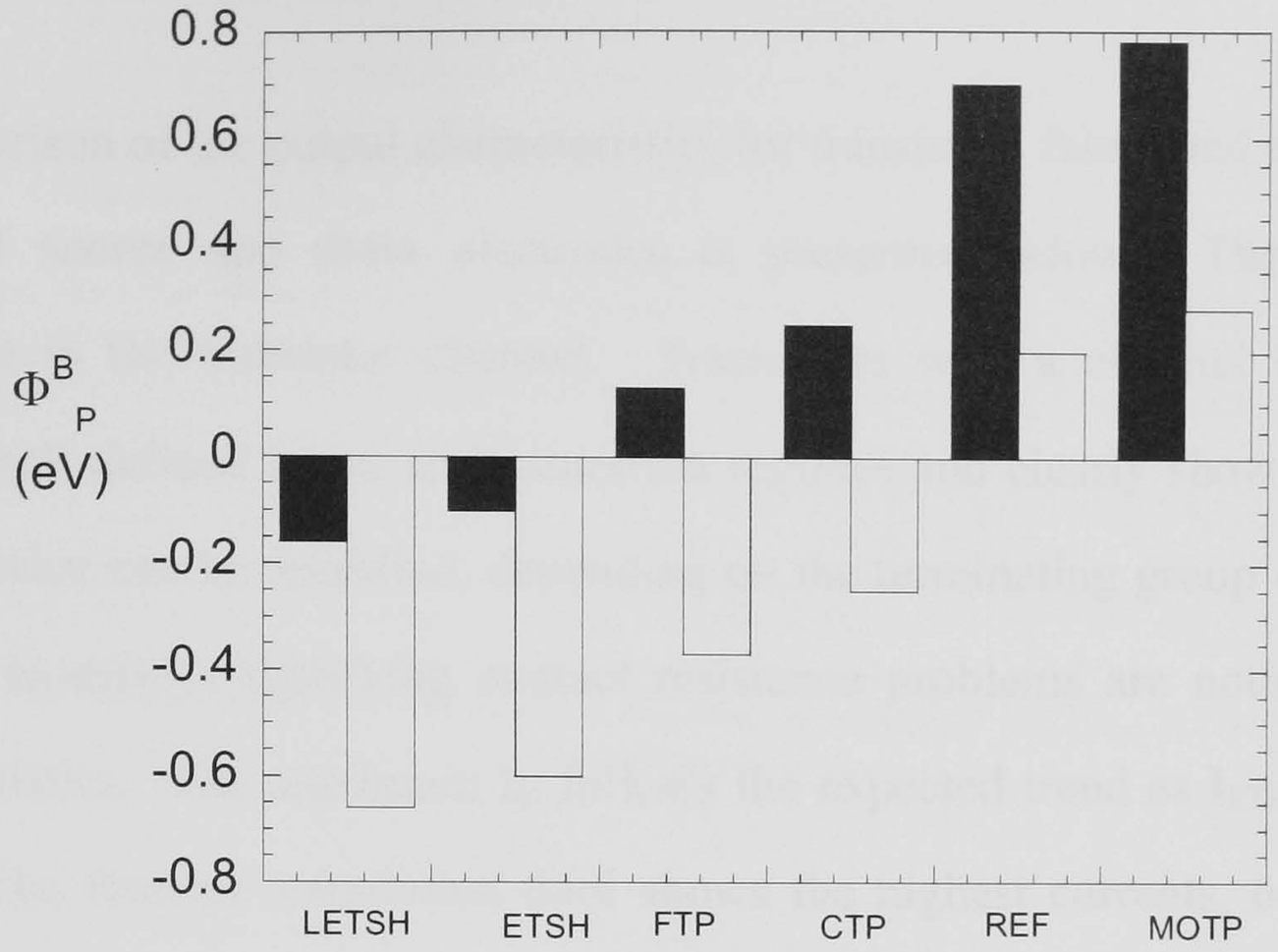


Figure.5.11. Estimation of the hole injection barrier for the different thiols assembled onto gold. The filled bars assume the reference workfunction of gold to be 4.6eV (as measured by calibration of Kelvin probe) and the empty bars assume Φ_{Au} to be 5.1eV.

The HOMO of syn-pBTTT was deduced to be 5.3eV from UPS studies. Kelvin probe does not provide an absolute value of the workfunction, so we will first assume a standard accepted value of 5.1eV for gold. This is unlikely to be exact, as measurements to determine Φ_{Au} are carried out in ultrahigh vacuum. The substrates also have a 5nm chromium adhesion layer, which would also affect the pristine workfunction of the gold substrate. Calibrating the gold reference electrode revealed that the Φ was 4.6eV.* So, bearing in mind that we are concerned with general trends, and neglecting any additional interfacial effects, the effective hole injection energy barrier can be simply illustrated as above by the empty bars, assuming a Φ_{Au} of 5.1eV, or the solid bars, if Φ_{Au} is taken to be 4.6eV. The bottom half of the figure (negative values) indicates no injection barrier, whilst the top half illustrates the effective barrier to hole injection. In both cases, the fluorinated and chlorinated thiols should provide ohmic contacts for hole injection.

* See Section 2.2.2.

5.2.4. I-V characteristics

A comparison of the output characteristics for transistors fabricated on aromatic thiol modified source and drain electrodes is presented below. There is no silane treatment in the transistor channel. Transistors with a channel length of 20μm exhibit well-defined linear and saturation regimes and clearly show that the current in the device can be modified, depending on the terminating group of the thiol. No obvious hysteresis signifying contact resistance problems are noticeable from the characteristics. The maximum I_D follows the expected trend as $I_{FTP} > I_{CTP} > I_{REF} > I_{MOTP}$. The fluorine substituted thiol shows the highest currents, being nearly five times greater than the reference sample. Indeed, the methoxyl substituted thiol displays the worst behavior as is to be expected if the barrier to hole injection is increased.

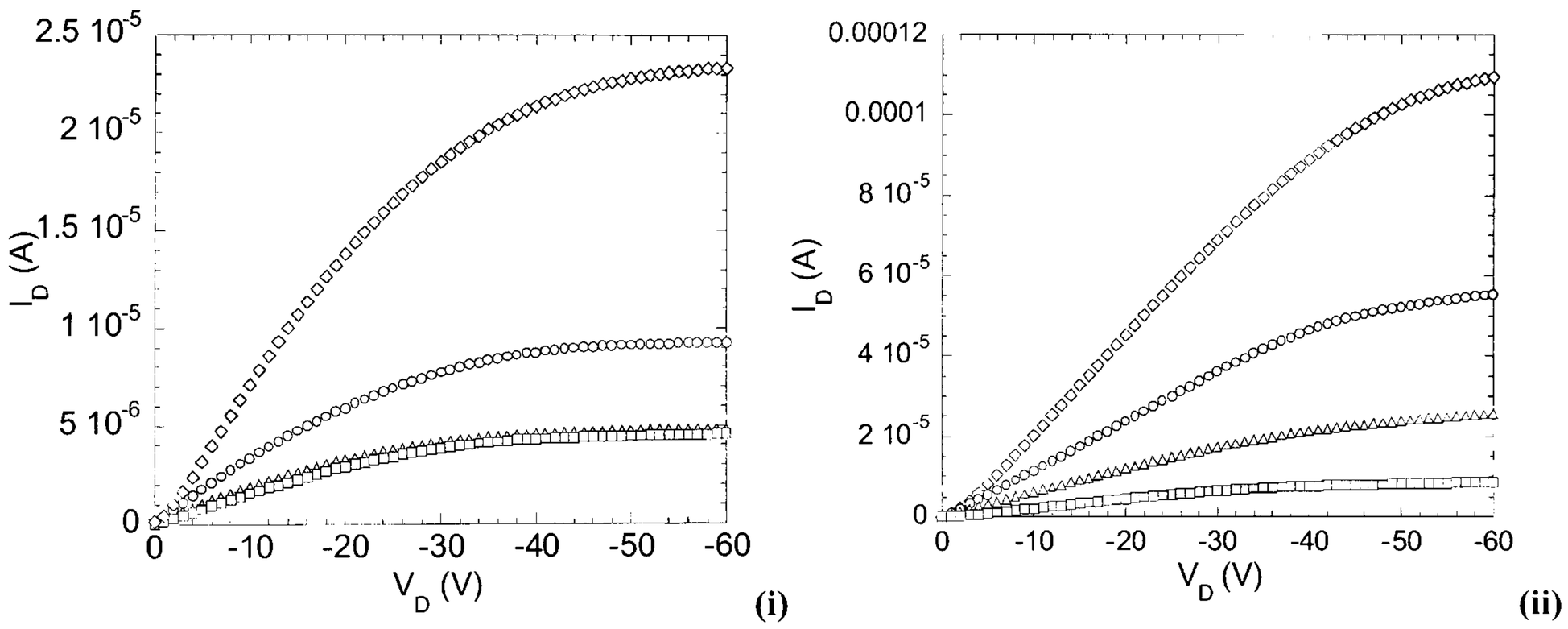


Figure.5.12. Output characteristics comparing aromatic thiol treated syn-pBTTT transistors at a gate voltage of -40V of FTP (diamonds), CTP (circles), a reference (triangles), and MOTP (squares) thiol modified electrodes with channel length (i) 20μm and (ii) 5μm. The channel width is 1cm.

The same trend is followed for transistors with channel length 5μm, though a more noticeable difference is evident between the reference and MOTP devices. The ratio between the saturated drain currents for the FTP transistor in relation to the reference

sample is still similar (~ 4 times greater) to that of the 20μm channel length transistor, as is that of the CTP device (still 2 times greater). The difference in saturated drain currents for the MOTP and reference sample is 3 times worse for the 5μm transistor, a more pronounced increase than that of the longer channel device. This effect is further increased and decreased for 2.5μm and 10μm channel length devices, respectively. As we saw in the previous Chapter, injection problems due to contact resistance are heightened for transistors with shorter channel lengths, so it follows that MOTP treated contacts exhibit worsened characteristics if the channel length is decreased. This corroborates the idea that the injection barrier to hole injection is increased for the MOTP device.

Saturated transfer characteristics presented in semi logarithmic format for a range of substituted thiophenols are displayed below, for the same 20μm channel length transistors.

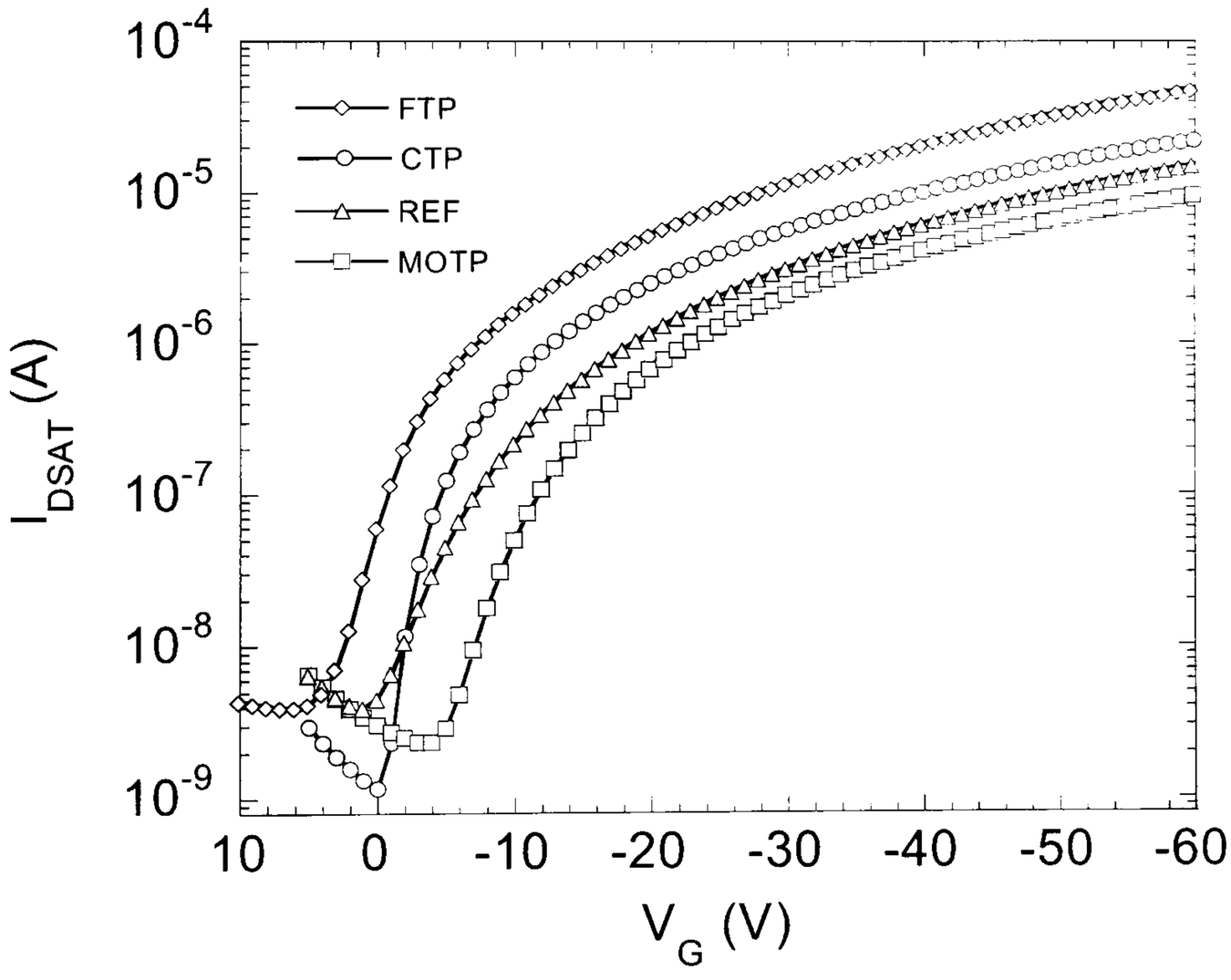


Figure.5.13. Saturated transfer characteristics comparing the same aromatic thiol treated syn-pBTTT transistors as in Fig.5.12. Again diamonds represent FTP, circles CTP, triangles the reference electrode, and squares the MOTP modified electrode.

The switch-on voltage V_0, which signifies the flat band condition, shifts from +4V to -5V, depending on the thiol treatment. The only treatment with a negative turn-on voltage is with MOTP, suggesting that the transistor is completely switched-off at zero gate bias. On the other hand, the FTP treated transistor is switched on at zero gate bias. V_0 follows the trend $V_{0\,(FTP)} > V_{0\,(CTP)} > V_{0\,(MOTP)}$ with an identical pattern observed for transistors of 2.5, 5 and 10μm channel length. V_0 depends on the presence of mobile carriers at the polymer /dielectric interface which is determined by the mismatch between the contact workfunction and HOMO of the polymer, as well as any charge due to interfacial states and dipoles. Thiols are only assembled at the gold contact (not in the channel) and as the barrier to hole injection follows the same pattern as $V_{0,}$ suggests that the variation is due to improved (FTP, CTP) or worsened (MOTP) injection with respect to the reference electrode.

So far, only the aromatic thiols have been considered. Fig.5.14 demonstrates the effect of limited injection as a result of the spacer group, by comparing the output characteristics of the conjugated fluorinated thiol (FTP) with the fluorinated alkane chain thiol (ETSH). The latter, though raising the gold workfunction, functions as an insulating layer resulting in non-linear characteristics and lower currents, as it is harder for the charge carriers to tunnel through the monolayer. A difference in the injection barrier would depend on the conjugation of the spacer group, and its length. Though the injection may seem to be more favourable if only considering the induced surface dipole, we have not taken into account the tunnelling process required for injection to occur.

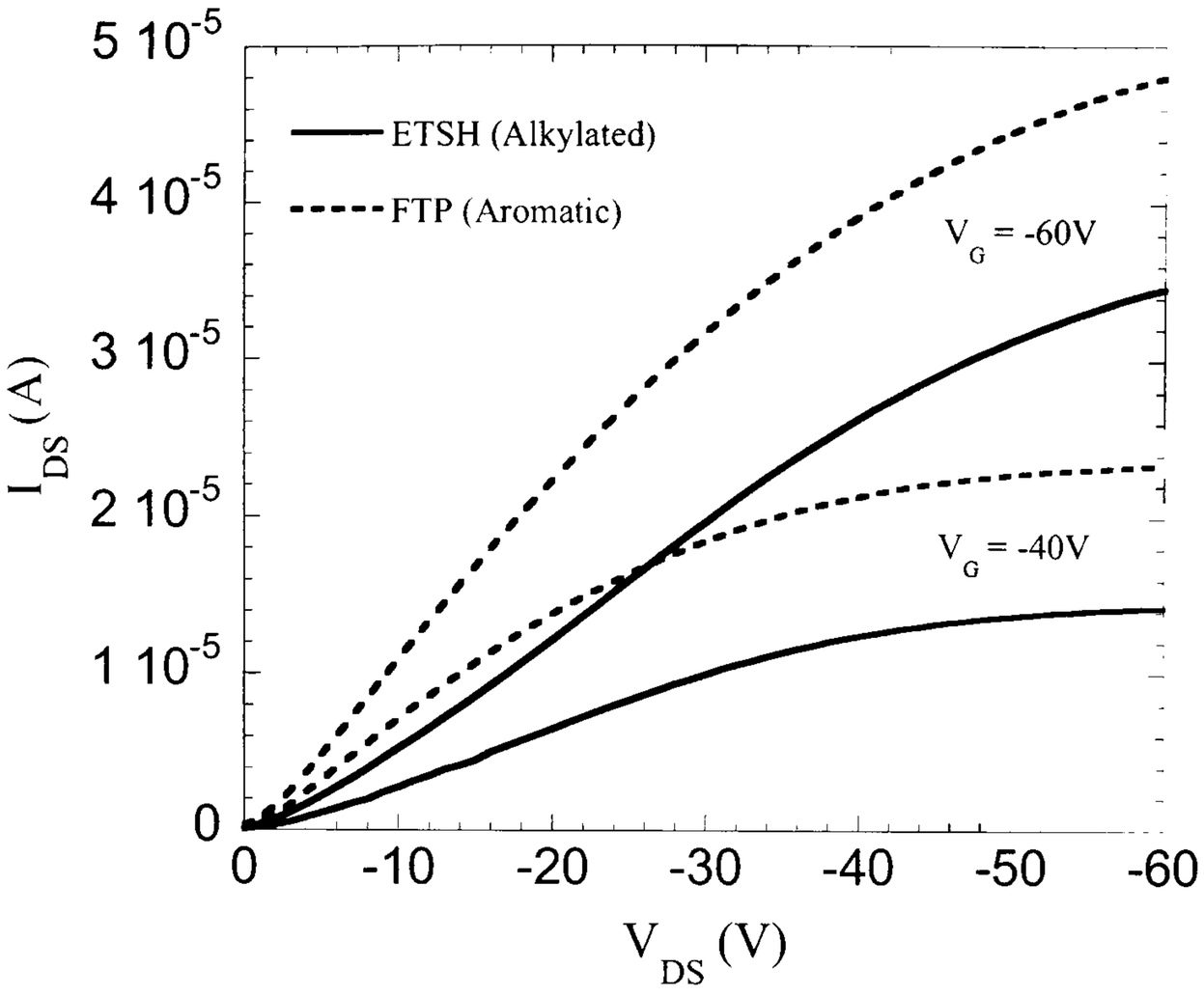


Figure.5.14. Comparison between the output characteristics of the ETSH alkylated thiol (solid line) and FTP aromatic thiol (dashed line) for 20µm channel length and 1cm channel width syn-pBTTT transistor. Thought ETSH treated electrodes should result in improved hole injection the characteristics are worsened showing injected limited currents at low drain voltages, indicating that the unconjugated spacer group is to blame.

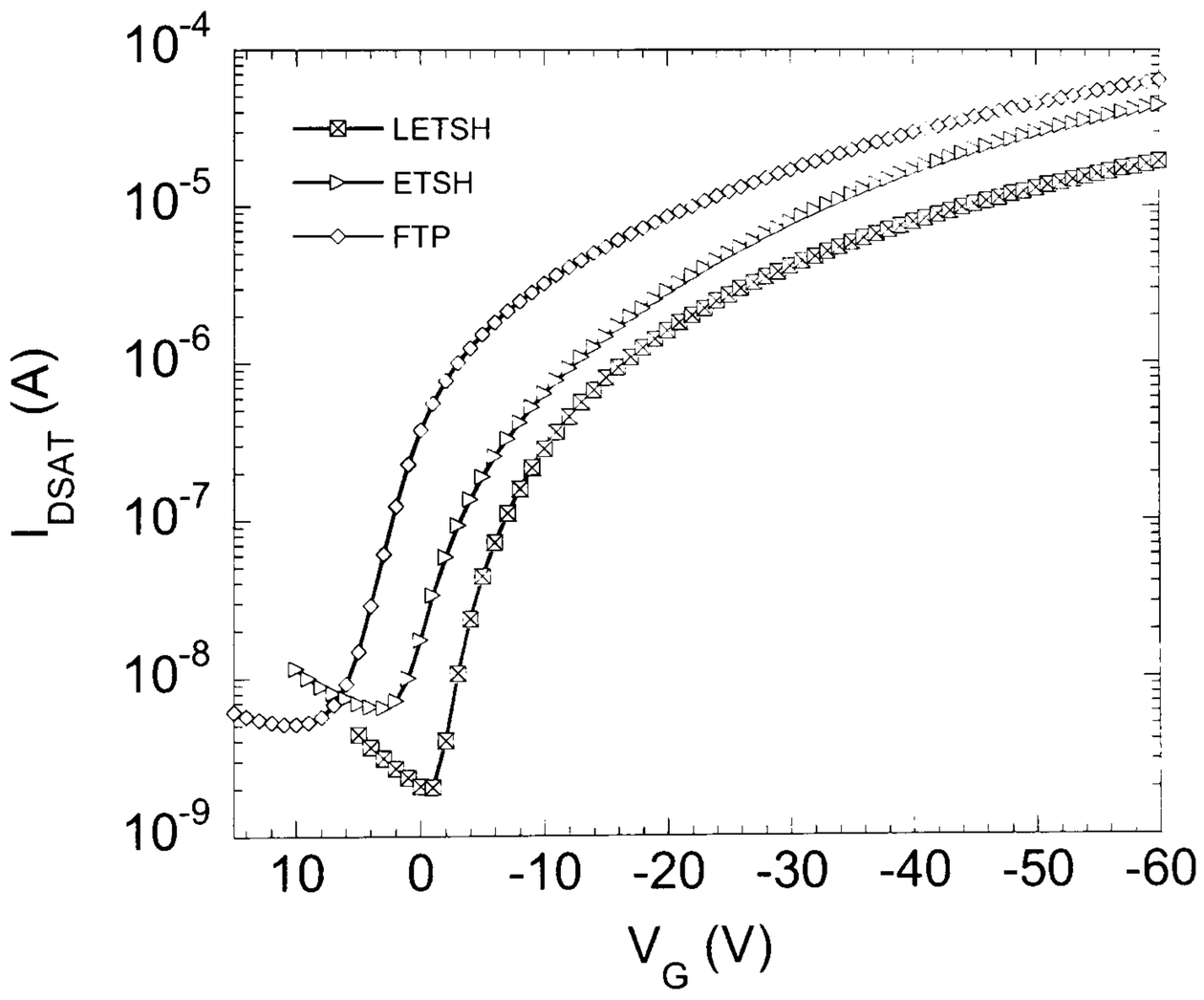


Figure.5.15. Saturated transfer characteristics comparing fluorinated thiol treated syn-pBPTTT transistors with different spacer groups. The dimensions of the transistors are L=20µm and W=1cm.

The switch-on voltages for the range of fluorinated thiols is illustrated in Fig.5.15 and shifts from positive to negative with decreasing conjugation and increasing spacer group length. This tendency is also confirmed if we consider the output plot of the three thiols at zero applied gate bias.

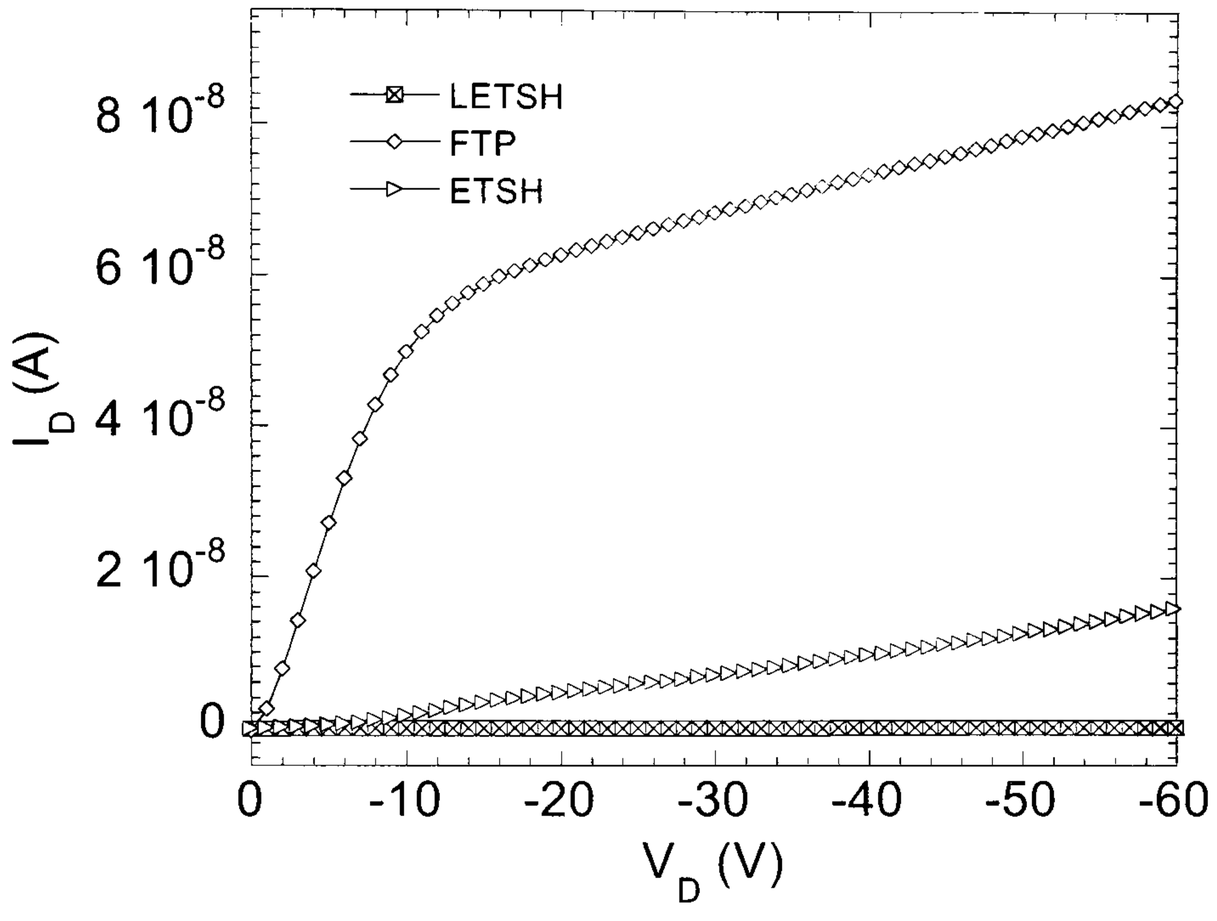


Figure.5.16. Output characteristics comparing the magnitude of charge already accumulated in the channel at zero gate bias for fluorinated thiol treated syn-pBTTT transistors with different spacer groups.

This is essentially a measure of any charge present in the polymer layer at zero gate bias. All the fluorinated thiols raise the workfunction of the gold electrodes, charges could be injected into the channel at no applied bias. It would be expected that more charge would be injected in the case of the LETSH thiol as it raises the workfunction by +0.86eV. However, it shows a negative switch-on voltage and negligible bulk conductivity. Coupled with the severe non-linearity in the linear output characteristics, this is suggestive of injection-limited currents, due to the methyl groups providing a barrier to tunnel through. ETSH has a shorter spacer group so the charge carriers have a smaller tunnelling barrier to overcome. FTP has a conjugated spacer group, and consequently has the highest turn-on voltage and bulk conductivity currents at zero V_G. This fits with the hypothesis that the charge has to

be injected through the monolayers, and this inhibits the currents for the more insulating thiols.

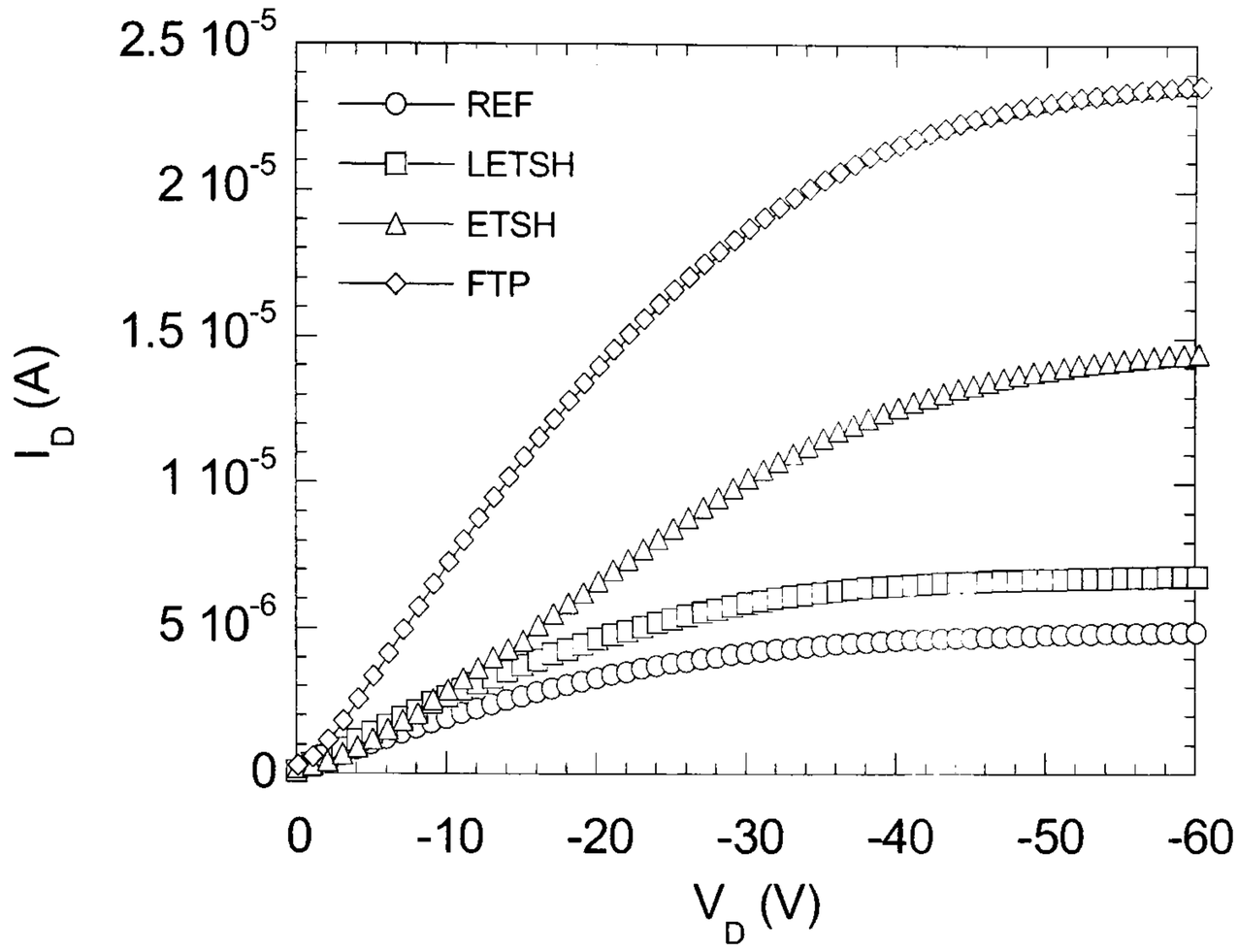


Figure.5.17. Output characteristics at V_G = -40V comparing fluorinated thiol treated syn-pBTTT transistors with different spacer groups with respect to an untreated device.

However, though it should be noted that even though the alkylated thiols hinder injection by acting as insulating layers, the improvement in Φ_{Au} by the dipole of the fluorinated terminal group is sufficient to improve charge transfer with respect to an untreated device. Correspondingly, the variation of the drain current is in accordance with $I_{FTP} > I_{ETSH} > I_{LETSH} > I_{REF}$, as can be observed in the comparison of output characteristics (V_G=-40V) in Fig.5.17.

5.2.5. Wettability and contact angle measurements

Contact angle measurements were carried out by Saghar Khodabakhsh on the same substrates as used for Kelvin probe studies.[20]

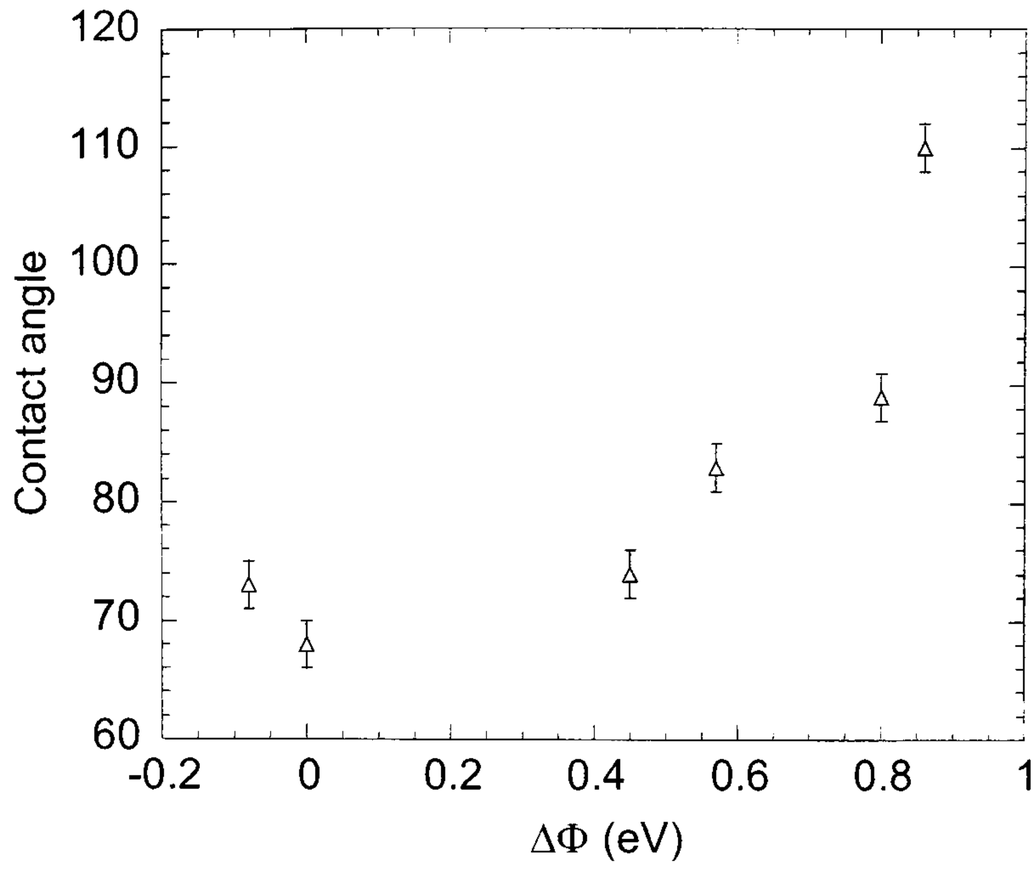


Figure.5.18. Relationship between the contact angle (water) and change in gold workfunction as measured by Kelvin probe.

A relation between the workfunction change of the gold electrode and the wettability is clearly evident from Fig.5.18. A higher $\Delta\Phi$ is consistent with thiols of higher dipole moment. Fluorine terminated thiols have the highest contact angles. Water has a high surface tension due to hydrogen bonding, and a low contact angle indicates that the surface in question has a similar surface energy – thus the droplet spreads. If the contact angle is high, the surface energy of water and the surface are different. Fluorine is the most electronegative element and fluorinated terminated thiols form unreactive hydrophobic monolayers. Most polymers are insoluble in water (a polar solvent), so low energy hydrophobic (non-ionisable) surfaces are more favourable. However, as can be seen from Fig.5.19 and the summary in Fig.5.23, the wettability of the electrodes does not have a big impact on the currents, contact resistance or mobility. After all, it does not affect the interface where the channel is accumulated and transport occurs.

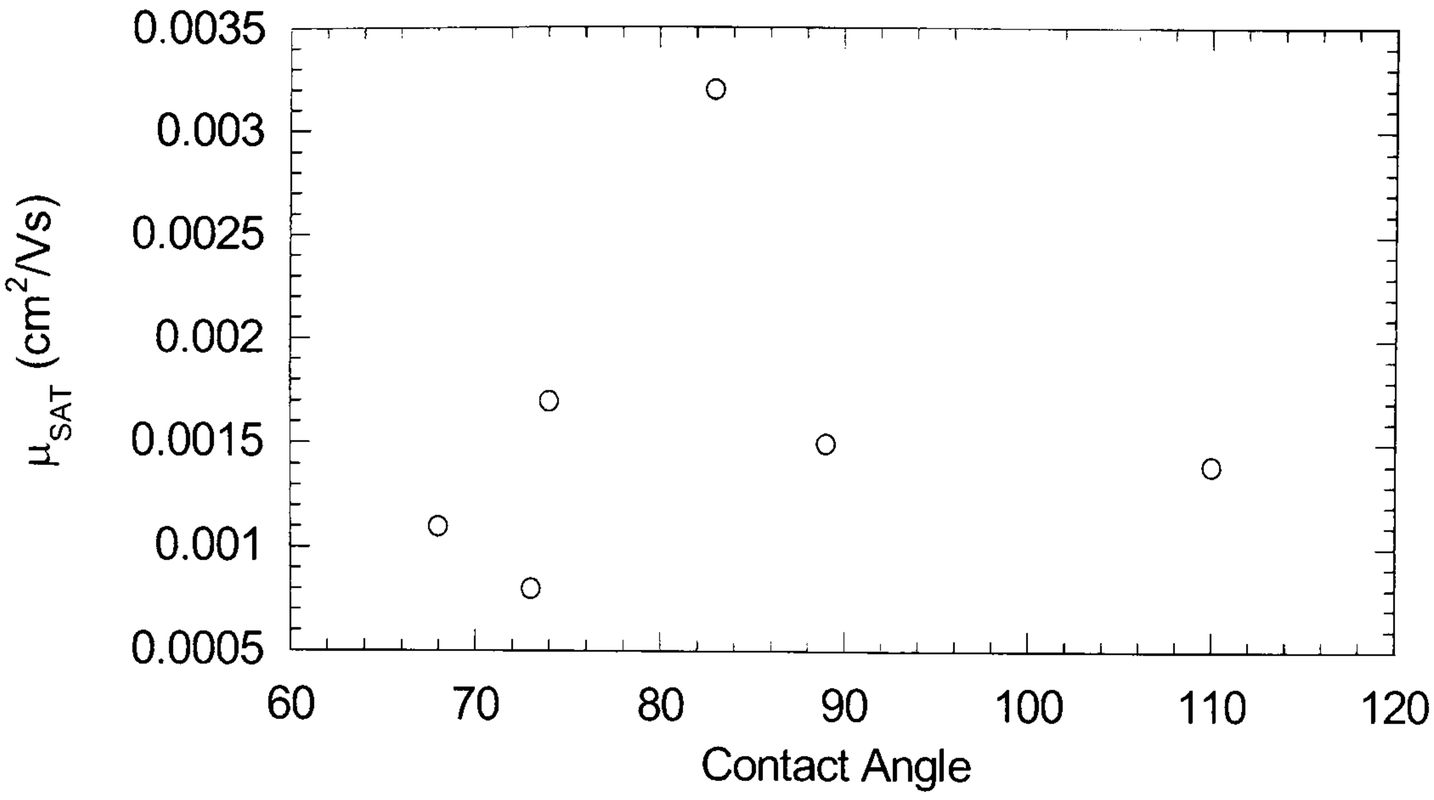


Figure.5.19. Relationship between the saturated mobility and wettability of the gold electrodes.

5.2.6. The effect of thiols on the contact resistance

As discussed in the previous chapter, the contact resistance in a polymer transistor is dependent on the injection barrier. It depends on both the workfunction mismatch and the morphology near the contacts, which can also physically inhibit injection. To correctly evaluate the performance of an OFET one needs to take into account this contact resistance, R_C. It also provides an indication of the magnitude of the metal-polymer injection barrier, so would be a useful tool for estimating the hole injection barriers for different thiol treatments. Using the linear transmission method described previously,[25] the contact resistance was estimated for each thiol, with respect to the gate voltage.

The contact resistance, calculated at a gate voltage of -40V, for the different thiol treated substrates is depicted in Fig.5.20. The injection of a hole from the electrode into the polymer can be thought of as a sum of two processes; surmounting the energy barrier created by the workfunction difference, and a tunnelling event. If a monolayer is assembled at the interface, it would provide an addition tunnelling

distance. So even though the workfunction mismatch may be reduced, the inhibition of direct tunnelling from the metal into the polymer suggests that SAMs can also worsen transistor performance.

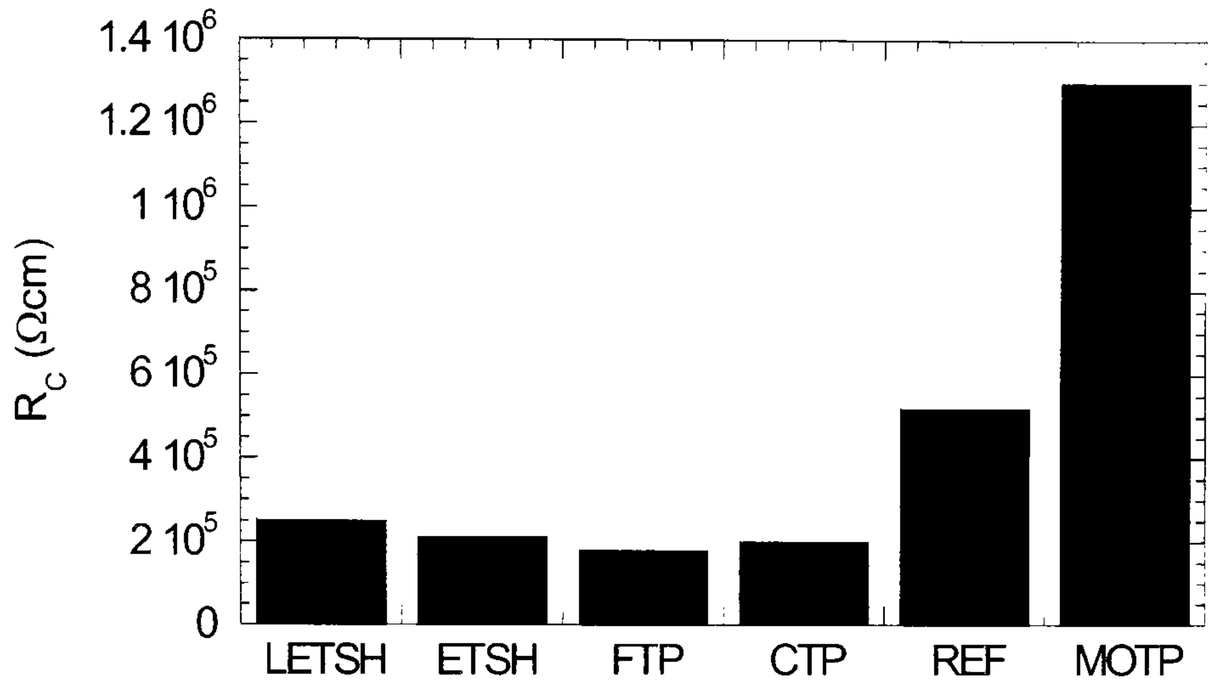


Figure.5.20. Variation of the contact resistance extracted at V_G = -40V for the different thiol treatments.

Taking this into account, two trends that one would expect would be

(i) Lowest contact resistance for the terminal group that minimises the workfunction difference between the gold and the polymer (if spacer group is identical)

(ii) Highest contact resistance for the thiol with the most insulating spacer group (if terminal group is the same)

Analysis of the contact resistance shows that both predictions are met. Consider the series of aromatic thiols. The fluorine terminated thiol increases Φ_{Au} the most – reducing the workfunction mismatch and hole injection barrier. Chlorine has a slightly lower dipole moment than fluorine, whilst a methoxy group donates electrons. It follows that the R_C for aromatic thiol SAM treated transistors follows the trend $R_{C\ FTP} < R_{C\ CTP} < R_{C\ REF} < R_{C\ MOTP}$.

Fig.5.21 illustrates the relationship between the contact resistance and gate voltage for different aromatic thiol treatments. R_C varies between 1.5MΩ to 12kΩ over a voltage range of -10V to -60V for the reference sample. This increases to 5.4MΩ to 0.6MΩ for the MOTP transistor, and decreases to 23kΩ to 0.6kΩ for the CTP treated transistor. This supports the predictions for the effective barrier height of hole injection based on induced interfacial dipoles.

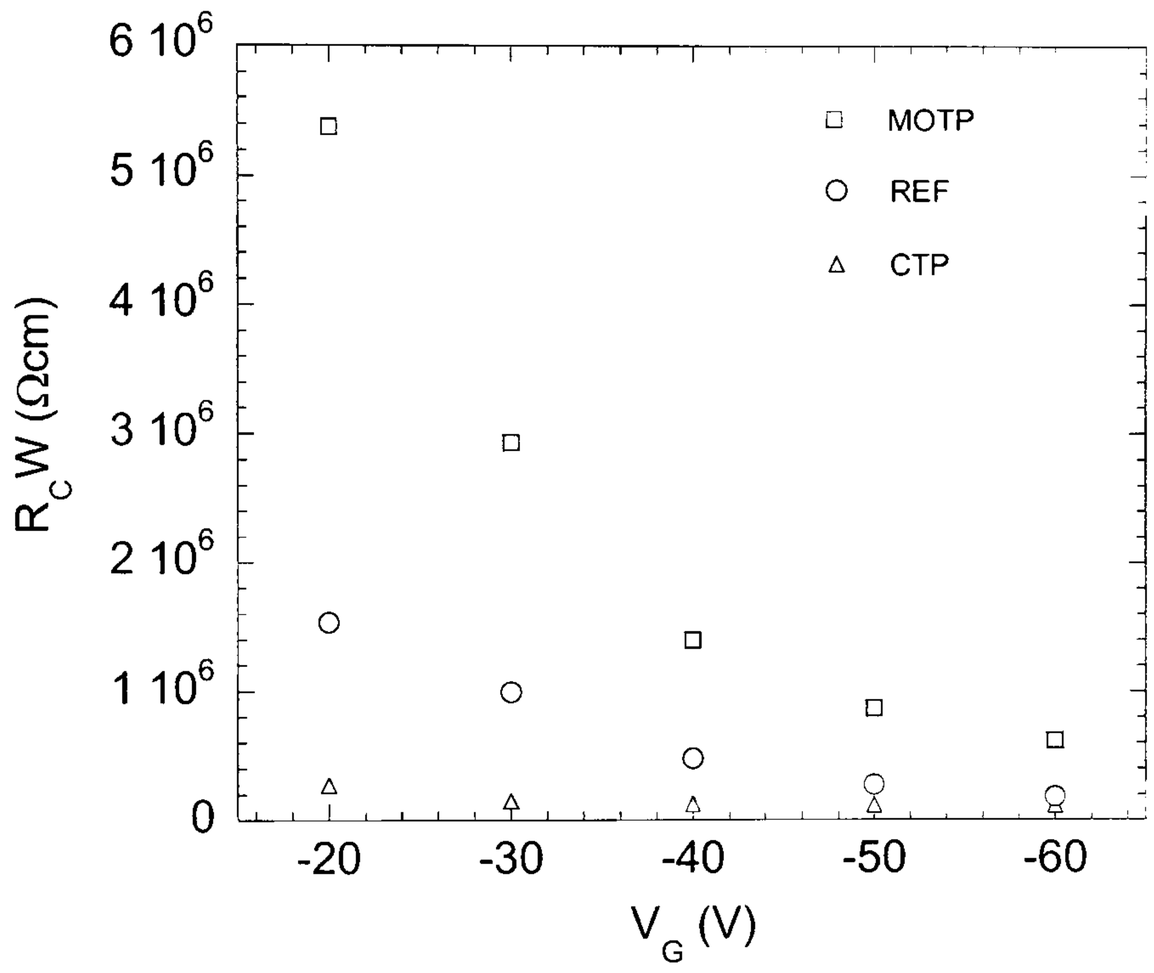


Figure.5.21. illustrates the relationship between the contact resistance and gate voltage for different aromatic thiol treatments. This supports the predictions for the effective barrier height of hole injection based on induced interfacial dipoles.

If the effect of the spacer group is considered, the contact resistance is largest for the most insulating spacer group, as $R_{C\ (FTP)} < R_{C\ (ETSH)} < R_{C\ (LETSH)}$. However, as we saw with the I-V characteristics, even treating the electrodes with the longest fluorinated thiol LETSH gives enhanced performance to untreated devices. Thus the choice of both terminal and spacer groups is important to optimise the gold/thiol/polymer system.

5.2.7. How do thiols affect the mobility?

The mobility can be thought of as defining the overall performance of the transistor. The table in Fig.5.23 summarises the saturated mobility of the 20μm channel length transistors. The field-effect mobility is increased by up to three times with a FTP monolayer and is decreased for MOTP treated transistors - the saturated mobility of the reference sample is 1.4 times bigger. In fact the same trend as the I-V characteristics of $\mu_{FTP} > \mu_{CTP} > \mu_{REF} > \mu_{MOTP}$ and $\mu_{FTP} > \mu_{ETSH} > \mu_{LETSH} > \mu_{REF}$ is followed.

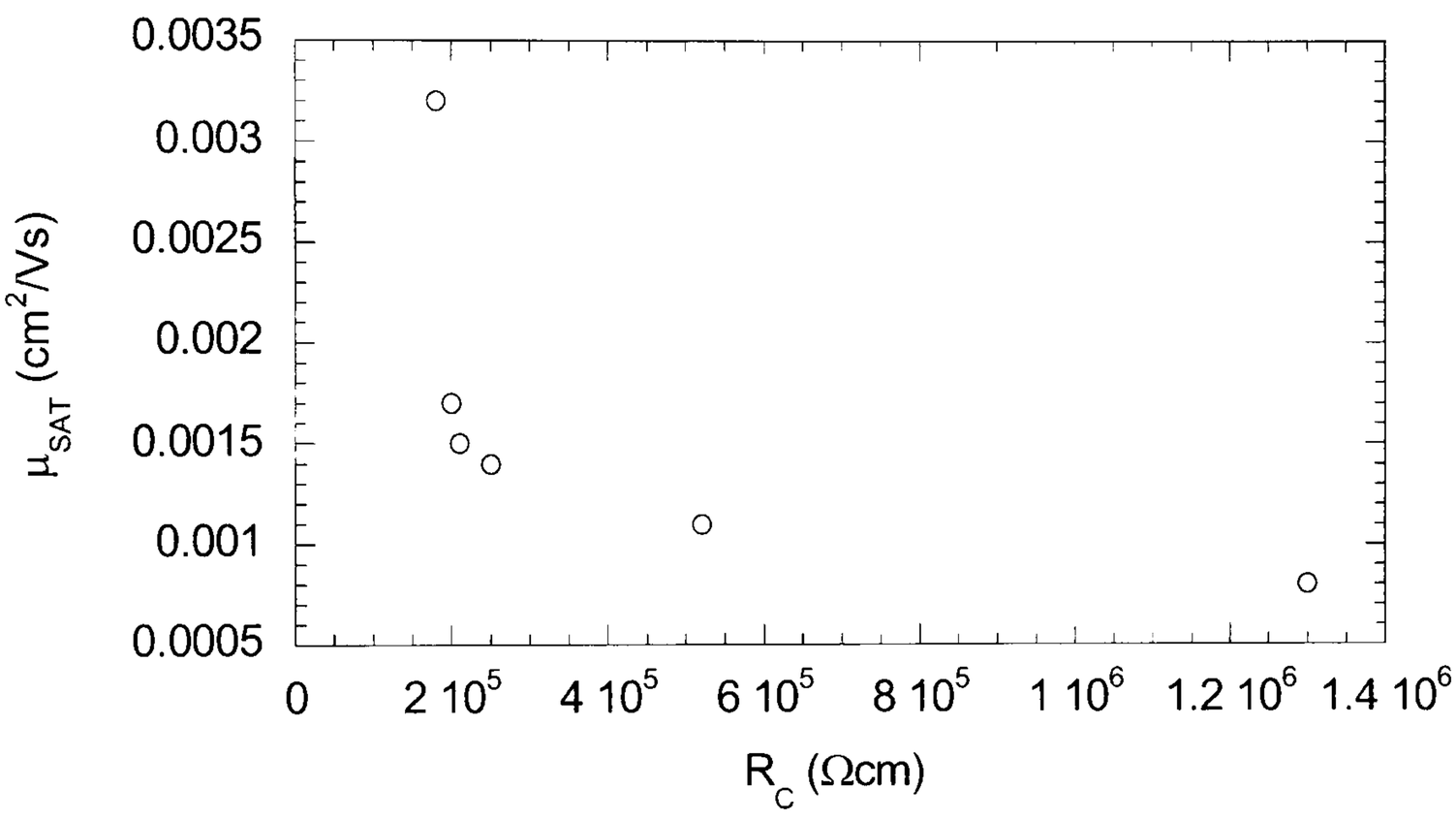


Figure.5.22. illustrates the relationship between the contact resistance and the saturated mobility for 20μm channel length syn-pBTTT transistors. The derivation of the saturated mobility should be independent of contact resistance effects.

Fig.5.22 illustrates the relationship between the contact resistance and the saturated mobility. Linear mobilities follow the same pattern. The mobility is increased, as expected with injection improving SAMs, thus for lower contact resistances the mobility is increased. The same trend is noted for all channel lengths, further corroborating that injection is improved by using fluorinated non-insulating thiols to raise Φ_{Au} and reduce the hole injection barrier.

5.2.8. Summary of transistor performance with thiol modified electrodes

In conclusion, we have demonstrated that the field-effect mobility is limited by injection and contact resistances originating from a workfunction mismatch between the metal and organic layer.

	LETSH	ETSH	FTP	CTP	REF	MOTP
ΔΦ (eV)	+0.86	+0.80	+0.57	+0.45	0.0	-0.08
Contact angle (°)	110±2	89±2	83±2	74±2	68±2	73±2
μ_{sat} (cm^2/Vs)	0.0014	0.0015	0.0032	0.0017	0.0011	0.0008
R_c† (Ωcm)	$2.5x10^5$	$2.1x10^5$	$1.8x10^5$	$2.0x10^5$	$5.2x10^5$	$1.3x10^6$

Figure.5.23. Tabulated device characteristics for 20μm channel length syn-pBTTT transistors. The channel width is 1cm.

This injection barrier can be reduced or increased by modifying the metallic electrode using thiols to induce a dipole at the interface. The magnitude and direction of this dipole directly affects values derived for the contact resistance and mobility. The contact resistance is the only parameter investigated that follows a direct relationship with the mobility, as it takes into account both the change in Φ_{Au} and insulating effect of the monolayer. The fluorinated aromatic thiol performed best, as

† R_C at V_G = -40V

the short, conjugated spacer group did not significantly inhibit injection, as compared to alkyl spacer groups. This is definitely a useful technique to combat the problem of non-ohmic injection in transistor structures, which is becoming more commonplace as more air-stable polymers tend to have ionisation potentials higher than the gold.

5.3. Improving interfacial molecular order using silanes

Considering that the channel extends up to 5nm into the bulk film, it is unsurprising that the performance of OFETs depends strongly on the molecular order of the polymer at the semiconductor/dielectric interface. Silylating SAMs such as hexamethyldisilazane (HMDS) and alkyltrichlorosilanes are commonly used to modify the naturally hydrophyllic SiO_2 surface of OFETs prior to the deposition of organic material. The mechanism of formation essentially replaces the hydroxyl groups with apolar methyl groups, resulting in a more hydrophobic surface and promoting adhesion of the polymer layer.

5.3.1. Formation of silane monolayers

Five silanes were used in this study and their chemical structures are shown in Fig.5.24. All silanes were purchased from Aldrich. For trichlorosilane surface preparation, substrates were immersed in 10mM solutions of octyltrichlorosilane (OTS) or octadecyltrichlorosilane (ODTS) in toluene. A small amount of water is needed for the reaction to occur but too much causes the development of a white precipitate in the solution, as it polymerises. Hexadecane is a better solvent for this purpose as it does not pick up much water due to evaporative cooling, though is not as readily available as toluene. The latter was used as no difference was apparent from device performances, but it was ensured that new solutions were made up

before use to avoid any precipitation problems. Prepared devices were simply immersed in fresh solution for 15 minutes at 60°C in ambient. They were then sequentially rinsed in toluene, acetone and isopropanol. Complete dewetting at the acetone stage is an easy way to see if the process has been successful, but contact angle measurements were carried out on off-cuts prepared alongside the FET substrates as a quality check.

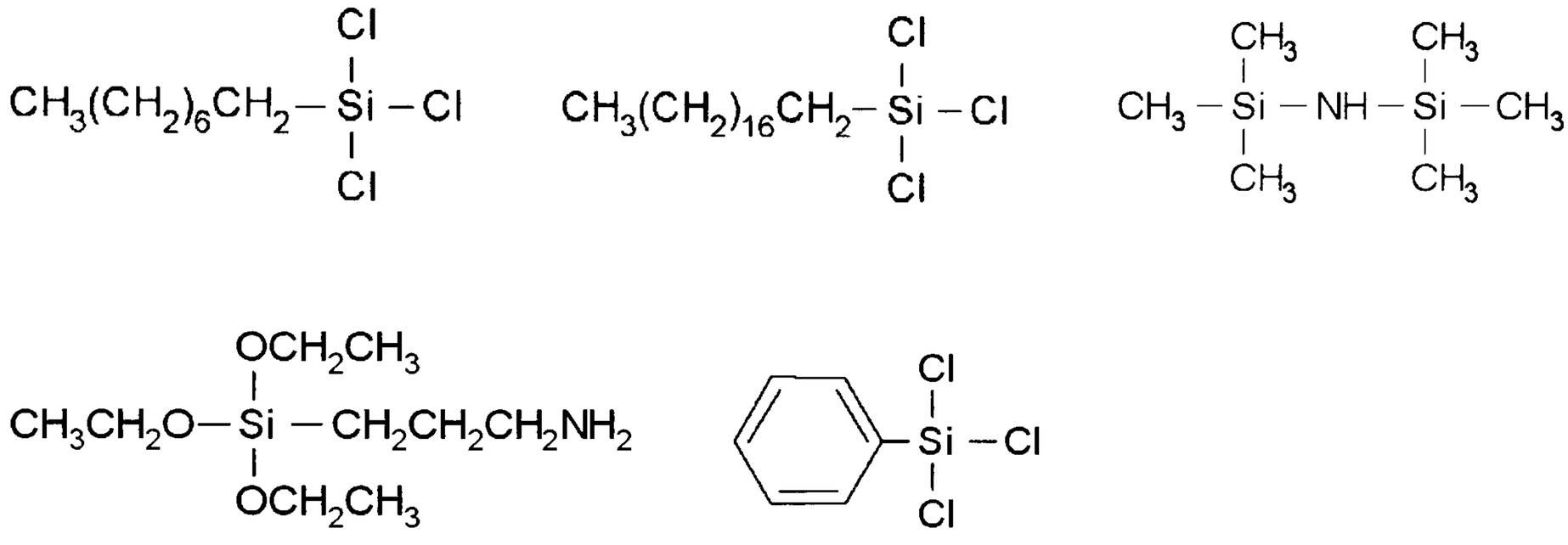


Figure.5.24. From top left going clockwise the names and chemical structures of the silanes used in this work are described: octyltrichlorosilane (OTS), octadecyltrichlorosilane (ODTS), 1, 1, 1, 3, 3, 3-Hexamethyldisilazane (HMDS), phenyltrichlorosilane (PETS), and (3-aminopropyl)triethoxysilane (APTS).

Hydrolysis of Si-Cl to form Si-OH is followed by adsorption onto the silicon dioxide surface and the creation of a cross-linked polymerised Si-O-Si network via condensation reactions. Molecular packing and the consequent quality of coverage of the monolayer is determined by the Si-O-Si system, not as for thiols in which it is dictated by the epitaxial arrangement on the gold.[26] An additional step of annealing the SAM for up to an hour on a hotplate in ambient completes the polymerisation and further improves device characteristics. An alternate silylating treatment involves refluxing in 1, 1, 1, 3, 3, 3-hexamethyldisilazane (HMDS) at 150°C for 2-3

hours. Though this method was employed for comparative studies, the harsher reaction conditions required discouraged its use and surface treatments involving trichlorosilanes were preferentially used.

Further surface studies should be carried out to assess the quality of the monolayers, though as the same method was used for all trichlorosilane (and triethoxysilane) treatments we can assume that the surface coverage is similar. In addition, the contact angle of each substrate does not vary significantly from one area to another – indicating that the monolayer coverage is adequate. The average error was ±2° at most.

5.3.2. I-V characteristics

The same polymer solution was used in the spin-coating of all devices. As this was a comparative study, devices were prepared and measured as close as possible to each other. The saturated transfer characteristics of 10μm channel length syn-pBTTT transistors with different surface treatments are displayed in Fig.5.25. It is clear that silane treatments produce more dramatic differences in the I-V characteristics than thiol SAMs. The currents are much higher for silane treated transistors, and as silanes are only present at the dielectric interface, indicates that interfacial properties dominate those associated with injection. The saturated drain currents are highest for ODTS treatment, being almost 500 times more than for the APTS SAM. The trend follows $I_{ODTS} > I_{OTS} > I_{HMDS} > I_{PETS} > I_{APTS}$, which is also the case for the mobilities.

Another obvious difference is the turn-on voltage V_0. As the impurity level of the organic material is the same for all transistors, the individual surface treatments must be responsible for this variation. The turn-on voltage for the ODTS, OTS and HMDS transistors is more or less zero. The PETS and APTS devices show much

lower drain currents and are switched-off at zero applied gate bias. As a negative gate bias is required to turn the transistor on, they are operating as depletion mode devices.

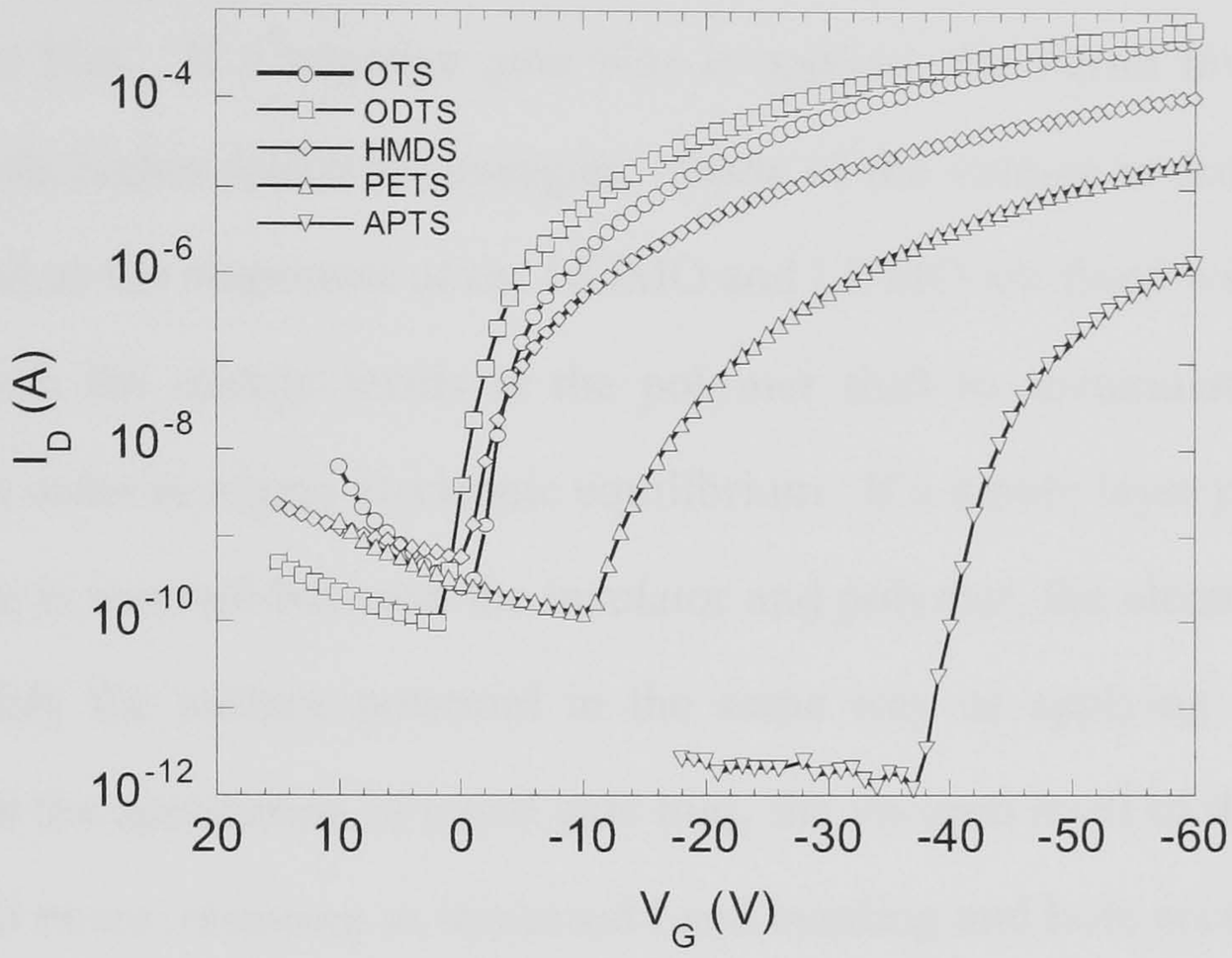


Figure.5.25. The saturated transfer characteristics of 10μm channel length syn-pBTTT transistors with different surface treatments.

Pernstich et al. also noted shifted turn-on and threshold-voltage characteristics for a range of silane surface treated transistors, using pentacene as the active layer.[27] They attributed variations in device characteristics to the dipole associated with the monolayer inducing charge in the channel. This is similar to the principle behind assembling fluorinated thiol monolayers on the injecting electrodes of OFETs in order to modify the interfacial dipole and reduce the hole injection barrier, as the shifts in V_0 can be attributed to the electronegativity of the terminal group. The more electronegative the terminal group, the more electrons from the polymer film are attracted to the monolayer, leaving behind mobile holes. This reasoning fits the shift of turn-on voltage observed; $V_{ODTS} \approx V_{OTS} \approx V_{HMDS} > V_{PETS} > V_{APTS}$.

The mechanism for charge accumulation would be different to the thiol case. In this instance the monolayer is assembled at the interface between the dielectric (SiO_2) and the polymer film. If the molecules possess a dipole moment, an electric field would be induced at the insulator interface, which can then be superimposed onto the applied gate bias. If a negative gate bias is applied, the Fermi level of the metal shifts towards higher (electron) energies. Some of the voltage is dropped across the insulator and as the alignment of the HOMO and LUMO are fixed with respect to the vacuum level, the energy levels in the polymer shift to accumulate charge at the interface, in order to regain electronic equilibrium. If a dipole layer pointing towards the interface is inserted between the insulator and polymer, the electric field induced would modify the surface potential in the same way as applying a negative gate voltage. On the application of a real gate bias, the vacuum level of the insulator is in effect raised twice, resulting in increased band bending and hole accumulation in the channel. An electron donating molecule such as PETS results in a dipole pointing away from the interface and acts as a positive gate voltage.

The turn-on voltage is negative for PETS and APTS transistors, and they are completely switched off at zero gate bias. This suggests that carriers are depleted rather than accumulated. Amine-terminated silanes have been shown to possess a permanent dipole moment of 1.04D.[28] The part of the monolayer adjacent to the polymer film should have a slight positive charge, attracting electrons towards the interface. It should also be noted that charge transfer between the assembled molecule and polymer could occur with APTS, as lone electron pairs on the nitrogen atoms could donate charge. The unpaired electron of the amino group could also act to trap positive carriers and further reduce hole transport in FET channel. In this case, the surface potential of the insulator is reduced, analogous to applying a positive gate bias. Thus the bands bend downwards, depleting carriers.

Alkyl-terminated SAMs (OTS, ODTS and HMDS) possess a very small dipole moment along the axis of the molecule, so are not be expected to bring about significant changes to the surface potential. The OTS, ODTS and HMDS treatments do not shift V_0 significantly and are centred on 0V.

5.3.3. The effect of silanes on ambipolar transport in transistors

P-type transport is prevalent in OFETs. Electron and hole transport has been shown to occur in many polymeric materials, but as electron transport is sensitive to trapping, hole transport usually dominates. Positive gate biasing regimes should enable n-type transport in polymer transistors, though this is rarely observed. Solution-processible blends of syn-pBTTT and PCBM have recently been realised as the active layer in ambipolar thin film field-effect transistors.[28] Considering the dipole argument we have just addressed, either electron or hole (n-type or p-type) transport could be preferentially observed by choosing different silane treatments. The transistor data included in Fig.5.26 and 5.27 were carried out by Richard Simms.

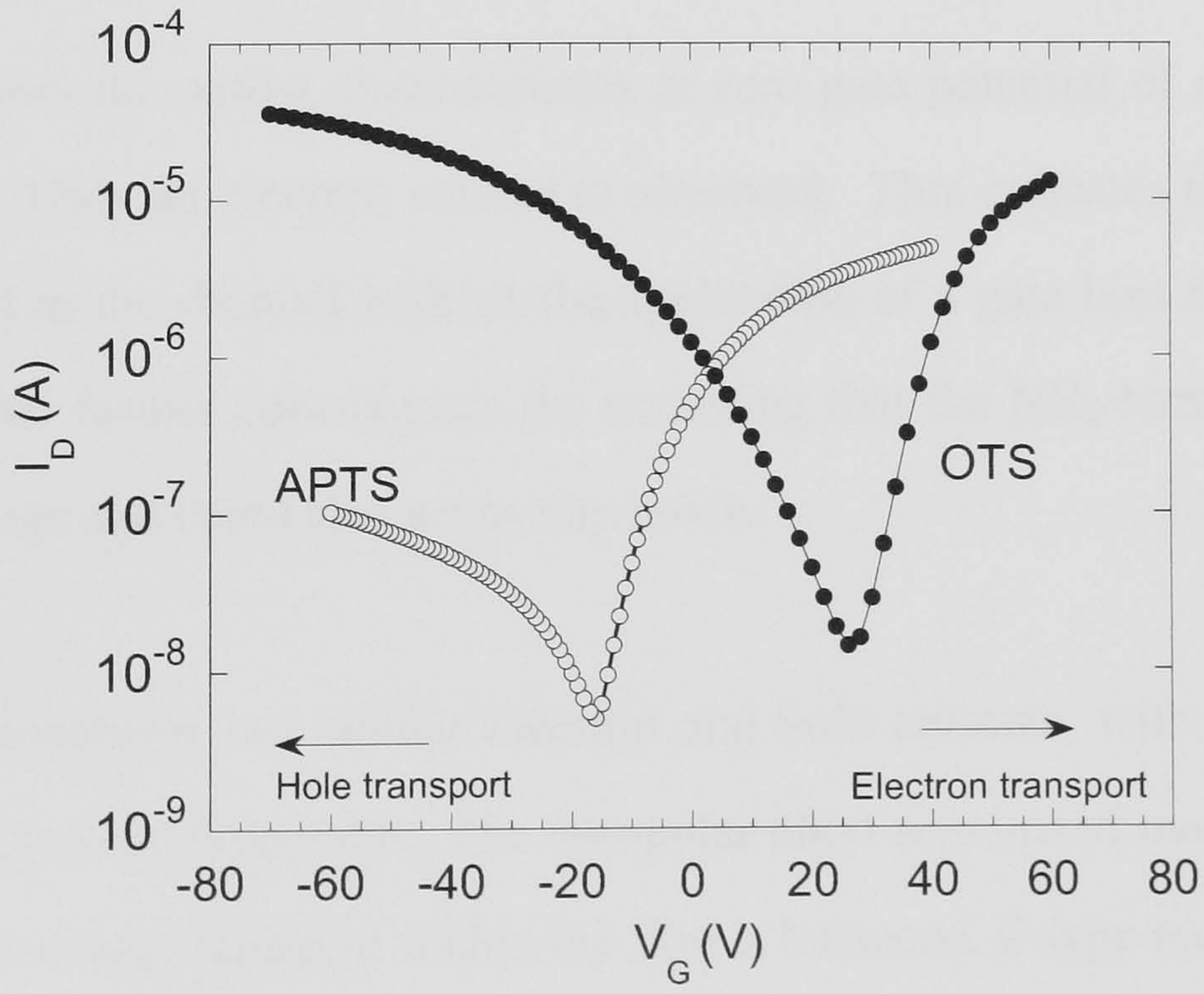


Figure.5.26. illustrates the difference between saturated transfer scans for 10µm channel length syn-pBTTT/PCBM blended transistors with APTS and OTS surface treatments.

Fig.5.26 illustrates saturated transfer scans for 10μm channel length syn-pBTTT/PCBM blended transistors with APTS and OTS surface treatments. Ambipolar transport is observed, with the amine-terminated silane clearly enhancing electron transport. Hole transport (negative voltage regime) is substantially lower, by two orders of magnitude.

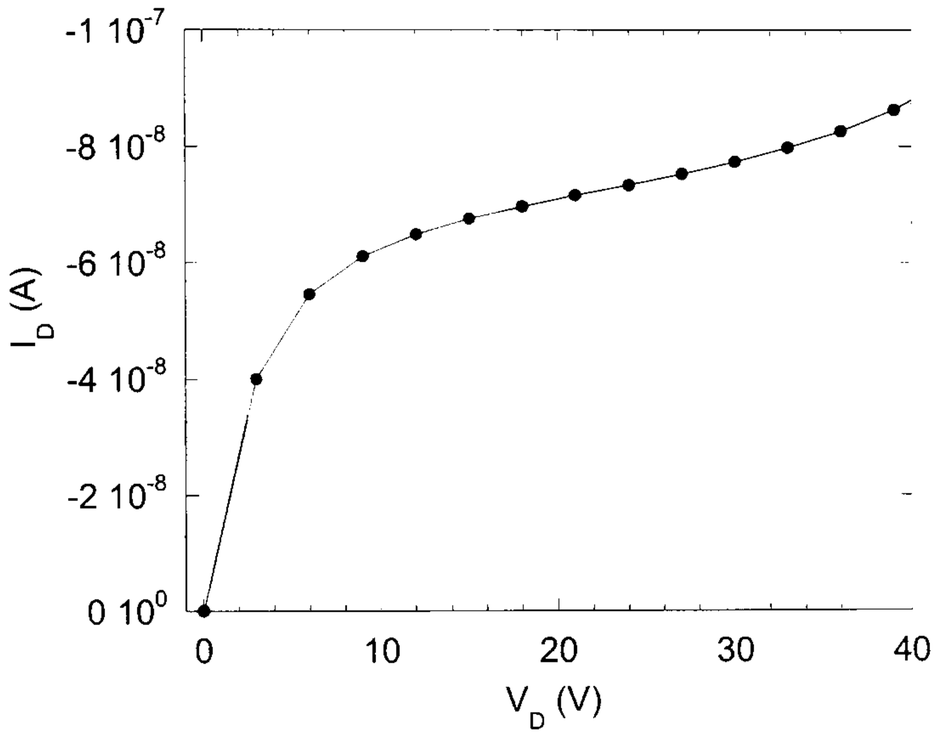


Figure.5.27. shows the output characteristics at zero gate potential of the 10μm channel length syn-pBTTT/PCBM blended transistors with APTS surface treatment.

Fig.5.27 shows the output characteristics at zero gate potential of an APTS treated transistor. Only an electron current is observed. This indicates that electrons are accumulated in the channel without the application of a gate bias for APTS treated devices. This further corroborates the reasoning that the NH_2-termination depletes positive charge and could also act to trap holes.

The OTS monolayer has similar electron and hole currents, with p-type transport being slightly more favourable. The non-polar alkyl terminated monolayers possess no dipole, so charge transport within the film is balanced. P-type transport is slightly favourable as electrons are more susceptible to trapping. The switch-on voltage of the OTS treated transistor is shifted to the positive due to the PCBM present in the

film. This is the same effect noted when V_0 shifted to the positive for doped P3HT transistors in Chapter 3. ODTS treated devices performed similarly to the OTS monolayers.

Salleo et al. suggested that the carrier mobility does not only depend on the surface energy of the dielectric but is also due to the steric interaction of the self-assembled monolayer with the polymer microstructure.[10] They found no direct corroboration between the surface energy and mobility, but noted that silanes with alkane chains showed improved characteristics. For example, the alkane chains in octyltrichlorosilane (OTS) extend perpendicularly to the surface. Interlocking of these chains would improve the π-π stacking of F8T2 chains in the direction of current flow as the aromatic rings would preferentially orientate out of plane. Thus, the mobility is increased. This would be a similar situation for P3HT and syn-pBTTT.

5.3.4. Wettability and contact angle measurements

Let us now consider the wettability factor. As previously demonstrated, the wettability of the self-assembled monolayer can be modified by substituting different terminal groups onto the molecules. This would be expected to make a more significant difference in silane monolayers, than for thiols, as the silanes are assembled on the silica interface at which the channel is accumulated and charge transport occurs.

A clear relationship exists between the saturated mobility and contact angle, with the mobility increasing for lower energy surfaces. This is depicted in Fig.5.28, overleaf, and is expected as lower energy hydrophobic surfaces are more favourable to

polymers. Thus the polymer film has better order, leading to improved charge transport and I-V characteristics.

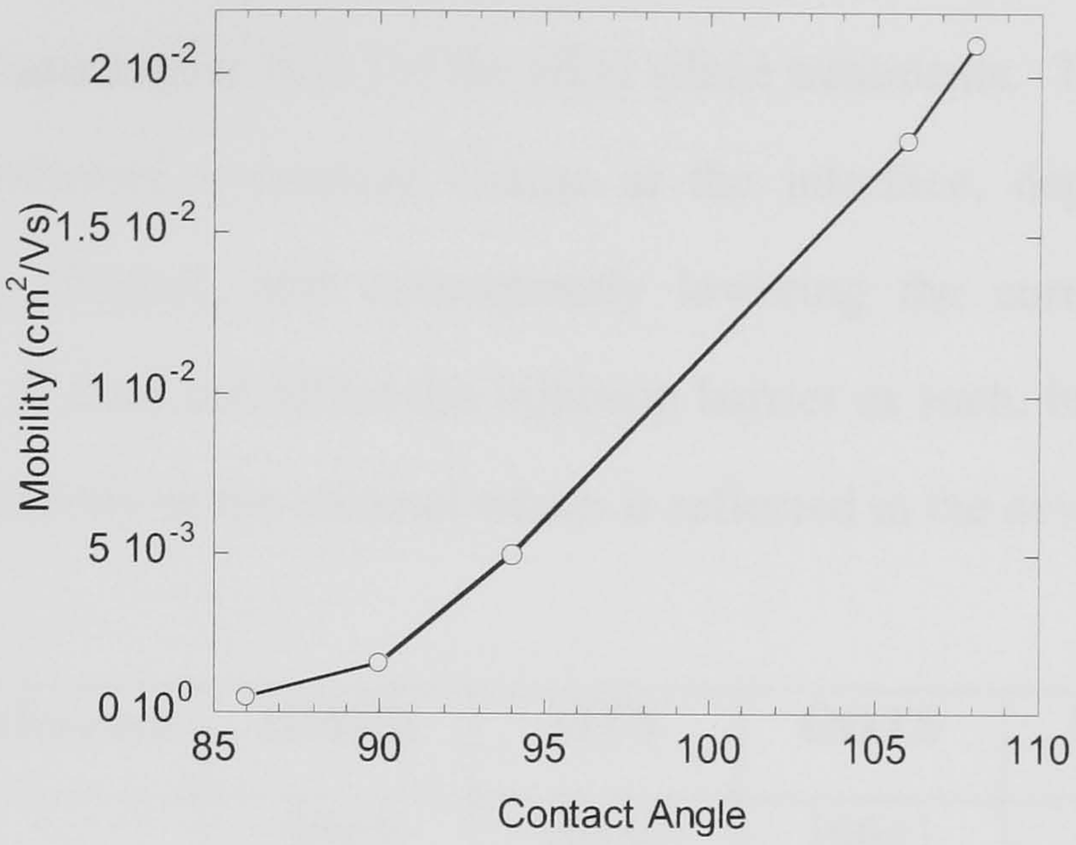


Figure.5.28. Relationship between the saturated mobility and wettability of the silica interface.

The amine terminated silane has the lowest contact angle (not including the ozone treated reference sample, which has an immeasurable contact angle as the surface is completely wetted due to favourable energetic interaction with the hydroxyl ions present at the surface). This is as expected, as though amines are not ionisable, they can readily act as H-bond acceptors. The polymer chains are consequently less organised on the APTS surface, the interchain distance (rate-limiting factor of mobility – See Chapter 6) is larger and the transistor characteristics are worsened.

5.3.5. Contact Resistance

The contact resistance shouldn't be affected by silane surface treatments as the SAMs are localised to the silica interface and should play no part in the injection properties of the system. The contact resistance for each of the silane treatments was extrapolated using the TLM method, as described previously. Unfortunately this was not possible for the APTS treated devices, as carrier injection was so limited that the non-linearity in the output characteristics was too great to extract any reasonable

values from. PETS showed increased non-linearity in the linear regime, as compared to OTS, ODTS and HMDS treated transistors, but data fitting were still possible. The derived estimate of contact resistance for PETS was 2.1MΩcm at V_G = -40V, an order of magnitude higher than for the alkyl silane treatments. This concurs with the PETS SAM inducing a positive charge at the interface, depleting the majority carriers in the channel, and consequently lowering the currents and switch-on voltage. Thus, it does not affect the injection barrier as such, but does diminish the charge carrier density in the channel which is reflected in the device characteristics.

	Reference	**HMDS**	**OTS**	**ODTS**	**PETS**	**APTS**
Contact Angle (°)	-	94±3	105±1	106±1	90±3	86±2
μ_{sat} (cm^2/Vs)	1.1×10^{-3}	5.0×10^{-3}	1.8×10^{-2}	2.1×10^{-2}	1.6×10^{-3}	0.5×10^{-4}
On/off ratio	10^4	10^4	10^5	10^6	10^5	10^6
R_C‡ (Ωcm)	2.1×10^5	4.9×10^5	4.8×10^5	5.1×10^5	2.1×10^6	-

Figure.5.28. Tabulated device characteristics for 10μm channel length syn-pBTTT transistors with various surface treatments. The channel width is 1cm.

Let us now concern ourselves with the differences between the OTS, ODTS and HMDS treatments. These surface treatments don't seem to affect carrier accumulation, as are not polar, which is confirmed by analysis of the contact resistance. A summary of the contact resistance is given in Fig.5.28 along with the other parameters discussed so far. The contact resistance does not exhibit significant

‡ Contact resistance at V_G = -40V

variation between these treatments, ranging between 490-510kΩcm (V_G = -40V) for transistors with OTS, ODTS, HMDS and a reference sample with no surface treatment. After all, silanes are only located at the polymer/dielectric interface and should not affect the hole injection barrier, as thiol treatment does. As the mobility varies from 0.0011 to 0.021cm^2/Vs for the untreated and ODTS treated devices respectively, the improvement in device characteristics must be due to the surface energy or improved molecular order at the interface.

5.3.6. Temperature studies

We have already mentioned that the molecular order at the interface plays an important role in the performance of thin film transistors. Temperature studies can give an indication of the level of order in the system, by extracting estimates of the positional and energetic disorder. If the order is improved at the interface, molecular packing is enhanced, resulting in more efficient charge transport and better device characteristics. Thus the energetic disorder can give an indication of the molecular order at the interface, if derived from OFET measurements. Disorder is inherent in all polymer systems, and detailed discussion of the differences between bulk and surface properties will be given in the following Chapter. For now, we aim simply to approximate values of the energetic disorder for OTS, ODTS, HMDS and untreated surfaces in transistor structures, for comparative purposes.

The disorder formalism, derived by Bassler and co-workers, offers a quantative estimate of the energetic disorder present in a disordered system.[29] Monte-Carlo simulations of the Miller-Abrahams hopping rate counteracts the complex problem of analytically solving charge transport within a hopping framework with a Gaussian density of states. The energetic disorder parameter σ^2 (σ is the standard deviation of the Gaussian DOS) can give an indication of improved charge transport, with lower

values suggesting a higher mobility as the level of energetic disorder in the system is reduced.

Positional disorder and energetic disorder both are taken into account in the simulations, which leads to the expressions below:

$$\mu = \mu_0 \exp\left[-\left(\frac{2\sigma}{3k_BT}\right)^2\right] \times \begin{cases} \exp\left[C\left\{\left(\frac{\sigma}{k_BT}\right)^2 - \Sigma^2\right\}\sqrt{E}\right] & \Sigma \geq 1.5 \\ \exp\left[C\left\{\left(\frac{\sigma}{k_BT}\right)^2 - 2.25\right\}\sqrt{E}\right] & \Sigma \leq 1.5 \end{cases} \quad \{5.3\}$$

where μ is the mobility, C is a constant, μ_0 is a prefactor, T is the temperature, E the electric field, and σ and Σ the energetic and positional disorder parameters respectively. It follows that μ_0 can be derived from the intercept, and σ from the gradient, of the plot ln $|\mu_{(E=0)}|$ versus $1/T^2$.

The activation energy is instead given by an Arrhenius relation, as shown below, and can give an indication of the energy level of traps or interface states.[30]

$$\mu_{E=0} = \mu_0 \exp\left(-\frac{\Delta}{kT}\right) \quad \{5.4\}$$

A summary of results are given in the table in Fig.5.29. A more detailed discussion of the Gaussian Disorder Model (GDM) and further instruction on the methodology used can be found in Chapter 6.

	Reference	HMDS	OTS	ODTS
Δ (eV)	0.103	0.101	0.092	0.087
σ (eV)	0.057	0.058	0.053	0.052

Figure.5.29. Difference in the activation energy Δ and energetic disorder σ for 20μm channel length syn-pBTTT transistors with different surface treatments.

Let us first consider the results with respect to the GDM. The values of σ are relatively small for a conjugated polymer (typically 0.1eV) indicating, as we know, that syn-pBTTT is a highly ordered material. There is a correlation between decreased energetic disorder and a higher mobility. The energetic disorder is less for the OTS and ODTS trichlorosilane treated transistors, implying that the order at the interface is improved. This supports the consensus that molecular order at the interface is improved by better backbone stacking as the side alkyl chains and those of the SAM interlock. The HMDS and reference sample have similar energetic disorder values, higher than those of OTS or ODTS, yet HMDS displays a 5 times higher mobility. This suggests that the surface energy also plays an important part in device performance. The table in Fig.5.28 shows that the trend of increasing mobility is mirrored with the contact angle, with best performance achieved for lower energy surfaces.

A similar trend is also found for the activation energy, with lower values corresponding to higher device mobilities. Traps are due to specific chemical impurities, conformational defects or chain end groups. Even if these have trap energies which lie outside the energy gap, these can reduce the mobility by forming a spatial barrier which a carrier must pass round. ODTS and OTS surface treatments have activation energies around 0.09eV, whilst those of the ozone cleaned and HMDS samples are approximately 0.1eV. This implies that the trap depth is smaller in the case of OTS/ODTS devices and the mobility is consequently increased.

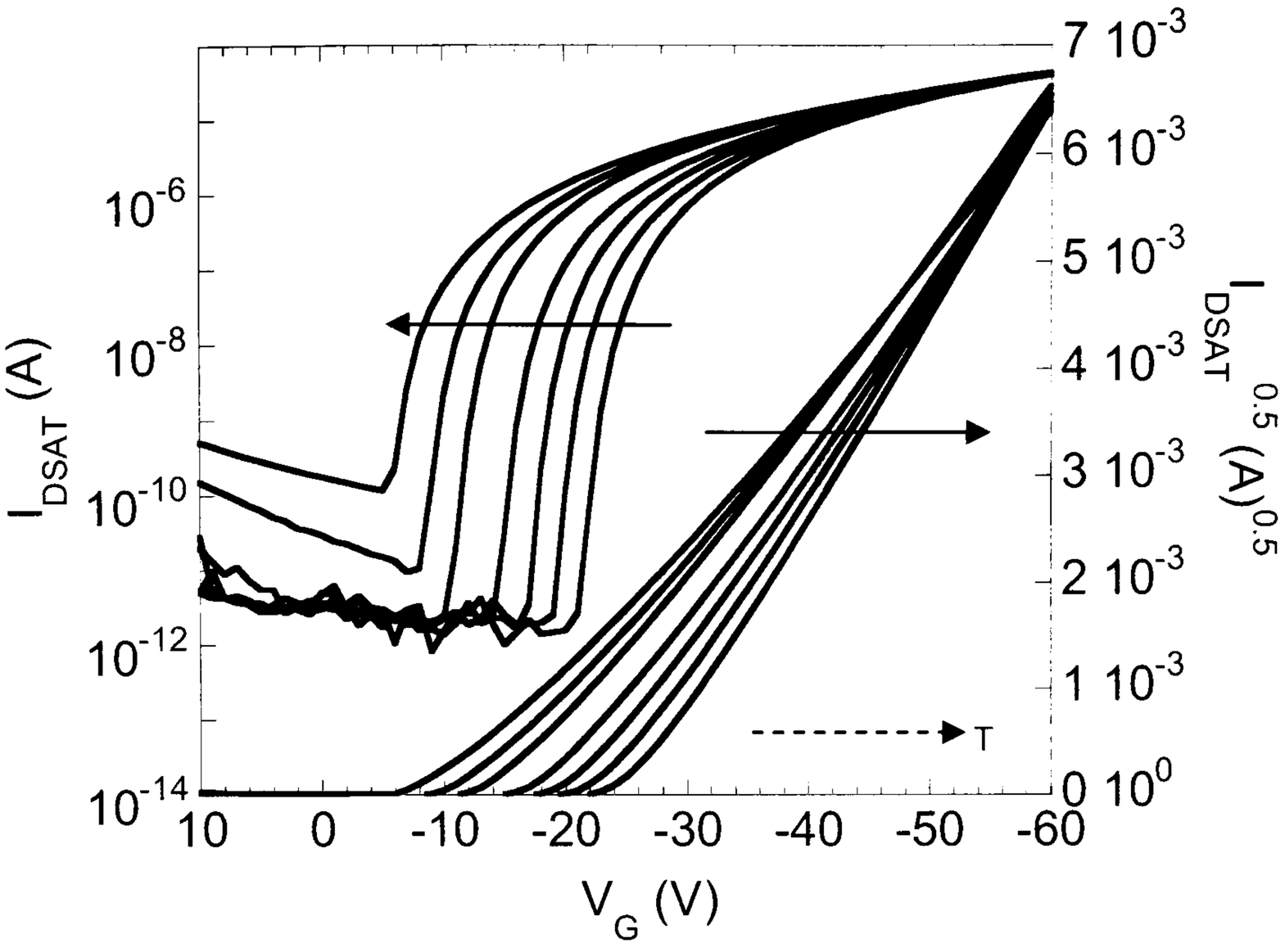


Figure.30. Saturated transfer characteristics for 20µm channel length syn-pBTTT ozoned transistors with temperature. The dotted arrow indicates the direction of the evolution of the characteristics with temperature. The solid arrows link the data with their respective axes.

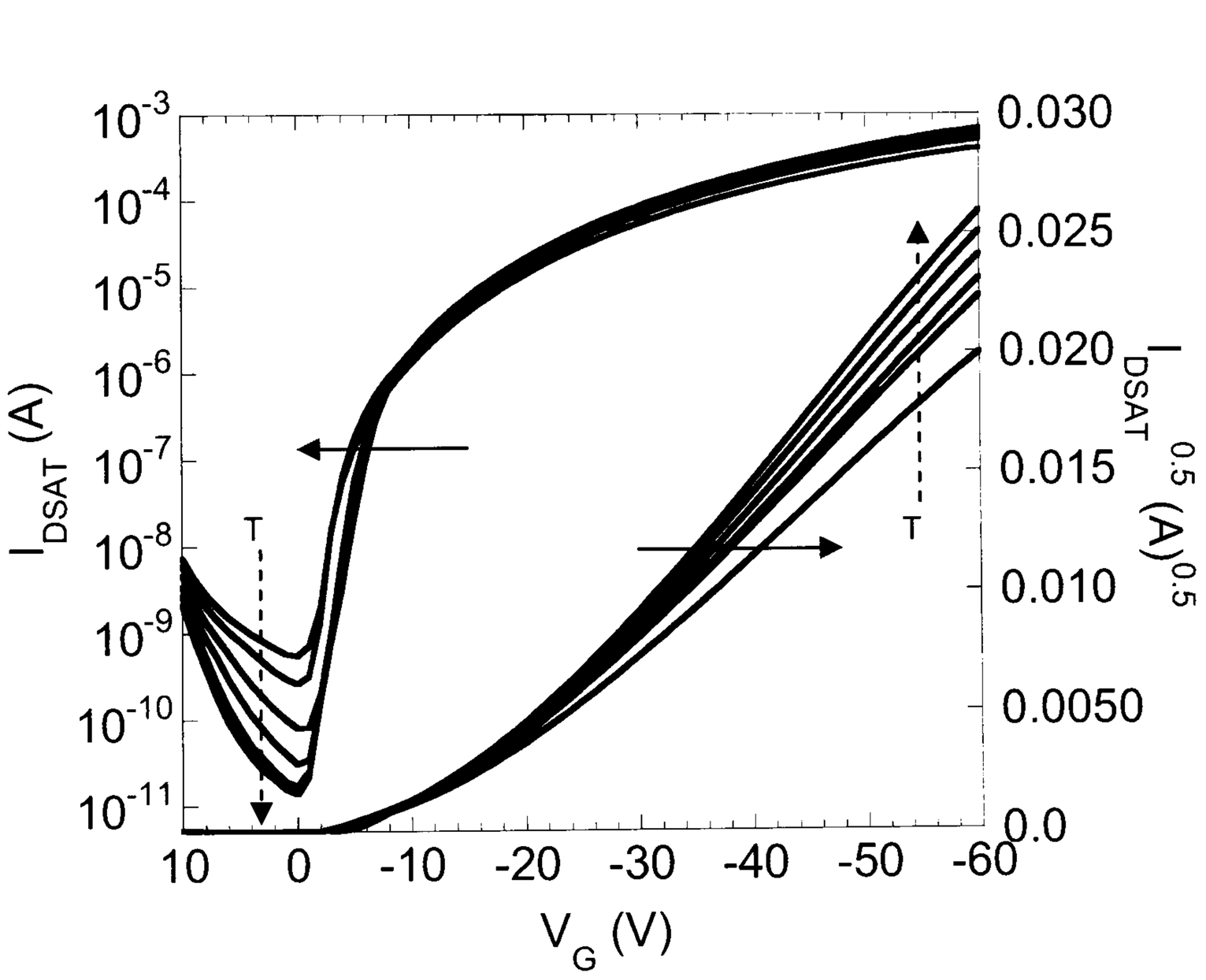


Figure.5.31. Saturated transfer characteristics for 20µm channel length syn-pBTTT OTS treated transistors with temperature. The dotted arrow indicates the direction of the evolution of the characteristics with temperature. The solid arrows link the data with their respective axes.

An interesting anomaly was noted if the transfer characteristics were plotted in semilogarithmic format with regard to the temperature. Notably different trends are observed on comparing the temperature dependence of an ozone-cleaned sample with a silane-treated device, as is evident from Fig.5.30 and 5.31.

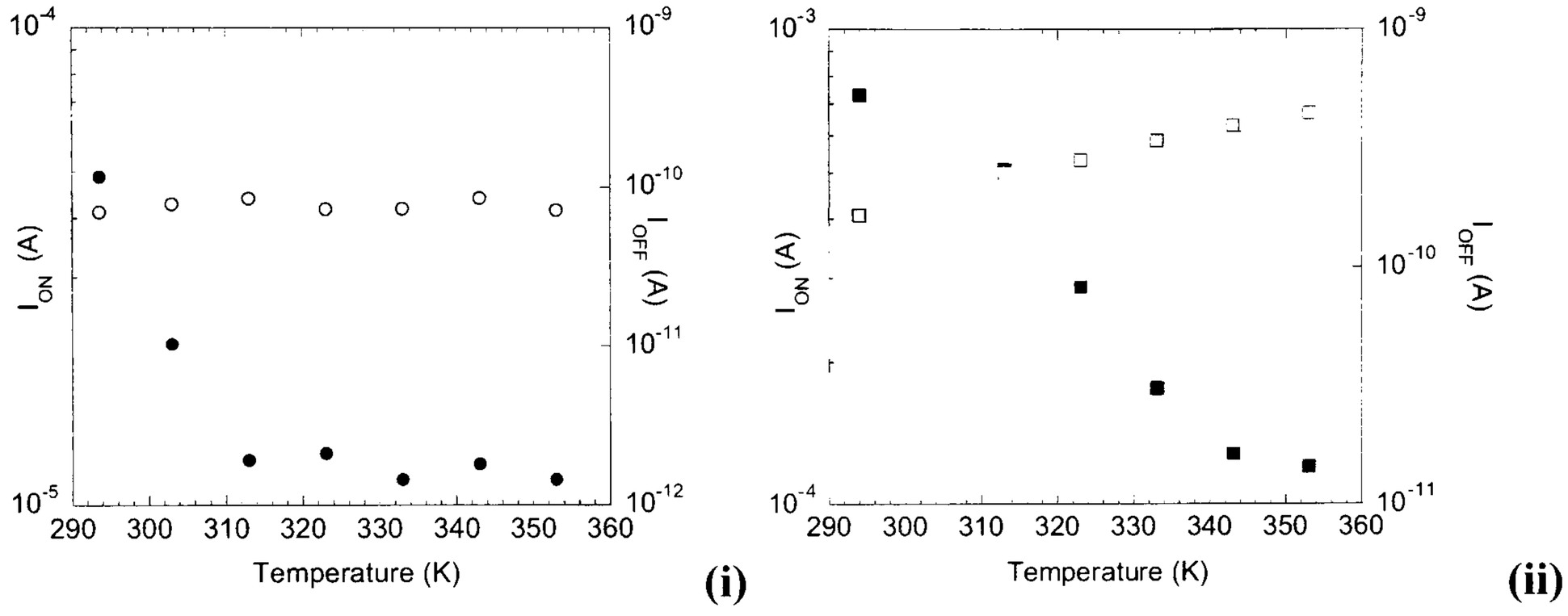


Figure.5.32. illustrates the relationship between the on (empty shapes) and off-currents (filled shapes) with temperature for the (i) ozone treated and (ii) OTS treated syn-pBTTT transistors.

In both cases, the off-current decreases with increasing temperature. This is more rapid for the ozoned device. After a temperature increase of just 20K, the off current drops to pA levels before levelling off. This current decrease is much slower for the OTS treated transistor, with currents only beginning to stabilise at 10pA after a 50K temperature increase. The on-current increases slightly and then becomes stable, fluctuating within a current range of 42 to 44μA, for the ozoned transistor. This corresponds to the temperature at which the off-current stabilises. The on-currents increase steadily for the OTS treated device, in parallel to the off-currents that are continually decreasing.

The switch-on voltage and threshold voltage shift negatively for the ozoned transistor with increasing temperature, but remains constant for the OTS treated device. We have already discussed how this can depend on the electron acceptance of the terminating group, as any surface charge present at the interface can influence

the surface potential, translating to a shifting V_0. The same effect can also be observed if hydroxyl ions, water molecules, or mobile ions are present at the interface. Though all the fabrication steps involving the polymer were carried out under nitrogen (H_20 and O_2 typically <0.1ppm level), simply ozone treating the surface introduces hydroxyl ions at the interface, which can then act as electron accepting traps. The hydroxyl groups on the surface of the oxide are in effect passivated by silane treatment.

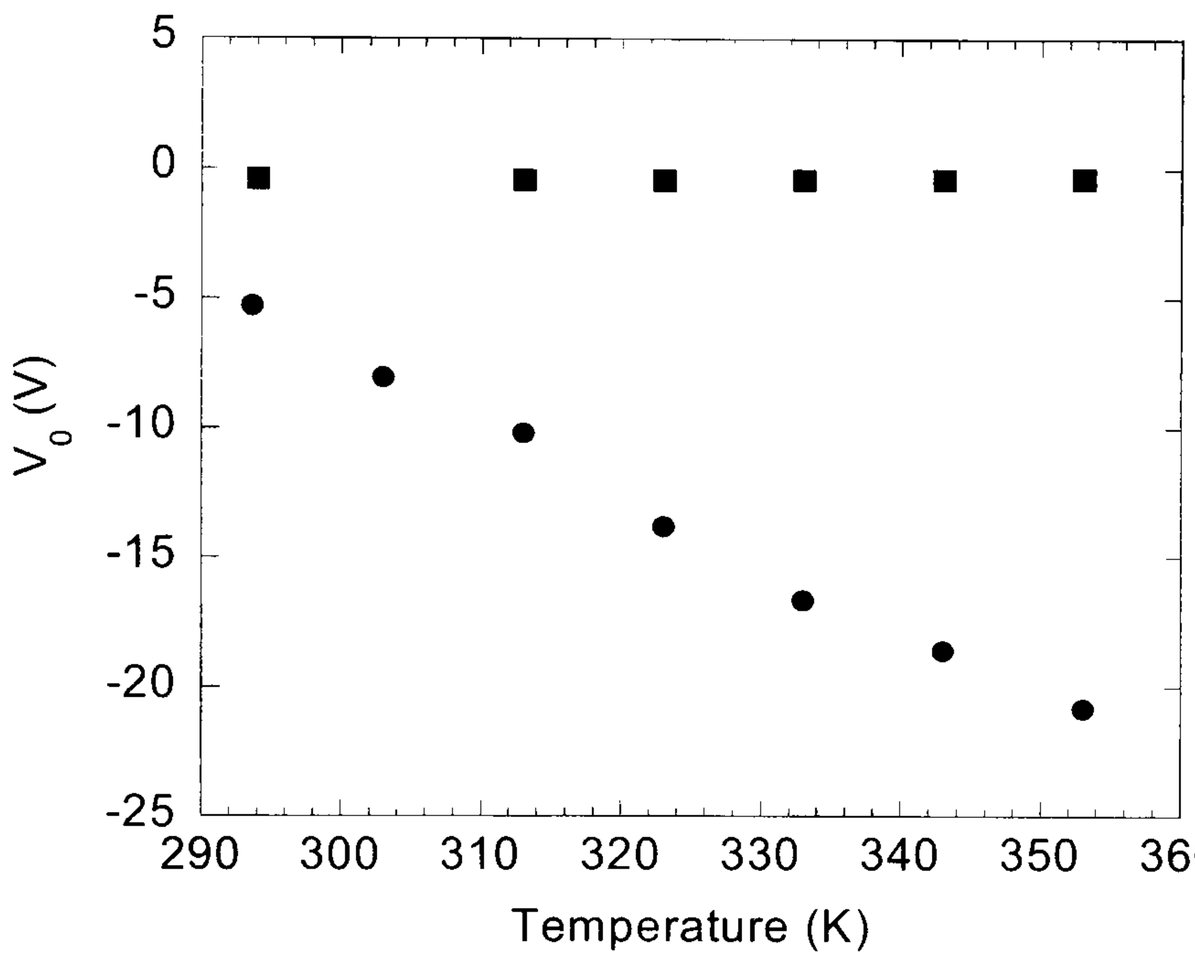


Figure.5.32. illustrates the relationship between the switch-on voltage and temperature for ozoned (filled circles) and OTS treated (filled squares) 20µm channel length syn-pBTTT transistors.

Let us first consider the OTS treated device. V_0 is approximately zero and remains constant with increasing temperature. In the ozone treated case, V_0 is less than zero and this value shifts negatively with increasing temperature. If we assume that the switch on voltage is made up of a combination of the workfunction mismatch, interface charges and injection barrier, we can write V_0 in accumulation as follows:

$$V_0 = \Phi_{ms} + \frac{Q_{is}}{C_i} + V_{inj} \qquad \{5.5\}$$

Φ_{ms} depends on the relative level of dopants (N_D and N_A in the silicon and polymer, respectively) and should be similar for both the OTS and ozone treated devices. Only the switch-on voltage of the ozone treated transistor varies with temperature, so it is unlikely that a changing concentration of acceptor dopants with temperature is responsible for the shift. Injection should improve with increasing temperature, but this should lead to V_0 shifting positively towards zero. Thus, interface states must play a role in the negative shifting of V_0.

As the switch-on voltage for the ozoned transistor is negative, it would be expected that the interface states are either neutral when full and positive when empty or negative when full and neutral when empty. As the gate voltage is swept from zero to V_0, either holes are arriving or electrons are leaving. Bearing in mind that the switch-on voltage is negative, and we know that hydroxyl groups at the interface trap electrons, we can assume that electrons are trapped and as the temperature is increased a larger proportion of interface trap states are empty as electrons are released. As the surface charge density in the interface states can be approximately calculated as: [32]

$$N_{is} = \frac{C_i V_0}{q} \qquad \{5.6\}$$

Fig.5.33 estimates the change in the trap density of negative insulator states on increasing the temperature. Let us assume that states exist deep in the energy gap with large activation energies. Heating would release trapped electrons. This reduces the negative charge density at the interface, decreasing the concentration of holes accumulated and shifting the switch-on voltage to more negative values. This also corresponds to the decrease in the off-currents.

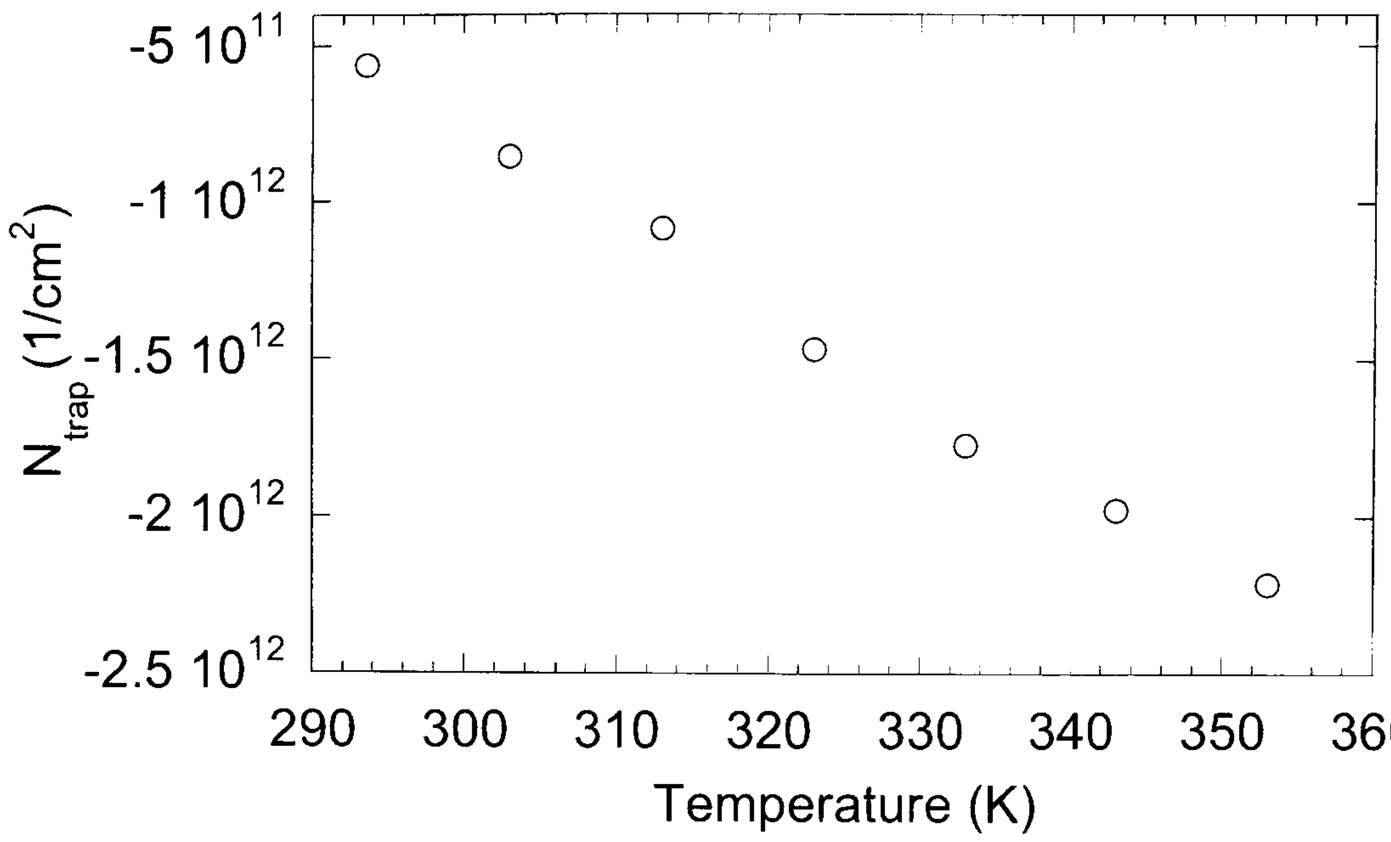


Figure.5.33. illustrates the relationship between the trap density and temperature for the ozoned 20μm channel length syn-pBTTT transistor.

This is far more rapid for the non-silylated interface. Chua et al. suggest that OTS treatment can not completely passivate interface states and though the proportion is reduced the residual concentration is still significant (uncondensed groups in the O-Si-O network can also contribute to the number of hydroxyl groups present).[32] The self-assembled monolayer also provides a physical barrier between the channel and interface states. The reduced concentration of negative charge due to trapped electrons is partially screened and electrons have to tunnel through the monolayer to fill or empty the traps. V_0 consequently does not shift and the off-current decreases at a slower rate than the non-ozoned device.

5.3.8. Summary of silane treatments

Silane layers act in two ways to improve the performance of PFETs. They improve organisation at the interface by encouraging ordered packing via the interlocking of alkyl chain side groups, enabling more efficient charge transport along the π-π conjugated backbone. Preliminary experiments show that this corresponds to a smaller energetic disorder parameter. Silanes can also induce charge at the interface, which acts to shift the switch-on voltage. Electron accepting or donating terminal

groups affect the charge distribution at the interface (i.e. channel). This is useful for polymers with a very positive or negative turn-on, as a silane treatment can be chosen accordingly. For example, F8T2 often has V_0 of ~ -5V so treatment with a fluorinated silane could encourage this to shift positively. Finally, if silicon dioxide is used as the dielectric in organic transistors, hydroxyl groups will naturally be present at the surface. These hydroxyl groups act to trap electrons forming interface states that can affect the transistor characteristics via higher off currents and a shifting switch-on voltage with temperature. These states can, to an extent, be passivated by a silane monolayer.

5.4. Combination of surface treatments

The next logical step is to combine both thiol and silane surface treatments. This should provide enhancement of the mobility from both an injection and morphological point of view. Contact angle studies indicate that silanes could assemble onto freshly ozone-cleaned gold surfaces, which is also confirmed by increased non-linearity in the linear portion of the transistor output characteristics. Hydroxyl groups could temporarily be induced onto the gold by ozone treatment, but are unstable and dissipate within a couple of hours. Thus ozone-cleaned substrates were stored under nitrogen for two to three hours before silane treatment, and this was indeed found to improve any non-linearity in the output characteristics. Thiols were assembled before silane surface treatments were undertaken, as the Au-S process is more selective. The same process described in Section 5.2.2 was used, and silane treatment then carried out according to 5.3.1.

5.4.1. Combination of surface treatments for syn-pBTTT

The image in Fig.5.34 denotes the spreading of a water droplet on an off-cut of a pre-patterned thiol and silane surface treated silicon wafer. The grey and white sections are representative of the silicon dioxide and gold surfaces, respectively, and the gold

is patterned so that four strips lead off from a central square. The water droplet dewets from the more hydrophobic silylated silicon dioxide and sticks preferentially onto the thiol-treated gold, as the surface energies are more similar.

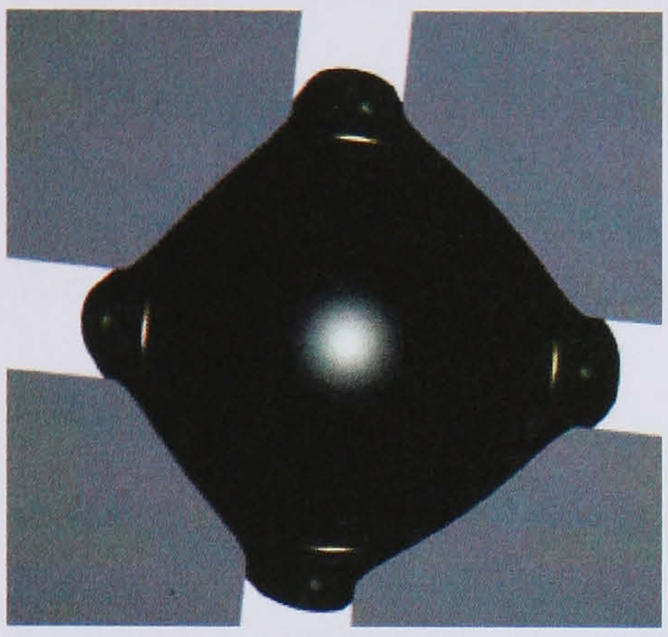


Figure.5.34.The image depicts the spreading of a water droplet on an off-cut of a pre-patterned thiol and silane surface treated silicon wafer. The grey and white sections represent the silicon dioxide and gold surfaces, respectively, and the gold is patterned so that four strips lead off from a central square. The water droplet dewets from the more hydrophobic silylated silicon dioxide and sticks preferentially onto the thiol-treated gold.

Fig.5.35 displays the saturated transfer characteristics of a FTP, OTS, and FTP/OTS treated syn-pBTTT transistor.

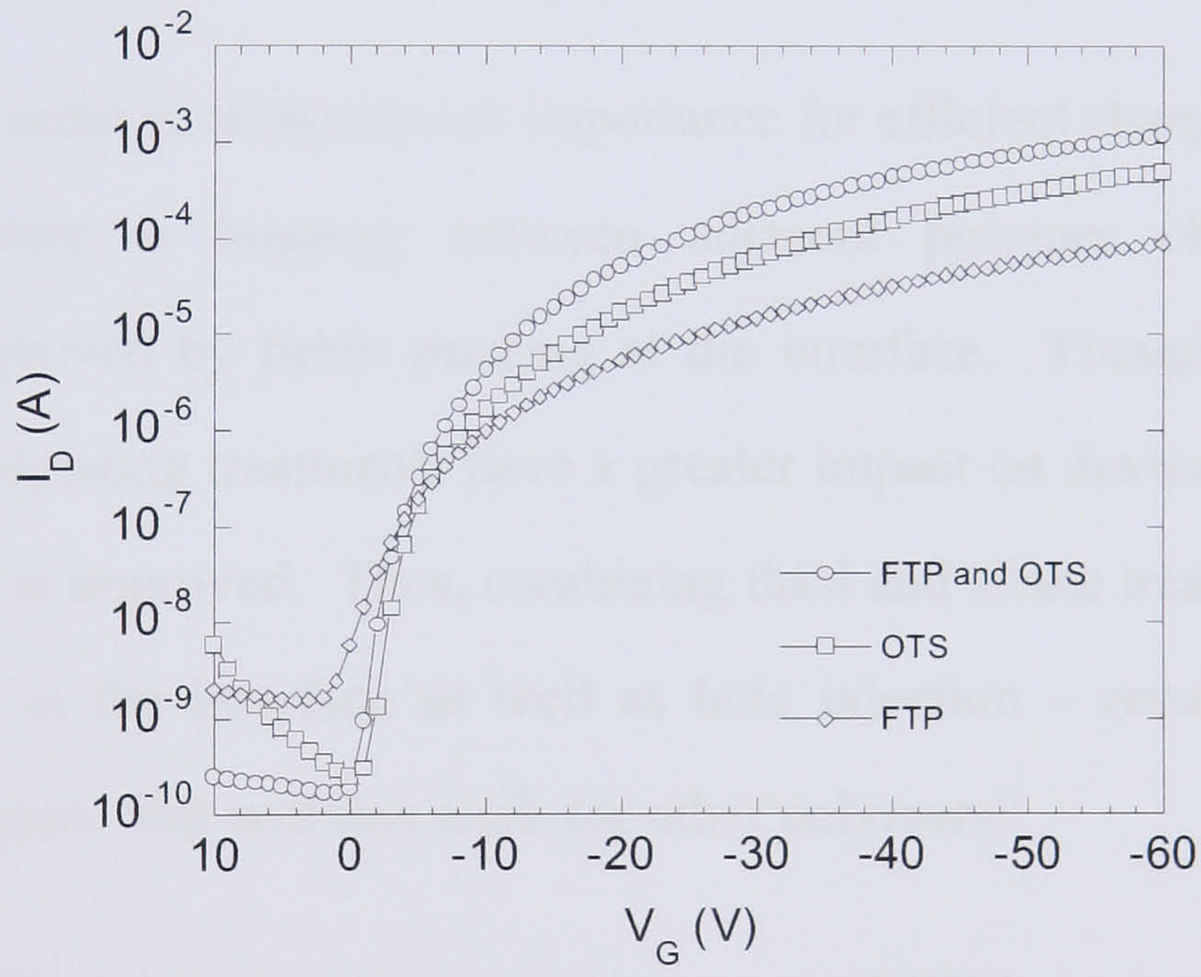


Figure.5.35. Saturated transfer characteristics of FTP, OTS, and FTP/OTS treated syn-pBTTT transistors. The channel length and channel width is 10μm and 1cm, respectively.

The channel length and channel width is 10μm and 1cm, respectively. The saturated mobility of the OTS treated transistor is nearly 6 times higher than the FTP devices, 0.02cm^2/Vs as compared to 0.0035cm^2/Vs. The saturated mobility of the FTP/OTS treated transistor is 0.041cm^2/Vs, nearly 12 times higher than the FTP one, and

double that of the OTS treated device. The drain currents increase in the trend $I_{FTP/OTS} > I_{OTS} > I_{FTP}$ and are highest for the FTP/OTS treated devices, which shows that holes are more easily accumulated than in the OTS treated transistor. This is as expected, as we have seen that FTP assembled on the electrodes reduces the barrier to hole injection for the polymer/gold system.

We can suppose that there is a greater proportion of holes present in the channel with the FTP treated transistor, which is corroborated by the more negative switch-on voltage of the OTS treated device – approximately 0V rather than +5V. The FTP/OTS transistor also shares a V_0 of ~ 0V, which indicates that similarity of interface states for the silylated devices plays a greater role than V_{inj} when determining V_0. Improved injection properties for the FTP/OTS transistor are clearly evident from the higher currents.

Good molecular order is of paramount importance for efficient charge transport. The rate-limiting factor is hopping between adjacent polymer chains, which is significantly improved by better packing at the interface. Though thiols improve hole injection, silylating treatments have a greater impact on device performance as charge transport is improved. Thus, combining thiol and silane treatments improves molecular order at the interface as well as hole injection – resulting in the best overall performance. But will this work for other polymers?

5.4.2. Combination of surface treatments for ant-pBTTT

The effects of thiol and silane treatments were also investigated for ant-pBTTT. In this case the HOMO level was estimated from UPS studies to be 5.1eV, as discussed in Chapter 3. Fig.5.36 shows the difference in output characteristics for a -30V gate bias for a FTP/OTS, CTP/OTS and OTS treated 20μm transistor. Fig.5.38 shows the linear and saturated transfer characteristics for the same transistors as in Fig.5.37. The currents are highest for the FTP/OTS device, followed by the CTP/OTS and

then the OTS treated transistor, as in the case of transistors fabricated from syn-pBTTT it follows the trend $I_{FTP/OTS} > I_{CTP/OTS} > I_{OTS}$. The saturated mobility for the OTS treated transistor was $0.13cm^2/Vs$ and CTP/OTS treatment increased it to $0.22cm^2/Vs$. The mobility was highest for the FTP/OTS treated transistor at $0.29cm^2/Vs$.

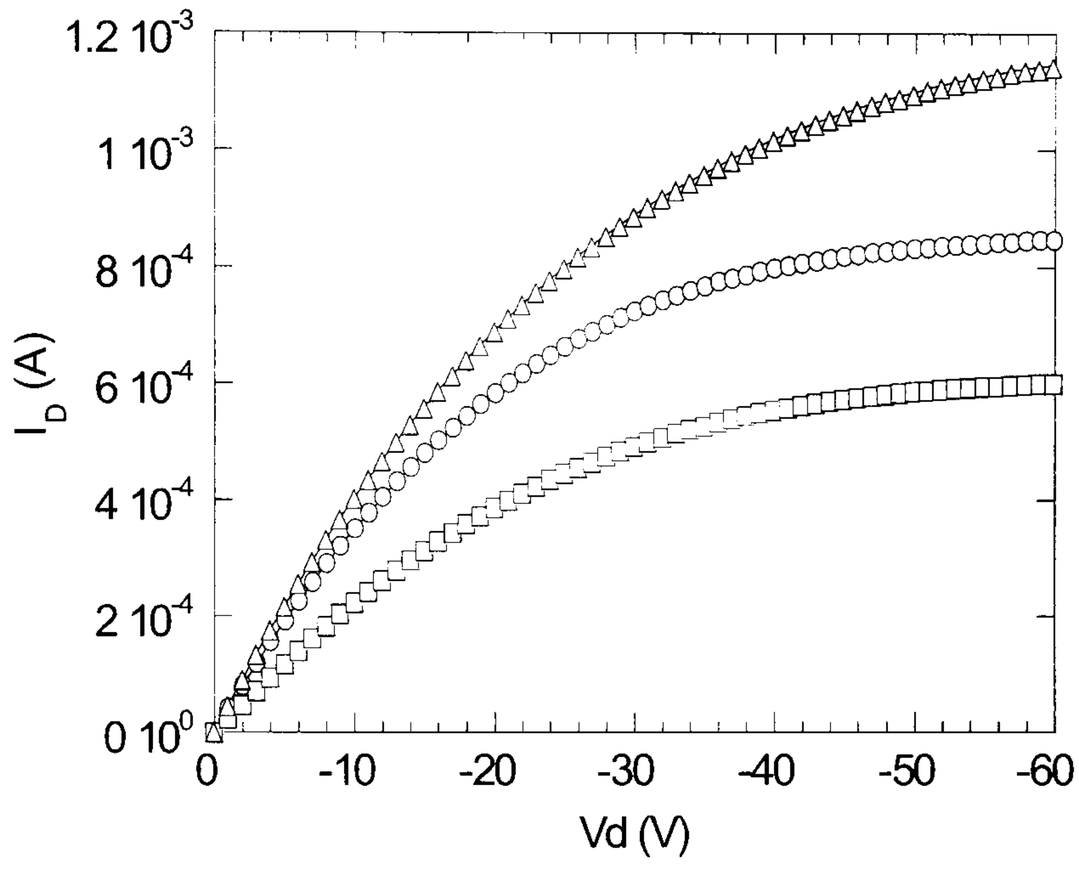


Figure.5.37. Output characteristics for a FTP/OTS (open triangles), CTP/OTS (open circles) and OTS (open squares) treated 20µm transistors at V_G=-30V.

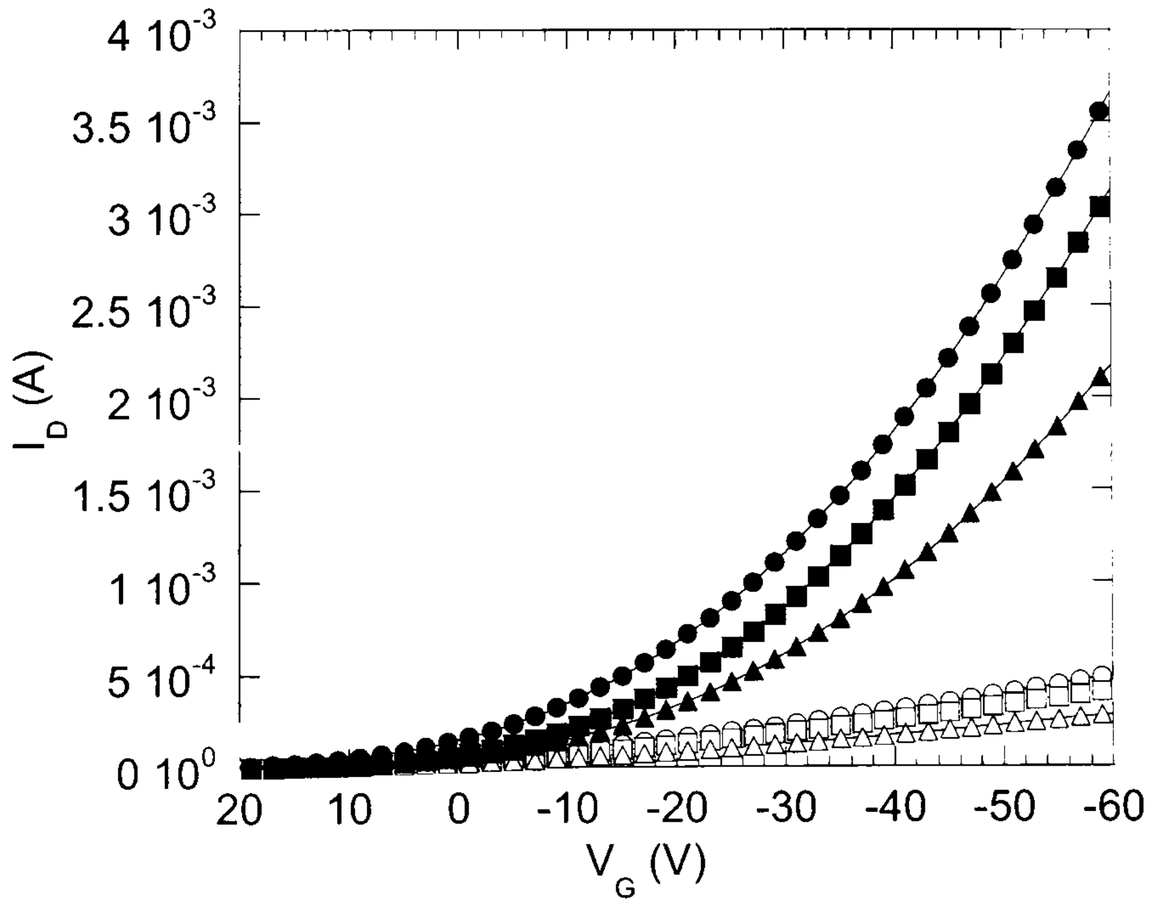


Figure.5.38. Linear (open shapes) and saturated (filled shapes) for FTP/OTS (circles), CTP/OTS (squares) and OTS (triangles) treated 20µm transistors.

Though the hole injection barrier is smaller for ant-pBTTT than syn-pBTTT, the combination of FTP and OTS treatment improved device characteristics. FTP self-assembled monolayers raise the workfunction of the gold injecting electrodes, decreasing the barrier to hole injection with respect to the HOMO of the polymer. There should in theory be no barrier to hole injection between gold and ant-pBTTT, but the composite material systems has not been studied and as we have seen the Φ_{Au} can be reduced by 0.5eV if measured under nitrogen. Introduction of the SAM at the electrode enables higher charge densities of carriers to be injected into the polymer, significantly improving the mobility and on-currents. This results in some of the highest mobilities reported for solution-processible polymers, making it a very valuable tool for use in device fabrication.

5.5. Conclusions and further work

In this Chapter we have seen that the device characteristics of polymer field-effect transistors can be significantly modified by using self-assembled monolayers. The operation of PFETs is mainly affected by the charge transport in the channel and injection limitations. The former is dependent on molecular order and the packing of the polymer chains adjacent to the dielectric/semiconductor interface, whilst the foremost factor affecting injection is the injection barrier, estimated from the difference between the workfunction of the metallic electrode and HOMO (or LUMO for n-type transport) of the polymer. SAMs enable both of these factors to be optimised through simple surface chemistry.

The sulphur containing head group of thiols preferentially adsorbs to gold. If the molecule is chosen to possess a dipole moment, assembly onto the gold electrodes has the equivalent effect of the insertion of a dipole layer between the metal and polymer. If the terminal group is electronegative this acts to raise the workfunction of the gold, reducing the hole injection barrier. If the terminal group is chosen to be

electron donating, Φ_{Au} is decreased and the barrier to hole injection is increased. The device characteristics of polymer transistors can thus be improved or worsened via selection of the appropriate thiol. The choice of spacer group also affects the injection, as charge carriers have to physically tunnel through the monolayer into the polymer. Aromatic thiols were best suited for this purpose and injection limited I-V characteristics and increased contact resistances were observed with increasing spacer group length. 4-fluorothiophenol (FTP) was found to improve device characteristics best for syn-pBTTT transistors, and a three times increase in mobility was achieved.

Silanes self-assemble into ordered monolayers via condensation reactions. These enhance the mobility by improving the stacking of the conjugated backbones, as the perpendicular side chains of the polymer can interlock with the alkyl chains protruding upwards from the interface. Silane surface treatment also makes the interface more hydrophobic as it replaces the naturally occurring polar hydroxyl groups of silica with apolar methyl groups (thus improving adhesion of the polymer). This also acts to passivate the interface, as hydroxyl groups are known to act as electron traps. This results in a significant improvement of the mobility of up to 16 times for octyltrichlorosilane (OTS) treatment.

The chemical selectivity of self-assembled monolayer allows thiol and silane surface treatments to be combined in order to achieve the best overall performance. Combining FTP and OTS treatments improves the mobility by 40 times with reference to an untreated syn-pBTTT transistor. Improved device characteristics were also observed for ant-pBTTT transistors. Not only is this beneficial for improving device performance, but it gives us an insight into the relation between charge transport and injection in these systems. Good molecular order at the interface (efficient charge transport) has a bigger impact on the mobility and device characteristics, than the injection alone.

In this work, self-assembled monolayers were systematically studied in syn-pBTTT and ant-pBTTT polymers, but promising results were seen for preliminary experiments concerning the polyfluorene polymers, F8T2 and PFO. Further work needs to be undertaken to look at different and composite material systems (both for the electrodes[§] and the polymers). This simple generic technique helps to solve injection problems that arise from the use of high I_P polymers, so designed to combat instability in air.

[§] Though thiols can only be used with metals, the same principles could be applied to other electrode materials.

References

1. I. H. Campbell, J. D. Kress, R. L. Martin, D. L. Smith, N. N. Barashkov, J. P. Ferraris, *Appl. Phys. Lett.* **71** 3528 (1997)

2. I. H. Campbell, S. Rubin, T. A. Zawodzinski, J. D. Kress, R. L. Martin, D. L. Smith, N. N. Barashkov, J. P. Ferraris, *Phys. Rev. B* **54** 20 (1996)

3. Y. Park, V. Choong, Y. Gao, B. R. Hsieh, C. W. Tang, *Appl. Phys. Lett.* **68** 19 (1996)

4. J. Lee, B-J. Jung, H. Y. Chu, L-M. Do, H-K. Shim, *J. Mater. Chem.* **12** 3494 (2002)

5. C. Ganzorig, K. J. Kwak, K. Yagi, M. Fujihia, *Appl. Phys. Lett.* **79** 2 (2001)

6. S. F. J. Appleyard, S. R. Day, R. D. Pickford, M. R. Willis, *J. Mater. Chem.* **10** 1 (2000)

7. A. Vilan, A. Shanzer, D. Cahen, *Nature* **404** (2002)

8. C. D. Dimitrakopoulos and P. R. L. Malenfant, *Adv. Mater.* **14** 2 (2002)

9. P. Stoliar, R. Kshirsagar, M. Massi, F. Biscarini, *Conf. Proc. ECM* (2005)

10. A. Salleo, M. L. Chabinyc, M. S. Yang, R. A. Street, *Appl. Phys. Lett.* **81** 23 (2002)

11. S. M. Sze, Physics of Semiconductor Devices, 2nd Edition, John Wiley & Sons (1981)

12. H. Ishii, K. Sugiyama, E. Ito, K. Seki, *Adv. Mater.* **11** 605 (1999)

13. J. C. Scott and G. G. Malliaras, *Chem. Phys. Lett.* **299** 115 (1999)

14. I. D. Parker, *J. Appl. Phys.* **75** 1656 (1993)

15. P. R. Entage, J. J. O'Dwyer, *Phys. Rev. Lett.* 16 **356 (1966)**

16. J. Campbell Scott, *J. Vac. Sci. Technol.* **21** 3 (2003)

17. R. G. Nuzzo, D. L. Allara, *J. Am. Chem. Soc.* **104** 4481 (1983)

18. B. Livesay, *Masters Thesis* (2002)

19. P. W. Atkins, *Physical Chemistry*, 5th Edition, Oxford University Press (1994)

20. S. Khodabakhsh, *PhD Thesis* (2005)

21. J. H. Fendler, *Chem. Mater.* **13** 10 (2001)

22. F. T. Cavadas, PhD Thesis (2003)

23. A. Vilan, A. Shanzer, D. Cahen, *Nature* **404** 166-168 (2000)

24. A. Kahn, N. Koch, W. Y. Gao, *J. Pol. Sci. B* **41** 21 (2003)

25. S. Luan and G. Neudeck, *J. Appl. Phys.* **72** 2 (1992)

26. D. K. Schwartz, *Ann. Rev. Phys. Chem.* **52** 107-137 (2001)

27. K. P. Pernstich, C. Goldmann, C. Krellner, D. Oberhoff, D. J. Gundlach, B. Batlogg, *Synth. Met.* 146 (2004) 325-328

28. M. Shkunov, R. Simms, M. Heeney, S. Tierney, I. McCulloch, *Adv. Mater.* **17** 21 (2005)

29. H. Bässler, *Phys. Stat. Sol. (b)* **175** 15 (1993)

30. M. Borsenberger and D. S. Weiss, *Organic Photorecep tors for Xerography*, M. Dekker Ltd. (1998).

31. K. P. Pernstich, S. Haas, D. Oberhoff, D. J. Gundlach, B. Batlogg, A. N. Rashid, G. Schitter, *J. Appl. Phys.* **96** 11 (2004)

32. L.-L. Chua, J. Zaumseil, J.-F. Chang, E. C.-W. Ou, P.K.-H. Ho, H. Sirringhaus, R. H. Friend, *Nature* **434** 194-199 (2005)

Chapter 6

Bulk and interface mobility comparisons

The differences between the bulk mobility, measured by the TOF photocurrent technique, versus the field-effect mobility are explored in this Chapter. Though the charge density is lower in time of flight measurements, μ_{TOF} is significantly higher than that of transistors, for the materials studied. Transistors represent a lower mobility as the two-dimensional charge transport occurs in the first few polymer chains adjacent to the interface, making it more sensitive to disorder and interfacial traps. Temperature measurements confirm that the disparity between the bulk and interface mobility is due to increased energetic disorder and a longer interchain hopping distance at the interface. If the molecular order of the transporting layer is improved, by using silanes or annealing, the mobility of the transistor is improved and it approaches μ_{TOF}. Temperature dependent transistor comparisons of an amorphous polymer to the polycrystalline polymers used in the prior Chapters signify further that increased morphological disorder directly translates to lower mobilities, a longer interchain hopping distance, increased energetic disorder and a higher activation energy.

The previous Chapters have demonstrated the effect the interface, morphology and injecting contacts have on the mobility of field-effect transistors and has found μ_{FET} to be dependent on the efficiency of charge transport in the accumulation layer and the charge carrier density. The mobility of a material can be defined as the magnitude of the drift velocity per unit electric field.[1] The time of flight technique (TOF), in which the transit time of optically generated carriers across a film is measured, is typically used to determine the mobility of organic systems and provide a reliable estimate of the bulk mobility (μ_{BULK}) at low charge carrier densities. This can also be extracted from space-charge limited current (SCLC) transient dark injection and steady state J-V measurements. Comparisons of these methodologies have yielded mobility values differing by several orders of magnitude for the same materials, with a considerable variation often noted between the bulk and field-effect mobility.

Another feature of disordered systems is that the mobility is often observed to be strongly field and temperature dependent. As charge transport occurs via a hopping mechanism it is understandable that the mobility depends on the electric field, since the application of an electrostatic potential would tilt the DOS and in doing so reduce the average barrier height for energetic uphill jumps in the direction of field. This tends to follow a 'Poole-Frenkel' like dependence, $\ln|\mu|$ varying linearly with respect to the square root of the applied electric field. Temperature-wise, the mobility is generally observed to increase with rising temperature, further evidence that the transport in such disordered systems is via a hopping mechanism.[2] Though it should be noted that band-like transport has been detected for the crystalline, small molecule pentacene at low temperatures (<150K).[3]

TOF and fitting from I-V characteristics sample different electric field and charge density regimes. TOF is used to measure mobility for E-fields from about

$5x10^4$V/cm to $1x10^6$ V/cm and is restricted to low carrier densities ($<10^{13}cm^{-3}$). Fitting single-carrier space charge limited diode J-V characteristics probes the mobility from fields from 10^5V/cm to 10^6 V/cm and carrier densities from 10^{16} to $10^{18}cm^{-3}$. It is much less sensitive to trapping effects than TOF as a comparatively large density of injected carriers can fill moderate densities of traps without affecting the mobility measurement. Transistors operate in an even higher charge carrier density regime of $>10^{18}cm^{-3}$.[4] In interpreting charge transport within the framework of the multiple trapping and release model (MTR), it is assumed that a charge carrier spends longer escaping from deep tail sites. If the carrier density is so high that these sites can be thought of as effectively filled, 'excess' charge carriers can move via the shallower sites, reducing on average the time a carrier spends being trapped. This should consequently increase the mobility and suggests that for a given material the field-effect mobility should be larger than that derived from TOF measurements.

Scheinert et al. and Grecu et al. noted that the mobility derived from capacitance-voltage (C-V) measurements on polythiophene-based MIS diodes was four orders of magnitude lower than that of similarly fabricated FETs.[5,6] Tanase et al. also demonstrated similar differences between the field-effect mobility and mobility as derived from hole-only diodes, attributing it to a charge carrier density dependence of the mobility in disordered hopping systems, as described above.[7] However, mobilities derived from time of flight studies can be higher than those from transistors - indicating this is not the entire story.

Another considerable difference between the bulk and field-effect mobility can be attributed to different device geometries from which they are extracted. The charge transport in a diode or TOF device is typically perpendicular to the substrate, with charge carriers traversing the bulk of the film. In a transistor, efficient charge transport is required in the channel adjacent to the interface between the dielectric

and semiconducting polymer, in a direction parallel to the substrate. In addition to the common factors that affect the mobility in organic systems, such as the tunnelling rate between polymer chains, positional and energetic disorder, and the activation energy (depending on model used), interface effects can also affect the field-effect mobility. We have already seen that specific interface trap states can arise from the hydroxyl groups terminating a silica dielectric. Interface states could also arise due to polarisation interactions of organic insulators, diffusion of ions or from any contaminants at the interface. The surface roughness of the insulator is also crucial, as could disrupt charge transport at the interface. Not only would any physical obstructions have to be circumnavigated by the charge carriers, but this could also affect the chain packing and conformation, so increasing the disorder in the film.

To summarise, in disordered systems such as conjugated polymer semiconductors, charges are 'trapped' at lower energy sites, moving from one site to the next via a hopping mechanism. The mobility consequently increases with applied electric field as hopping in the direction of the field is enhanced. One would expect the field-effect mobility to be higher than that derived from time of flight measurements if the mobility is dependent on the charge carrier density – as there is a higher probability that the transport sites are occupied. However, the positional and energetic disorder are likely to be increased at the interface and the presence of any interface trap states would act to reduce the field-effect mobility.

In this work, I shall look at the differences between the bulk mobility, measured by the TOF photocurrent technique and SCLC diode characterisation, versus the field-effect mobility. Differences between room temperature results will initially be addressed, before looking at the temperature dependence of the mobility. This gives us an indication of the effect different device structures and charge density regimes

have on parameters such as the energetic disorder, interchain distance, traps and polaronic effects.

6.2 Experimental techniques

6.2.1. The time of flight photocurrent technique

The time of flight (TOF) technique has become the conventional method for determining charge carrier mobilities in these amorphous materials. TOF is a straightforward technique by which a planar sheet of charges is photoinduced at the edge of the polymer film. The application of a bias sweeps the charges across the film, and their mobility can consequently be determined by the time taken to transverse the sample (of known thickness).

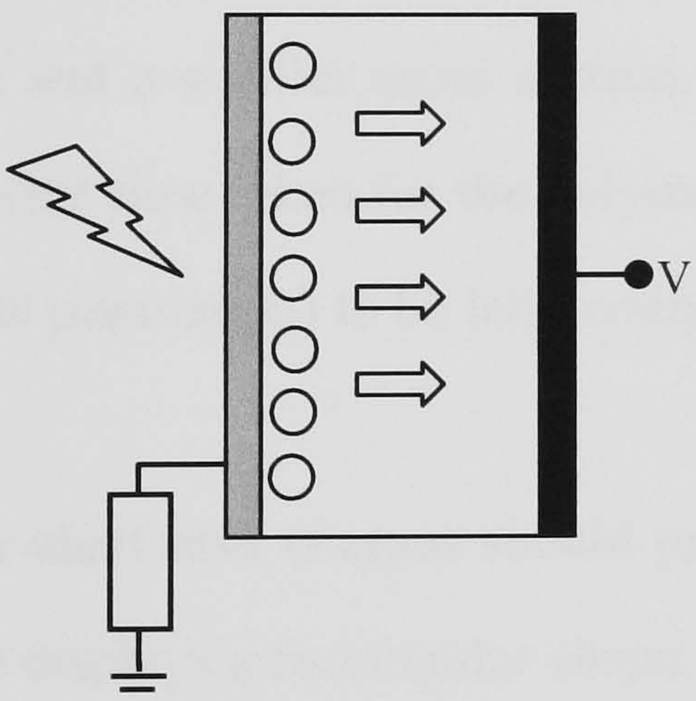


Figure.6.1. Schematic of a time-of-flight device. A pulse of incident light photogenerates a thin sheet of electron-hole pairs adjacent to the semi-transparent blocking electrode. Whether holes or electrons traverse the film depends on the bias at the counter electrode. The current is measured as a time varying voltage drop across the resistor connected in series to the device.

The sandwich device structure typically consists of a semitransparent blocking contact (20-30nm Al)/polymer film (>1μm thick)/contact (ITO). A thin sheet of e-h pairs is created adjacent to the semi-transparent contact on excitation by an optical pulse. The absorption depth of the optical excitation must be small compared to the film thickness, $\delta << d$, or bulk generation could occur. The optical pulse duration should also be short compared to the transit time of the charged carriers across the

sample. It is important that the amount of charge generated is relatively small so that space charge effects do not appreciably change the spatially uniform electric field in the device. Ideally, the injected charge Q_0 (estimated by integrating the area under the photocurrent transient) should be no more than 5%CV where C is the capacitance of the device and V is the applied voltage.

The application of a field causes the electron-hole pairs to separate and drift in a sheet across the film to the opposite electrode. This induces a time dependent photocurrent to flow in the external circuit, from which the transit time can be deduced. The time constant of the circuit should be much smaller compared with the average drift time of the charges, otherwise the RC decay and not the photocurrent would be observed. This can be achieved by reducing the resistance or capacitance. The resistance has a lower limit as decreasing R reduces the signal-to-noise ratio of the oscilloscope. As capacitance is proportional to the device area and inversely proportional to sample thickness, a smaller capacitance can be obtained with thicker films and a smaller cross section. It is also necessary for the dielectric relaxation time (the time taken for the polymer film to return to a neutral state after a change in carrier population) to be long compared to the transit time.

In an ideal case charges should propagate in a plane wave so that the photocurrent pulse displays a rectangular shape, with it immediately falling to zero when the sheet of carriers reaches the opposite electrode, as depicted in Fig.6.2. The situation which actually occurs is portrayed by the dashed and dotted lines. The so-called tail of the transient is attributed to the circuit reaction delay and decays exponentially. A diffusive broadening of the distribution of charges causes deviation from the ideal case with the shape of the transient being non-dispersive if it is assumed that the carriers possess similar drift velocities. Sometimes there is an initial current spike due to carriers of the opposite sign leaving, but fundamentally the current rapidly

drops and remains constant to a point where it gradually falls off – the time taken for the first carriers to traverse the sample. This point is called the effective transit time τ_0.

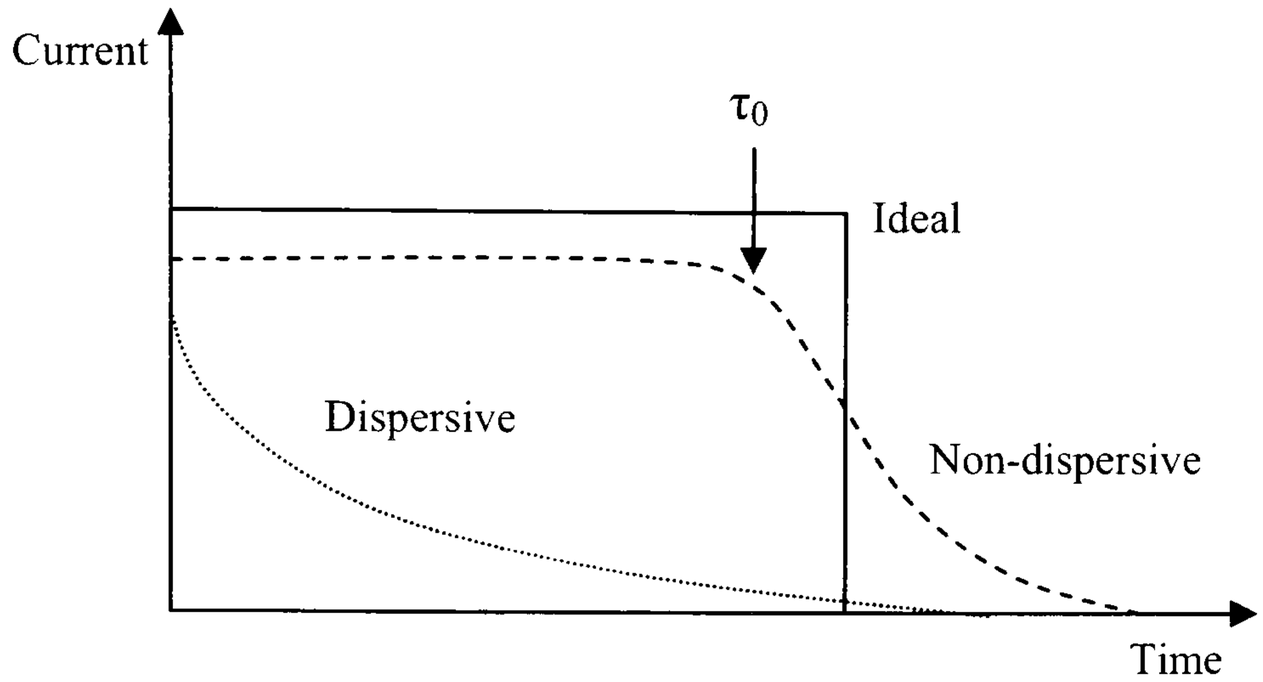


Figure.6.2. Illustration of ideal (solid line), non-dispersive (dashed line) and dispersive (dotted line) TOF transients. τ_0 represents the transit time of the non-dispersive transient.

Transport in conjugated polymers can be highly dispersive, meaning that if the distribution of the carrier drift velocities is extensive an almost featureless photocurrent can be obtained. This is a general feature of disordered systems and can lead to problems in determining the transit time, as the point at which the first carriers reach the opposite electrode may not be clearly defined. In this case the transient is classified as dispersive and the data are plotted on a log I-log t axis, with the transit time being determined by the intersection of asymptotes to the plateau and declining slope of the current transient.

The carrier mobility is determined from the carrier transient time by:

$$\mu = \frac{d^2}{\tau V} \qquad \{6.1\}$$

where d is the film thickness, τ is the transit time and V is the applied voltage. Thus, the mobility in this case is derived from the bulk of the film.[2,8]

6.2.2. Device fabrication

Pre-patterned indium tin (II) oxide (ITO) on glass substrates were supplied by CRL Optics for fabrication of time of flight samples and diodes. Substrates were thoroughly cleaned using the procedure outlined in Section 2.3. No surface treatments were used in this Chapter, though for diode fabrication poly (ethylenedioxythiophene)/polystyrene sulphonic acid (PEDOT: PSS) was spin-coated in a saturated acetone atmosphere and annealed at 100°C for ten minutes, before polymer deposition (if the ITO/PEDOT: PSS electrode was used as the hole injecting contact). The PF polymers were dissolved in xylene* at concentrations of 60 to 120 mg/ml for F8T2 and PFB time of flight samples, respectively. The solution concentration was dependent on the molecular weight of the material and the resulting viscosity and was chosen so that the film was smooth and at least 1μm thick when spin-coated onto the substrates at 1500rpm. Concentrations of 10-30mg/ml were used for diode studies and gave films with a thickness of 200nm.

Semitransparent aluminium (40nm thick) top electrodes deposited by shadow-mask evaporation completed the time of flight devices. Gold or aluminium electrodes 100nm thick were evaporated in the case of the diodes. The same device structure was used for both devices, and the average device area was 0.04 cm^2. This is illustrated in Fig.6.3. The polymer was carefully scratched off with a toothpick to make contact with the bottom ITO electrode, and conductive silver paste used to make contacting the devices easier.

* AnalaR grade (>99.5% purity) xylene is used for solution preparation.

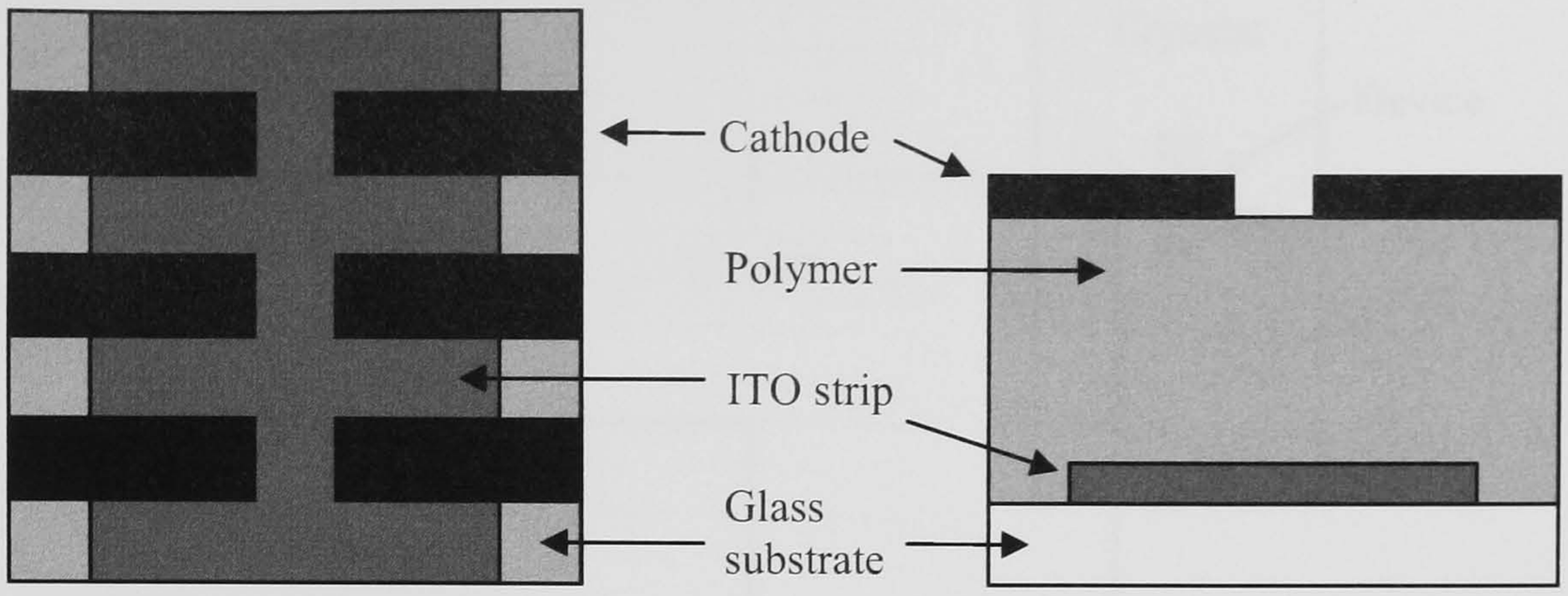


Figure.6.3. Schematic diagram of a plan and cross-sectional view of a standard diode/TOF device.

6.2.3. Time of flight measurements

Absorption measurements were initially carried out on the material using a UV-VIS Spectrometer, as this enables a suitable wavelength to be chosen for the exciting source. The absorption coefficient α should be high at the excitation wavelength as a localised sheet of charge carriers is required, rather than bulk generation. A frequency tripled Quantel ND:YAG ns-pulsed laser (λ_{ex} = 355 nm) was used as the photoexcitation source for PFMO and PFB devices, but a dye laser was used for F8T2 in order to shift the photoexcitation wavelength to 460nm, as both wavelength outputs of the ND:YAG laser lie either side of the absorption maximum of F8T2. As well as setting the power level of the laser, the intensity could be adjusted by using Neutral Density (ND) filters. This was optimised to provide maximum photocurrent signal, whilst ensuring that the amount of photogenerated charge Q remained <5% than $Q_0 = CV$.

A schematic of the TOF experimental set up is illustrated in Fig.6.4, overleaf. The field was applied using a high voltage DC power supply, and as hole transport was of interest, a negative voltage supplied to the collecting electrode.

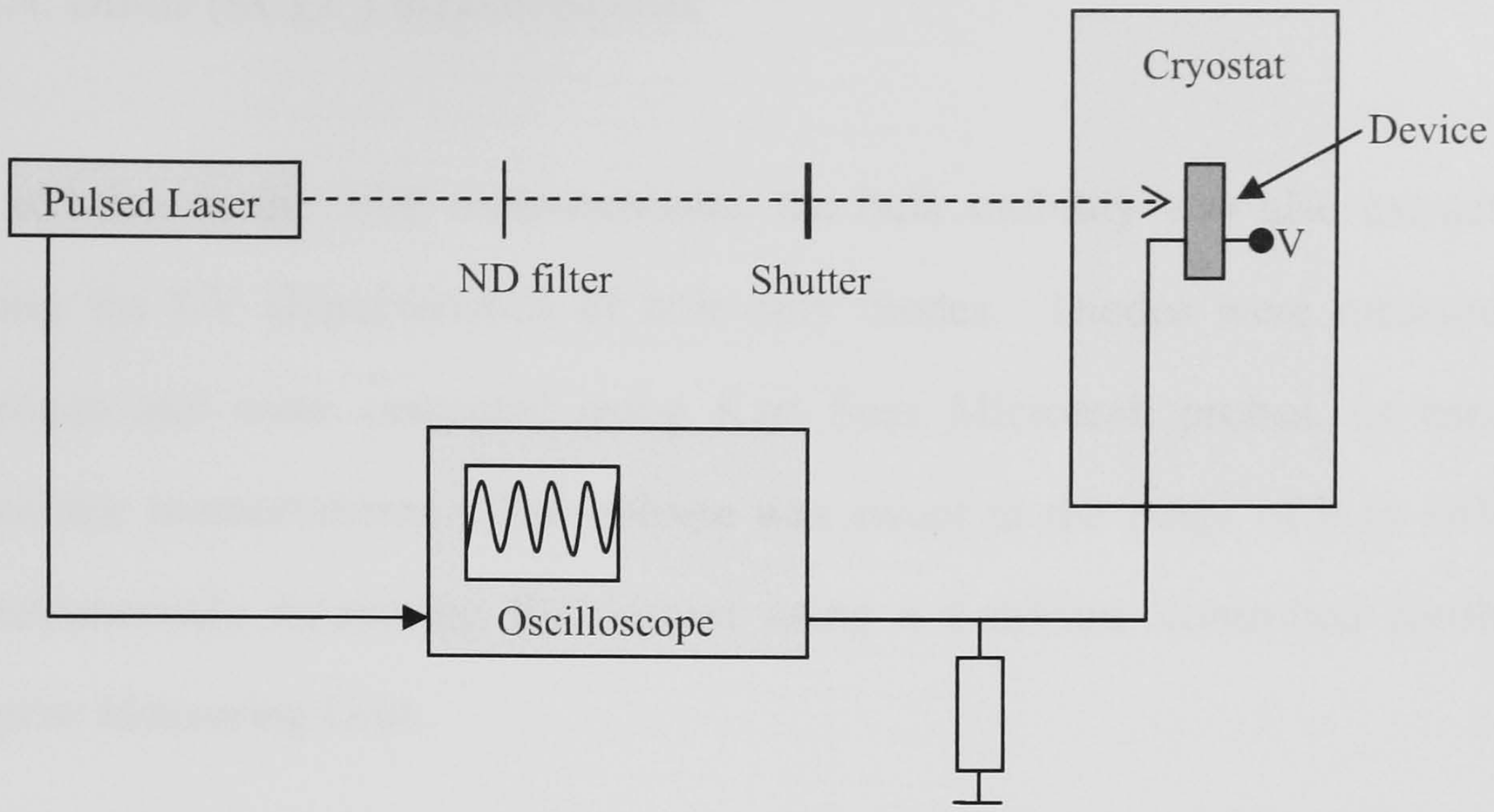


Figure.6.4. Schematic diagram of the TOF experimental set up. Adapted from[9]

The photocurrent was measured via a digital 500 MHz Tektronics TDS 3052 oscilloscope as the voltage drop across the series resistor with time. 256 averages were typically taken for each measurement. A shutter was used to block the sample off from the laser in order to take a baseline scan of the noise signal generated by the laser. The noise was then subtracted from the 'real' signal numerically.

The sample was securely mounted in a helium-exchange gas Oxford Instruments Optistat^{DN} cryostat. This enabled measurements to be taken in an inert atmosphere whilst an integrated thermocouple allowed temperature measurements in the range of 77K to 500K to be made. The F8T2 sample was measured in a different set up at the physics department of Queen Mary and Westminster University in which no cryostat was available. A thermocouple was built into a copper block underneath the sample holder and enclosed in a sealed box that was purged with nitrogen. In this case, measurements could only be undertaken above room temperature.

6.2.4. Diode (SCLC) measurements

In addition to the TOF measurements, the bulk mobility was also extracted from fitting the I-V characteristics of hole-only diodes. Diodes were measured under nitrogen and were contacted using Karl Suss Microtech probes, as used in the transistor measurements. The voltage was swept in the range of 0 to +6V, whilst simultaneously measuring the current using a LabView controlled Keithley 237 Source Measuring Unit.

The carrier mobility is the main factor that determines the current-voltage characteristics of single-carrier SCLC diodes. The current flowing through a device can be either transport or injection limited, depending on the barrier height. The space charge limited current (SCLC) represents the maximum single carrier current that can flow under any circumstances. It only occurs if the contact is Ohmic (essentially unlimited supply of carriers). If the barriers to carrier injection are small and the conductivity of the material is relatively low, the rate limiting step of current flow will be bulk transport. The simplest type of bulk transport at a given temperature is single carrier Ohmic conduction:

$$J = \frac{qn\mu V}{d} \qquad \{6.2\}$$

J is the current density, q the electronic charge ($\pm 1.6 \cdot 10^{-19}$C), n (or p in the case of holes) the charge carrier concentration, μ the mobility, V the applied bias, and d is the device thickness. The field (V/d) is taken to be constant and it is assumed that the field due to the presence of the carriers is negligible. However, a significant number of carriers have to be injected for a current to flow in organic materials. If the injecting contact is Ohmic, the steady-state current will now be limited by the

space-charge in the sample. Not only would the charge carriers interact, but their induced field would no longer be negligible in comparison to the applied field so that V/d gives only an average approximation of the electric field in the device.

However, we know that transport in disordered semiconductors is localised and moves via a hopping mechanism. The presence of trap states reduces current levels at low charge carrier densities as they capture and immobilise a large proportion of the injected charge. The distribution of trap energies is proposed to be exponential, though it has been suggested that this could be correlated to the deep sites in the tail of the Gaussian DOS. After all, hopping sites can be looked upon as traps, depending on their depth, so it is hard to distinguish between trapped and mobile states in a disordered system – which makes modelling difficult.

If we assume that transport is trap-free but follows a Poole-Frenkel like dependence on the electric field {6.4}, the resulting steady-state current density as a function of applied voltage is numerically given by:

$$J(V) = \frac{9}{8}\varepsilon_r \varepsilon_0 \mu_0 \exp\left(0.89\left(\frac{V}{E_0 d}\right)^{1/2}\right)\frac{V^2}{d^3} \qquad \textbf{\{6.3\}}$$

This allows for the observed square-root dependence of the mobility with electric field, though is only applicable if the injecting contact is Ohmic, as if this is not the case the current can be influenced by the properties of the electrode and not those of the bulk material.[10] From {6.3.} we can see this criterion is fulfilled if the correct thickness dependency is observed, which is how one can distinguish between SCLC and injected limited currents if the voltage dependencies are similar. The above

model can be fitted to find the parameters μ_0 and E_0, which can be further substituted into:

$$\mu = \mu_0 \exp\left(\sqrt{\frac{E}{E_0}}\right) \quad \{6.4\}$$

to gain an estimate of how the mobility varies with electric field, so as to contrast it with TOF results. However, as we have just discussed, it should be remembered that V/d is only a measure of the average electric field of the diode, though this should be sufficient to make comparisons.

6.3. Room temperature mobility measurements

This Chapter is concerned with the properties of hole-transporting dioctylfluorene-triarylamine conjugated copolymers. The arylamine donor functionality leads to a decrease in the ionisation potential with respect to polyfluorene (PFO – 5.8eV), improving hole injection and the ohmicity of the contact with respect to gold or ITO/PEDOT: PSS. Thus, the ionisation potential of the polymer is reduced to 5.09eV and 4.98eV for PFB and PFMO, respectively.[11] In addition to this, the film structure is expected to be more amorphous as the aromatic rings can rotate more freely (the dioctylfluorene structure of PFO is rigid), allowing more degrees of freedom. Differential scanning calorimetry (DSC) results for these materials are ambiguous. Only slight changes in the heat capacity indicate that the glass transition temperature T_G for PFB is ~ 140°C, as shown in Fig.6.5. The amorphous nature of the films was also confirmed by no observable difference to the mobility or device characteristics with heat treatment, once the solvent had fully evaporated. Any mobility differences due to anisotropy can thus be neglected.

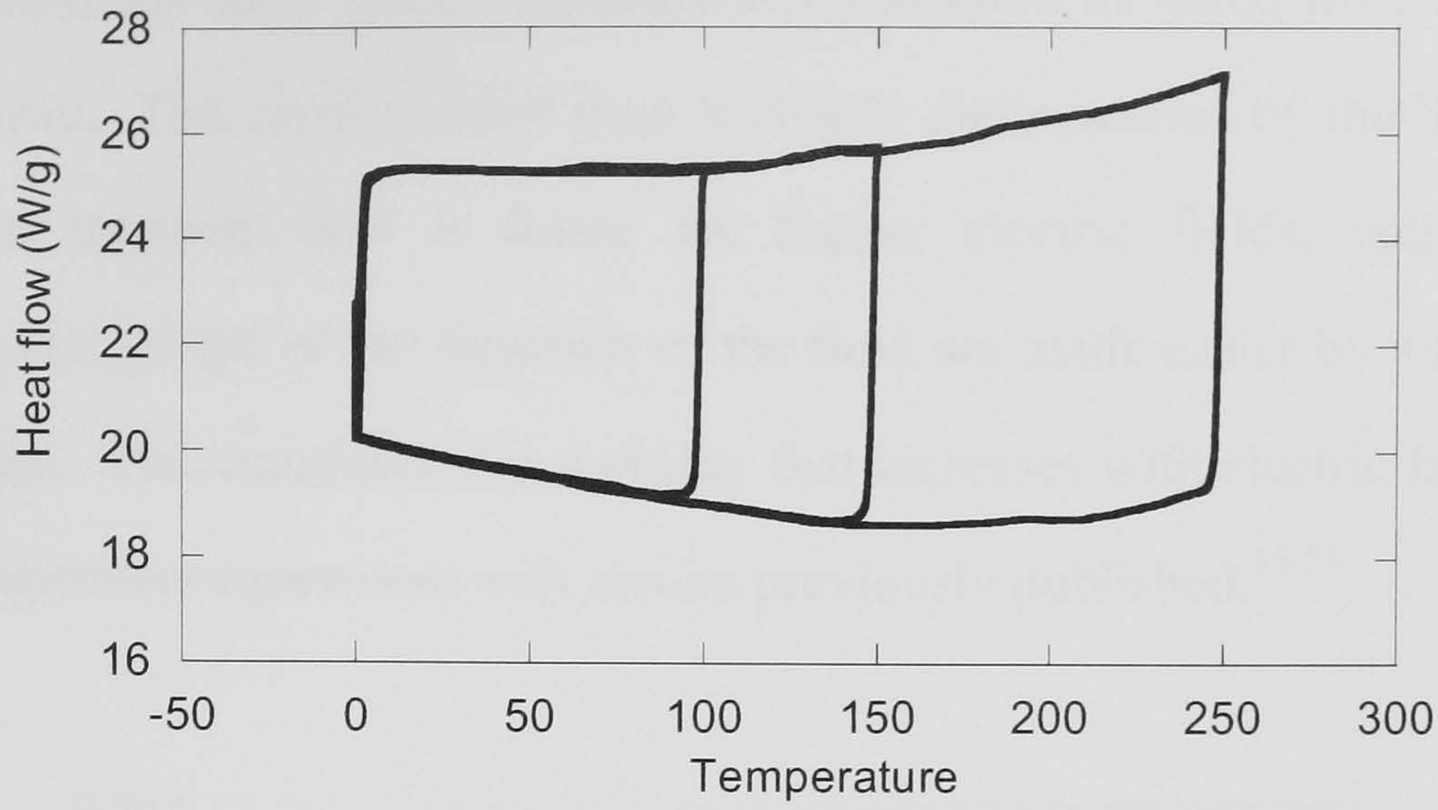


Figure.6.5. Differential scanning calorimetry scan of PFB showing the consecutive first, second and third heatings at a ramp rate of 10°C/min.

6.3.1. Bulk mobility measurements of amorphous materials

Time of flight measurements were the main method used to provide an estimate of the bulk mobility. Fig.6.6 shows typical room temperature hole transients for PFB at different field strengths.

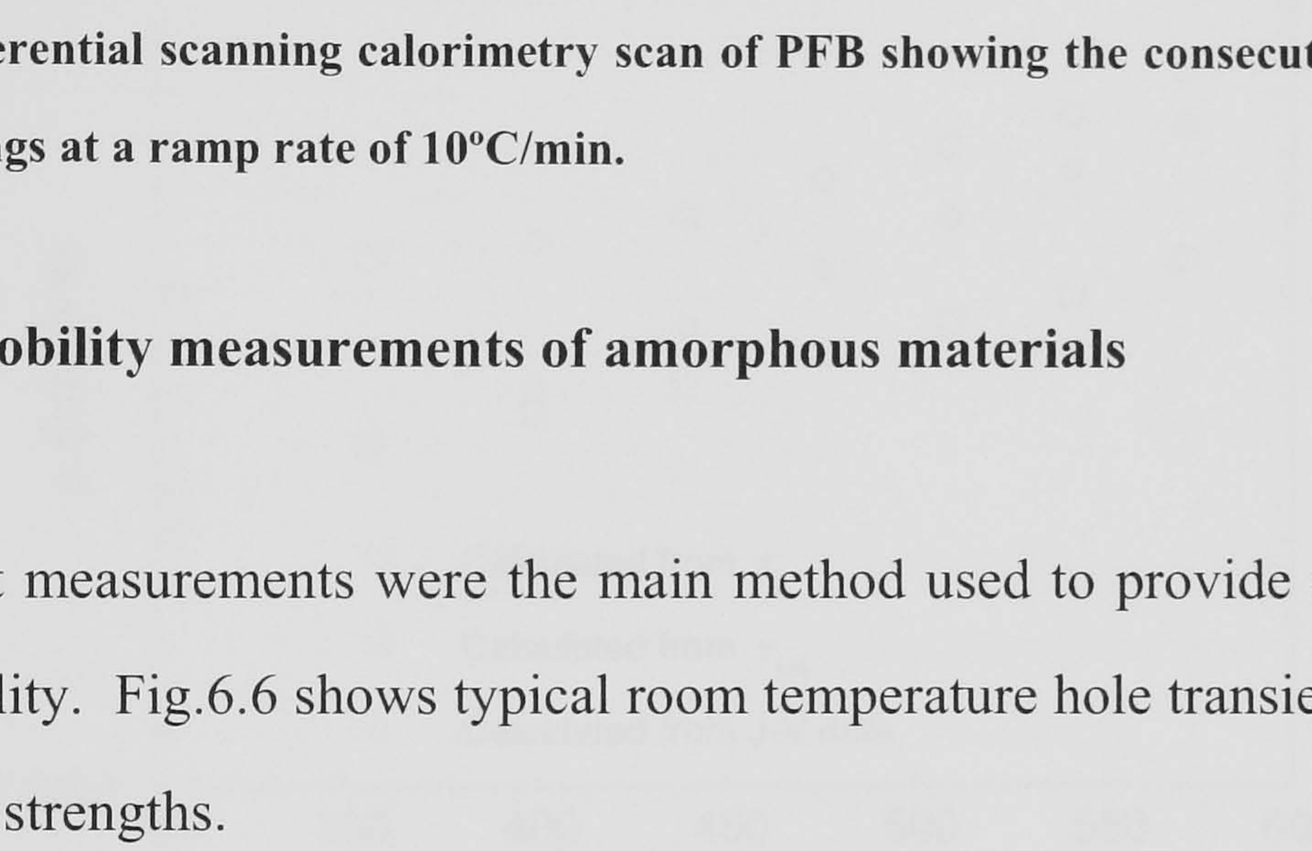


Figure.6.6. Non-dispersive hole transients for PFB at 3 different field strengths. The transit time can be taken at τ_0 or $\tau_{1/2}$, the former representing the time taken for the fastest carriers to traverse the film and the latter the time it takes for the current to drop to half of its initial value. The film thickness is 1.6μm.

The hole transients show good non-dispersive transport, as noted from the constant current plateau. The carrier transit time is clearly distinguished by the 'knee' of the photocurrent transient and is faster for higher electric fields, confirming the assumption that jumps in the direction of the field are made easier by a reduction in barrier height. This translates to a mobility that increases with electric field. These data are in excellent agreement with results previously published.[11-13]

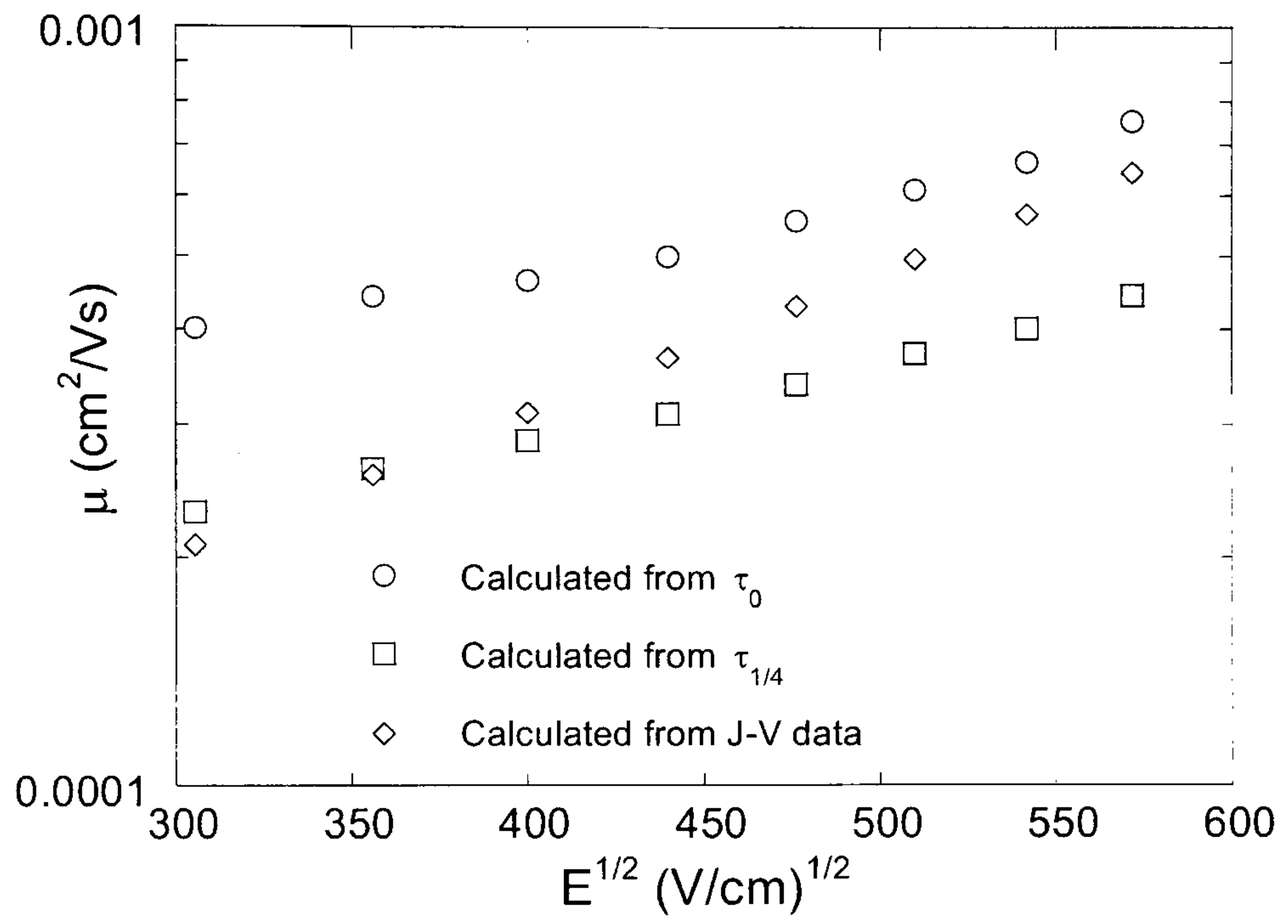


Figure.6.7. Comparison of the mobility derived from time of flight (μ_{TOF}) measurements and fitting of diode data (μ_{SCLC}), as a function of the square root of the electric field for PFB. The quarter-life of the transient $\tau_{1/4}$ represents a more average value of the bulk mobility.

The graph above shows a comparison of the mobility derived from time of flight (μ_{TOF}) measurements and fitting of diode data (μ_{SCLC}), as a function of the square root of the electric field. Diode and dark injection studies have already shown PFB to display no thickness dependence in the range d ~ 100nm to 1μm. This indicates good Ohmic contacts with respect to gold and ITO/PEDOT: PSS hole injecting contacts, as the condition for SCLC is met.[9] μ_{TOF} calculated from τ_0 is consistently higher than μ_{SCLC}, which is easily explainable. Physically, this relates to the time taken for the fastest carriers to traverse the sample, and taking the transit time to be

the point at which this value is halved, or even quartered, gives a more realistic average value.[2] Indeed, if $\tau_{1/4}$ is taken to the time for the carriers to traverse the sample, more of an average value, the mobility is in the same range as that derived for the diode. The bulk mobility consequently ranges from $6 \cdot 10^{-4} cm^2/Vs$ to $4 \cdot 10^{-4} cm^2/Vs$ for PFB, as measured at E = 0.26MV/cm. Again, this is good agreement with data in presented in the literature.[9,13]

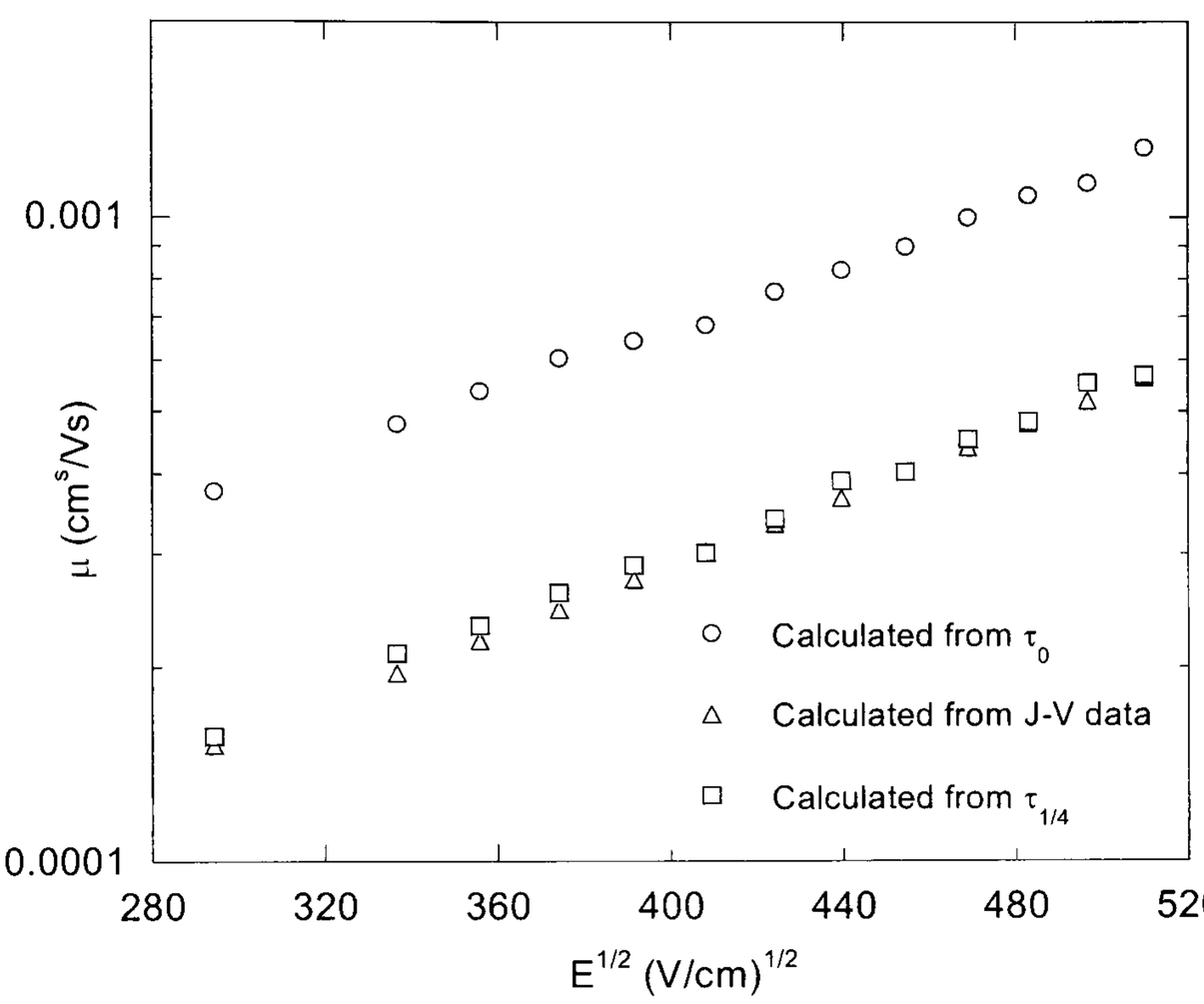


Figure.6.9. Comparison of the mobility derived from time of flight (μ_{TOF}) measurements and fitting of diode data (μ_{SCLC}), as a function of the square root of the electric field for PFMO. The quarter-life of the transient $\tau_{1/4}$ represents a more average value of the bulk mobility.

These results are further corroborated with comparison using poly (9,9-dioctylfluorene-co-bis-N,N'-(4-methoxyphenyl)-bis-N,N'-phenyl-1,4-phenylenediamine (PFMO), in which the butane end groups of PFB are replaced by methoxyl groups. PFMO is also an inherently amorphous material and has been shown to possess an ionisation potential of 4.8eV and display an Ohmic contact to gold and PEDOT: PSS electrodes.[9,12] As for PFB, μ_{TOF} represents the highest derived value of the bulk mobility for PFMO devices. In this case an even better match between diode and TOF devices is observed if $\tau_{1/4}$ is used to determine the mobility.

and values of $8.0 \cdot 10^{-4} cm^2/Vs$ and $3.9 \cdot 10^{-4} cm^2/Vs$ are calculated from τ_0 and $\tau_{1/4}$, respectively, at E = 0.26MV/cm. The mobility derived from the J-V characteristics of $3.8 \cdot 10^{-4} cm^2/Vs$ (at the same E-field strength) is very similar to that derived from $\tau_{1/4}$.

6.3.2. Field-effect transistor measurements of amorphous materials

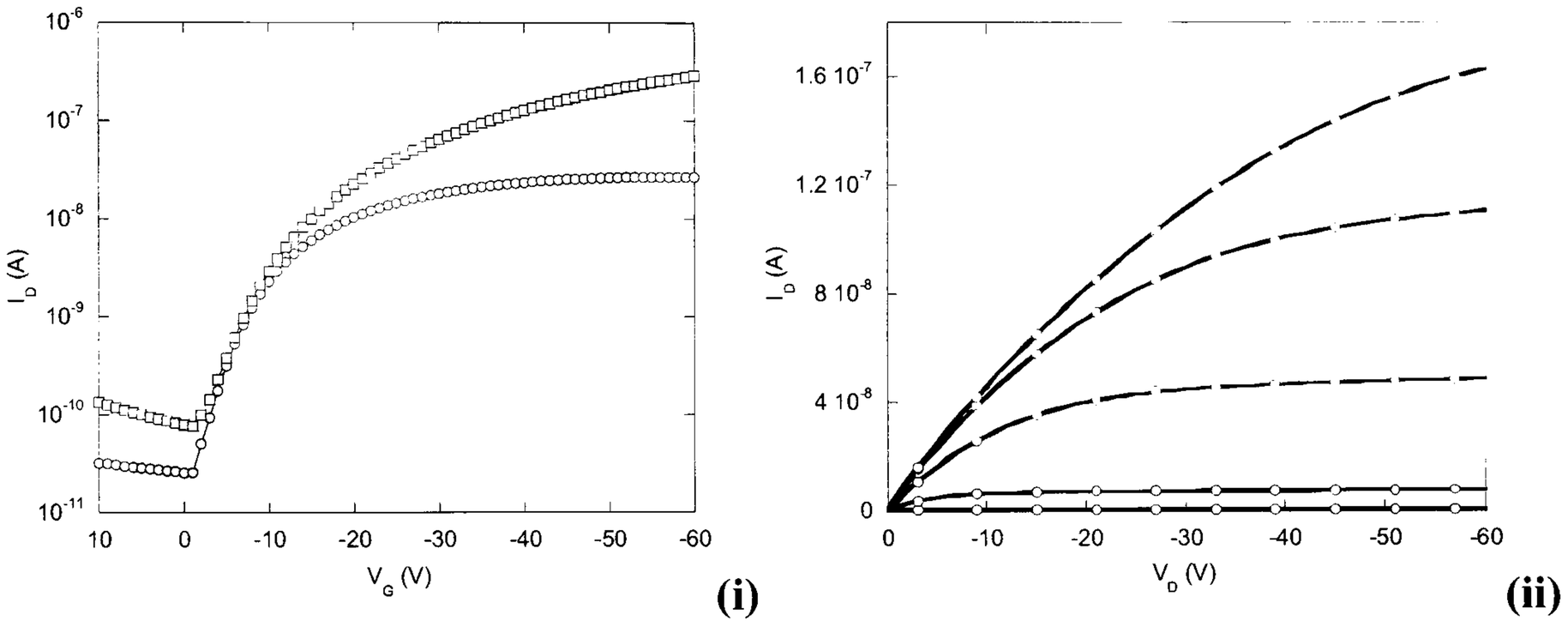


Figure.6.8. (i) Linear (V_D=-5V) and saturated (V_D=-60V) transfer scans of a PFB transistor with 10μm channel length and 1cm channel width. (ii) Output characteristics for the same transistor with V_G increased in -15V steps.

Fig.6.8 shows the transfer and output characteristics of a 10μm channel length PFB transistor. All samples were annealed at 100°C for 10minutes to remove all traces of solvent and water from the film. The linear and saturated mobilities were calculated using the customary equations to be $7.2 \cdot 10^{-6} cm^2/Vs$ and $1.3 \cdot 10^{-5} cm^2/Vs$, respectively. The output characteristics clearly indicate Ohmic contacts, which is inferred from the low ionisation potential (5.08eV) and prior studies concerning hole injection. Again, no non-linearity is evident from the linear region of the output characteristics and both the linear and saturation regimes are well defined.

The transfer and output characteristics of a PFMO transistor are shown in Fig.6.10. The linear and saturated field-effect mobilities were calculated using the customary equations to be $8.8 \cdot 10^{-5} cm^2/Vs$ and $1.4 \cdot 10^{-4} cm^2/Vs$, respectively. Again, these mobility values are lower than those derived from bulk characteristics.

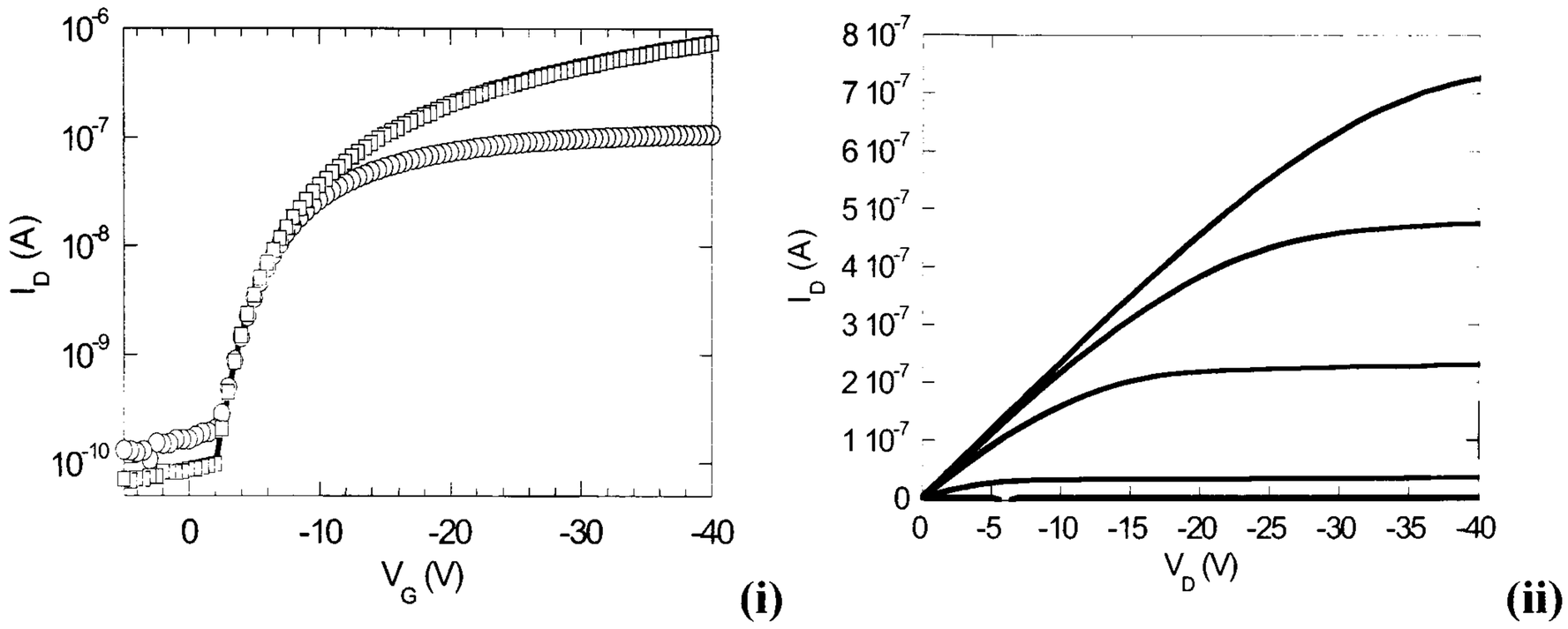


Figure.6.10. (i) Linear (V_D=-5V) and saturated (V_D=-40V) transfer scans of a PFMO transistor with 10μm channel length and 2cm channel width. (ii) Output characteristics for the same transistor with V_G increased in -10V steps.

Using no surface treatment gives an estimate of the lowest derivable field-effect mobility, and this case is illustrated. As we have seen, μ_{FET} can vary over several orders of magnitude by modifying the dielectric interface, improving injection from the contacts, and enhancing the molecular order via alignment or annealing techniques. The amorphous nature of these polymers suggests that promotion of self-organisation is unlikely to occur with silane treatments, though some local self-alignment may still be possible in the first couple of monolayers. Other benefits of silane treatments, such as a reduced concentration of trap sites and a more favourable surface energy could act to improve the mobility.

In fact, the mobility of the PFB transistors can be improved 14 times to $2.2 \cdot 10^{-4} cm^2/Vs$ simply by using an octyltrichlorosilane (OTS) interface layer, which is of a similar order to the average bulk mobility derived estimate. As there are no

problems with hole injection, and no obvious hysterisis and trapping effects that in themselves are detrimental to the mobility, this can be considered as the maximum mobility achievable in the device geometry used, as PFB is an amorphous material so further alignment techniques would not improve it further. The mobilities are much lower than those demonstrated thus far for the thiophene-based polymers, because PFB and PFMO films are more disordered and charge transport is thus not as efficient as in microcrystalline films.

6.3.3. Bulk and field-effect mobility measurements for F8T2

Let us compare these results with those of a liquid crystalline polyfluorene copolymer. Poly-9, 9' dioctyl-fluorene-co-bithophene (F8T2), is such a block copolymer, comprising of a polyfluorene unit and two thiophenes. F8T2 has been shown to possess a nematic liquid crystalline (LC) phase above 265°C and mobility anisotropy has been demonstrated in field-effect transistors by Sirringhaus et al.[14] They achieved this by aligning the active F8T2 layer both parallel to and perpendicularly to the channel, using a directionally rubbed polyimide alignment layer. The field-effect mobility was found to be 10^{-2}cm^2/Vs for parallel aligned film, and between 5-8 times lower for the film aligned perpendicular to the current flow in the channel.

Even without alignment procedures, we found dramatic differences in the mobility, ranging from $1.3 \cdot 10^{-5}$cm^2/Vs for an untreated, unannealed interface, to $9.3 \cdot 10^{-4}$ cm^2/Vs for annealed devices. This reflects the range of different structural phases which can occur in F8T2, as depending on the details of sample preparation, different amounts of crystalline, aggregate and amorphous material may be present. These crystalline, aggregate and liquid-crystalline phases can possess different electron affinities and ionisation potentials compared to the amorphous, glassy

phase. These more ordered phases can both reduce and enhance the mobility by acting as trapping sites at low concentrations, or by decreasing the interchain hopping distance, polaron relaxation energy, and energetic or positional disorder. But does the maximum observed field-effect mobility correspond to that derived from the bulk?

Time of flight measurements have not yet been reported for this material, which is surprising as it is a promising material for field-effect transistors. Fig.6.11 depicts the absorption spectrum of a thin film of F8T2 spun onto a Spectrosil B (transparent) disc. The absorption maximum is at a wavelength of 460nm, so the wavelength controllable Nd:YAG pumped type II BBO Optical Parameter Oscillator laser at Queen Mary was used, as the Nd:YAG laser at Imperial could only generate outputs of 355nm and 532nm (second and third harmonics).

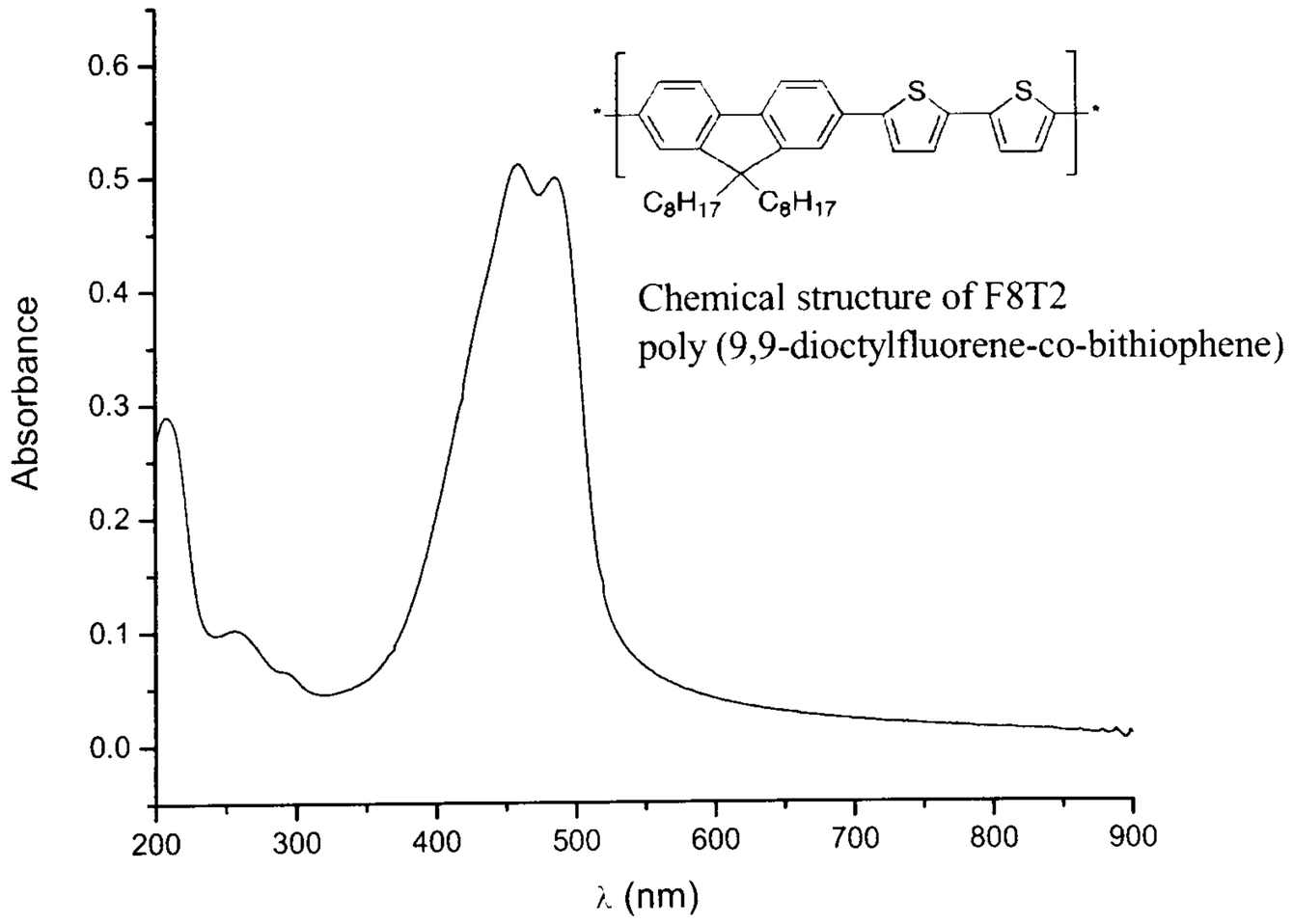


Figure.6.11. Absorption spectrum of a thin film of F8T2 spun onto a Spectrosil B disc. The inset displays the chemical structure of the material.

Fig.6.12 illustrates room temperature hole transients for as spun, un-annealed F8T2. The transients scale with field, with the transit time being quicker at higher E-fields.

The hole transients are much more dispersive than for PFB, and in this case the transit time is obtained from the asymptotes of a double logarithmic I-t plot, as shown in the inset. The sample thickness was 1.2μm, but the measurements had to be recorded at fields an order of magnitude lower than those used for PFB. Hole transport is significantly faster in F8T2 than in PFB, as at higher fields the transients were too fast to measure. Thicker films resulted in severely dispersive transients, such that transit times could not be extracted. As one of the main contributors to dispersivity is the presence of traps, we can assume that a greater proportion of trapping states exists in the thicker layer. In the trade off between the thickness of the film and the fields used, the sample with d~1.2μm gave the best compromise.

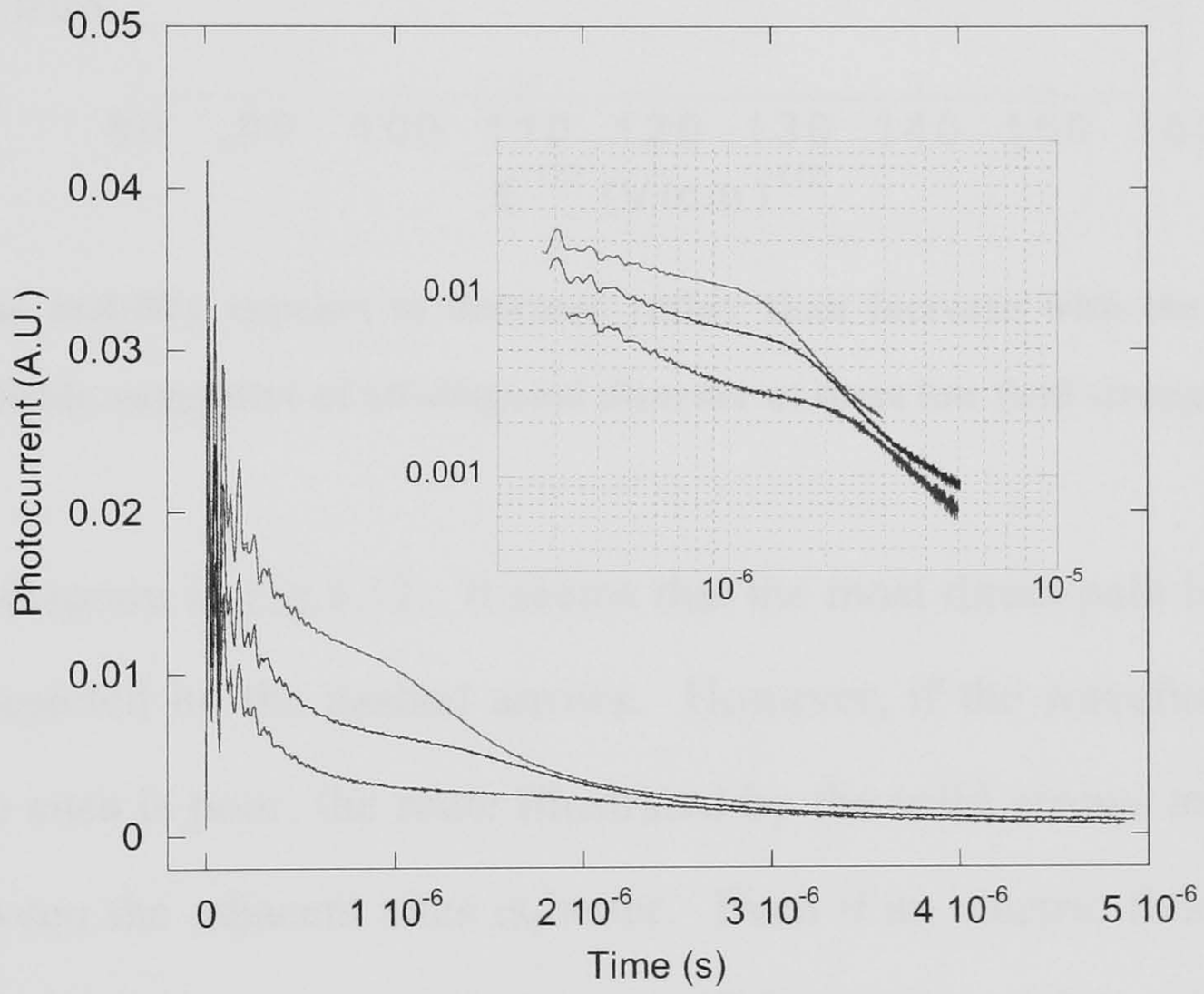


Figure.6.12. Hole transients for as-spun F8T2 at 3 different field strengths. The inset depicts the transients in log-I log-t format, in which the transit time can be determined from the intersection of the asymptotes. The film thickness in this case is 1.2μm.

The values of μ_{TOF} for F8T2 of $7 \cdot 10^{-3}$ at 10^4 V/cm are some the highest reported for an amorphous, non-aligned semiconducting polymer.[15,16] TOF transients on annealed samples were found to be even faster than those shown here, implying even better transport. The transit times increase with increasing electric field. However, if we

look at the mobility relation with the square root of the electric field, we observe that the mobility decreases rather than increases at higher fields, as can be seen in Fig.6.11 overleaf. This is often accounted for within the framework of the GDM, by positional or off-diagonal disorder.[2]

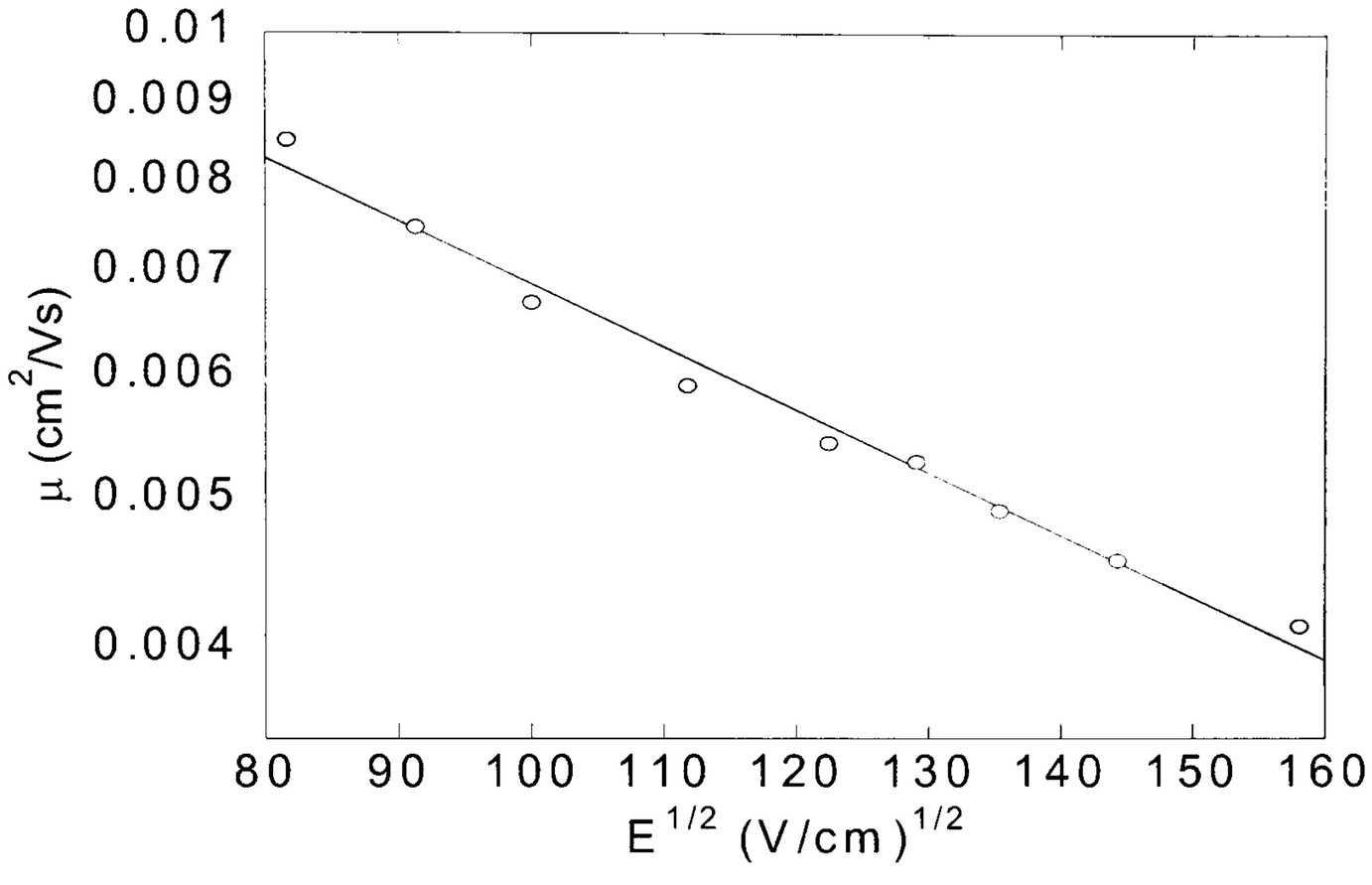


Figure.6.11. The mobility appears to decrease rather than increase with the square root of higher electric fields, suggestive of off-diagonal disorder at these low field strengths.

Consider the diagram in Fig.6.12. It seems that the most direct path between points A and B is depicted by the dashed arrows. However, if the wavefunction overlap between these sites is poor, the route illustrated by the solid arrows may be faster if coupling between the adjacent sites is better. Even if an electric field is applied in the direction of the direct pathway, it may still be preferential to take the indirect route at lower field strengths. This leads to the observed anomaly of the mobility decreasing (low E-fields) then increasing with escalating electric fields. Alternative explanations of a decreasing mobility at low E-fields have been attributed to delayed injection from the injection layer or delayed germinate pair dissociation in the bulk. Also, if the transit time is large it is more likely that a charge carrier can be captured by a low concentration of deep traps. This would also lower the effective mobility.

Off-diagonal disorder seems a reasonable explanation in our case, as our measurements are recorded at lower than usual field strengths.

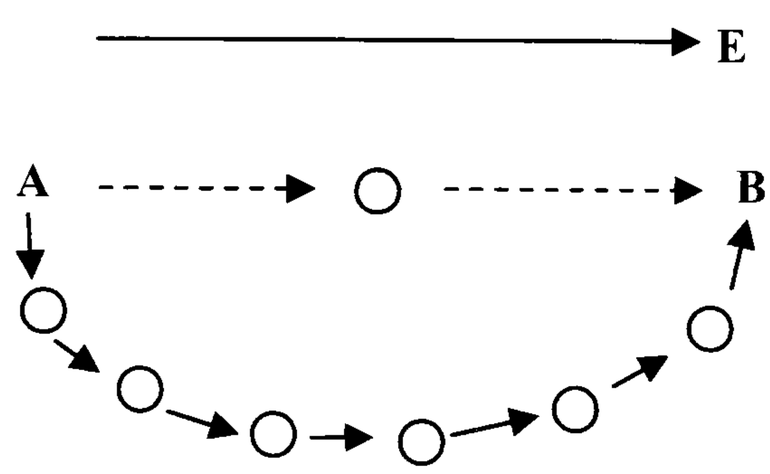


Figure.6.12. A charge carrier may follow a more indirect path (solid arrows) if the wavefunction overlap between sites is better. On application of a low electric field E, the indirect path can still dominate (resulting in a lower mobility) until larger field strengths eliminate these routes.

We still find that the top range of transistor mobilities is in keeping with the TOF results. Fig.6.13 illustrates the spread of μ_{FET} for amorphous films where the F8T2 has been annealed, but not aligned.

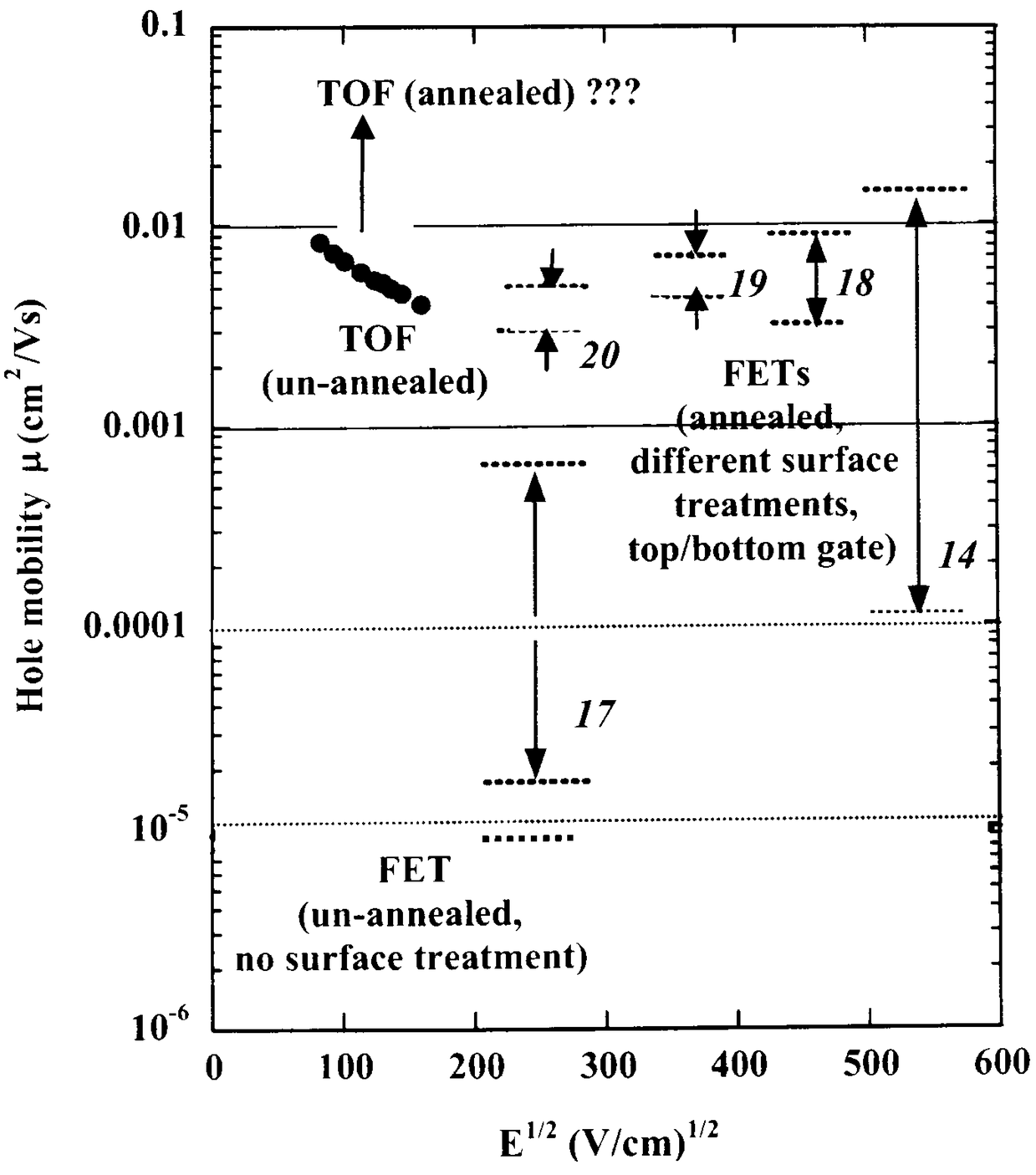


Figure.6.13. This figure illustrates the range of mobility values in this work, and the literature, for F8T2 transistors in comparison those derived from the unannealed TOF devices. The considerable range of mobilities is a result of different molecular weights, surface treatment, device configuration and annealing temperatures.

All values for the annealed devices show μ_{FET} values at or below μ_{TOF} for the un-annealed bulk film.[14,17-20] Given that preliminary measurements for μ_{TOF} of annealed bulk films indicate that the mobility is even higher, μ_{FET} is again less than μ_{TOF}.

6.3.4. Comparisons of the bulk and field-effect mobility

To summarise, we have seen that the bulk mobility can be derived from time of flight measurements. Time of flight gives mobilities an order of magnitude higher than SCLC measurements, though this is dependant on how one defines the transit time. If it is taken to be the time at the 'knee' when the photocurrent starts to drop off (τ_0) the maximum value is obtained, with the time taken for the photocurrent to fall to a half or quarter of the original value representing a more average value of the carriers mobility. If the mobility is calculated from $\tau_{1/4}$, it is similar to that derived from the SCLC regime. There is clearly a range of mobility values due to the dispersivity of these amorphous systems. We can thus take the upper and average limits of the mobility in the bulk to be as calculated from τ_0 (maximum) and from $\tau_{1/4}$ (average). Both TOF and SCLC measurement follow a Poole-Frenkel like relation with the electric field and values are consistent with those published in the literature.

Let us now concern ourselves with μ_{FET}. This is also an I-V fitting, though the equations used do not allow for a mobility variation with lateral field in the direction of charge transport. Tanase et al. reported a relationship between the charge density and mobility of SCLC diodes and field-effect transistors.[21] Comparative measurements of poly (3-hexyl thiophene) (P3HT) and a soluble poly (phenylene vinylene) derivative gave a bulk SCLC mobility lower than the FET mobility. They suggested that the high carrier densities at the FET interface filled deep sites 'permanently'. Charge carriers were therefore free to hop between shallower sites, and never having to spend time escaping from the deep sites gives a mobility which

is consequently carrier density dependant. This was proposed to be a universal model to explain charge transport in transistors and why the field-effect mobility should be greater than the bulk mobility.

Charge transport in a field-effect transistor occurs in a thin layer at the semiconductor-insulator interface. The charge density of this accumulation layer is found to vary exponentially with respect to increasing distance from the interface and μ_{FET} was determined as such. However, the mobility as calculated from the linear equation {1.5} correlates with that determined at a distance of 1nm from the interface, which in turn is an estimate of the magnitude of the accumulation layer depth - being only a few polymer chains wide. Thus {1.5} can serve as a good approximation for estimating the mobility.[21]

The results presented here indicate that the bulk mobility can be higher than the FET mobility, regardless of the charge density. Time of flight results show the highest mobilities, whilst having the lowest charge carrier densities. Integrating the area under the photocurrent transient and dividing by the device dimensions enables the charge density per cubic cm to be estimated. At a field of $1 \cdot 10^5$V/cm, the charge density per unit volume is estimated at 10^{14}. The charge density ρ in a transistor can also be simply estimated by using calculating the surface charge density ρ_s and assuming that the majority of charge is contained in the first monolayer. For our transistors, this corresponds to a ρ of 10^{19}. The situation is more complex and can not be explained solely by the charge density relationship, as our results clearly indicate that higher mobilities do not necessarily correlate to higher charge densities in different device configurations.

We have seen that the mobility of a transistor can be dependent on charge density. μ_{FET} can also depend on the surface energy of the interface and the molecular order

in the film. The structure of diodes and TOF devices are similar, with transport occurring through the bulk of the film. FET transport is along the interface, a couple of polymer chains deep, which is more likely to be influenced by any disruptions or even different polarisation reactions and disorder due to the 2-dimensionality of the system. For example, a chain at the interface will not experience the same level of polarisation interactions from the surrounding medium as a chain in the bulk, so this could shift the polaron levels into the energy gap to act as trap states. All these factors would reduce the field-effect mobility.

We also have to consider the ranges over which mobility values are spread. The highest obtained mobilities for PFB transistors were $1.1 \cdot 10^{-4} cm^2/Vs$ and $2.2 \cdot 10^{-4} cm^2/Vs$, 14 and 17 times higher than those extracted for transistors with untreated interfaces. In this case the substrates were treated with OTS before film deposition. As PFB is an amorphous material, this vast improvement could be due to a surface energy effect or better packing of the conjugated backbone as the side alkyl chains interlock with those of the silanes at the interface. There is not such a wide spread of values compared to more crystalline polymers as self-ordering morphology related effects can to an extent be discounted.

Maybe what we should be considering are mobility ranges for material systems. For PFB, this varies from the mobility in an untreated transistor of $7.2 \cdot 10^{-6} cm^2/Vs$ to $6 \cdot 10^{-4} cm^2/Vs$, as derived from τ_0 in a TOF device. The mobility of the OTS treated transistor is approaching this value, and is only two times less than the average bulk mobility. It seems that derivation of the mobility from TOF measurements presents the maximum mobility of the material (remember charge carriers are photogenerated so there are no injection problems), and limiting factors such as contact resistance and increased disorder or traps at the interface have to be overcome to achieve this in a transistor structure. The same principles apply to PFMO.

In the case of F8T2, the mobility ranges from the bulk estimate of $7 \cdot 10^{-3}$ at 10^4V/cm to $1.3 \cdot 10^{-5}$cm^2/Vs for unannealed films, and $9.3 \cdot 10^{-4}$cm^2/Vs for annealed films. Preliminary TOF measurements show the transport in annealed films to be even faster, but more measurements are needed to extract reliable data. Literature values show a wide range of μ_{FET} values, depending on surface treatments, annealing conditions, device configuration, and even the molecular weight. The morphology of these films, especially at the interface, affects the transistor performance significantly. Variation of the field-effect mobility with molecular weight has previously been attributed to varying degrees of crystallite formation, resulting in carrier trapping at the grain boundaries. The large mobility deviation demonstrates that crystalline polymers are more sensitive to preparation conditions, as these can affect the proportions of crystalline and amorphous regions in the film. Polythiophene is also known to possess different morphologies of crystalline and amorphous phases, and the considerable spread of μ_{FET} values in the literature supports this further.[23] However, PFB and PFMO are amorphous materials that are not expected to be affected by such phenomena and the smaller variation in device performance reflects this.

6.4. Temperature dependence of the mobility

Temperature measurements can give us an indication of the activation energy and amount of disorder present in a material. The dependence of the mobility on the temperature is not yet satisfactorily described by a single model. At higher temperatures ($T > 100$K) the charge carrier mobility will tend to increase with increasing temperature, indicative of a polaron hopping regime. Such thermally activated processes tend to follow Arrhenius-like behaviour, which predicts a linear relationship of $\ln|\mu|$ with T^{-1}. However, a mobility increase with decreasing temperature has been observed at low temperatures ($T < 100$K) for some small

molecules, suggesting that at these lower temperatures transport switches to a more band-like regime. Band-like transport in small molecules has been attributed to the presence of highly crystalline regions (grains), with the grain boundaries limiting the charge transport. This effect has not yet been observed for conjugated polymer systems. Polymer systems are generally more disordered, but the limited temperature range that experimental measurements can be carried out at makes differentiation between transport models ambiguous. Often the precise temperature dependence of the mobility can only be distinguished at very low temperatures, which are difficult to measure.

6.4.1. The Bässler (GDM) and Holstein (Arrhenius) Models

An Arrhenius model predicts a linear relation of $\ln|\mu|$ with T^{-1}. This enables the activation energy E_A to be extracted from the gradient of:

$$\mu(T) = \mu_0 \exp(-(E_A/kT)) \qquad \{6.5\}$$

as well as μ_0 from the y-intercept. This mobility relation often holds true for high temperatures, but the linear fits usually deviate at temperatures below 200K.[8]

Holstein assumed that the transport of charge carriers in organic materials derives from small polaron hopping, the mobility of which can also be described by an Arrhenius-like dependence. In this case E_A can be approximated as $E_B/2$, half of the polaron binding energy.[24] E_B is partially determined by polarisation interactions with the surrounding environment, so would be affected by variations in chain packing or by being close to the dielectric-semiconductor interface. If these interactions dominate the effect of energetic disorder, one could expect the temperature dependence of the mobility should follow {6.5}. A similar situation might also be

expected if a single energy deep trap or interface state controlled the charge transport. In this case the trap depth (or trap energy) E_T would be analogous to E_A.

Bassler et al. derived an alternative temperature model specifically for disordered organic semiconductors.[2] This assumes that the energy of each site is distributed in accordance with Gaussian statistics and is so named the Gaussian Disorder Model (GDM). It does not take into account any correlation between site energies and each jump is supposedly unrelated to its predecessor. Polaronic effects are also neglected. As mentioned in the previous Chapter, the GDM predicts a linear relationship between $\ln|\mu|$ and T^{-2}, as well as a Poole-Frenkel like relationship with the electric field. As the zero-field mobility $\mu_{(E = 0)}$ is found by taking the intercept at $E^{1/2} = 0$ from a plot of μ against $E^{1/2}$, for $E = 0$, Equation {5.3} reduces to:

$$\mu_{(E=0,T)} = \mu_0 \exp(-(2\sigma/3kT)^2) \qquad \{6.6\}$$

μ_0 can thus be derived from the intercept of a plot of $\ln|\mu_{(E = 0)}|$ against T^{-2} and the energetic disorder, σ, extracted from the slope. This model has also been shown to fit experimental data for higher temperature ranges well, and could dominate the Arrhenius model if the system was governed by energetic disorder.

6.4.2. Temperature dependence of the mobility for PFB

Fig.6.14 shows the compilation of hole mobilities deduced from time of flight data (τ_0) at different field strengths. This field dependence fits in well with the expected Poole-Frenkel like behaviour. Unfortunately, the device structure of the field-effect transistors did not allow for measurements at low temperatures as they could not be

used in conjunction with the cryostat. The system was heated rather than cooled, and the temperature range studied was typically limited to between 300K and 400K.

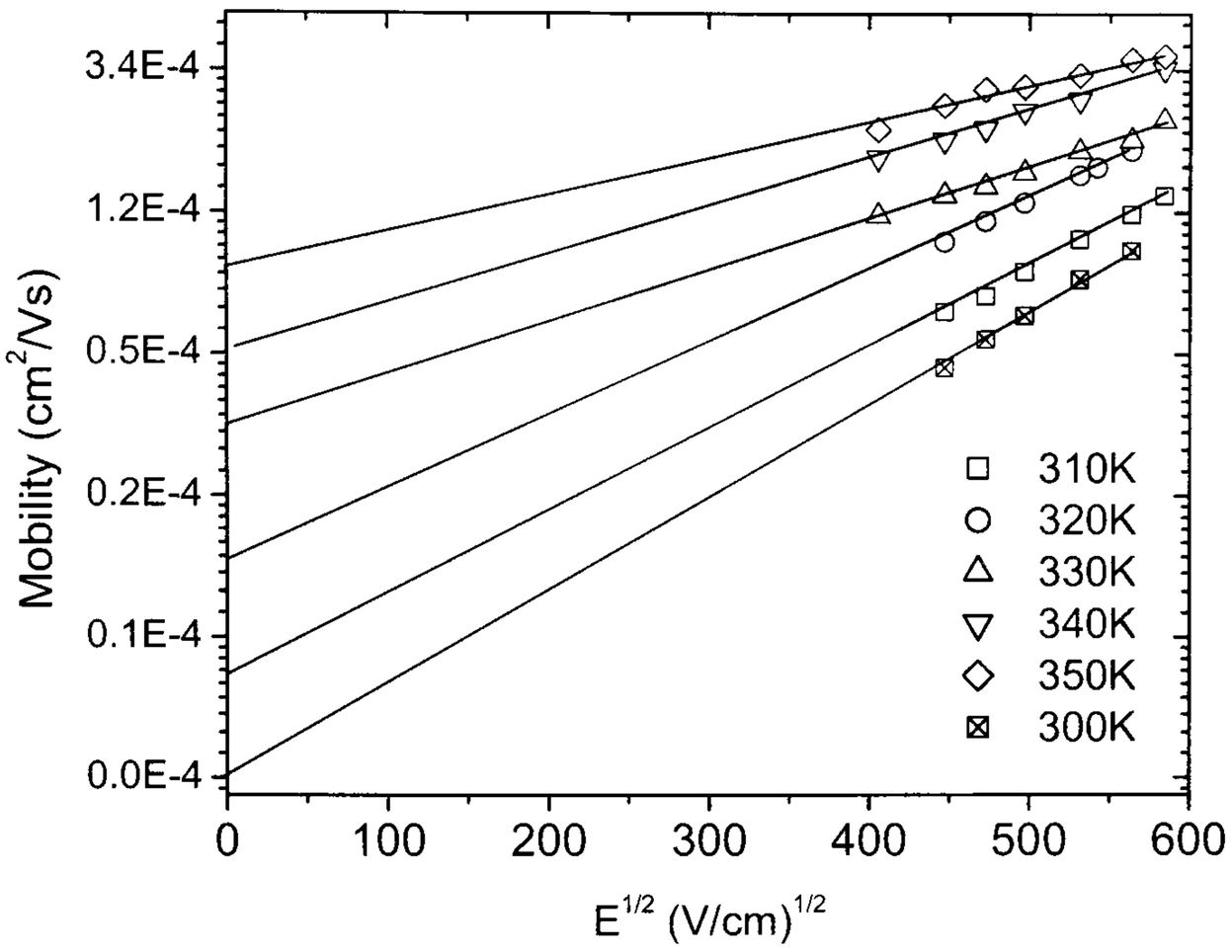


Figure.6.14. Poole-Frenkel plot of time-of-flight hole mobilities for a 1.6μm thick PFB film at increasing temperatures.

Low temperature measurements (150K) were also carried out for PFB and the fit parameters were found to correspond well to those extracted from the data collected in the higher temperature regime. A transition from non-dispersive to dispersive transport often occurs at low temperatures limiting the measurement range. In this case, an anomaly appears at higher temperatures. Instead of a constant current plateau, the photocurrent rises to the point where it corresponds to the 'knee' and then drops. This effect is similar to that of excess space charge generated in the sample, but this was not responsible as reducing the power of the laser or increasing the neutral density (thus attenuation of the laser) did not affect it. Additionally, when the charge generated was calculated by integrating the area under the transient it was found to be 7% of the total charge, which is still acceptable. This cusp was also observed in[25] and as a consequence the temperature was only measured up to 350K for TOF measurements.

The FET characteristics were also measured with temperature for PFB (These data are not shown). The FET mobility μ_{FET} was then derived from the transfer characteristics using {1.4} and {1.5} as PFB does not exhibit a significant variation of mobility with gate bias (charge density). Given that the channel length for the transistors used in this work was 10μm and that V_{DS} used was -5V or -60V, the average field strength between the source and drain is between one to two orders of magnitude smaller than the field range used for TOF measurements. The field responsible for the movement of holes from the source to the drain is the bias applied between the source and the drain, V_{DS}. To compare the results we assume that:

$$\mu_{FET(T)} = \mu_{(E=0,T)} \qquad \{6.7\}$$

so the calculated mobilities are plotted directly against T^{-1} or T^{-2}.

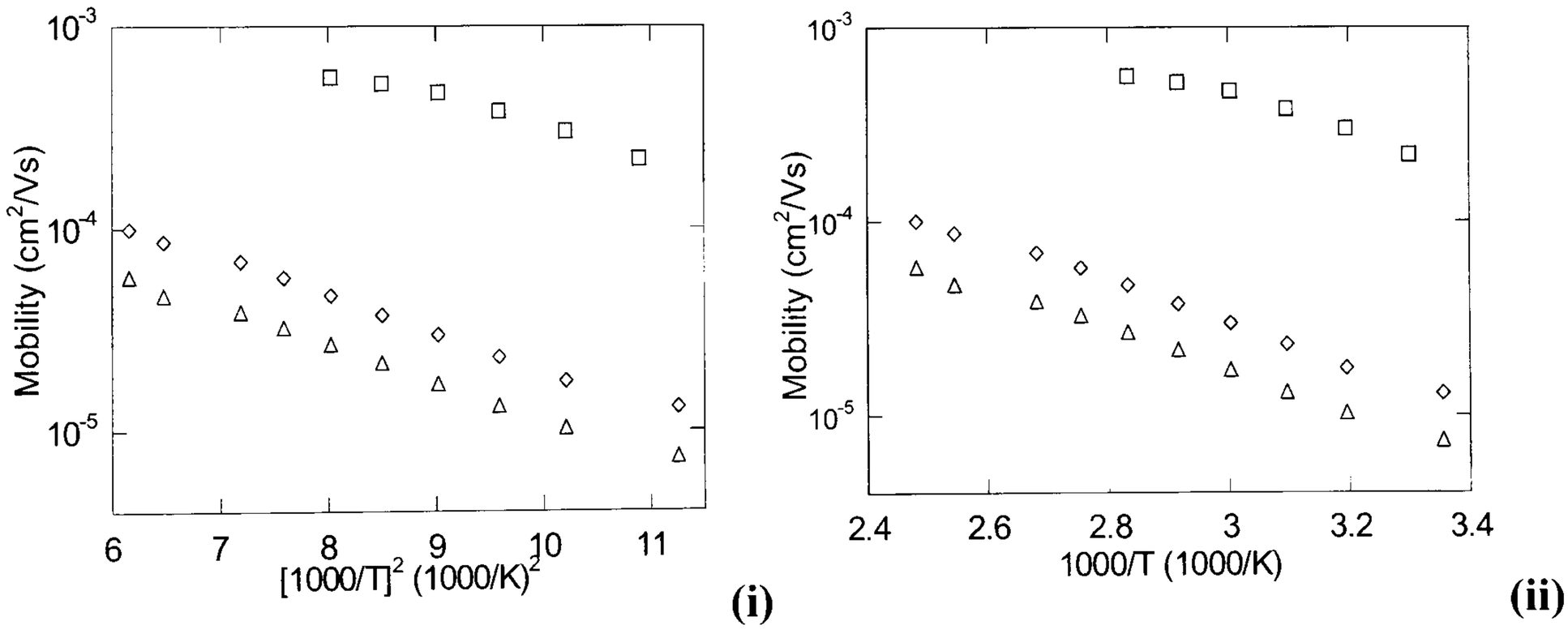


Figure.6.15. Temperature dependence of TOF (squares), and transistor derived linear (triangles) and saturated (diamonds) mobilities following (i) the GDM (ii) an Arrhenius relationship for PFB.

Device	Mobility	Arrhenius Model		GDM	
		μ_0	E_A	μ_0	σ
TOF	$6 \cdot 10^{-4}$	0.185	200	0.016	0.08
FET (Lin)	$7.6 \cdot 10^{-6}$	0.027	210	7.1×10^{-4}	0.089
FET (Sat)	$1.3 \cdot 10^{-5}$	0.042	215	1.3×10^{-3}	0.087

Figure.6.16. Table comparing the GDM and Arrhenius model parameters for PFB devices.

The table in Fig.6.16 lists the values of σ, μ_0 and E_a derived from the data shown in Fig.6.15. Unfortunately, our limited temperature range can not distinguish whether the Bässler or Holstein model is a better fit. Veres et al. also looked at the temperature activation of amorphous triarylamines and found the quadratic temperature dependence to describe the fitting better.[16] This makes sense, as the GDM was designed for amorphous disordered systems. Following similar reasoning, Majewski et al. also compared the models for the small molecule pentacene and regioregular polythiophene. In this case the Holstein model was found to fit the data better.[26] This is not surprising as pentacene is crystalline and the thin film structure of RR P3HT consists of microcrystalline regions embedded in an amorphous matrix.[27] The crystallinity of this material concurs with the concept of an activation energy, with transport best described by the multiple trapping and release model. The better fit of the mobility with an inverse temperature relation is not necessarily an indication of the polaron regime, but what it does indicate is that Bässlers model may not be satisfactorily applied to crystalline systems. Veres at al. also compared the parameters derived from TOF and transistor measurements.[16] They also found μ_{TOF} to represent the maximum mobility, and demonstrated that the transistor mobility was improved by using low dielectric insulators. They attributed

this to a reduction of polarisation interactions at the interface, leading to reduced energetic disorder.

The values of σ for the TOF results of 0.08 is typical of a disordered organic semiconductor, and is in agreement with literature data measured over a low temperature range.[9] The FET values of σ are slightly higher than those for TOF suggesting that energetic disorder is increased at the transistor interface. TOF samples are typically over 1μm thick, and solutions have to be made suitably viscous to achieve this. Perhaps this viscosity and reduction of solvent may also lead to improved energetic disorder in the film. Transistors and TOF samples were also fabricated on different substrates (Glass and n^{++}-Si/SiO_2). The surface energies were similar before deposition, though there may be differences in trap states.

What about some change in the polaron binding energy at the interface due to polarisation interactions with the insulator? What about some new deep trap state or deep interface state at the insulator-semiconductor boundary? The values of E_A from the TOF results are slightly less, though still similar, to those derived from transistors. The OTS treated PFB transistor had a significantly increased mobility and such surface treatments are known to reduce the energetic disorder and concentration of interface trap states present at the interface. It also significantly reduces the activation energy. This suggests that there are interface states present in the case of the PFB transistor that are unlikely to affect the bulk material properties.

Let us now consider μ_0. The FET value of μ_0 is one order of magnitude smaller than the TOF value and μ_{FET} is about one order of magnitude smaller than μ_{TOF}. Lower values are derived from the GDM, though the same patterns are followed. μ_0 is related to the average interchain hopping distance *a*. The average intersite hopping distance experienced by a charge carrier at the insulator-semiconductor interface is

larger than in the bulk material. This is most likely due to chain packing at the interface being poorer than in the bulk material, also a result of increased energetic disorder. The data given in Appendix I for F8T2 temperature comparisons of the bulk and field-effect mobility also corroborate this.[17] This is further supported by FET mobility measurements of P3HT devices which show that a two order of magnitude increase in μ_{FET} can be related to an improvement in interchain packing and a decrease in the hopping distance perpendicular to the interface.[23]

The table in Fig.6.17 below, compares temperature FET data for the three microcrystalline thiophene based polymers with PFB.

Material	**Mobility**	**Arrhenius Model**		**Gaussian**	
		μ_0	**E_A**	**μ_0**	**σ**
PFB	$1.3 \cdot 10^{-5}$	0.042	210	1.3×10^{-3}	0.087
P3HT	$3.4 \cdot 10^{-2}$	0.38	20	0.027	0.025
Ant-pBTTT	$1.5 \cdot 10^{-1}$	2.30	65	0.69	0.044
Syn-pBTTT	$1.8 \cdot 10^{-2}$	0.15	103	0.014	0.057

Figure.6.17. Table comparing the GDM and Arrhenius model parameters for amorphous PFB and self-ordering polycrystalline thiophene based transistors.

The mobility is at least three orders of magnitude higher for the microcrystalline polymer systems. This increased order also reflects the decreased energetic disorder parameter and activation energy. There appears to be a definite correlation between all of these parameters and the mobility extracted from the transistor. Ant-pBTTT is the highest mobility material, and μ_0 reflects this. μ_0 decreases in accordance with the observed mobility decrease. The activation energy and energetic disorder parameter are smaller for P3HT, though this could just be due to experimental error.

Majewski et al. showed a wide range of values for the activation energy in the literature for P3HT, ranging from 84meV to 115meV, depending on the surface treatment or regioregularity.[26] The energetic disorder parameter also varied from 45.5meV to 54meV. However, this related to increased energetic disorder when the Al_2O_3 dielectric was treated with OTS, which is contradictory to our findings for OTS on SiO_2. They put forward an explanation that the GDM was unsuitable for polycrystalline systems, though their mobility values for the 98.5% RR material were very low at $2.8 \cdot 10^{-4} cm^2/Vs$, increasing to $5 \cdot 10^{-3} cm^2/Vs$ for the OTS treated interface. They also noted that the activation energy increased for the OTS treated devices.

What is certain for our data is that E_A and σ are significantly smaller for the polycrystalline systems than for amorphous PFB. μ_0 follows the closest relation to the derived mobility values, suggesting that the interchain hopping distance is a crucial factor in determining the device mobility.

6.5. Conclusions and further work

The mobility derived from time of flight measurements are an order of magnitude higher than SCLC measurements if the transit time is calculated from τ_0, though if the mobility is calculated from $\tau_{1/4}$ it is similar to that derived from the SCLC regime. Our results clearly indicate that higher mobilities do not necessarily correlate to higher charge densities in the different device configurations as the bulk mobility was found to be higher than the field-effect mobility. Mobilities approaching that of the bulk can be achieved in transistors by using silane treatments to reduce the energetic disorder and traps at the interface, or by annealing - if the polymer has crystalline properties.

Temperature measurements indicated that the rate-limiting step which determines the charge transport is thermally-assisted tunnelling between chains. This is determined by a range of factors. The tunnelling rate varies exponentially with the interchain hopping distance *a*, as has been noted in molecularly doped polymers. The mobility is also dependent on the level of energetic and spatial disorder. The former is due to variations in chain conformation and packing giving each chain site a different energy. The latter is due to variations in interchain distance and orientation. A chain at the polymer interface experiences more energetic disorder than one in the bulk of the film. This, in combination with an increased interchain hopping distance, limits the mobility of transistors and is responsible for the difference between the bulk and field-effect mobility.

Preliminary temperature experiments, similar to those carried out for PFB, were done for F8T2 and PFMO systems and their data is given in Appendix I. More experimental work needs to be carried out on these materials as discrepancies were found between batches. The batch of PFMO used for preliminary experiments gave significantly different results to those from a different batch. The transistor set up needs to be modified so temperature measurements can be carried out to low temperatures, in order to get more reliable results. Attempts were made to investigate the time of flight of aligned F8T2 films were unsuccessful. More work needs to be done on TOF for F8T2, concentrating on the thickness dependency and effect of the molecular weight.

References

1. C. Kittel, *Introduction to Solid State Physics*, 7th Edition, John Wiley & Sons (1996)

2. H. Bässler, *Phys. Stat. Sol.* (b) **175**, 15 (1993)

3. N. Karl, *Syn. Met.* **133** 649-657 (2003)

4. I. H. Campbell & D. L. Smith, *Physics of Organic Electronic Devices,* in Solid State Physics **55,** Academic Press (2001)

5. S. Scheinert and W. Schliefke, *Syn. Met.* **139** 501-509 (2003)

6. S. Grecu, M. Bronner, A. Opitz, W. Brütting, *Syn. Met.* **146** 359-363 (2004)

7. C. Tanase, E. J. Meijer, P. W. M. Blom, D. M de Leeuw, *Phys. Rev. Lett.* **91** 21 (2003)

8. M. Borsenberger and D. S. Weiss, *Organic Photoreceptors for Xerography,* M. Dekker Ltd. (1998).

9. D. Poplavskyy, *PhD Thesis* (2003)

10. T. H. Richardson, *Functional Organic and Polymeric Materials: Molecular Functionality – Macroscopic Reality*, John Wiley & Sons (2000)

11. A. J. Campbell, D. D. C. Bradley, and H. Antoniadis, *J. Appl. Phys.* **89** 3343-3351 (2001)

12. M. Redecker, D. D. C. Bradley, M. Inbasekaran, W. W. Wu and E. P. Woo, *Adv. Mater.* **11** 241-246 (1999)

13. D. Poplavskyy, T. Kreouzis, A. J. Campbell, J. Nelson and D.D.C. Bradley, *Mat. Res. Soc. Symp. Proc.* **725** 1.4.1-1.4.11 (2002)

14. H. Sirringhaus, R. J. Wilson, R. H. Friend, M. Inbasekaran, W. Wu, E. P. Woo, M. Grell, and D. D. C. Bradley, *Appl. Phys. Lett.* **77** 3 (2000)

15. M. Redecker, D. D. C. Bradley, M. Inbasekaran and E. P. Woo, *Appl. Phys. Lett.* **74**, 1400 (1999)

16. J. Veres, S. D. Ogier, S. W. Leeming, D. C. Cupertino, S. M. Khaffaf, *Adv. Funct. Mater.* **13** 199 (2003)

17. R. Rawcliffe, D.D.C. Bradley and A. J. Campbell, *Proc. SPIE* **5217**, 25-34 (2003)

18. D. J. Brennan et al, *Proc. SPIE* **5217** 1-6 (2003)

19. C. J. Newsome et al, *Proc. SPIE* **5217** 16-23 (2003)

20. P. H. Townsend et al, *International PolyScene-Workshop on Polymer Electronics proceedings Munich* 9-16 (2002)

21. C. Tanase, E. J. Meijer, P. W. M. Blom, D. M. de Leeuw, *Organic Electronics* **4** 33-37 (2003)

22. W. Brütting, *Physics of Organic Semiconductors,* VCH Verlagsgesellschaft Germany (2005)

23. H. Sirringhaus et al, *Synth. Met.* **111** 129-132 (2000)

24. G. Horowitz, *Adv. Mater.* **10** 5 (1998)

25. D. Hertel, H. Bässler, U Scherf, H. H. Hörhold, *J. Chem. Phys.* **110** 18 (1999)

26. L. A. Majewski, R. Schroeder, M. Grell, P. A. Glarvey, M. L Turner, *J. Appl. Phys.* **96** 10 (2004)

27. H. Sirringhaus, P.J. Brown, R. H. Friend, M. M. Nielsen, K. Bechgaard, B. M. W. Langeveld-Voss, A. J. H. Spiering, R. A. J. Janssen, E. W. Meijer, P. Herwig, and D. M. de Leeuw, *Nature* **401** 685-688 (1999)

Chapter 7

Conclusions and further work

This chapter presents the key points of this thesis, Chapter by Chapter, along with ideas for further work necessary to corroborate or extend the findings.

There are many unanswered questions concerning the operation of polymer field-effect transistors, and this research aims to further our understanding of these devices. The work presented in this thesis was predominantly concerned with improving device performance using novel, high mobility, solution-processible thiophene based conjugated polymers as the active layer. Not only were some of the highest mobilities for conjugated polymer field-effect transistors realised, but several other significant inferences were made and are highlighted in this final Chapter:

In ambient conditions, water is more detrimental to the operational stability of transistors than oxygen. This indicates that initial fabrication steps can be carried out in a low humidity environment before employing encapsulation techniques to hinder diffusion of ambient species into the film prolonging device performance.

Ionisation potentials can predict the stability of transistors in ambient. Neglecting any overpotentials if a neutral polymer chain has an ionisation potential less than 4.97eV it can be oxidised by oxygen and water, and if an oxidised polymer chain has an I_P of more than 4.97eV, it can be reduced. Electron accepting dopants break the conjugation of the backbone, resulting in a higher Ip and increased stability, though the switch-on voltage and off-currents will be increased due to the introduction of charged carriers into the bulk.

Detailed cyclic voltammetry studies and capacitance measurements (to detect dopant densities) would be required to fully understand these effects. This work only provides an introduction to the causes of instability in these systems and though the effects of humidity and ionisation potential were discussed, further work needs to be done to confirm the precise mechanisms involved. The addition of antioxidants has also been shown to improve ambient stability, as has blending insulators with the semiconducting polymer. There is also a great deal of further work to be done in this

field involving combining spectroscopic measurements (such as photoluminescence photo-oxidation and FTIR studies), cyclic voltammetry, and modelling of dopant densities using capacitance measurements. Clear differentiation should also be made of operational and shelf-life stability before we can fully understand the processes contributing to degradation.

The hole injection barrier should be minimised to negate short channel effects in transistors. Scaling down of device dimensions should result in enhanced currents, a higher operational frequency and a higher mobility, as the drain current is inversely proportional to L and the maximum switching frequency is proportional to μ/L^2. Injection problems are often noticeable from the non-linearity of the output characteristics for shorter channel length transistors ($L \leq 5\mu m$). These effects can be minimised by using a thinner dielectric thickness (and reducing the corresponding voltages) or by reducing the barrier to hole injection. This can be achieved by decreasing the thickness of the chromium adhesion layer so the potential distribution due to V_G is proportionally higher over the gold part of the electrode, or by using an ITO adhesion layer, as the workfunction of ITO is a closer match to that of gold.

Electroluminescence is observed close to the drain electrode in the saturation regime. Finite output conductance is also observed at high drain voltages when the pinch-off region expands from the drain into the channel, leads to enhanced transport in bulk and in some cases electron injection. Equations derived for calculating the saturated mobility are no longer applicable in this case, as the channel length is significantly shortened. Emission is observed close to the drain electrode as the high lateral fields modify the HOMO–LUMO of the organic material at the drain to enable electron tunnelling into the LUMO of the organic material in the pinch-off region. The EL corresponds to the PL and the luminescence intensity is dependent

on the drain bias. Light emission is very sensitive to oxygen levels and trapping, as is also only observed if pulsed or swept biases are applied.

An interesting trend observed concerned the polymers that exhibited electroluminescence. Preliminary photoluminescent quantum efficiency (PLQE) measurements estimated the quantum efficiency of syn-pBTTT to be less than 1%. This is interesting as more 'luminescent' materials such as PFB, PFMO and PFO do not exhibit observable light emission in a transistor structure. Perhaps the level of thr LUMO is crucial to observing this effect. It would be interesting to carry out further PLQE measurements of thin films, diodes and OLET of the materials concerned to see what correlation exists.

The device characteristics of polymer transistors can be improved or worsened by using thiols to modify the workfunction of the gold injecting electrode. The sulphur containing head group of thiols preferentially adsorbs to gold, and if the molecule is terminated with an electronegative moiety, the workfunction of gold will be increased and the barrier to hole injection reduced. The choice of spacer group also affects the injection, as charge carriers have to physically tunnel through the monolayer into the polymer. The contact resistance is the only parameter investigated that follows a direct relationship with the mobility, as it takes into account both the change in Φ_{Au} and insulating effect of the monolayer. A fluorinated aromatic thiol performed best, increasing the mobility threefold, as fluorine is the most electronegative element and the short, conjugated spacer group does not significantly inhibit injection. This is definitely a useful technique to combat the problem of non-Ohmic injection in transistor structures, which is becoming more commonplace as more air-stable polymers tend to have ionisation potentials higher than gold.

Device characteristics can be optimised by combining thiol and silane treatments. Silanes enhance charge transport by improving the stacking of the conjugated backbones, as the perpendicular side chains of the polymer can interlock with the alkyl chains protruding upwards from the interface, and making the interface more hydrophobic. They in effect passivate the interface as polar hydroxyl groups, known to act as electron traps, are replaced by apolar methyl groups, improving the surface energy and adhesion of the polymer. This results in a significant improvement of the mobility of up to 16 times for octyltrichlorosilane (OTS) treatment. The chemical selectivity of self-assembled monolayer allows thiol and silane surface treatments to be combined in order to achieve the best overall performance. Combining FTP and OTS treatments improves the mobility by 40 times for syn-pBTTT transistors. Not only is this beneficial for improving device performance, but it gives us an insight into the relation between charge transport and injection in these systems. Good molecular order at the interface (efficient charge transport) has a bigger impact on the mobility and device characteristics, than the injection alone.

Self-assembled monolayer have been systematically studied in two polymers, syn-pBTTT and ant-pBTTT polymers, and very promising results have also been seen for preliminary experiments concerning the polyfluorene polymers, F8T2 and PFO. Further work needs to be undertaken to look at different and composite material systems (both for the electrodes* and polymers). This simple generic technique helps to solve injection problems that arise from the use of high I_P polymers, so designed to combat instability in air.

The mobility derived from TOF data represents that of the fastest carriers and transistor performance can approach this value if molecular order is improved and the concentration of interface states reduced, effectively reducing the energetic

* Though thiols can only be used with metals, the same principles could be applied to other electrode materials.

disorder and interchain hopping distance. Though the charge density is lower in time of flight measurements, μ_{TOF} is still significantly higher than that of transistors, for the three PF copolymers studied. Transistors represent a lower mobility as the two-dimensional charge transport occurs in the first few polymer chains adjacent to the interface, making it more sensitive to disorder and interfacial traps. Temperature measurements confirm that the disparity between the bulk and interface mobility is due to increased energetic disorder and a longer interchain hopping distance at the interface. If the molecular order of the transporting layer is improved, by using silanes or annealing, the mobility of the transistor is improved and it approaches μ_{TOF}. Temperature dependent transistor comparisons of an amorphous polymer to the polycrystalline polymers used in the prior Chapters signifies further that increased morphological disorder directly translates to lower mobilities, a longer interchain hopping distance, increased energetic disorder and a higher activation energy.

Appendix I

In this Appendix, parameters derived from the Gaussian Disorder Model (GDM) and Holstein (Arrhenius) Models are presented for F8T2. These are not included in the main text of the thesis because further evidence is needed to corroborate the values obtained. TOF measurements could only be taken at low E-fields, as the thickness of the film could not be increased since this increases the dispersivity of the film. The decrease of the mobility with increasing electric field was attributed to off-diagonal order as low E-fields are involved. These measurements should be carried out over a larger temperature range in future.

The temperature dependence of the mobility with respect to the square root of the electric field is shown in Fig(i) below, and the extracted parameters are displayed in the table in Fig(ii).

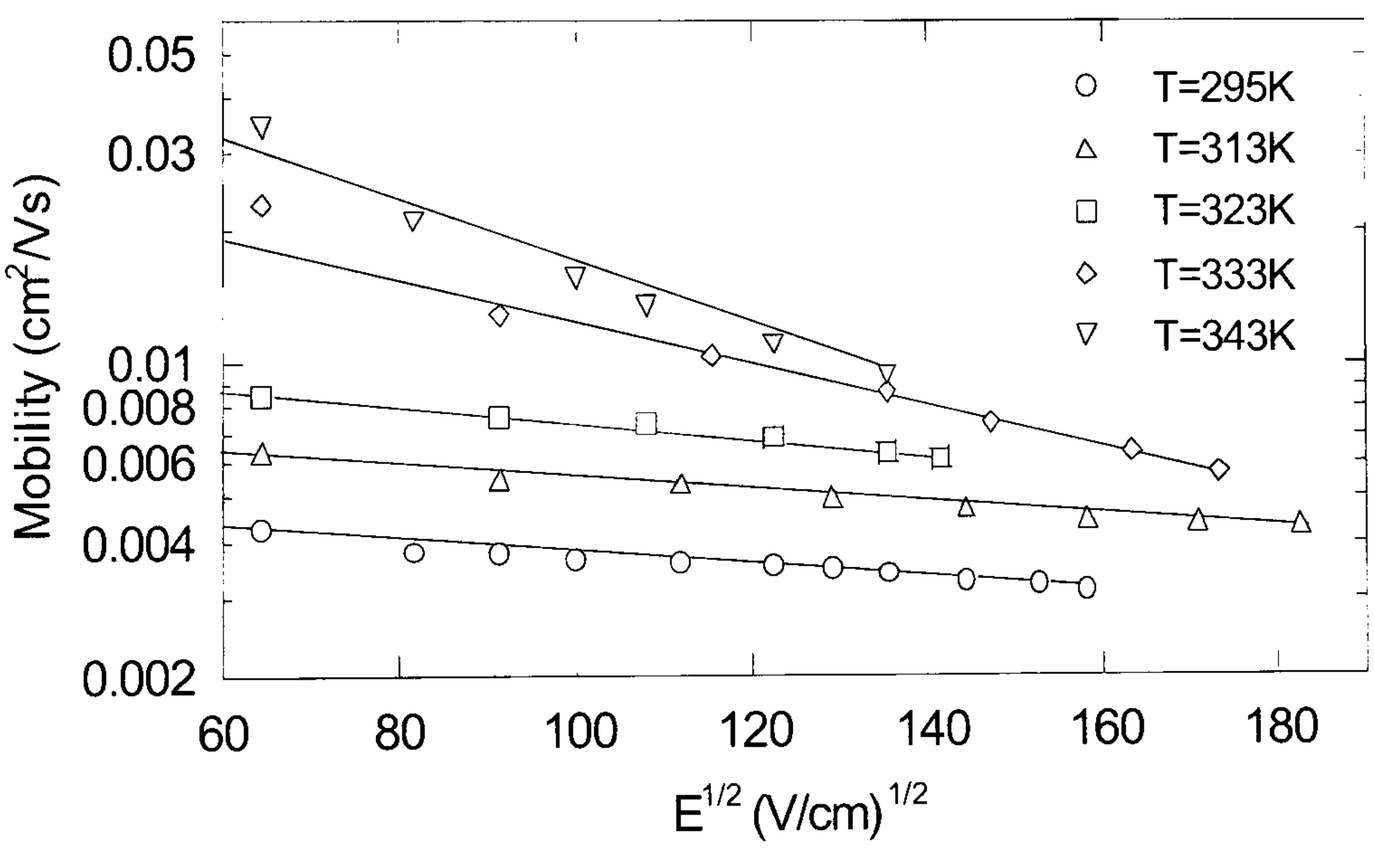


Figure (i). Temperature dependence of the mobility, extracted by the time of flight photocurrent technique, with respect to the square root of the electric field for an unannealed F8T2 device 1.2μm thick.

Device	Mobility	Arrhenius Model		GDM	
		μ_0	E_A	μ_0	σ
TOF	$7.1 \cdot 10^{-3}$	615	0.33	13.6	0.093
FET	$9.2 \cdot 10^{-6}$	$1.4 \cdot 10^{-4}$	0.11	$3.1 \cdot 10^{-5}$	0.088

Figure (i). Table comparing the GDM and Arrhenius model parameters for F8T2 devices.

In this case, the energetic disorder and activation energy are smaller for the field-effect mobility. This is unexpected as the bulk mobility is larger than μ_{FET} and one would expect the energetic disorder at the interface to be larger than in the bulk of the film, as we saw in Chapter 6. F8T2 is a crystalline material, and though no surface treatment was used for these measurements, a degree of self-ordering could occur at the interface that is not present in the bulk of the film. Preliminary TOF measurements also indicate that F8T2 is sensitive to trapping, as the dispersivity of the transient increased with film thickness. As the TOF sample is twenty times thicker than in the active layer of the transistor, we can assume that more trap states are present. The FET derived value of μ_0 is considerably smaller than that extracted from TOF measurement, corresponding to the difference between bulk and interface mobility. This corroborates the reasoning that was put forward in Chapter 6; that the mobility difference is due to the interchain hopping distance. However, more systematic studies need to be carried out before a definite conclusion can be made.